



# Uncertainty analysis of 100-year flood maps under climate change scenarios

---

Saba Mirza Alipour

---



Saba Mirza Alipour

# Uncertainty analysis of 100-year flood maps under climate change scenarios

Dissertation for the degree philosophiae doctor (ph.d.)

University of Agder  
Faculty of Engineering and Science

2022

Doctoral dissertations at the University of Agder 392

ISSN: 1504-9272

ISBN: 978-82-8427-105-7

© Saba Mirza Alipour, 2022

Print: 07 Media

Kristiansand



To the brave women all over the world, particularly the women in my country, Iran, who stand for their rights and fight for equality and emancipation.



## **Acknowledgements**

I would like to thank to all of those who have contributed either directly or indirectly to my research.

My thanks go particularly to my supervisor, Dr. Joao Leal for being available whenever I needed help and trusting my capability to do independent research. His supervision, valuable advice, and constant support made this thesis possible. I learned a lot from you.

Next, I would like to extend my sincerest gratefulness to my co-supervisor, Dr. Kolbjørn Engeland, whose help and support greatly improved the quality of this thesis through his numerous valuable insights and advice.

I would also like to express my gratitude to many wonderful people that I met in UiA. Emma Hornemann for her helps, kindness, and continuous support, and all my friends and colleagues in UiA, especially renewable energy department for their smiles, lunch time stories and kindness. Your friendship will always remain in my heart.

I would also like to express my gratefulness to Dr. Daniel Conde and Dr. Rui Ferreira for providing the simulation tool (HiSTAV) and their help on setting up the simulations.

Last, but not least, no word can describe my gratefulness to my husband, Sepehr Bapiri, who always believed in me, and his unconditional love and support was always with me throughout this journey.



## Summary

Floods are natural disastrous hazards that throughout history have had and still have major adverse impacts on people's life, economy, and the environment. One of the useful tools for flood management are flood maps, which are developed to identify flood prone areas and can be used by insurance companies, local authorities and land planners for rescue and taking proper actions against flood hazards.

Developing flood maps is often carried out by flood inundation modeling tools such as 2D hydrodynamic models. However, often flood maps are generated using a single deterministic model outcome without considering the uncertainty that arises from different sources and propagates through the modeling process.

Moreover, the increasing number of flood events in the last decades combined with the effects of global climate change requires developing accurate and safe flood maps in which the uncertainty has been considered.

Therefore, in this thesis the uncertainty of 100-year flood maps under 3 scenarios (present and future RCP4.5 and RCP8.5) is assessed through intensive Monte Carlo simulations. The uncertainty introduced by model input data namely, roughness coefficient, runoff coefficient and precipitation intensity (which incorporates three different sources of uncertainty: RCP scenario, climate model, and probability distribution function), is propagated through a surrogate hydrodynamic/hydrologic model developed based on a physical 2D model. The results obtained from this study challenge the use of deterministic flood maps and recommend using probabilistic approaches for developing safe and reliable flood maps. Furthermore, they show that the main source of uncertainty comes from the precipitation, namely the selected probability distribution compared to the selected RCP and climate model.

## **Sammendrag**

Flom er naturkatastrofer som har hatt og fortsatt har store konsekvenser for menneskers liv, økonomi og miljø. Et nyttig verktøy for flomhåndtering er flomkart, som er utviklet for å identifisere flomutsatte områder og kan brukes av forsikringsselskaper, lokale myndigheter og planleggere for redning og iverksetting av riktige tiltak mot flomfare.

Utviklingen av flomkart blir ofte gjort ved hjelp av flommodelleringsverktøy som 2D hydrodynamiske modeller. Men flomkart er ofte skapt ved å bruke en enkelt årsaksbestemt modell, uten å ta hensyn til usikkerheten som oppstår fra forskjellige kilder og som forplanter seg gjennom modelleringsprosessen.

Dessuten krever det økende antallet flomhendelser de siste tiårene - kombinert med virkningene av globale klimaendringer - utvikling av nøyaktige og sikre flomkart der usikkerheten er vurdert.

Derfor, i avhandlingen er usikkerheten til 100-års flomkart under tre scenarier (nåværende og fremtidig RCP4.5 og RCP8.5) vurdert gjennom intensive Monte Carlo-simuleringer. Usikkerheten introdusert ved innmating av modell data: ruhetskoeffisient, avrenningskoeffisient og nedbørsintensitet (som inkluderer tre forskjellige kilder til usikkerhet: RCP-scenarier, klimamodell og sannsynlig fordelingsfunksjon), forplantes gjennom en surrogat-hydrodynamisk/hydrologisk modell som er utviklet basert på en fysisk 2D-modell. Resultatene fra denne studien utfordrer bruken av årsaksbestemte flomkart og anbefaler bruk av sannsynlighetsbestemte tilnærminger for å utvikle sikre og pålitelige flomkart. Videre viser de at hovedkilden til usikkerhet kommer fra nedbøren, nemlig valgt sannsynlighetsfordeling sammenlignet med valgt RCP og klimamodell.

# Table of Contents

<b>Acknowledgements</b> .....	<b>VII</b>
<b>Summary</b> .....	<b>IX</b>
<b>Table of Contents</b> .....	<b>XI</b>
<b>List of Figures</b> .....	<b>XIII</b>
<b>List of Tables</b> .....	<b>XIV</b>
<b>List of Publications</b> .....	<b>XV</b>
<b>Structure of the Thesis</b> .....	<b>XVI</b>
<b>1. Introduction</b> .....	<b>1</b>
1.1. Scope and motivation .....	1
1.2. Problem statement and research objectives .....	4
<b>2. Methods</b> .....	<b>7</b>
2.1. Case study .....	7
2.2. 2D hydrodynamic simulations.....	8
2.3. Sensitivity analysis using Taguchi method and ANOVA analysis .....	12
2.4. Surrogate Hydrodynamic model (Emulator) .....	15
2.5. Uncertainty Analysis (Probabilistic approach).....	15
2.6. Deterministic approach.....	17
<b>3. Results</b> .....	<b>19</b>
3.1. Outline of results .....	19
3.2. Paper I: A practical methodology to perform global sensitivity analysis for 2D hydrodynamic computationally intensive simulations .....	19
3.3. Paper II: Return levels uncertainty under effect of climate change .....	20
3.4. Paper III: Representation of 100-year design rainfall uncertainty in catchment-scale flood modeling: A MCMC Bayesian approach .....	21
3.5. Paper IV: Emulation of 2D Hydrodynamic Flood Simulations at Catchment Scale Using ANN and SVR .....	22
3.6. Paper V: Uncertainty Assessment of Flood Maps: A Comparison of Bootstrap and Monte Carlo Methods .....	23
3.7. Paper VI: Uncertainty analysis of 100-year flood maps under climate change scenarios .....	24
<b>4. Conclusions and recommendations</b> .....	<b>27</b>
4.1. Conclusions .....	27
4.2. Limitations and future directions.....	29

<b>List of references.....</b>	<b>31</b>
<b>Appendices .....</b>	<b>39</b>



## List of Figures

Figure 1. (a) Map of Tovdal river's catchment area. (b) The case study area region, inundated in 2017 flood event.....	8
Figure 2. Spatial distribution of the precipitation stations and the interpolated precipitation over the catchment. ....	11
Figure 3. Taguchi ANOVA method workflow. ....	13
Figure 4. Performance of the developed SVR surrogate model.....	23

## List of Tables

Table 1. The recorded data of the flood event in the study area (water level and discharge refer to Flakksvann, in Figure 1).....	7
Table 2. Selected input descriptions and assigned ranges. ....	16

## List of Publications

The following papers have been published or submitted for publication in peer reviewed international conference proceedings and journals.

**Paper I:** Alipour, S.M., Engeland, K., Leal, J., 2021a. A practical methodology to perform global sensitivity analysis for 2D hydrodynamic computationally intensive simulations. Hydrology Research.

DOI:<https://doi.org/10.2166/nh.2021.243>

**Paper II:** Alipour, S.M., Leal J., 2019. Return levels uncertainty under effect of climate change. Proceedings of the IAHR World Congress. ISSN: 2521-7119. s 256 - 264. DOI:[10.3850/38WC092019-1230](https://doi.org/10.3850/38WC092019-1230).

**Paper III:** Alipour, S.M., Engeland, K., Leal, J., 2021b. Representation of 100-year design rainfall uncertainty in catchment-scale flood modeling: A MCMC bayesian approach. [VANN](#), 04.

**Paper IV:** Alipour, S.M., Leal, J., 2021. Emulation of 2D Hydrodynamic Flood Simulations at Catchment Scale Using ANN and SVR. Water, 13(20): 2858.

DOI:[10.3390/w13202858](https://doi.org/10.3390/w13202858)

**Paper V:** Alipour, S.M., Leal, J., Engeland, K., 2022. Uncertainty Assessment of Flood Maps: A Comparison of Bootstrap and Monte Carlo Methods. Proceedings of the 39th IAHR World Congress (19–24 June 2022, Granada, Spain): 6422-6430. DOI:[doi://10.3850/IAHR-39WC2521716X2022651](https://doi.org/10.3850/IAHR-39WC2521716X2022651)

**Paper VI:** Alipour, S.M., Leal, J., Engeland, K., 2022. Uncertainty analysis of 100-year flood maps under climate change scenarios. (Submitted to the Journal of Hydrology, Manuscript Number: HYDROL47552)

## **Structure of the Thesis**

This thesis is a collection of six technical publications addressing the uncertainty analysis of 100-year flood maps. Chapters 1 and 2 provide an introduction into the topic and describe the methods and the approach used in this thesis. Chapter 3 summarizes the main findings of the thesis in a modified format based on the published papers. In chapter 4, main conclusions and recommendations for future work are presented. Finally, in Appendices, the scientific publications from this thesis are presented.

# 1. Introduction

## 1.1. Scope and motivation

Floods are one of the world's major natural disasters, occurring all over the world. One very recent example was the flood of July 2021 in several European countries including Germany, Belgium and the Netherlands, in which over 200 people were killed and billions of euros economic losses happened (UNRIC, 2022). In recent years, flood losses have increased considerably (Nicholls *et al.*, 2015, Paprotny *et al.*, 2018). In Norway floods have also caused severe damages and billions of NOK losses (Roald, 2021). According to the latest report from the Intergovernmental Panel on Climate Change (IPCC) the number and severity of extreme flood events are expected to increase (Masson-Delmotte *et al.*, 2021). Therefore, it is important to identify flood prone regions and properly manage flood risks accounting for the uncertainty induced by climate change.

Flood inundation maps are useful tools to delineate inundated regions and are the primary step for the subsequent flood risk management. In Norway, flood maps are mostly developed by the Norwegian Water Resources and Energy Directorate (NVE) and private actors such as insurance companies which use them to determine insurability and compensation cost. These maps are mostly developed using 1D or 2D hydrological/hydrodynamic models with a deterministic approach, rendering floodplain boundaries as a single line. Deterministic approach, which assumes known values for input data and provides fixed outputs, is subjected to considerable criticism since it inevitably masks out a wide range of probable outputs. Unfortunately, despite the advances in computational power and uncertainty analysis techniques, environment agencies, authorities and engineering consultancies rarely adopt probabilistic approaches. There is significant uncertainty associated with flood maps which stems from different sources and from the complex nature of flooding. Therefore, flood maps should not be defined as a single deterministic border. Looking at flood insurance claims of recent flood events, shows that a remarkable number of claims have occurred out of the identified hazard zones (Brody *et al.*, 2013, Howard, 2022). This confirms the inefficiency of deterministic maps to present a safe realization of flood extents. Furthermore, probabilistic flood maps have proven to be preferable to single deterministic maps of inundation extent and are likely to be more in demand in the near future (Teng *et al.*, 2017).

Uncertainty analysis is an unavoidable part of flood modeling. To date, many studies have been conducted highlighting the importance of this issue and have developed different frameworks or approaches to deal with uncertainty systematically (e.g., Refsgaard *et al.*, 2007, Beven *et al.*, 2011, Dottori *et al.*, 2013, Ahmadisharaf *et al.*, 2018). One of the widely used approaches for uncertainty analyses purposes, is the probabilistic approach in which the uncertainty is described by means of probability distribution functions (PDFs). Input parameters are treated as random variables with known PDFs, and the result is a PDF of an output parameter (Komatina and Branisavljevic, 2005). In general, based on the literature, the following steps should be carried out to address the uncertainty: firstly, to identify the sources of uncertainty; secondly, to quantify and rank the uncertainty sources and finally representing the uncertainty through uncertainty analysis methods.

Uncertainty can be introduced to the outputs throughout the modeling process by several sources such as uncertain input parameters, modeling assumptions and limitations, model structure and parameters, calibration, and validation of the model. According to the literature, the key sources of uncertainty in flood modeling are: (1) input parameters such as hydraulic roughness coefficient in the river channel and flood plains, precipitation, discharge and design hydrograph (e.g., Sampson *et al.*, 2014, Das and Umamahesh, 2018, Vojtek *et al.*, 2019, Chen *et al.*, 2018, Ahmadisharaf *et al.*, 2018, Lawrence, 2020), topography/bathymetry and digital terrain models (DTM) (e.g., Savage *et al.*, 2016, Abily *et al.*, 2016, Lim and Brandt, 2019, Neal *et al.*, 2015, Van Vuren *et al.*, 2015, Mejia and Reed, 2011), (2) model parameters and structures like boundary conditions (Pappenberger *et al.*, 2006), mesh generation (Kim *et al.*, 2014), modeling assumptions and simplifications (Wagenaar *et al.*, 2016), and (3) validation data (Stephens *et al.*, 2012, Thielen *et al.*, 2015). The uncertainty in these sources is described by statistical probabilistic methods.

Sensitivity analysis (SA) is a commonly used technique in environmental modeling for identifying the influential parameters and ranking them. By performing sensitivity analyses we can determine which input uncertainty sources affect more the output and accordingly pay additional attention to the uncertainty they introduce. In practice SA methods are classified into local and global methods (Saltelli *et al.*, 2004). In the local approach, input parameters are varied one factor at a time while keeping the other inputs as fixed. Conversely in global approach the inputs are varied simultaneously, and the variation is assessed in output. A

review of existing SA methods, types and their applications can be found in the studies by Song *et al.* (2015) and Pianosi *et al.* (2016). Global SA methods are computationally intensive, time-consuming, and require a high number of simulations. Therefore, it is often difficult to apply these methods.

One possible solution to overcome the computational burden of global SA methods is to statistically design the simulations (Rao, 1947). This method which is called DoE (design of experiments) effectively reduces the number of simulations (experiments) and explores the relationship between the input parameters (predictor variables) and the generated output (response variables), as well as various interactions that may exist between the input variables.

Taguchi (1986) has developed a methodology for the application of designed experiments based on orthogonal design to reduce the number of experimental combinations. Using orthogonal arrays allows us to collect the necessary information by testing specific combinations, instead of examining all possible combinations. In this study we used Taguchi method for sensitivity analysis. To validate the results, analysis of variances (ANOVA) was performed additionally.

Assessing and communicating the identified uncertainties in previous steps is a crucial step which can be done through different methods. Generally, to explore the propagated uncertainty, the uncertain parameters' spaces are sampled using a Monte Carlo-based framework and an ensemble of probable model outputs is generated. There are different methods to assess uncertainty, such as Monte Carlo (Hong *et al.*, 2006, Apel *et al.*, 2008), Bayesian methods (Yang *et al.*, 2007, Han and Coulibaly, 2017, Guo *et al.*, 2020), generalized likelihood uncertainty estimation (GLUE) (Zheng and Keller, 2007, Jung and Merwade, 2012, Nott *et al.*, 2012), bootstrap (Selle and Hannah, 2010, Bomers *et al.*, 2019), fuzzy set approach (Maskey *et al.*, 2004, Arunraj *et al.*, 2013) and others. Each of these methods has advantages and drawbacks. As an example, the GLUE methodology proposed by Beven and Binley (1992) as a commonly used method for uncertainty assessment has been criticized by a number of researchers (*e.g.*, Mantovan and Todini, 2006, Stedinger *et al.*, 2008, Alazzy *et al.*, 2015). Among the proposed methods Monte Carlo method is yet a powerful and reliable method to capture the uncertainty.

Uncertainty analyses generally requires many model realizations. Consequently, it is often hampered by the intensive computational burden of the 2D models. There are different solutions to overcome this constrain such as: *i*) using optimized sampling techniques (*e.g.*, Wang *et al.*, 2004, Hossain *et al.*, 2006, Shields *et al.*, 2015), *ii*) advanced computational tools (*e.g.*, Conde *et al.*, 2020, Kalyanapu *et al.*,

2011), *iii*) simplified conceptual models (Lhomme *et al.*, 2008, Teng *et al.*, 2015, Guo *et al.*, 2021), and *iv*) surrogates or emulators (*e.g.*, Laloy *et al.*, 2013, Bermúdez *et al.*, 2018, Zahura and Goodall, 2022).

In general, surrogates or emulators, also referred as metamodels (Razavi *et al.*, 2012), are developed using different types of methods such as polynomial regression (Castro-Gama *et al.*, 2014; Yu *et al.*, 2015), radial basis functions (Luo and Lu, 2014), kriging methods (Bacchi *et al.*, 2019) and smoothing splines (Villa-Vialaneix *et al.*, 2012). Amongst the proposed methods for development of the surrogates or emulators, machine learning techniques are popular methods which have been widely applied in flood related studies (*e.g.*, Ghalkhani *et al.*, 2013, Chu *et al.*, 2020, Xie *et al.*, 2021).

## **1.2. Problem statement and research objectives**

Floods and their link with climate change are nowadays a concern for society. In Norway, unexpectedly high flood levels occurred in recent years and have caused awareness about the inefficiency of deterministic flood maps with 100-year return period, with insurance companies paying high losses and menacing not ensuring anymore properties close to rivers. For hydropower companies, the knowledge of floods and their proper management is important to secure the downstream valleys, but also to minimize the losses of water through dams' spillways that does not pass the turbines, representing a direct economic loss.

The present work aims to contribute to the understanding about uncertainty in 2D flood modeling and to establish a comprehensible and feasible methodology to assess it under climate change scenarios. The following specific objectives are defined:

**Objective 1:** Identification and characterization of the uncertainties associated to the model input parameters taking into consideration different climate change scenarios.

**Objective 2:** Identification of the most influencing input parameters on the model output.

**Objective 3:** To create a less computationally demanding model to estimate flood inundation maps.

**Objective 4:** Representing the uncertainty of the 100-year flood maps obtained using a Monte Carlo framework under present and future scenarios.

**Objective 5:** Comparing and exploring the differences arising from adopting the deterministic and probabilistic approaches.



The following specific research questions should be answered within this study:

- Can a simple DoE approach, like Taguchi method, be used for a global SA?
- What are the main sources of uncertainty in flood modelling?
- Is it possible to detect a climate change pattern with nonstationary Generalized Extreme Value (GEV) model from observed data in stations?
- Can a low computational cost data-driven surrogate/emulator of 2D hydrological/hydrodynamic simulations be developed with reasonable accuracy?
- What is the contribution of climate change uncertainty to the overall uncertainty?
- What are the most relevant assumptions on climate change modelling to flood map uncertainty assessment?
- To each extent we can avoid the use of a computationally intensive Monte Carlo framework by using simpler sampling/ensemble techniques, like bootstrap?
- What are the main differences between deterministic and probabilistic flood maps, and what we might have been overlooking by just using the former ones?



## 2. Methods

### 2.1. Case study

Birkeland town area, located in Agder province (Norway), is selected as the case study since in recent years floods have become a major concern there. Birkeland is located beside a river named Tovdal, where the river debouches into a small natural lake called Flakksvann (Figure 1). The length of the main river reaches approximately 130 km, and the catchment with an area of about 1,767 km<sup>2</sup> is dominated by forests (about 74%). The elevation ranges from 10.00 to 872.34 m.a.s.l, and the average slope of the catchment along the river is about 0.65%. The mean annual precipitation is approximately 1,261 mm, with most of the rainfall occurring between October and March (about 60%).

On 2<sup>nd</sup> of October 2017, an extreme flood event occurred in this area which was the highest ever recorded flood in this river, with an estimated return period over 100 years (Langsholt and Holmqvist, 2017). Recorded data of the event (Table 1) (including water level, discharge, flood hydrograph at Flakksvann cross-section (CS), and flood maps) will be used to calibrate the 2D hydrodynamic model and to validate the methodology.

Table 1. The recorded data of the flood event in the study area (water level and discharge refer to Flakksvann, in Figure 1).

Date	Precipitation (mm)	Maximum water level (m)	Maximum discharge (m <sup>3</sup> /s)
30.09.2017	45.1	21.40	501.28
01.10.2017	173.1	24.57	1,061.19
02.10.2017	63.6	25.56	1,194.88

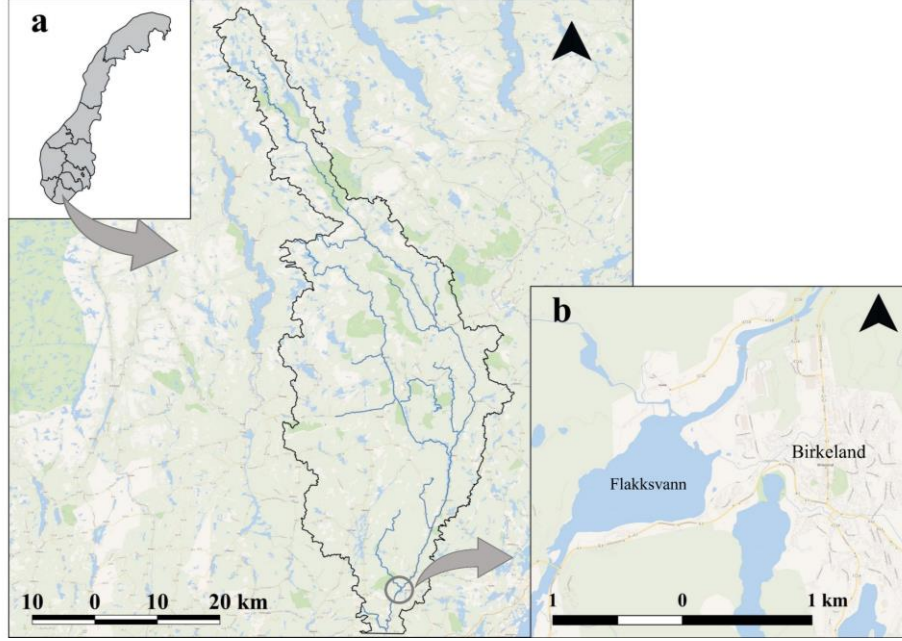


Figure 1. (a) Map of Tovdal river's catchment area. (b) The case study area region, inundated in 2017 flood event.

## 2.2. 2D hydrodynamic simulations

There are a variety of tools for flood modeling and among those hydrodynamic modeling groups have received a considerable attention. Hydrodynamic models can be classified into one-dimensional (1D), two-dimensional (2D) and three-dimensional (3D) models that simulate water movement by solving flow equations. In the current study a GPU based 2DH (two dimensional horizontal) hydrodynamic model, named HiSTAV has been used to simulate floods. The model was originally proposed by Ferreira *et al.* (2009) and optimized by Conde *et al.* (2020). The core of the model is a hyperbolic system of partial differential equations expressing mass and momentum conservation principles for flow. In this framework, the Navier-Stokes system is vertically integrated between the bed and the free surface, leading to the following depth-averaged form of the conservation laws for total mass and horizontal momentum (*Eq. 1* and *Eq. 2*) (Conde *et al.*, 2020).

$$\partial_t h + \partial_x(hu) + \partial_y(hv) = h_p - \partial_t z_b \quad \text{Eq. 1}$$

$$\begin{aligned} \partial_t(hu_i) + \partial_{x_i}(hu_i^2) + \partial_{x_j}(hu_i u_j) \\ = -\partial_{x_i}(gh^2/2) - gh\partial_{x_i}z_b + (\tau_{w,i} - \tau_{b,i})/\rho \end{aligned} \quad \text{Eq. 2}$$

Where  $t$  is time,  $x_i$  stands for the horizontal space coordinates  $i = x$ , and  $y$ ,  $h$  is the flow depth,  $z_b$  is the bed elevation,  $u_i$  is the depth-averaged velocity in the  $x_i$  direction, and  $g$  is the gravitational acceleration. In *Eq. 2*  $\tau_{w,i}$  and  $\tau_{b,i}$  are the wind

and bed shear stresses, respectively,  $\rho$  is depth-averaged density, and  $gh\partial_{x_i}z_b$  represents the bottom slope contribution. The local source terms for total mass are the bed evolution  $\partial_t z_b$  and the effective precipitation intensity  $h_p$ . The bed shear stress,  $\tau_{b,i}$ , is given by Manning-Strickler equation:

$$\tau_{b,i} = \frac{\rho g}{K_S^2 h^{1/3}} |u_i|^2 \quad \text{Eq. 3}$$

where  $K_S$  is the Strickler coefficient (inverse of Manning's coefficient).

The equations are solved using a finite volume scheme which is applied on a spatial discretization using unstructured meshes. The discretization method allows body fitting unstructured grids. These can optimize the computational workload by using large cells, where flow gradients are expected to be mild, and small cells in specified areas.

The hyperbolic non-homogeneous system, composed by quasi-linear first order *Eq. 1* and *Eq. 2*, can be compactly rewritten in the form of *Eq. 4* (please see Conde *et al.*, 2020, for details):

$$\frac{\partial U}{\partial t} + \vec{\nabla} \cdot (\mathbf{E} - \mathbf{T}) = S \quad \text{Eq. 4}$$

where,  $U$  is the vector of conserved (or state) variables and  $\mathbf{E}$  is the conservative fluxes vector,  $\mathbf{T}$  represents source terms as non-conservative fluxes (LeFloch and Novotny, 2003) and  $S$  defines source terms that are only locally determined. A finite volume formulation is obtained by integrating *Eq. 4* over a time-invariant volume  $\mathcal{V}$  and applying the Gauss theorem to the flux terms, resulting in

$$\frac{\partial}{\partial t} \int_{\mathcal{V}} \mathbf{U} d\mathcal{V} + \oint_{\partial\mathcal{V}} (\mathbf{E} - \mathbf{T}) \cdot \mathbf{n} dA = \int_{\mathcal{V}} \mathbf{S} d\mathcal{V} \quad \text{Eq. 5}$$

where  $\mathbf{n}$  is the outward unit vector normal to the volume surface  $dA$ . Considering a Gudonov-type average representation of the integrated quantities, *Eq. 5* can be discretized as (see Conde *et al.*, 2020, for details):

$$\frac{\mathbf{U}_i^{m+1} - \mathbf{U}_i^m}{\Delta t} A_i + \sum_{k=1}^{K_i} (\Delta_k \mathbf{E}_i^m - \mathbf{T}_{i_k}^m) n_{i_k} l_{i_k} = \mathbf{S}_i^m A_i \quad \text{Eq. 6}$$

where  $\mathbf{U}_i^m$  is the state vector, averaged over volume  $i$  at time step  $m$ ,  $A_i$  is the base area and  $\Delta t$  is the time step. Index  $k$  represents the  $k^{\text{th}}$  edge of volume  $i$ , from a total  $K_i$  edges, with  $l$  and  $n$  being the respective length and  $i$ -outward normal. The  $\Delta_k$  operator denotes a quantity jump across the  $k^{\text{th}}$  edge, so that  $\Delta_k E_i^a = E_{j(i_k)}^a - E_i^a$  with  $j(i_k)$  being the volume adjacent to  $i$  through edge  $i_k$ . The non-conservative

flux  $T_{i_k}^a$  is integrated across each edge  $i_k$  as defined by Murillo *et al.* (2009) and Parés and Castro (2004).

To simulate the flow, the model solves the equations over the entire catchment based on the following sources: *i*) input variables, *ii*) computational mesh and *iii*) initial and boundary conditions.

The 2D model used here requires different data sets as input namely: (a) raster data structures (including topo-bathymetric dataset, Strickler roughness coefficient values and runoff coefficient values), and (b) precipitation intensity.

Raster data structures and grids are used to present the catchment discretization and to describe spatially distributed terrain parameters (*i.e.*, elevation, bathymetry, land use, etc.). A  $10 \times 10 \text{ m}^2$  Digital Terrain Models (DTM) of the catchment, including the river bathymetry information, is used to represent topographic features that determine hydrologic characteristics (*i.e.*, slope, flow direction, flow accumulation, stream network, etc.).

Hydraulic roughness is inserted in the model in the form of grid structure raster file ( $100 \times 100 \text{ m}^2$  resolution), in which each cell represents Strickler roughness values. The spatial distribution of roughness values is determined based on  $100 \times 100 \text{ m}^2$  land cover maps (obtained from <https://land.copernicus.eu/> “Corine Land Cover (CLC) 2018, Version 20”). Subsequently, using engineering knowledge and standard tables Strickler roughness coefficients, the roughness values were assigned for each cell. These values were determined by firstly identifying an average value for each land type and assuming a 50% upper and lower band as the variation range. Secondly, the ranges were expanded or narrowed down using the values reported in the literature (*e.g.*, Nicholas and Lewis, 1980, Asante *et al.*, 2008, Kaiser *et al.*, 2011, Papaioannou *et al.*, 2018).

The runoff coefficient  $C$  is a dimensionless factor that is used by HiSTAV to convert the rainfall amounts to runoff (effective precipitation  $h_p = C \cdot i_p$  in Eq. 1, being  $i_p$  the precipitation intensity). Similar to hydraulic roughness values, runoff coefficient values are used in form of raster data and represent the integrated effect of catchment losses (like infiltration and surface retention). Therefore, the coefficient value depends on different parameters such as land cover and use, slope, soil moisture, and rainfall intensity (Goel, 2011). Using land cover maps and recommended values of runoff coefficient for different types of areas (Subramanya, 2013), a range was determined for each cell. Similar to the roughness ranges, the ranges initially were identified based on an average value

with 50% bounds and then the ranges were corrected using values reported in the literature (*e.g.*, Lewis *et al.*, 2006, Dhakal, 2012, Mahmoud and Alazba, 2015, Sriwongsitanon and Taesombat, 2011).

HiSTAV applies the precipitation as a constant intensity (mm/h) over the study domain for a given time. In other words, the model assumes the precipitation as a spatially and temporally constant variable. This assumption is against what happens in real nature. As a result, to apply a spatially varying precipitation we used the runoff coefficient to artificially vary the precipitation intensity over the study domain. For this purpose, focusing on the flood of 02.10.2017, daily precipitation data were obtained from 37 stations (Figure 2). The rainfall observations within the spatial distribution of stations were interpolated to delineate the precipitation zones. The inverse distance weighting interpolation method (IDW) was used, giving similar precipitation patterns as the ones presented the Norwegian Meteorologic Institute ([www.seNorge.no](http://www.seNorge.no)). The precipitation zones were delineated as Figure 2. The combination of the two mentioned approaches was used to calculate final runoff coefficient in each cell,  $C_{total}$ , as follows:

$$C_t = C \times \left( \frac{i_{P_{cell}}}{i_{P_{max}}} \right) \quad Eq. 7$$

where  $i_{P_{max}}$  is the maximum amount of precipitation intensity among the recorded values,  $i_{P_{cell}}$  is the recorded precipitation intensity in each cell and  $C$  is the runoff coefficient (Alipour *et al.*, 2021a) (Paper I). Resuming the explanations presented above, in this study the precipitation is adopted as spatially varying and temporarily constant. This assumption showed good results for the validation made of the 02.10.2017 flood event.

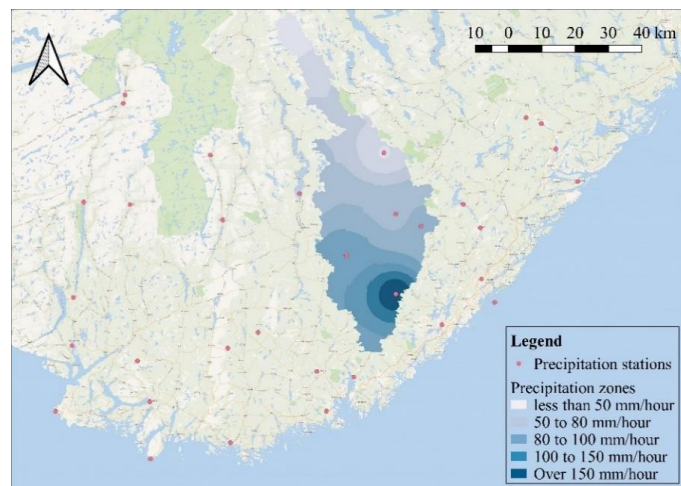


Figure 2. Spatial distribution of the precipitation stations and the interpolated precipitation over the catchment.

HiSTAV adopts triangular meshes to discretize the computational domain and balance the computational workloads, different detail levels, and complex geometry fitting capabilities (Conde *et al.*, 2015). In this study, by employing Godunov's finite volume approach (LeVeque, 2002), a mixed mesh of triangular cells are constructed in three sizes over the computational domain by Gmsh (Geuzaine and Remacle, 2009), which is a free finite element grid generator with a built-in CAD engine and post-processor. The small cells or so-called finer resolutions are assigned to the cells where the flow gradients are expected to be large such as the river channel, medium-sized cells, or average resolution over the flood plain, and coarser resolution over other parts of the catchment, where flow gradients are expected to be mild. In the post-processing step, the constructed meshes were checked for shape and size quality. In total, 401,769 cells, including 106,088 of small cells, 40,172 of medium cells and 255,509 of large cells, were adopted for the study domain.

Water enters the domain only through rainfall, hence there are not inlet boundaries. The only open boundary is at the outlet (downstream) where free outflow is assumed. The computational domain was extended about 7 km downstream Flakksvann, so that this boundary condition does not influence the flow conditions there. Warm-up simulations were performed starting from initial conditions with zero water depth and zero discharge everywhere (completely dry catchment conditions) until reaching the normal water level across the entire catchment. A 9-day precipitation with the intensity of 2 mm/h was found to be long enough to fill the river basin and the lakes with steady flow over the main water courses. These were then used as the initial conditions for all the simulations.

To make sure that all the values and assumptions are valid, a validation using the 02.10.2017 flood event data is performed. The weighted average of precipitation intensities which occurred 1.5 days before the 2017 flood event was used as the reference precipitation (Table 1). Subsequently, by adjusting the friction factor and the runoff coefficient values for each land class in a trial-and-error process, calibration was performed such that simulated water level and discharge resembled the event's recorded information (Table 1).

### **2.3. Sensitivity analysis using Taguchi method and ANOVA analysis**

Taguchi developed a system of tabulated designs (arrays) that allows for the maximum number of main effects to be estimated in an unbiased manner while using only a minimum number of experimental tests (Taguchi 1986). Depending



on the number of parameters and the levels of variation for each parameter, there are standard orthogonal arrays available. As an example, assessing possible combinations for four parameters with three levels, corresponds to 81 number of simulations (called full factorial design). However, to effectively reduce the number of experiments, the Taguchi method proposes two possible orthogonal arrays, namely L27 and L9. The L27 consists of 27 sets of combinations and assesses the main effects and the interaction between the parameters, while the L9 consists of nine combinations, which only concentrates on main effects and ignores the interactions.

The process of Taguchi analysis can be summarized into seven steps (Bao *et al.* 2013). The flow chart of the whole process is illustrated in Figure 3 (Alipour *et al.*, 2021a (Paper I)).

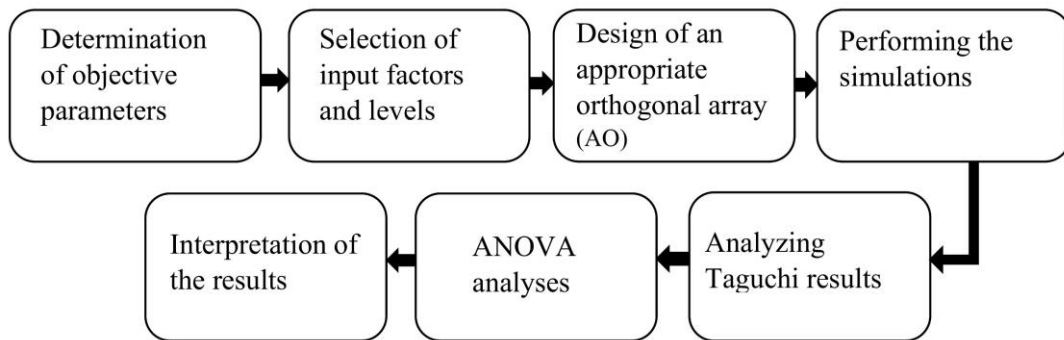


Figure 3. Taguchi ANOVA method workflow.

The simulated cross-sectional water level at different locations and total flooded area are selected as the target outputs (called response in Taguchi framework). The inputs (called factors in Taguchi framework) namely: mesh size, hydraulic roughness parameter ( $K_s$ ), runoff coefficient ( $C$ ), and precipitation intensity ( $i_p$ ) are selected as the uncertainty sources whose influence on the target outputs we aim to identify. Three levels were established for the input parameters. These levels were obtained based on the average values of the parameters observed in the 2017 flood event (level 2) with 50% upper and lower bounds (level 1 and 3, respectively). The mesh size space was set at three levels of refinement named fine, medium, and coarse resolution. Different combination of the inputs with different levels were designed based on Taguchi method and the model is executed for each combination. Details of the process can be found in Alipour *et al.* (2021a) (Paper I).

Taguchi design uses the signal-to-noise ratio (SNR) (Eq. 8) to measure the deviation of the response from the mean value.

$$\text{SNR} = -10 \times \log \left( \frac{1}{n} \sum_{i=1}^n \frac{1}{Y_i^2} \right) \quad \text{Eq. 8}$$

Where  $Y_i$  represents the result in the  $i$ th simulation,  $n$  is the number of simulations,  $\bar{Y}$  is the average of the results and  $\sigma$  represents the standard deviation of  $Y$ . Once the SNR is calculated for each combination, the average of the SNR is calculated for each factor  $j$  at level  $l$  using Eq. 9.

$$\text{MSNR}_{\text{Factor}=j}^{\text{Level}=l} = \frac{1}{n_{jl}} \sum_{i=1}^{n_{lj}} [\text{SNR}_{\text{Factor}=j}^{\text{Level}=l}]_i \quad \text{Eq. 9}$$

where  $n_{jl}$  is the number of simulations that have factor  $j$  at level  $l$ , and  $i$  represents the  $i$ th simulation with factor  $j$  at level  $l$ . The parameters producing the highest variation in MSNR are identified as the most influencing parameters.

In addition to the SNR analyses, analysis of variance (ANOVA) was performed to identify the most significant factors/parameters and their potential interactions. This method focuses on the analysis of the variance around the mean of the performance characteristics and is accomplished by estimating the Fischer's test value ( $F$ -value). The impact of any parameter is explained by its  $F$ -value and corresponding sum of squares. Higher  $F$ -value and sum of squares of any parameter indicates its relative importance in the process of the response (Karmakar *et al.*, 2018). Moreover, to explore the impacts of individual parameters the percentage contribution ( $PC$ ) of each parameter are calculated using the following equation (Yang and Tarnng, 1998):

$$PC = \frac{SS_j}{SS_T} \times 100 \quad \text{Eq. 10}$$

where,  $SS_T$  is the total sum of squares and  $SS_j$  is the sum of squared deviations for each factor  $j$ . Both can be calculated using Eq. 11 and Eq. 12, respectively:

$$SS_T = \sum_{i=1}^n (Y_i - \bar{Y})^2 \quad \text{Eq. 11}$$

$$SS_j = \sum_{j=\text{factors}}^1 \sum_{i=1}^l n_{jl} (\bar{Y}_{jl} - \bar{Y})^2 \quad \text{Eq. 12}$$

Where  $n$  is the number experiments/simulations,  $Y_i$  represents the result in the  $i$ th simulation,  $\bar{Y}$  is the average of results,  $\bar{Y}_{jl}$  is the mean of results for the factor  $j$  at level  $i$  (for example mean of results when precipitation is at level 1, etc.),  $n_{jl}$  is the number of simulations that have factor  $j$  at level  $l$  (Alipour *et al.*, 2021a) (Paper I).

## 2.4. Surrogate Hydrodynamic model (Emulator)

Despite the fact that the HiSTAV is a high-performance model optimized to run in several GPUs (Conde *et al.*, 2020), the simulation time for the computational domain of the case study (composed of 401,769 mixed mesh elements) is about 12 GPU hours. As a result, this long run time inhibits the application of HiSTAV for uncertainty analysis in which a large number of realizations is required. To overcome this limitation, we developed an emulator based on 1,200 different simulations performed with the 2D hydrodynamic model.

The details of the model and the emulation procedure can be found in Alipour and Leal (2021) (Paper IV). In summary, by sampling the input parameters spaces namely precipitation intensity, roughness, and runoff coefficient values for each land type in the catchment, 1,200 simulations were performed. The ranges for roughness and runoff coefficients were made based on the land type, vegetation, and average antecedent soil moisture, and they reflect a reasonable variation range. In this study we aimed to emulate the 100-year return period flood water level. Therefore, 100-year design precipitation range was obtained by fitting the Generalized Extreme Value (GEV) distribution to the annual maxima series in different stations and finally selecting a sufficiently wide range as the precipitation range. The range corresponds to 5% and 95% confidence intervals of the estimated design precipitation (details are presented in Alipour *et al.*, 2021b (Paper III)). These simulations were then used to develop two emulators using Artificial Neural Network (ANN) and Support Vector Regression (SVR). The developed emulators were optimized in a subsequent step by dimension reduction techniques and removing the less correlated inputs. The trained emulator was updated later with more simulations, covering wider ranges of the precipitation, to be used in this study.

## 2.5. Uncertainty Analysis (Probabilistic approach)

The input parameters namely: hydraulic roughness parameter ( $K_S$ ), runoff coefficient ( $C$ ) and precipitation intensity ( $i_p$ ) are selected as the uncertain input variables which HiSTAV uses to simulate the flow. The hydraulic roughness and runoff coefficient parameter spaces are constructed for each of them based on a range which reflects the reasonable variation range. The choice of ranges was made based on the land type, vegetation, and average antecedent soil moisture, as explained before in pages 10 to 11.

Estimation of precipitation intensity is a crucial step in rainfall-runoff modelling practices which is incorporated with uncertainty due to the limited historical data, climate variability/change and complex and chaotic nature of climate. This is even more challenging for estimates under future scenarios. In this study, we used three scenarios (present, future-RCP 4.5 and future-RCP 8.5) along with a Bayesian Markov chain Monte Carlo (MCMC) approach to define a range for 100-year precipitation intensity (detailed information is presented in Papers IV and V). Table 2 presents the considered input variables with their descriptions and specified ranges used in this study. Runoff coefficient values and Strickler roughness values are assigned to each cell based on the land type.

Table 2. Selected input descriptions and assigned ranges.

Parameters		Acronym	Range	Distribution of the values
Precipitation intensity (mm/h)		$i_p$	[3-16]	Empirical distributions
Strickler roughness ( $m^{1/3}/s$ )	Urban lands	$K_s_U$	[40-70]	Uniform
	Forests (broad-leaved, coniferous)	$K_s_F$	[15-40]	Uniform
	Moors and heathland	$K_s_{Mo}$	[18-30]	Uniform
	Arable lands	$K_s_A$	[18-37]	Uniform
	Agriculture and vegetated areas	$K_s_{Ag}$	[18-37]	Uniform
	River and water courses	$K_s_R$	[20-50]	Uniform
	Mineral sites	$K_s_{Mi}$	[30-60]	Uniform
Runoff coefficient (%)	Urban lands	$C_U$	[80-90]	Uniform
	Forests (broad-leaved, coniferous)	$C_F$	[50-70]	Uniform
	Moors and heathland	$C_{Mo}$	[60-80]	Uniform
	Arable lands	$C_A$	[40-60]	Uniform
	Agriculture and vegetated areas	$C_{Ag}$	[40-60]	Uniform
	Mineral sites	$C_{Mi}$	[70-90]	Uniform

The uniform distribution is selected for roughness and runoff coefficient values since there is insufficient information to assume that any value in the range is more likely than any other value (Dalbey *et al.*, 2008). Therefore, we used a uniform distribution, ensuring equal probability for each value and avoiding any prior assumptions about the parameter distribution. The precipitation intensity distributions are empirical distributions with different ranges. These distributions were obtained from fitting different distributions (GEV, Gumbel, Generalized Logistic, Log-normal, and Pearson type III) into different annual maximum precipitation (AMP) series extracted from simulated future data (future scenario) and measured data (present scenario) (for details please see the section named “Probabilistic approach (Monte Carlo simulations)” in Paper VI).

Uncertainty analyses generally require a large number of model realizations. This is often hampered by the high computational costs necessary to simulate flood using 2D models. The developed emulator allows us to overcome the computational burden and perform uncertainty analysis within a thorough Monte Carlo framework. For Monte Carlo simulations, *i*) the input parameters are randomly sampled with replacement from the assigned distributions, *ii*) the model is executed for each combination of inputs and finally *iii*) the ensemble of the output of interest (water level) is generated.

## **2.6. Deterministic approach**

In contrast to the probabilistic approach, deterministic approach assumes known values for input data and provides a single fixed value output. These methods are subjected to considerable criticism since they inevitably mask out a wide range of probable outputs. In this study, to explore the difference between the probabilistic and deterministic modeling, we present the flood maps based on both approaches. To obtain the deterministic water level, the 100-year precipitation value is estimated by fitting the GEV distribution to the AMP series observed in Dovland station, identifying the quantile which corresponds to the probability of 0.99 of not being exceeded (0.99 quantile). We only considered the GEV distribution, since it is the distribution which is widely used to estimate extreme events such as 100-year precipitation. Similar to the probabilistic approach, we used Bayesian MCMC method to fit the distribution to the data series, however instead of a range of values, the value with the highest probability (maximum likelihood) is selected as the deterministic 100-year precipitation (*i.e.*, the peak point of the GEV distribution in Figure 3). The other inputs (namely, roughness and runoff

coefficient values) were determined based on the median values of the specified ranges of the parameters presented in Table 2. Using the deterministic inputs, the deterministic 100-year flood water level is simulated (present-deterministic).

The future deterministic precipitation accounting for climate changes is calculated by multiplying the estimated value (present-deterministic) to a climate factor equal to 1.2, as proposed by Hanssen-Bauer *et al.* (2009).

The results obtained from probabilistic and deterministic approaches are compared in terms of inundation map and the areas that deterministic map fails to cover are highlighted.

## **3. Results**

### **3.1. Outline of results**

Six papers are presented in the appendices and a summary of their main results is described in this section. The papers are presented in an order to follow the steps of the uncertainty analysis framework explained in the method section and to provide a most straightforward structure for this thesis. Paper I describes the identification of uncertainty sources (precipitation, roughness coefficient, runoff coefficient and mesh size) and presents a sensitivity analysis using Taguchi method to rank the parameters based on their importance. Once the parameters are ranked, the uncertainty of the most influential parameter (precipitation) is treated in detail in Papers II and III. These papers, describe the assessment of the uncertainty of the precipitation parameter and determine a range for the 100-year precipitation. For uncertainty analysis of 100-year flood maps, a large number of model realizations was needed and using the 2D hydrodynamic model, which took 12 GPU hours for each simulation, was not feasible. Therefore, in Paper IV, the development of an emulator as a fast and accurate alternative is presented. Paper V seeks to compare two uncertainty analysis techniques namely the bootstrap method which does not require many model realizations versus the Monte Carlo method which requires intensive number of model realizations. Finally, Paper VI, compares the deterministic and probabilistic methods and presents the uncertainty associated with 100-year flood maps under climate change scenarios.

### **3.2. Paper I: A practical methodology to perform global sensitivity analysis for 2D hydrodynamic computationally intensive simulations**

In this study we used Taguchi method coupled with ANOVA to perform a global sensitivity analysis. It should be reminded that in this step we used only the 2D hydrodynamic model with the intensive computational demands (the emulator was developed latter). Therefore, we choose the Taguchi method which offers an effective and practical way to rank the influencing parameters, to quantify the contribution of each parameter for the variability of the outputs, and to investigate the possible interaction between the input parameters.

Taguchi method uses an optimum design for input combination (called orthogonal design) to reduce the number of combinations (*i.e.*, experiments or simulations) needed to perform the sensitivity analysis. The successful application of the

Taguchi method can be found in laboratory experimental practices, manufacturing, and design processes. But no previous study has used the Taguchi method in hydrodynamic flood simulations.

In this paper the input parameters (namely, precipitation, roughness coefficient, runoff coefficient) and the computational mesh size are assumed as the sources of the uncertainty. The relevant spaces of the parameters (except the mesh size) for sensitivity analysis were determined based on the values of the parameters observed and calibrated in the October 2017 flood event with  $\pm 50\%$  bounds. The mesh size space was set at three levels of refinement named fine, medium, and coarse resolution in the paper. Three levels of variation (minimum, average and maximum) were assumed for each input to design the experiments. Following an orthogonal design, two designs namely: the L9 and L27 orthogonal arrays (consisting of 9 and 27 combinations, respectively) were constructed based on the Taguchi method (Kacker *et al.* 1991) to identify the contribution of the inputs into the target outputs (cross sectional water level and flooded area).

The results obtained from this paper indicated that the precipitation intensity is by far the most important parameter (contributing about 80%), while the mesh refinement is the least contributing parameter (contributing about 1%). To validate the results, in addition to the Taguchi method, the analysis of variance (ANOVA) was also applied. The results of ANOVA analysis were consistent with those of Taguchi method. Furthermore, a comparison between Taguchi design results with those of full factorial design (*i.e.*, all possible 81 input combinations) confirmed the validity of the implemented method.

Therefore, the estimation of 100-year precipitation and its uncertainty became the most important issue and the uncertainty analysis of this parameter is further treated in detail (Papers II and III). The mesh refinement uncertainty is neglected in the subsequent papers due to its little contribution.

### **3.3. Paper II: Return levels uncertainty under effect of climate change**

This paper seeks to detect a climate change pattern using trend analysis and compares the nonstationary GEV model against stationary GEV using discharge and precipitation data.

The purpose of a trend test was to determine whether the time series has a general increase or decrease. But since increasing or decreasing behavior of the series does not always indicate non-stationarity (Yilmaz *et al.*, 2014), we adopted different



nonstationary GEV models (location and scale parameters as time varying parameters) for each of the stations and compared them with the stationary GEV. The results do not reveal significant trends, neither in the location nor the scale parameters. The goodness of fit for the developed models were also assessed through the Akaike information criterion (AIC) and the Bayesian information criterion (BIC). The small differences in AIC values for all the developed models unable us to make definitive conclusions about which model is better and if there is a clear signal of nonstationary. Nevertheless, it can be seen that even if trend analyses did not show any significant trend, in some cases nonstationary models adjust slightly better than the stationary model.

In a subsequent step, the analysis (not presented in this paper) was extended to the other stations of the catchment and similar results were obtained. Therefore, we decided to use a stationary model for this catchment to estimate the 100-year precipitation.

### **3.4. Paper III: Representation of 100-year design rainfall uncertainty in catchment-scale flood modeling: A MCMC Bayesian approach**

Estimation of precipitation intensity is a crucial step in rainfall-runoff modelling practices which is incorporated with uncertainty due to the limited historical data, climate change and complex and chaotic nature of climate.

In this study, a Bayesian inference with prior knowledge about the shape parameter was applied to fit the GEV distribution for annual maximum rainfall data. The method was used for different data sets, namely *i*) station based data which involves the recorded data at each station, *ii*) catchment based data in which the estimated posteriors of the stations were merged into one sample, and *iii*) gridded data that are presented by MET Norway ([www.seNorge.no](http://www.seNorge.no)) and are developed based on interpolation of observations at approximately 400 precipitation stations (Dyrddal *et al.*, 2016). Finally, the 100-year precipitation and the incorporated uncertainty is calculated for each data set.

Figure 4 in the paper displays the uncertainty ranges. Most of the estimates from different data sets are not significantly different and are practically similar. However, since we do not want to under-estimate the uncertainty, we selected to use the estimates from Dovland station which provides slightly wider range. To transfer the climate change effects and possible future changes, the identified range was multiplied by a climate factor equal to 1.2.

### **3.5. Paper IV: Emulation of 2D Hydrodynamic Flood Simulations at Catchment Scale Using ANN and SVR**

Once the uncertainty sources are identified and the uncertainty of the sources are quantified, the propagated uncertainty in results should be assessed through uncertainty analysis methods such as Monte Carlo.

As stated, earlier 2D hydrodynamic models are usually computationally intensive and require long run time. In the current catchment considering the resolution of the DTM and the number of mesh elements (401,769 mixed mesh elements), each simulation takes about 1.5 hours using 8x NVIDIA Tesla P100 (16GB) GPU (Model: 2x Intel(R) Xeon(R) CPU E5-2698 v4 @ 2.20GHz). Therefore, uncertainty analysis, which require a large number of model realizations (often more than 1,000), is not feasible using the 2D model. To overcome this limitation, we developed an emulator based on 1,200 different simulations performed with the physical-based 2D model. Paper IV describes the process of developing an emulator as a fast and accurate alternative to replace the 2D model.

To develop the emulator, 14 input variables (seven different Strickler friction coefficient ranges assigned for each land type, six types of runoff coefficient ranges assigned for each land type, and 100-year precipitation intensity range) were sampled, and 1,200 simulations were performed. Uniform distribution was selected for the inputs ensuring equal probability for each value and avoiding any prior assumptions about the parameter distribution. The selected range for precipitation was wide compared to the other ranges. Thus, the precipitation intensity probability distribution was divided into three equal uniformly distributed intervals with equal probabilities (1/3) and the values were sampled from these intervals to ensure all the intensities from low to extreme rainfalls were sampled for training the emulator.

The cross-sectional water levels resulting from 1,200 simulations were then used to develop two data-driven emulators using Artificial Neural Network (ANN) and Support Vector Regression (SVR). The performance of the proposed emulators is assessed by computing several metrics such as mean squared error (*MSE*) and correlation coefficient (*R*), root mean square error (*RMSE*), mean relative absolute error (*MRAE*), coefficient of determination ( $R^2$ ) and maximum absolute error (*MaxAE*) to ensure the reliability of the emulator. The developed emulators were optimized in a subsequent step by dimension reduction techniques and removing the less correlated inputs. Table 3 in the paper presents the performance of the

trained emulators on a test set. Finally, the SVR based emulator, which uses as input set the precipitation ( $i_p$ ), the forest runoff coefficient ( $C_F$ ), the river friction ( $K_{s_R}$ ) and the forest friction ( $K_{s_F}$ ), was selected as the best model that mimics the physical-based 2D model. The choice of SVR was made based on different error structure analysis (Figures 8 and 9 in the paper). The performance of the SVR surrogate model against the 2D hydrodynamic model is shown in Figure 4. The use of this surrogate 2D hydrodynamic model (with an accuracy of  $R^2 = 0.999$ ) allows us to overcome the unaffordable computational resources of running the physical-based model.

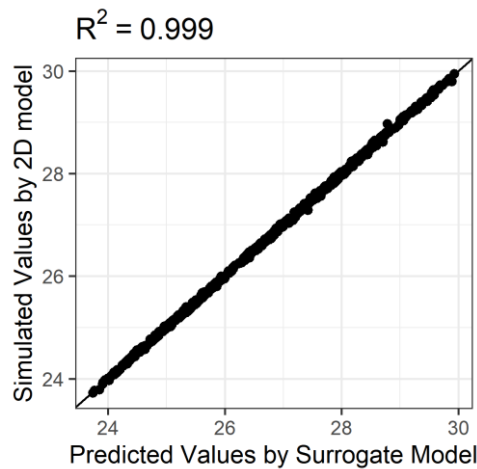


Figure 4. Performance of the developed SVR surrogate model.

### 3.6. Paper V: Uncertainty Assessment of Flood Maps: A Comparison of Bootstrap and Monte Carlo Methods

The emulator enables us to rapidly perform a large number of simulations which is required by Monte Carlo based uncertainty analysis method. However, it is important to know to each extent we can avoid the use of a computationally intensive Monte Carlo framework by using simpler sampling/ensemble techniques, like bootstrap. To answer this question and highlight the importance of the emulator, we performed a comparison between the Monte Carlo method and the bootstrap method in Paper V.

The bootstrap method is usually introduced as a robust and powerful technique for uncertainty analysis in limited and small samples where the large number of realizations are not feasible. This method relies on drawing random samples with replacement from the available dataset and thereby allow to carry out statistical inference on a wide range of estimators, like the mean value, without imposing

much structural assumptions on the underlying data-generating random process (Kreiss and Lahiri, 2012). In fact, the bootstrap assumes that the data provide the best estimate of the distribution from which the data were drawn.

In Monte Carlo framework, the input parameters are sampled from the assigned spaces, the model is executed for each combination of inputs and finally the ensemble of output of interest (water level) is generated. The number of simulations in MC is identified based on the convergence of the process (*e.g.*, the fluctuation in output mean).

The results presented in this paper indicate that the bootstrap technique is dependent on the original sample and the degree of representativeness of the original sample. Accordingly, in small samples the bootstrap method performs poorly and provides unrealistic description of uncertainty. The bootstrap technique performs well in large samples, and to achieve reliable inferences, it requires samples sizes as large as the Monte Carlo method does. Paper V demonstrated that uncertainty assessment is not possible without a large number of model realizations, enhancing the need for a computationally fast emulator.

### **3.7. Paper VI: Uncertainty analysis of 100-year flood maps under climate change scenarios**

The studies presented thus far, were the preliminary steps for the study presented in Paper VI. This paper has been divided into four parts. The first part deals with estimation of 100-year precipitation distributions under 3 different modeling scenarios, namely: present, future (RCP 4.5) and future (RCP 8.5). The data sets that are used to estimate 100-year precipitation distributions are observed data (for present scenario) and simulated data by global/regional climate models (for future scenarios). The data were fitted to six different PDFs (Gumbel, GEV, GEV with prior on shape, Log-normal, Generalized Logistic and Pearson type III) using Bayesian MCMC method and, consequently, six 100-year precipitation distributions were derived for each scenario (see Figure 3 in Paper VI). In the second part, the flood is simulated using deterministic and probabilistic approaches. The deterministic input values are the 100-year precipitation estimated by GEV distribution under present scenario (the peak point of the 100-year precipitation distribution derived from GEV distribution, present scenario in Figure 3) multiplied by a climate factor, and the roughness and runoff values were assumed equal to the median values of the ranges reported in Table 1 in Paper VI. Using the deterministic input set, deterministic flood water level is simulated. In

probabilistic approach, the identified ranges for the inputs (Figure 3 and Table 1 in Paper VI) are sampled in a Monte Carlo framework for 100,000 times and the water level distributions (Figure 4) are estimated with the emulator. The third part discusses the convergence issue in Monte Carlo simulations and finally in the fourth part, the main source of uncertainty (precipitation) is decomposed into the uncertainty of individual parameters namely: RCP scenario, climate model, and PDF.

The results presented in this paper suggest that the use of probabilistic approach for 100-year flood studies, as opposite of deterministic approach, results in safer predictions and more accurate risk analysis due to the large uncertainties found in flood water level estimation. According to the results obtained from probabilistic approach (Figure 4 in the paper), future floods are expected to be larger in magnitude. A comparison between different quantiles of the estimated water level under different scenarios indicates that, the changes are not homogeneous between different quantiles and become more pronounced in higher quantiles. This result challenges the use of constant climate factors for estimation of future flood magnitude.

The uncertainty decomposition revealed that selection of the precipitation PDF is the main source of uncertainty, while selection of the future RCP scenario, which is the subject of debate in climate change mitigation and adaptation guidelines, is the least important parameter for uncertainty estimation.



## 4. Conclusions and recommendations

### 4.1. Conclusions

Flood modeling and mapping are fundamental parts of flood management. However, this is not a static process and changes over time. Especially according to the probable changes in future climate and their impact on floods, the flood maps should be reviewed and updated. Additionally, estimation of flood magnitude is subject to uncertainty from various sources. This thesis presents the 100-year flood maps under present and future scenarios, explores the uncertainty associated with those maps and seeks to provide insights and tools for flood modelers and managers.

In this thesis, we explained the uncertainty introduced by model input parameters, namely, roughness coefficient, runoff coefficient and precipitation intensity (which incorporates three different sources of uncertainty: RCP scenario, climate model, and PDF), propagated through a 2D hydrodynamic/hydrologic model and how it affects flood estimates. The long run time of the 2D model and the intensive number of simulations required to perform an uncertainty analysis, eventuated to develop an emulator which mimics the 2D model and requires significantly less computational effort. Finally, through an intensive set of Monte Carlo simulations the uncertainty of 100-year flood maps was presented.

The main conclusions of this thesis are presented as follow:

- Despite the wide input ranges for the roughness and runoff coefficients, the precipitation uncertainty, which incorporates three different sources of uncertainty (RCP, PDF, CM), is by far the main source of uncertainty in flood simulations and should require more attention from modelers.
- Taguchi–ANOVA approach which explores multiple combinations of the inputs through orthogonal design, can successfully rank the influencing parameters and identify their contribution. Due to its low computational costs, this approach can be used as an efficient global SA method in 2D flood modeling to quantify and rank the affecting parameters.
- To overcome the computational costs of uncertainty assessment, machine learning based surrogates (emulators) can be developed and used as a reliable and fast alternative for flood simulation. We recommend measuring the emulators performance through both aggregated metrics (*e.g.*, *RMSE*) and the metrics that assess the accuracy at individual points (*e.g.*, *MaxAE*). A simple SVR method was able to generate a very accurate emulator.

- The use of simpler sampling/ensemble techniques, like bootstrap, is attractive, but the results show that to produce accurate results they require as many number of simulations as Monte Carlo method. So, they do not avoid the burden of the computational cost.
- The uncertainty analysis of 100-year flood water level, assessed through intensive MC simulations, shows that there is a large variability in the results. Therefore, we highly recommend taking the uncertainty into account. This uncertainty is mainly introduced by precipitation.
- A comparison of the simulated water level under present scenario with future scenarios (RCP 4.5 and 8.5) indicate that flood magnitudes are expected to increase in future. However, this increment is not homogeneous for different quantiles and become more pronounced in higher quantiles. This result challenges the application of climate factors for projecting the future changes, since in probabilistic approaches a range of values is obtained and these factors cannot be multiplied as a constant to the whole range.
- The flood maps based on the deterministic approach considerably underestimate the future flood's magnitude, even if a climate factor is included.
- The selection of the precipitation PDF is the main source of precipitation uncertainty, while selection of the future RCP scenario (which is the subject of debate in climate change mitigation and adaptation guidelines) is the least important parameter for uncertainty estimation.
- The lower quantiles (such as q1 and median) of 100-year precipitation ensembles are mostly influenced by climate models and as we move to the higher quantiles the PDFs influence becomes larger. As a result, we suggest in studies where the most likely situation is the focus (for example, design based on the maximum likelihood value), the attention should be paid to the selection of climate models. Conversely, if the focus is on highly unlikely extreme events, such as in risk analysis, the PDF selection for precipitation should be considered as the major uncertainty source that can considerably change the results.

Finally, given the large uncertainties observed in the results, the uncertainty analysis is essential for safe decision-making. To overcome the computational constrains, which is the main obstacle in probabilistic approaches, surrogate



models can be an efficient alternative. In fact, using the surrogate model enabled us to perform this study with intensive number of MC simulations (a total of 1,800,000 simulations were performed). Therefore, we suggest flood modelers to use surrogate models as a complementary tool to perform uncertainty analysis and make more safe decisions. If the application of the probabilistic approach is not feasible, we suggest to at least to simulate several precipitation values obtained from different PDFs, instead of using a single deterministic approach.

Estimation of future floods is a significant challenge and as we showed in this study, future floods are being underestimated by using current recorded data along with climate factors. Two possible solutions for this problem, are to perform uncertainty analysis and make the decisions based on the estimates derived from higher quantiles of the analysis (quantiles of the distribution tail) or using higher return periods (more than 100-year) in preparation of flood maps.

#### **4.2. Limitations and future directions**

- The focus of this study has been on the uncertainty of 100-year flood maps, using a 2D hydrologic/hydrodynamic model at catchment scale. Therefore, water level was considered as the output of interest. There are other outputs such as flow velocity or discharge that play important roles in flood events. Further analyses are required to assess the uncertainty of these parameters.
- Due to time-consuming simulations, we used a time invariant precipitation intensity in this study. The more complex approach such as using synthetic hyetographs was avoided which would increase the number of inputs and consequently would increase the total number of simulations. Furthermore, for the same reason the uncertainty sources are limited to the input variables and the uncertainties associated with other sources such as sampling uncertainty, modeling, and method uncertainty are not addressed in this study.
- The developed emulator performance depends on the data set used for training. Therefore, the application of the emulator is limited to the trained ranges. For values outside of this range, the training process should be updated.

Nevertheless, the referred limitations do not invalidate the main conclusions presented above.



## List of references

- Abily, M., Delestre, O., Gourbesville, P., Bertrand, N., Duluc, C.-M., Richet, Y., 2016. Global sensitivity analysis with 2D hydraulic codes: application on uncertainties related to high-resolution topographic data, *Advances in Hydroinformatics*. Springer, pp. 301-315.  
DOI:[https://doi.org/10.1007/978-981-287-615-7\\_21](https://doi.org/10.1007/978-981-287-615-7_21)
- Ahmadisharaf, E., Kalyanapu, A.J., Bates, P.D., 2018. A probabilistic framework for floodplain mapping using hydrological modeling and unsteady hydraulic modeling. *Hydrological Sciences Journal*, 63(12): 1759-1775.
- Alazzy, A.A., Lü, H., Zhu, Y., 2015. Assessing the uncertainty of the Xinanjiang rainfall-runoff model: effect of the likelihood function choice on the GLUE method. *Journal of Hydrologic Engineering*, 20(10): 04015016.
- Alipour, S.M., Engeland, K., Leal, J., 2021a. A practical methodology to perform global sensitivity analysis for 2D hydrodynamic computationally intensive simulations. *Hydrology Research*.  
DOI:<https://doi.org/10.2166/nh.2021.243>
- Alipour, S.M., Engeland, K., Leal, J., 2021b. Representation of 100-year design rainfall uncertainty in catchment-scale flood modeling: A MCMC bayesian approach. *VANN*, 04.
- Alipour, S.M., Leal, J., 2021. Emulation of 2D Hydrodynamic Flood Simulations at Catchment Scale Using ANN and SVR. *Water*, 13(20): 2858.  
DOI:10.3390/w13202858
- Apel, H., Merz, B., Thielen, A.H., 2008. Quantification of uncertainties in flood risk assessments. *International Journal of River Basin Management*, 6(2): 149-162.
- Arunraj, N., Mandal, S., Maiti, J., 2013. Modeling uncertainty in risk assessment: An integrated approach with fuzzy set theory and Monte Carlo simulation. *Accident Analysis & Prevention*, 55: 242-255.
- Asante, K.O., Artan, G.A., Pervez, S., Bandaragoda, C., Verdin, J.P., 2008. Technical manual for the geospatial stream flow model (GeoSFM). *World Wide Web*, 605: 594-6151.
- Bacchi, V., Hamdi, Y., Foch, M., Pheulpin, L., 2019. Development of a new approach for the assessment of Flood Hazard through a kriging surrogate: application to the bi-dimensional model of the Loire River, *Advances in Extreme Value Analysis and Application to Natural Hazards, EVAN*.
- Bermúdez, M., Ntegeka, V., Wolfs, V., Willems, P., 2018. Development and comparison of two fast surrogate models for urban pluvial flood simulations. *Water Resources Management*, 32(8): 2801-2815.  
DOI:<https://doi.org/10.1007/s11269-018-1959-8>
- Beven, K., Binley, A., 1992. The future of distributed models: model calibration and uncertainty prediction. *Hydrological processes*, 6(3): 279-298.
- Beven, K., Leedal, D., McCarthy, S., Lamb, R., Hunter, N., Keef, C., Bates, P., Neal, J., Wicks, J., 2011. Framework for assessing uncertainty in fluvial flood risk mapping. *FRMRC Research Rep. SWP1*, 7.
- Bomers, A., Schielen, R.M., Hulscher, S.J., 2019. Decreasing uncertainty in flood frequency analyses by including historic flood events in an efficient

- bootstrap approach. *Natural hazards and earth system sciences*, 19(8): 1895-1908.
- Brody, S.D., Blessing, R., Sebastian, A., Bedient, P., 2013. Delineating the reality of flood risk and loss in Southeast Texas. *Natural Hazards Review*, 14(2): 89-97.
- Castro-Gama, M.E., Popescu, I., Li, S., Mynett, A., van Dam, A., 2014. Flood inference simulation using surrogate modelling for the Yellow River multiple reservoir system. *Environmental modelling & software*, 55: 250-265. DOI:<https://doi.org/10.1016/j.envsoft.2014.02.002>
- Chen, S., Garambois, P.-A., Finaud-Guyot, P., Dellinger, G., Mose, R., Terfous, A., Ghenaïm, A., 2018. Variance based sensitivity analysis of 1D and 2D hydraulic models: An experimental urban flood case. *Environmental Modelling & Software*, 109: 167-181. DOI:<https://doi.org/10.1016/j.envsoft.2018.08.008>
- Chu, H., Wu, W., Wang, Q., Nathan, R., Wei, J., 2020. An ANN-based emulation modelling framework for flood inundation modelling: Application, challenges and future directions. *Environmental Modelling & Software*, 124: 104587. DOI:<https://doi.org/10.1016/j.envsoft.2019.104587>
- Conde, D.A., Canelas, R.B., Ferreira, R.M., 2020. A unified object-oriented framework for CPU+ GPU explicit hyperbolic solvers. *Advances in Engineering Software*, 148: 102802. DOI:<https://doi.org/10.1016/j.advengsoft.2020.102802>
- Conde, D.A., Telhado, M.J., Baptista, M.A.V., Ferreira, R.M., 2015. Severity and exposure associated with tsunami actions in urban waterfronts: the case of Lisbon, Portugal. *Natural Hazards*, 79(3): 2125-2144. DOI:<https://doi.org/10.1007/s11069-015-1951-z>
- Dalbey, K., Patra, A., Pitman, E., Bursik, M., Sheridan, M., 2008. Input uncertainty propagation methods and hazard mapping of geophysical mass flows. *Journal of Geophysical Research: Solid Earth*, 113(B5): B05203. DOI:<https://doi.org/10.1029/2006JB004471>
- Das, J., Umamahesh, N., 2018. Assessment of uncertainty in estimating future flood return levels under climate change. *Natural Hazards*, 93(1): 109-124.
- Dhakal, N., 2012. *Development of Guidance for Runoff Coefficient Selection and Modified Rational Unit Hydrograph Method for Hydrologic Design*, Auburn University.
- Dottori, F., Di Baldassarre, G., Todini, E., 2013. Detailed data is welcome, but with a pinch of salt: Accuracy, precision, and uncertainty in flood inundation modeling. *Water Resources Research*, 49(9): 6079-6085. DOI:<https://doi.org/10.1002/wrcr.20406>
- Dyrddal, A.V., Skaugen, T., Stordal, F., Førland, E.J., 2016. Estimating extreme areal precipitation in Norway from a gridded dataset. *Hydrological Sciences Journal*, 61(3): 483-494.
- Ferreira, R.M., Franca, M.J., Leal, J.G., Cardoso, A.H., 2009. Mathematical modelling of shallow flows: Closure models drawn from grain-scale mechanics of sediment transport and flow hydrodynamics. *Canadian*

- journal of civil engineering, 36(10): 1605-1621.  
DOI:<https://doi.org/10.1139/L09-033>
- Geuzaine, C., Remacle, J.F., 2009. Gmsh: A 3-D finite element mesh generator with built-in pre-and post-processing facilities. *International journal for numerical methods in engineering*, 79(11): 1309-1331.  
DOI:<https://doi.org/10.1002/nme.2579>
- Ghalkhani, H., Golian, S., Saghafian, B., Farokhnia, A., Shamseldin, A., 2013. Application of surrogate artificial intelligent models for real-time flood routing. *Water and Environment Journal*, 27(4): 535-548.  
DOI:<https://doi.org/10.1111/j.1747-6593.2012.00344.x>
- Goel, M.K., 2011. Runoff Coefficient. In: Singh, V.P., Singh, P., Haritashya, U.K. (Eds.), *Encyclopedia of Snow, Ice and Glaciers*. Springer Netherlands, Dordrecht, pp. 952-953. DOI:[https://doi.org/10.1007/978-90-481-2642-2\\_456](https://doi.org/10.1007/978-90-481-2642-2_456)
- Guo, A., Chang, J., Wang, Y., Huang, Q., Li, Y., 2020. Uncertainty quantification and propagation in bivariate design flood estimation using a Bayesian information-theoretic approach. *Journal of Hydrology*, 584: 124677.
- Guo, K., Guan, M., Yu, D., 2021. Urban surface water flood modelling—a comprehensive review of current models and future challenges. *Hydrology and Earth System Sciences*, 25(5): 2843-2860.
- Han, S., Coulibaly, P., 2017. Bayesian flood forecasting methods: A review. *Journal of Hydrology*, 551: 340-351.
- Hanssen-Bauer, I., Drange, H., Førland, E., Roald, L., Børsheim, K., Hisdal, H., Lawrence, D., Nesje, A., Sandven, S., Sorteberg, A., 2009. Climate in Norway 2100. Background information to NOU Climate adaptation (In Norwegian: Klima i Norge 2100. Bakgrunnsmateriale til NOU Klimatilpassing), Oslo: Norsk klimasenter.
- Hong, Y., Hsu, K.I., Moradkhani, H., Sorooshian, S., 2006. Uncertainty quantification of satellite precipitation estimation and Monte Carlo assessment of the error propagation into hydrologic response. *Water resources research*, 42(8).
- Hossain, F., Anagnostou, E.N., Bagtzoglou, A.C., 2006. On Latin Hypercube sampling for efficient uncertainty estimation of satellite rainfall observations in flood prediction. *Computers & geosciences*, 32(6): 776-792.
- Howard, L.S., 2022. Floods Drive Economic Losses in 2021, but Only 25% of Risks Are Insured: Swiss Re, *Insurance journal*. *Insurance journal*.
- Jung, Y., Merwade, V., 2012. Uncertainty quantification in flood inundation mapping using generalized likelihood uncertainty estimate and sensitivity analysis. *Journal of Hydrologic Engineering*, 17(4): 507-520.
- Kaiser, G., Scheele, L., Kortenhaus, A., Løvholt, F., Römer, H., Leschka, S., 2011. The influence of land cover roughness on the results of high resolution tsunami inundation modeling. *Natural Hazards and Earth System Sciences*, 11(9): 2521-2540.

- Kalyanapu, A.J., Shankar, S., Pardyjak, E.R., Judi, D.R., Burian, S.J., 2011. Assessment of GPU computational enhancement to a 2D flood model. *Environmental Modelling & Software*, 26(8): 1009-1016.
- Karmakar, B., Dhawane, S.H., Halder, G., 2018. Optimization of biodiesel production from castor oil by Taguchi design. *Journal of Environmental Chemical Engineering*, 6(2): 2684-2695.  
DOI:<https://doi.org/10.1016/j.jece.2018.04.019>
- Kim, B., Sanders, B.F., Schubert, J.E., Famiglietti, J.S., 2014. Mesh type tradeoffs in 2D hydrodynamic modeling of flooding with a Godunov-based flow solver. *Advances in Water Resources*, 68: 42-61.
- Komatina, D., Branisavljevic, N., 2005. Uncertainty analysis as a complement to flood risk assessment. Faculty of Civil Engineering University of Belgrade: Beograd, Serbia.
- Kreiss, J.-P., Lahiri, S.N., 2012. Bootstrap methods for time series, *Handbook of statistics*. Elsevier, pp. 3-26.
- Laloy, E., Rogiers, B., Vrugt, J.A., Mallants, D., Jacques, D., 2013. Efficient posterior exploration of a high-dimensional groundwater model from two-stage Markov chain Monte Carlo simulation and polynomial chaos expansion. *Water Resources Research*, 49(5): 2664-2682.  
DOI:<https://doi.org/10.1002/wrcr.20226>
- Langsholt, E., Holmqvist, E., 2017. Flommen på Sørlandet 30.9-3.10. 2017. NVE rapport, 80: 2017.
- Lawrence, D., 2020. Uncertainty introduced by flood frequency analysis in projections for changes in flood magnitudes under a future climate in Norway. *Journal of Hydrology: Regional Studies*, 28: 100675.
- LeFloch, P.G., Novotny, J., 2003. Hyperbolic Systems of Conservation Laws: The theory of classical and nonclassical shock waves. *Appl. Mech. Rev.*, 56(4): B53-B54. DOI:<https://doi.org/10.1115/1.1579454>
- LeVeque, R.J., 2002. Finite volume methods for hyperbolic problems, 31. Cambridge university press, Cambridge.  
DOI:10.1017/CBO9780511791253
- Lewis, M., Cheney, C., O Dochartaigh, B., 2006. Guide to permeability indices.
- Lhomme, J., Sayers, P., Gouldby, B., Samuels, P., Wills, M., Mulet-Marti, J., 2008. Recent development and application of a rapid flood spreading method.
- Lim, N.J., Brandt, S.A., 2019. Flood map boundary sensitivity due to combined effects of DEM resolution and roughness in relation to model performance. *Geomatics, Natural Hazards and Risk*, 10(1): 1613-1647.  
DOI:<https://doi.org/10.1080/19475705.2019.1604573>
- Luo, J., Lu, W., 2014. Comparison of surrogate models with different methods in groundwater remediation process. *Journal of Earth System Science*, 123(7): 1579-1589. DOI:<https://doi.org/10.1007/s12040-014-0494-0>
- Mahmoud, S.H., Alazba, A., 2015. Hydrological response to land cover changes and human activities in arid regions using a geographic information system and remote sensing. *Plos one*, 10(4): e0125805.

- Mantovan, P., Todini, E., 2006. Hydrological forecasting uncertainty assessment: Incoherence of the GLUE methodology. *Journal of hydrology*, 330(1-2): 368-381.
- Maskey, S., Guinot, V., Price, R.K., 2004. Treatment of precipitation uncertainty in rainfall-runoff modelling: a fuzzy set approach. *Advances in water resources*, 27(9): 889-898.
- Masson-Delmotte, V., Zhai, P., Pirani, A., Connors, S.L., Péan, C., Berger, S., Caud, N., Chen, Y., Goldfarb, L., Gomis, M., 2021. Climate change 2021: the physical science basis. Contribution of working group I to the sixth assessment report of the intergovernmental panel on climate change: 2. DOI:<https://doi.org/10.1017/9781009157896>
- Mejia, A.I., Reed, S., 2011. Evaluating the effects of parameterized cross section shapes and simplified routing with a coupled distributed hydrologic and hydraulic model. *Journal of Hydrology*, 409(1-2): 512-524. DOI:<https://doi.org/10.1016/j.jhydrol.2011.08.050>
- Murillo, J., García-Navarro, P., Burguete, J., 2009. Conservative numerical simulation of multi-component transport in two-dimensional unsteady shallow water flow. *Journal of Computational Physics*, 228(15): 5539-5573. DOI:<https://doi.org/10.1016/j.jcp.2009.04.039>
- Neal, J.C., Odoni, N.A., Trigg, M.A., Freer, J.E., Garcia-Pintado, J., Mason, D.C., Wood, M., Bates, P.D., 2015. Efficient incorporation of channel cross-section geometry uncertainty into regional and global scale flood inundation models. *Journal of Hydrology*, 529: 169-183. DOI:<https://doi.org/10.1016/j.jhydrol.2015.07.026>
- Nicholas, F.W., Lewis, J.E., 1980. Relationships between aerodynamic roughness and land use and land cover in Baltimore, Maryland. US Government Printing Office.
- Nicholls, R., Zanuttigh, B., Vanderlinden, Jean P., Weisse, R., Silva, R., Hanson, S., Narayan, S., Hoggart, S., Thompson, R.C., Vries, W.d., Koundouri, P., 2015. Chapter 2 - Developing a Holistic Approach to Assessing and Managing Coastal Flood Risk. In: Zanuttigh, B., Nicholls, R., Vanderlinden, J.P., Burcharth, H.F., Thompson, R.C. (Eds.), *Coastal Risk Management in a Changing Climate*. Butterworth-Heinemann, Boston, pp. 9-53. DOI:<https://doi.org/10.1016/B978-0-12-397310-8.00002-6>
- Nott, D.J., Marshall, L., Brown, J., 2012. Generalized likelihood uncertainty estimation (GLUE) and approximate Bayesian computation: What's the connection? *Water Resources Research*, 48(12).
- Papaoannou, G., Efstratiadis, A., Vasiliades, L., Loukas, A., Papalexiou, S.M., Koukouvinos, A., Tsoukalas, I., Kossieris, P., 2018. An operational method for flood directive implementation in ungauged urban areas. *Hydrology*, 5(2): 24.
- Pappenberger, F., Matgen, P., Beven, K.J., Henry, J.-B., Pfister, L., 2006. Influence of uncertain boundary conditions and model structure on flood inundation predictions. *Advances in water resources*, 29(10): 1430-1449.



- Paprotny, D., Sebastian, A., Morales-Nápoles, O., Jonkman, S.N., 2018. Trends in flood losses in Europe over the past 150 years. *Nature communications*, 9(1): 1-12.
- Parés, C., Castro, M., 2004. On the well-balance property of Roe's method for nonconservative hyperbolic systems. Applications to shallow-water systems. *ESAIM: mathematical modelling and numerical analysis*, 38(5): 821-852. DOI:<https://doi.org/10.1051/m2an:2004041>
- Pianosi, F., Beven, K., Freer, J., Hall, J.W., Rougier, J., Stephenson, D.B., Wagener, T., 2016. Sensitivity analysis of environmental models: A systematic review with practical workflow. *Environmental Modelling & Software*, 79: 214-232. DOI:<https://doi.org/10.1016/j.envsoft.2016.02.008>
- Rao, C.R., 1947. Factorial experiments derivable from combinatorial arrangements of arrays. Supplement to the *Journal of the Royal Statistical Society*, 9(1): 128-139. DOI:<https://doi.org/10.2307/2983576>
- Razavi, S., Tolson, B.A., Burn, D.H., 2012. Numerical assessment of metamodelling strategies in computationally intensive optimization. *Environmental Modelling & Software*, 34: 67-86. DOI:<https://doi.org/10.1016/j.envsoft.2011.09.010>
- Refsgaard, J.C., van der Sluijs, J.P., Højberg, A.L., Vanrolleghem, P.A., 2007. Uncertainty in the environmental modelling process – A framework and guidance. *Environmental Modelling & Software*, 22(11): 1543-1556. DOI:<https://doi.org/10.1016/j.envsoft.2007.02.004>
- Roald, L.A., 2021. Floods in Norway. NVE Reports, nr. 1/2021
- Saltelli, A., Tarantola, S., Campolongo, F., Ratto, M., 2004. Sensitivity analysis in practice: a guide to assessing scientific models, 1. Wiley Online Library.
- Sampson, C.C., Fewtrell, T.J., O'Loughlin, F., Pappenberger, F., Bates, P.B., Freer, J.E., Cloke, H.L., 2014. The impact of uncertain precipitation data on insurance loss estimates using a flood catastrophe model. *Hydrology and Earth System Sciences*, 18(6): 2305-2324.
- Savage, J., Pianosi, F., Bates, P., Freer, J., Wagener, T., 2016. Quantifying the importance of spatial resolution and other factors through global sensitivity analysis of a flood inundation model. *Water Resources Research*, 52(11): 9146-9163. DOI:<https://doi.org/10.1002/2015WR018198>
- Selle, B., Hannah, M., 2010. A bootstrap approach to assess parameter uncertainty in simple catchment models. *Environmental Modelling & Software*, 25(8): 919-926.
- Shields, M.D., Teferra, K., Hapij, A., Daddazio, R.P., 2015. Refined stratified sampling for efficient Monte Carlo based uncertainty quantification. *Reliability Engineering & System Safety*, 142: 310-325.
- Song, X., Zhang, J., Zhan, C., Xuan, Y., Ye, M., Xu, C.J.J.o.h., 2015. Global sensitivity analysis in hydrological modeling: Review of concepts, methods, theoretical framework, and applications. 523: 739-757. DOI:<https://doi.org/10.1016/j.jhydrol.2015.02.013>



- Sriwongsitanon, N., Taesombat, W., 2011. Effects of land cover on runoff coefficient. *Journal of Hydrology*, 410(3-4): 226-238.
- Stedinger, J.R., Vogel, R.M., Lee, S.U., Batchelder, R., 2008. Appraisal of the generalized likelihood uncertainty estimation (GLUE) method. *Water resources research*, 44(12).
- Stephens, E.M., Bates, P., Freer, J., Mason, D., 2012. The impact of uncertainty in satellite data on the assessment of flood inundation models. *Journal of Hydrology*, 414: 162-173.
- Subramanya, K., 2013. *Engineering Hydrology*, 4e. Tata McGraw-Hill Education, New Delhi, India.
- Taguchi, G., 1986. *Introduction to Quality Engineering: Designing Quality Into Products and Processes*. Asian productivity Organization Tokyo.
- Teng, J., Jakeman, A.J., Vaze, J., Croke, B.F., Dutta, D., Kim, S.J.E.M., Software, 2017. Flood inundation modelling: A review of methods, recent advances and uncertainty analysis. 90: 201-216.  
DOI:<https://doi.org/10.1016/j.envsoft.2017.01.006>
- Teng, J., Vaze, J., Dutta, D., Marvanek, S., 2015. Rapid Inundation Modelling in Large Floodplains Using LiDAR DEM. *Water Resources Management*, 29(8): 2619-2636. DOI:10.1007/s11269-015-0960-8
- Thieken, A.H., Apel, H., Merz, B., 2015. Assessing the probability of large-scale flood loss events: a case study for the river Rhine, Germany. *Journal of Flood Risk Management*, 8(3): 247-262.
- UNRIC, 2022. 2021 floods: UN researchers aim to better prepare for climate risks.
- Van Vuren, S., Paarlberg, A., Havinga, H., 2015. The aftermath of “Room for the River” and restoration works: Coping with excessive maintenance dredging. *Journal of hydro-environment research*, 9(2): 172-186.  
DOI:<https://doi.org/10.1016/j.jher.2015.02.001>
- Villa-Vialaneix, N., Follador, M., Ratto, M., Leip, A., 2012. A comparison of eight metamodelling techniques for the simulation of N<sub>2</sub>O fluxes and N leaching from corn crops. *Environmental Modelling & Software*, 34: 51-66. DOI:<https://doi.org/10.1016/j.envsoft.2011.05.003>
- Vojtek, M., Petroselli, A., Vojteková, J., Asgharina, S., 2019. Flood inundation mapping in small and ungauged basins: sensitivity analysis using the EBA4SUB and HEC-RAS modeling approach. *Hydrology Research*, 50(4): 1002-1019. DOI:<https://doi.org/10.2166/nh.2019.163>
- Wagenaar, D., De Bruijn, K., Bouwer, L., Moel, H.d., 2016. Uncertainty in flood damage estimates and its potential effect on investment decisions. *Natural Hazards and Earth System Sciences*, 16(1): 1-14.
- Wang, R., Diwekar, U., Grégoire Padró, C.E., 2004. Efficient sampling techniques for uncertainties in risk analysis. *Environmental Progress*, 23(2): 141-157.
- Xie, S., Wu, W., Mooser, S., Wang, Q., Nathan, R., Huang, Y., 2021. Artificial neural network based hybrid modeling approach for flood inundation modeling. *Journal of Hydrology*, 592: 125605.  
DOI:<https://doi.org/10.1016/j.jhydrol.2020.125605>

- Yang, J., Reichert, P., Abbaspour, K.C., Yang, H., 2007. Hydrological modelling of the Chaohe Basin in China: Statistical model formulation and Bayesian inference. *Journal of Hydrology*, 340(3-4): 167-182.
- Yang, W.p., Tarnag, Y., 1998. Design optimization of cutting parameters for turning operations based on the Taguchi method. *Journal of materials processing technology*, 84(1-3): 122-129.  
DOI:[https://doi.org/10.1016/S0924-0136\(98\)00079-X](https://doi.org/10.1016/S0924-0136(98)00079-X)
- Yilmaz, A.G., Hossain, I., Perera, B.J.C., 2014. Effect of climate change and variability on extreme rainfall intensity–frequency–duration relationships: a case study of Melbourne. *Hydrol. Earth Syst. Sci.*, 18(10): 4065-4076.  
DOI:10.5194/hess-18-4065-2014
- Yu, J., Qin, X., Larsen, O., 2015. Uncertainty analysis of flood inundation modelling using GLUE with surrogate models in stochastic sampling. *Hydrological Processes*, 29(6): 1267-1279.  
DOI:<https://doi.org/10.1002/hyp.10249>
- Zahura, F.T., Goodall, J.L., 2022. Predicting combined tidal and pluvial flood inundation using a machine learning surrogate model. *Journal of Hydrology: Regional Studies*, 41: 101087.
- Zheng, Y., Keller, A.A., 2007. Uncertainty assessment in watershed-scale water quality modeling and management: 1. Framework and application of generalized likelihood uncertainty estimation (GLUE) approach. *Water resources research*, 43(8).

## Appendices



**Paper I:** A practical methodology to perform global sensitivity analysis for 2D hydrodynamic computationally intensive simulations

Alipour, S.M., Engeland, K., Leal, J., 2021a. A practical methodology to perform global sensitivity analysis for 2D hydrodynamic computationally intensive simulations. *Hydrology Research*. DOI:<https://doi.org/10.2166/nh.2021.243>



## A practical methodology to perform global sensitivity analysis for 2D hydrodynamic computationally intensive simulations

Saba Mirza Alipour <sup>a,\*</sup>, Kolbjørn Engeland<sup>b</sup> and Joao Leal<sup>a</sup>

<sup>a</sup> Department of Engineering and Science, University of Agder, Jon Lilletuns vei 9, 4879 Grimstad, Norway

<sup>b</sup> Norwegian Water Resources and Energy Directorate (NVE), P.O. Box 5091 Maj., 0301 Oslo, Norway

\*Corresponding author. E-mail: saba.m.alipour@uia.no

 SMA, 0000-0003-2078-3703

### ABSTRACT

Sensitivity analysis is a commonly used technique in hydrological modeling for different purposes, including identifying the influential parameters and ranking them. This paper proposes a simplified sensitivity analysis approach by applying the Taguchi design and the ANOVA technique to 2D hydrodynamic flood simulations, which are computationally intensive. This approach offers an effective and practical way to rank the influencing parameters, quantify the contribution of each parameter to the variability of the outputs, and investigate the possible interaction between the input parameters. A number of 2D flood simulations have been carried out using the proposed combinations by Taguchi (L27 and L9 orthogonal arrays) to investigate the influence of four key input parameters, namely mesh size, runoff coefficient, roughness coefficient, and precipitation intensity. The results indicate that the methodology is adequate for sensitivity analysis, and that the precipitation intensity is the dominant parameter. Furthermore, the model calibration based on local variables (cross-sectional water level) can be inaccurate to simulate global variables (flooded area).

**Key words:** 2D hydrodynamic flood modeling, ANOVA, global sensitivity analysis, Taguchi design

### HIGHLIGHTS

- A Taguchi–ANOVA approach can be used as an efficient sensitivity analysis method in 2D flood modeling.
- Necessity of considering both local- and global-scale calibrations is shown.
- The great importance of accurate estimation of precipitation intensity in flood simulation is presented.
- Mesh refinement sometimes can affect the results negatively.
- The significance of the input parameters can change depending on the hydrological conditions.

### INTRODUCTION

In hydrologic modeling, the use of 2D hydrodynamic models is common in applications like floods or water quality assessment (e.g., Yu & Lane 2006; Park *et al.* 2014; Zischg *et al.* 2018). Those models, based on the numerical solution of the 2D shallow water equations (SWEs), use different types of input parameters with complex domain spaces (e.g., hydrological data, floodplain and channel geometry, initial and boundary conditions, and roughness). Most of these parameters cannot be measured directly and can only be inferred by calibration to observed system responses (Ghasemizade *et al.* 2017; Zadeh *et al.* 2017). As a result, input parameters are one of the main sources of uncertainty in flood simulation processes, and a considerable amount of literature has investigated the relative importance of the inputs of interest and their contributions to the numerical models' outputs.

In 1D simulations, particular attention has been given to input parameters such as hydraulic roughness coefficient in the river channel and flood plains (e.g., Pappenberger *et al.*, 2005; Werner *et al.* 2005; Schumann *et al.*, 2007; Papaioannou *et al.*, 2017), discharge and design hydrograph (e.g., Ahmadisharaf *et al.* 2018; Chen *et al.* 2018; Vojtek *et al.* 2019). In 2D simulations, the analysis has been extended to other inputs such as topography/bathymetry and digital terrain model (DTM) resolution (e.g., Mejia & Reed 2011; Neal *et al.* 2015; van Vuren *et al.* 2015; Abily *et al.* 2016; Savage *et al.* 2016; Lim & Brandt 2019), mesh type, and mesh resolution (Schubert *et al.* 2008; Dottori *et al.* 2013; Zhang *et al.* 2016; Hu *et al.*

This is an Open Access article distributed under the terms of the Creative Commons Attribution Licence (CC BY 4.0), which permits copying, adaptation and redistribution, provided the original work is properly cited (<http://creativecommons.org/licenses/by/4.0/>).

2019). Among the considered parameters, hydraulic roughness is usually considered the most influential and is, therefore, given first consideration in the model calibration (Teng *et al.* 2017).

In recent years, due to the advances in computational power of computers and accessibility of graphics processing units (GPU), hydrodynamic models are becoming increasingly complex which intend to apply inputs and processes similar to what happens in nature such as spatially/temporally varying precipitation, high spatial resolution data that represent more details and infiltration/drainage processes. One example is the study conducted by Sauer & Ortlepp (2021), in which different rainfall scenarios are defined (time and space invariant, space invariant and time varying, and space and time varying) over a small area (12 km<sup>2</sup>), and the relative influence of hydraulic roughness coefficients and DTM resolution on the models' output has been roughly assessed with a simple sensitivity analysis (SA). They concluded that rainfall data, as well as the spatial resolution of the digital elevation model, have a strong influence on the surface runoff dynamics in terms of water levels in space and time. The effect of different input parameters including spatial resolution, rainfall inputs, and the parameters which are linked with the land-use information such as roughness and drainage has been investigated in a hydrodynamic urban flood simulation by Xing *et al.* (2021) using a detailed SA for a very small catchment (0.59 km<sup>2</sup>). They reported that model sensitivity to the input parameters can vary depending on the outputs choice. They found that the influence of the spatial resolution is more tightly related to the flood flow movements, whereas that of the rainfall inputs is more relevant to the flood water volume.

Most of the hydrodynamic simulations in the above-mentioned studies were performed in small areas or limited specific river reaches. Few studies were made at a bigger catchment scale. Some examples are the study by Fernández-Pato *et al.* (2016) that investigated the influence of infiltration, and the studies by Bellos *et al.* (2020) and Zischg *et al.* (2018) that analyzed the effect of precipitation spatial patterns. According to the literature, still little attention has been paid to the influence of parameters such as infiltration, runoff coefficient, spatially/temporally varying precipitation, and the possible interaction between them.

Beside the importance of input parameters in the modeling process, one of the key preliminary steps for the application of the physically based distributed modeling based on the 2D SWEs is the generation of a computational mesh (Ferraro *et al.* 2020). In this context, many studies have investigated the effect of mesh structure, shape, and size on the accuracy of the simulated results and computation time (Caviedes-Voullième *et al.* 2012; Gibson *et al.* 2016; Hu *et al.* 2018). Some of the studies reported that there is no optimal mesh type for 2D flood modeling, because each element type (e.g., triangle and quadrilateral) is advantageous under different circumstances (e.g., Kim *et al.* 2014), while some tried to address ways to generate the most optimum computational mesh (acceptable degree of accuracy and computational costs) (e.g., Bomers *et al.* 2019; Ferraro *et al.* 2020). Most of these studies were performed in small scales such as flood plain scale or urban areas, while a few studies have assessed the issue at the catchment scale with regard to possible interactions between land-related features (i.e., friction, infiltration, and runoff coefficient) (e.g., Caviedes-Voullième *et al.* 2012; Costabile & Costanzo 2021).

The quest for developing accurate and computationally efficient simulations prompts the need for understanding the models' behavior under different conditions, which can be offered by SA methods.

SA methods can be broadly classified into local and global methods (van Griensven *et al.* 2006; Campolongo *et al.* 2011; Tian 2013; Song *et al.* 2015). Local sensitivity measures, often referred to as 'one at a time' measures, assess how variation in one input affects the model output keeping the other inputs fixed to a nominal value (Campolongo *et al.* 2011). The main drawback of local SA methods is that interactions among inputs cannot be detected (Campolongo *et al.* 2011), which can render nonreliable results for complex and nonlinear systems (Yang 2011), where input factors usually interact with each other. In contrast, global SA methods can be used as a reliable approach to investigate the influence of inputs on outputs while they are varied simultaneously over their entire domain space. Song *et al.* (2015) reviewed various types of global SA methods in the field of hydrological modeling and provided a framework for SAs in hydrological modeling. Pianosi *et al.* (2016) also provided a comprehensive review of existing SA methods following different end purposes such as uncertainty assessment, model calibration, diagnostic evaluation, dominant control analysis, and robust decision-making in a classified context. SA methods have been used in hydrodynamic modeling, mainly focusing on the uncertainties arising from model parameters and inputs.

Most of the studies mentioned above use global SA methods. The main drawback of the global SA methods is that they are computationally intensive, time-consuming, and require too many simulations. Therefore, global SA is often difficult to be



applied in engineering practice and to overcome that the number of required simulations must be drastically reduced. In that path, the methods and expertise accumulated in the field of design of experiments (DoE) (named after Rao 1947) can be useful for developing a time and cost-effective design for performing SA under various conditions.

The DoE is a statistical approach to reaction optimization that allows the variation of multiple factors simultaneously in order to screen 'reaction space' for a particular process (Murray *et al.* 2016). Making an analogy between experiments and simulations, the statistical DoE can be implemented as a method to effectively reduce the number of simulations (experiments) and explore the relationship between the input parameters (predictor variables) and the generated output (response variables), as well as various interactions that may exist between the input variables (Yuangyai & Nembhard 2010; Khang *et al.* 2017; Whitford *et al.* 2018). This approach can be classified as a global SA method since several parameters are varied systematically and simultaneously to obtain sufficient information (Whitford *et al.* 2018).

Taguchi (1986) has developed a methodology for the application of designed experiments based on orthogonal design to reduce the number of experimental combinations. A large number of studies about the successful application of the Taguchi method can be found in laboratory experimental practices, manufacturing, and design processes (e.g., Rao *et al.* 2004; Sadeghi *et al.* 2012; Hadi *et al.* 2017). But no previous study has used the Taguchi method in hydrodynamic flood simulations.

The present study presents a global SA of flood simulations solving the 2D SWE at the catchment scale (for a big catchment, 1,767 km<sup>2</sup>), involving various parameters at different levels, in which each simulation takes a long time (about 3 h using 8× NVIDIA Tesla P100 (16 GB) GPU (Model: 2× Intel(R) Xeon(R) CPU E5-2698 v4@2.20 GHz)). Considering these features, the Taguchi method has been chosen. The main purpose of this paper is, therefore, to evaluate the application of the Taguchi method as a feasible engineering SA tool for 2D hydrodynamic simulations at the catchment scale and to identify the most influential parameters.

## CASE STUDY

Tovdal river, located in Agder province (Norway), is selected as the case study. The computational domain is the part of the catchment upstream of the small lake named Flaksvann, just beside a town called Birkeland (Figure 1). In order to avoid the outlet boundary interference, the domain was extended 11 km further to the downstream of the lake. The length of the main river reaches approximately 130 km, and the catchment with an area of about 1,767 km<sup>2</sup> is dominated by forests (about 74%). The elevation ranges from 10.00 to 872.34 m.a.s.l, and the average slope of the catchment along the river is about 0.65%. The mean annual precipitation is approximately 1,261 mm, with most of the rainfall occurring between October and March (about 60%). On 2 October 2017, an extreme flood event occurred in this area which was the highest ever recorded flood in this river. Recorded data of the event (Table 1) (including recorded water level, discharge, flood hydrograph at Flakksvann cross-section (CS), and flood maps) and a 2D hydrodynamic model were used to simulate the event and validate the methodology. For the calibration process, the weighted average of precipitation intensities which occurred 1.5 days before the 2017 flood event was used as the reference precipitation (Table 1). Subsequently, by adjusting the friction factor and the runoff coefficient values for each land class in a trial-and-error process, calibration was performed such that simulated water level and discharge resembled the event's recorded information (Table 1).

## METHODS

### Hydrodynamic model

In the current study, a GPU-based 2D horizontal hydrodynamic model named HiSTAV was used to simulate floods. The model was originally proposed by Ferreira *et al.* (2009) and optimized by Conde *et al.* (2020). The core of the model is a hyperbolic system of partial differential equations expressing mass and momentum conservation principles for flow. The model is closed in terms of flow resistance and a specific return-to-capacity parameter by a modified closure model. The SWEs are solved using a finite volume scheme, which is applied on a spatial discretization using unstructured meshes. The discretization method allows body fitting unstructured grids which can optimize the computational workload by using large cells, where flow gradients are expected to be mild and small cells in specified areas. The detailed information about HiSTAV and the model structure can be found in the study presented by Conde *et al.* (2020).

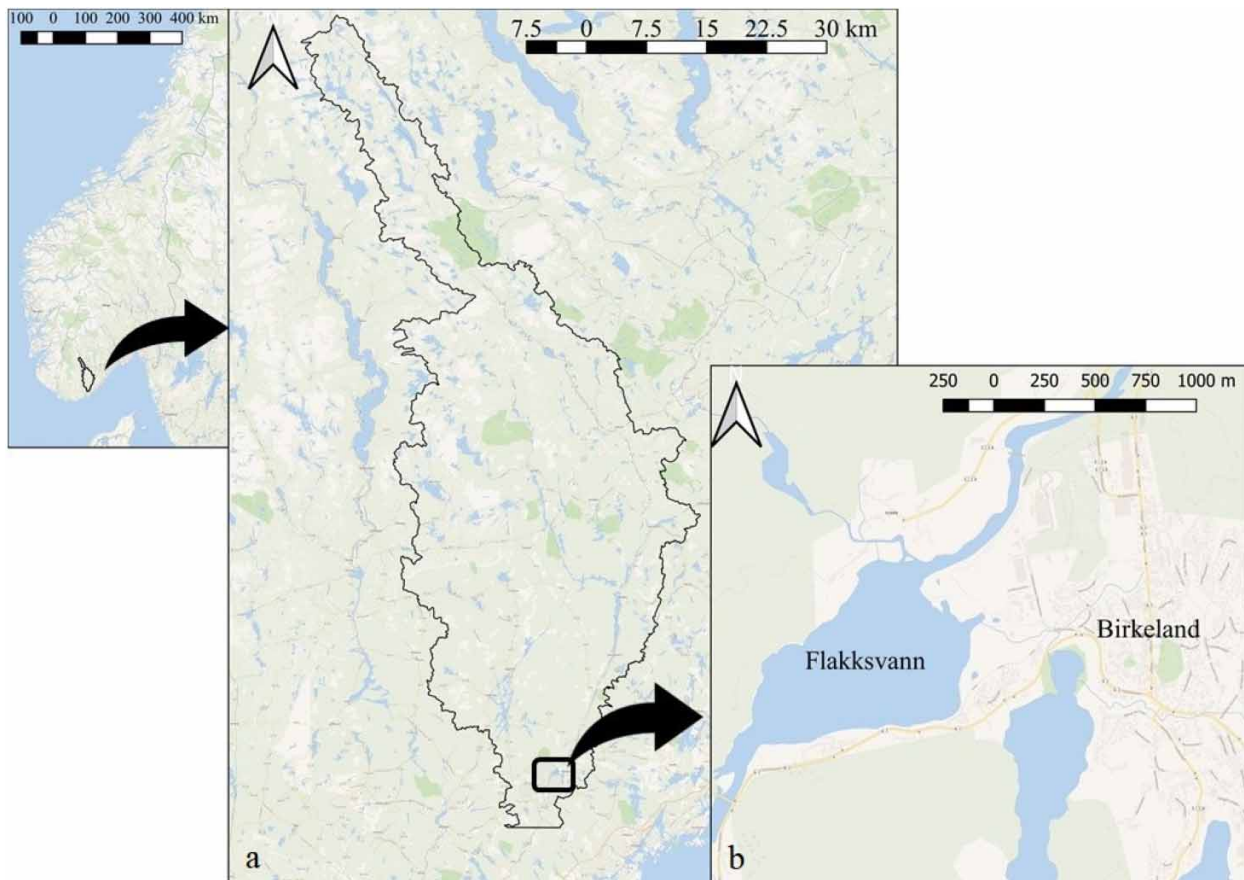


**Figure 1** | (a) Map of the Tovdal river catchment area until the computational domain and (b) the flooded area (Birkeland town area).

**Table 1** | The recorded data of the flood event in the study area (water level and discharge refer to Flakksvann, in Figure 1)

Date	Precipitation (mm)	Maximum water level (m)	Maximum discharge (m <sup>3</sup> /s)
30.09.2017	45.1	21.40	501.28
01.10.2017	173.1	24.57	1,061.19
02.10.2017	63.6	25.56	1,194.88

### Simulation set-up and approach

In order to simulate the flow, the model solves the equations based on the following sources:

1. Input variables
2. Computational mesh
3. Initial and boundary conditions

The 2D model used here requires different data sets drawn from two main sources: (a) raster data structures including the topo-bathymetric dataset, Strickler roughness coefficient values, and runoff coefficient values, and (b) precipitation records including the spatial distribution of rainfall measurement stations.

Raster data structures and grids are used to present the catchment discretization and to describe spatially distributed terrain parameters (i.e., elevation, bathymetry, land use, etc.). A  $10 \times 10$  m<sup>2</sup> DTM including the river bathymetry information is used to represent topographic features and derive hydrologic characteristics (i.e., slope, flow direction, flow accumulation, stream network, computational cascade for flow routing, etc.).

Hydraulic roughness is inserted in the model in the form of a grid structure raster file ( $100 \times 100 \text{ m}^2$  resolution), in which each cell represents Strickler roughness values. The spatial distribution of roughness values is determined based on  $100 \times 100 \text{ m}^2$  land cover maps (obtained from <https://land.copernicus.eu/>- 'Corine Land Cover 2018, Version 20'). Subsequently, using typical Strickler roughness coefficient tables, the roughness values were assigned for each cell (Arcement & Schneider 1989; Dorn *et al.* 2014). Different land types are classified in Table 2, and possible roughness variation ranges are assigned for each class.

The runoff coefficient  $C$  is a dimensionless factor that is used by HiSTAV to convert the rainfall amounts to runoff (effective precipitation  $h_p = C \cdot i_p$  in Equation (1), being  $i_p$  the precipitation intensity). In this study, we used the runoff coefficient as a parameter which reflects the lumped effect of several processes such as the antecedent conditions of the catchment and infiltration, land cover effect, and spatial variability of the rainfall intensity. The concept of event runoff coefficients is widely used in hydrologic modeling (e.g., Merz *et al.* 2006; Merz & Blöschl, 2009; Viglione *et al.* 2009; Chen *et al.* 2019). The choice of runoff coefficient values was based on the average antecedent conditions for the catchment and land features. The values were then calibrated in a way that the correspondence of the event's rainfall and 2017 flood flow (level and velocity) is achieved. Similar to the hydraulic roughness values, the runoff coefficient is used in the form of raster data.

In this study, a combination of two different approaches to calculate the runoff coefficient was used. Firstly, by using land cover maps and recommended values of runoff coefficient for different types of areas (Subramanya 2013), a range was determined for each cell. Secondly, since the HiSTAV model assumes a uniform spatial distribution of precipitation as input, the runoff coefficient was used as an artifact to introduce spatial variability of the precipitation. For this purpose, focusing on the flood of 2 October 2017, daily precipitation data were obtained from 37 stations (Figure 2). The rainfall observations at the stations were interpolated to delineate the spatial distribution of precipitation. For this purpose, the inverse distance weighting interpolation method was used, giving similar precipitation patterns like the one presented by the Norwegian Meteorologic Institute (<http://www.senorge.no/>). Thereafter, precipitation zones were delineated in Figure 2. The combination of the two mentioned approaches was used to calculate the final runoff coefficient in each cell,  $C$ , as follows:

$$C = C_{initial} \times \left( \frac{i_{p_{cell}}}{i_{p_{max}}} \right) \quad (1)$$

where  $i_{p_{max}}$  is the maximum amount of precipitation intensity among the recorded values,  $i_{p_{cell}}$  is the recorded precipitation intensity in each cell, and  $C_{initial}$  is the runoff coefficient with values displayed in Table 2 for each land cover class.

In order to define a reliable and time-consistent range to consider different flood magnitudes, three different rainfall intensities,  $i_p$  ranging from 3 to 9 mm/h, with a duration equal to 2 days, were considered for the simulations (Table 3). The range is obtained based on the average precipitation intensity that occurred in the flood event (6 mm/h) with 50% bounds. This means that the precipitation is treated as time invariant (or as block), which is rather a coarse and simplistic approach to the real conditions. Nevertheless, since the main goal of this study is to check the feasibility of using a simplified method (Taguchi method) for performing a global SA, we focus on reducing to a minimum number of inputs while having input ranges that cover in the full input-output space. This was needed because for such a big catchment, the inclusion of more inputs (like synthetic hyetographs defined by several parameters) would render many simulations.

**Table 2** | The land-use classes and corresponding ranges for the Strickler roughness coefficient and runoff coefficient

Land-use class	Occupied area (%)	Strickler roughness ( $K_s, \text{m}^{1/3}/\text{s}$ )	Runoff coefficient (C, %)
Constructed lands (discontinuous urban fabric, industrial, or commercial units)	0.40	40–70	80–90
Forests (broad-leaved, coniferous)	73.75	15–40	50–70
Moors and heathland	8.23	18–35	60–80
Agriculture and vegetated areas	12.82	18–37	40–60
Water courses and water bodies	4.76	20–50	100–100
Mineral extraction sites	0.04	30–60	70–90

Note: The median values of the specified ranges correspond to the calibrated values.

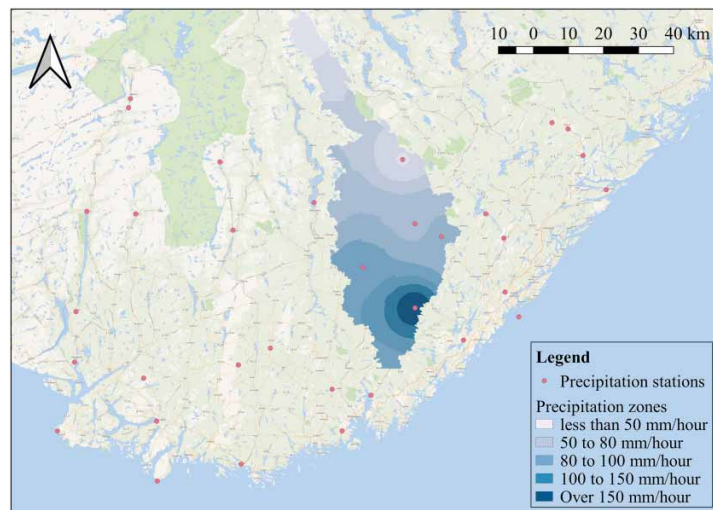


**Figure 2** | Spatial distribution of the precipitation stations and the interpolated precipitation over the catchment.

**Table 3** | Input parameters considered for the sensitivity analysis and their ranges of variation

Parameters		Level 1	Level 2	Level 3
Mesh size (m)	Maximum mesh length in the river (main channel)	15	20	25
	Maximum mesh in the flood plain	150	200	250
Precipitation intensity (mm/h)		3	6	9
Strickler roughness ( $m^{1/3}/s$ )	Constructed lands (discontinuous urban fabric, industrial, or commercial units)	40	50	70
	Forests (broad-leaved, coniferous)	15	25	40
	Moors and heathland	18	24	30
	Agriculture and vegetated areas	18	28	37
	Water courses and water bodies	20	35	50
	Mineral sites	30	40	60
	Runoff coefficient (%)	Constructed lands (discontinuous urban fabric, industrial, or commercial units)	80	85
	Forests (broad-leaved, coniferous)	50	60	70
	Moors and heathland	60	70	80
	Agriculture and vegetated areas	40	50	60
	Water courses and water bodies	100	100	100
	Mineral sites	70	80	90

Note: The levels 1, 2, and 3 for mesh size are representative of the fine resolution (total number of mesh elements: 582,161), the medium resolution (total number of mesh elements: 473,265), and the coarser resolution (total number of mesh elements: 401,769), respectively.

HiSTAV employs adaptable triangular meshes in order to discretize the catchment and balance acceptable computational workloads, different detail levels, and complex geometry fitting capabilities (Conde *et al.* 2015). In this study, by employing Godunov's finite volume approach (LeVeque 2002), a mixed mesh of triangular cells are constructed in three sizes over the computational domain by Gmsh (Geuzaine & Remacle 2009), which is a free finite element grid generator with a built-in CAD engine and post-processor. The small cells or so-called finer resolutions are assigned to the cells where the flow gradients are expected to be large such as the river channel, medium-sized cells, or average resolution over the flood plain, and coarser resolution over other parts of the catchment, where flow gradients are expected to be mild (Figure 3). In the post-processing step, the constructed meshes were checked for shape and size quality. The initial conditions for the equations are zero water depth and zero discharge everywhere (dry surface conditions). Water enters the domain only through rainfall; hence there are no inlet boundaries. The only open boundary is at the outlet (downstream), where free outflow is assumed. Warm-up



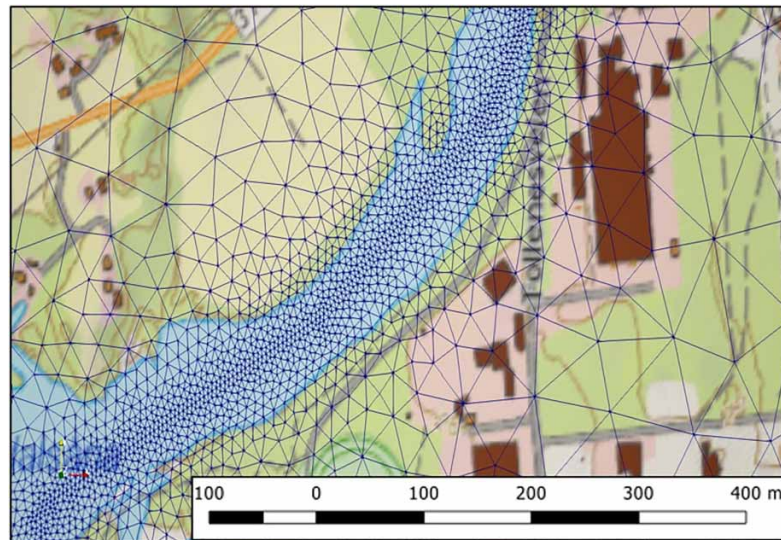


**Figure 3** | Finite volume meshes at three different sizes.

simulations were performed until reaching the normal water level in the river network. A 9-day precipitation with an intensity of 2 mm/h was found to be long enough to fill the river basin and the lakes with the steady flow over the main water courses.

### Taguchi method

Taguchi developed a system of tabulated designs (arrays) that allows for the maximum number of main effects to be estimated in an unbiased manner while using only a minimum number of experimental tests (Taguchi 1986). He introduced his approach using experimental design aiming to develop a process to be robust to component variation and also to minimize variation around a target value (Ross & Ross 1988).

The process of Taguchi analysis can be summarized into seven steps (Bao *et al.* 2013). The flow chart of the whole process is illustrated in Figure 4.

In this study, the local water level and total flooded area are selected as objective parameters. To calculate these parameters, nine different CS are specified in Figure 5. Several different CS were chosen to cover the changes in hydrodynamic behavior of the river, and the water level is observed at the time step equal to 34 h (this time step is selected based on the duration of the 2017 flood event). The CS were selected at different locations such as the areas of key importance, adjacent to bridge structures, adjacent to the flow measure stations (level and velocity), and at locations that represent different geometries of the river. Therefore, two of the CS were chosen on the lake where the geometry and flow conditions differ from other parts of the river to assess the flow behavior and water-level sensitivity.

The total flooded area was delineated as the subarea starting from the Birkeland city region and extended to the end of the computational domain, which represents around 11 km along the main river.

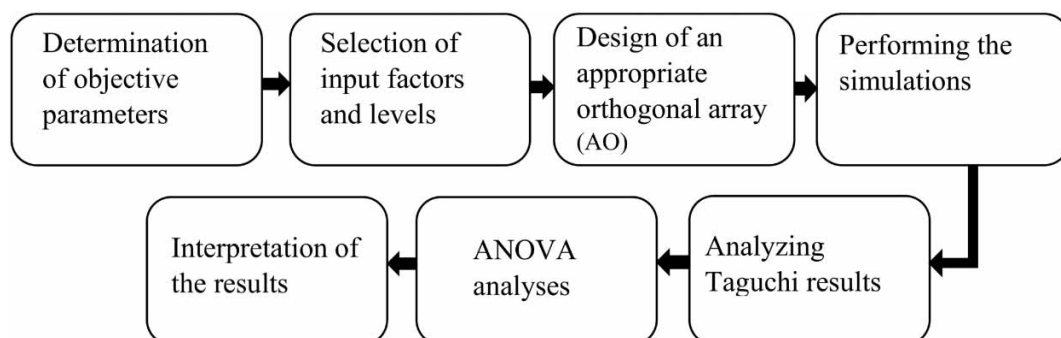


**Figure 4** | The general framework of Taguchi-ANOVA analyses.

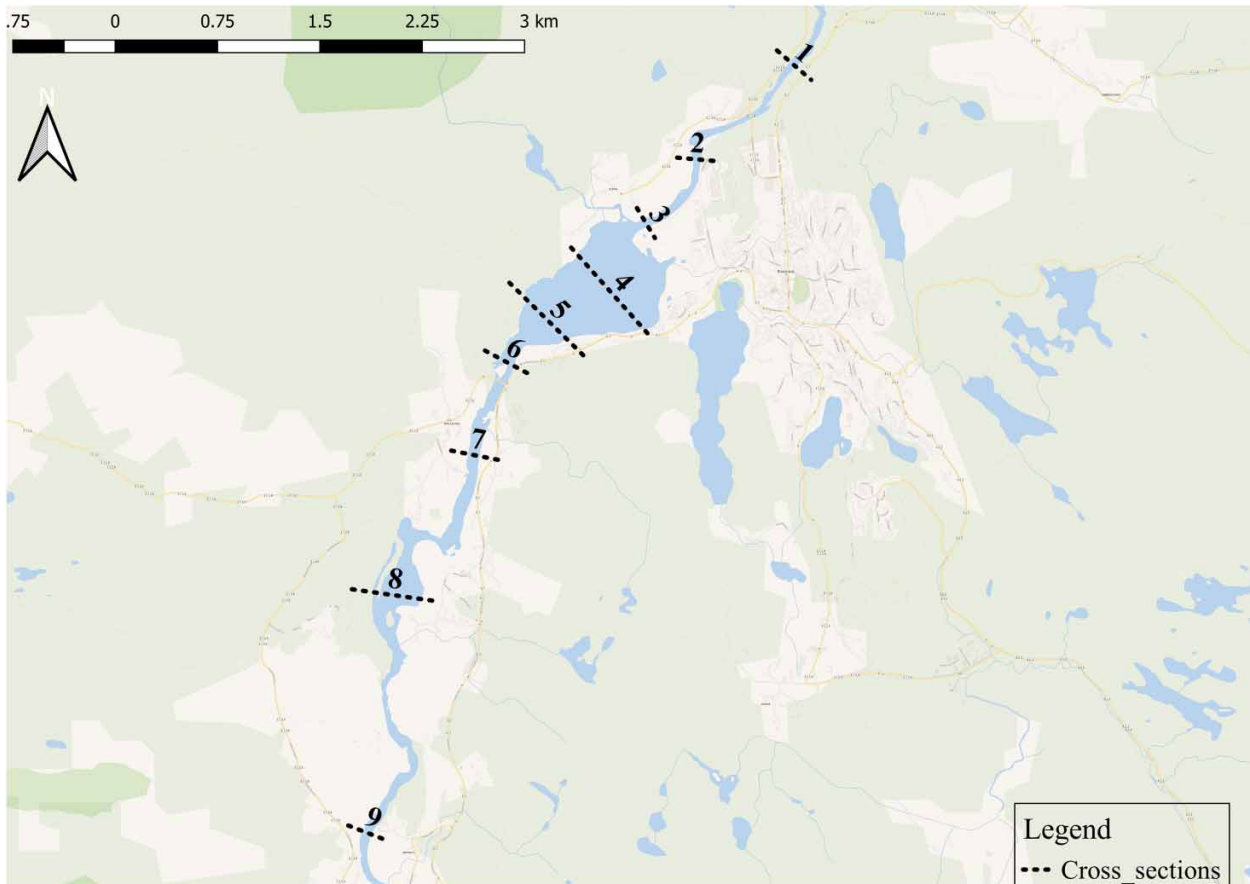


**Figure 5** | Cross-sections' locations.

The most important stage in the design of an experiment is the selection of the control factors. In this study, we selected the following four control factors: mesh size, hydraulic roughness parameter ( $K_S$ ), runoff coefficient ( $C$ ), and precipitation intensity ( $i_p$ ). These factors reflect the set of data, in which HiSTAV uses as an input to simulate the flow. We assigned three values to each of these control factors, as shown in Table 3. The three levels reflect the possible variation range for each parameter.

In the full factorial design, all possible combinations for a given set of factors are considered (Fanchi 2005), which, depending on the number of factors and associated levels, can result in a large number of experiments. The Taguchi method uses the orthogonal design to reduce the number of combinations. Using orthogonal arrays allows us to collect the necessary information by testing specific combinations, instead of examining all possible combinations. The orthogonal arrays have special properties such as (i) all the levels appear an equal number of times (balancing property), (ii) all the levels of parameters (factors) are used for conducting the experiments, and (iii) the array of each factor columns is mutually orthogonal to any other column (Kacker *et al.* 1991). Accordingly, the sequence of levels for conducting the experiments follows a standard sequence and cannot be changed. There are many standard orthogonal arrays available, depending on the number of parameters and the levels of variation for each parameter. Detailed information on the construction of orthogonal arrays can be found in the works presented by Plackett & Burman (1946) and Taguchi (1986).

The full combination of the experiments (full factorial design), considering four parameters with three levels, corresponds to 81 simulations. However, to effectively reduce the number of experiments, the Taguchi method proposes two possible orthogonal arrays, namely L27 and L9. The L27 consists of 27 sets of combinations and assesses the main effects and the interaction between the parameters, while the L9 consists of nine combinations, which only concentrates on main effects and ignores the interactions.

According to the importance of the interactions between the parameters in SA studies, this study is mainly focused on the L27 array. However, the results for the L9 array are also briefly presented to identify the possibility of performing the SAs

**Table 4** | L9 design and calculated SNR values for the water level at nine CS (CS1–CS9) and total flooded area

No.	Levels				SNR									
	Mesh	C	$K_s$	$i_p$	CS1	CS2	CS3	CS4	CS5	CS6	CS7	CS8	CS9	Area
1	1	1	1	1	30.674	26.598	26.505	26.502	26.502	26.495	26.372	26.248	25.089	6.833
2	1	2	2	2	31.016	27.283	27.213	27.213	27.213	27.197	27.071	26.913	25.828	8.331
3	1	3	3	3	31.536	28.353	28.343	28.343	28.343	28.307	28.167	27.907	26.866	10.385
4	2	1	2	3	31.072	27.390	27.330	27.330	27.330	27.312	27.180	27.022	25.869	8.606
5	2	2	3	1	30.613	26.358	26.292	26.293	26.293	26.285	26.201	26.136	24.926	6.419
6	2	3	1	2	31.167	27.748	27.679	27.677	27.676	27.661	27.488	27.271	26.101	9.136
7	3	1	3	2	30.844	26.764	26.707	26.707	26.707	26.697	26.607	26.491	25.319	7.312
8	3	2	1	3	31.378	28.222	28.171	28.169	28.168	28.148	27.967	27.711	26.535	9.931
9	3	3	2	1	30.758	26.632	26.563	26.562	26.562	26.554	26.452	26.342	25.167	6.943
Mean					31.006	27.261	27.200	27.199	27.199	27.184	27.056	26.893	25.744	8.211
Standard deviation					0.299	0.689	0.703	0.703	0.703	0.695	0.669	0.607	0.637	1.343
Coefficient of variation					0.010	0.025	0.026	0.026	0.026	0.026	0.025	0.023	0.025	0.164

with the minimum number of experiments. To validate the performance of the implemented method, the results were benchmarked against the results obtained from all the possible combinations of simulations (L81).

The L9 and L27 orthogonal arrays (see first five columns in Tables 4 and 5) were constructed using the aforementioned factors (Table 3) based on the Taguchi method (Kacker *et al.* 1991). Following the combinations constructed in the orthogonal tables, the simulations were then performed, and the identified objective outputs were calculated as the system's response.

The Taguchi design uses the signal-to-noise ratio (SNR) to measure the deviation of the response from the mean value (Wang *et al.* 2017). Based on the purpose of the experiment, SNRs can be classified into three types: smaller the better type (minimize the response), larger the better type (maximize the response), and nominal the best type (based on the SNR on standard deviation). The equation to calculate SNR values for larger the better type is presented in the following equation:

$$SNR = -10 \times \log \left( \frac{1}{n} \sum_{i=1}^n \frac{1}{Y_i^2} \right) \quad (2)$$

where  $Y_i$  represents the measured results in the  $i$ th experiment/simulation and  $n$  is the number of experiments/simulations.

To investigate the conditions that result in the major flood, the goal is defined as larger the better. Therefore, the larger values for the water level and the flooded area are desirable, and the SNR is calculated by Equation (2). The averages of the SNR values are calculated for each factor  $j$  at level  $l$  using the following equation to analyze the effect of each factor on the outputs:

$$MSNR_{Factor=j}^{Level=l} = \frac{1}{n_{jl}} \sum_{i=1}^{n_{jl}} [SNR_{Factor=j}^{Level=l}]_i \quad (3)$$

where  $n_{jl}$  is the number of experiments that have factor  $j$  at level  $l$  and  $i$  represents the  $i$ th experiment with factor  $j$  at level  $l$ . The significant parameters were then identified as those producing the highest difference in the mean SNR and mean response (target outputs) values. To find the rank of the effect of each parameter in the Taguchi analysis results, a parameter ( $\Delta_j$ ) is defined, which is the difference between the maximum and minimum SNR of all levels for each factor (see Figure 8 and the example in Figure 6(a)). Higher values for ( $\Delta_j$ ) indicate that the model has a higher sensitivity to factor  $j$ .

### Analysis of variance

In addition to the SNR analysis, analysis of variance (ANOVA) was performed to identify the most significant factors and their potential interactions. This method focuses on the analysis of the variance explained by each factor and is accomplished by estimating Fischer's test value ( $F$ -value). The impact of any factor is explained by its  $F$ -value and the corresponding sum of

**Table 5** | L27 design and calculated SNR values for the water level at nine CS (CS1–CS9) and total flooded area

No.	Levels				SNR									Area
	Mesh	C	K <sub>s</sub>	i <sub>p</sub>	CS1	CS2	CS3	CS4	CS5	CS6	CS7	CS8	CS9	
1	1	1	1	1	30.674	26.598	26.505	26.502	26.502	26.495	26.372	26.248	25.089	6.833
2	1	1	2	2	30.892	27.014	26.930	26.929	26.929	26.915	26.801	26.666	25.554	7.743
3	1	1	3	3	31.123	27.438	27.397	27.398	27.398	27.378	27.263	27.105	26.020	8.720
4	2	2	1	1	30.738	26.787	26.704	26.701	26.701	26.693	26.563	26.431	25.235	7.313
5	2	2	2	2	30.935	27.096	27.026	27.026	27.026	27.011	26.892	26.764	25.582	7.976
6	2	2	3	3	31.259	27.692	27.660	27.661	27.661	27.636	27.513	27.348	26.227	9.131
7	3	3	1	1	30.834	26.948	26.868	26.865	26.865	26.857	26.727	26.569	25.375	7.590
8	3	3	2	2	31.140	27.503	27.453	27.452	27.452	27.437	27.313	27.094	25.952	8.795
9	3	3	3	3	31.494	28.182	28.167	28.166	28.166	28.140	28.004	27.763	26.713	9.987
10	2	3	1	2	31.167	27.748	27.679	27.677	27.676	27.661	27.488	27.271	26.101	9.136
11	2	3	2	3	31.460	28.219	28.187	28.186	28.185	28.160	27.987	27.756	26.666	10.045
12	2	3	3	1	30.660	26.468	26.404	26.405	26.405	26.397	26.310	26.239	25.026	6.720
13	3	1	1	2	30.949	27.234	27.162	27.160	27.160	27.150	27.012	26.825	25.632	8.236
14	3	1	2	3	31.110	27.461	27.411	27.410	27.410	27.395	27.276	27.060	25.919	8.734
15	3	1	3	1	30.635	26.265	26.212	26.210	26.210	26.203	26.121	26.054	24.820	5.853
16	1	2	1	2	31.087	27.663	27.596	27.594	27.594	27.577	27.419	27.202	26.048	9.007
17	1	2	2	3	31.348	28.102	28.071	28.070	28.070	28.041	27.889	27.647	26.578	9.872
18	1	2	3	1	30.642	26.398	26.313	26.314	26.314	26.303	26.224	26.143	24.988	6.423
19	3	2	1	3	31.378	28.222	28.171	28.169	28.168	28.148	27.967	27.711	26.535	9.931
20	3	2	2	1	30.705	26.512	26.444	26.444	26.444	26.436	26.336	26.235	25.044	6.632
21	3	2	3	2	31.004	27.084	27.031	27.033	27.033	27.017	26.924	26.771	25.598	7.874
22	1	3	1	3	31.714	29.060	29.032	29.031	29.030	29.000	28.799	28.478	27.252	11.383
23	1	3	2	1	30.786	26.744	26.649	26.648	26.648	26.637	26.529	26.417	25.292	7.153
24	1	3	3	2	31.209	27.573	27.533	27.535	27.535	27.513	27.398	27.224	26.151	8.909
25	2	1	1	3	31.146	27.742	27.678	27.676	27.675	27.660	27.489	27.274	26.106	9.156
26	2	1	2	1	30.603	26.352	26.280	26.279	26.279	26.272	26.172	26.095	24.895	6.246
27	2	1	3	2	30.782	26.713	26.650	26.651	26.651	26.641	26.547	26.464	25.248	7.200
Mean					31.011	27.280	27.221	27.220	27.220	27.203	27.078	26.912	25.756	8.244
Standard deviation					0.293	0.676	0.690	0.690	0.690	0.683	0.657	0.597	0.623	1.358
Coefficient of variation					0.009	0.025	0.025	0.025	0.025	0.025	0.024	0.022	0.024	0.165

squares that represent variance. Higher  $F$ -value and sum of squares of any factor indicate its relative importance in the process of the response (Karmakar *et al.* 2018). Moreover, to explore the impacts of individual factors, the percentage contribution ( $PC$ ) of each factor is calculated using the following equation (Yang & Targ 1998; Sadrzadeh & Mohammadi 2008):

$$PC = \frac{SS_j}{SS_T} \times 100 \quad (4)$$

where  $SS_T$  is the total sum of squares and  $SS_j$  is the sum of squared deviations for each factor  $j$ . Both can be calculated using



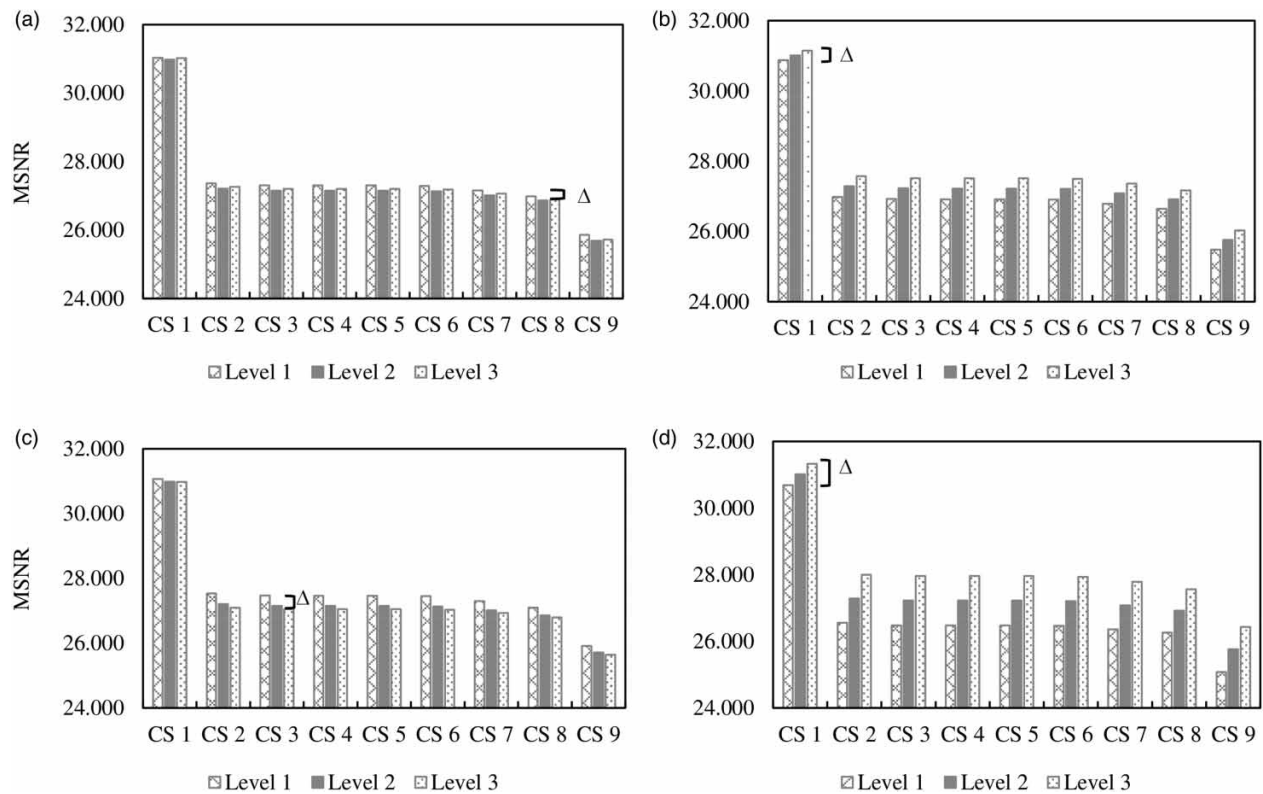


**Figure 6** | Calculated mean SNR at each level for (a) mesh parameter, (b) runoff coefficient, (c) roughness coefficient, and (d) precipitation intensity (considering the cross-sectional water level as a system response).

the following equations, respectively:

$$SS_T = \sum_{i=1}^n (Y_i - \bar{Y})^2 \quad (5)$$

$$SS_j = n_{jl} \sum_{i=1}^l (\bar{Y}_{ji} - \bar{Y})^2 \quad (6)$$

where  $n$  is the number of experiments/simulations,  $Y_i$  represents the measured results in the  $i$ th experiment/simulation,  $\bar{Y}$  is the average of results,  $\bar{Y}_{ji}$  is the mean of results for the factor  $j$  at level  $i$ , and  $n_{jl}$  is the number of experiments that have factor  $j$  at level  $l$  (Stahle & Wold 1989).

## RESULTS AND DISCUSSION

Following the combinations constructed in the Taguchi tables (Tables 4 and 5), 9 and 27 sets of simulations were performed. Two different output parameters, namely local water level and total flooded area, were considered as the system response to investigate the variation resulting from each combination and subsequently to explore the significance of each input parameter in the simulations. The calculated SNR values (based on Equation (2)) for the water level in each CS and the flooded area are presented in Tables 4 and 5.

The calculated standard deviation for the SNR values in each of the local responses (CS water level) ranges between 0.29 and 0.69 for L27 (see Table 5) and for the global response (flooded area) it is equal to 1.36. The coefficient of variation which is defined as the ratio of the standard deviation to the mean is calculated to measure the degree of variation in each of the results series (Tables 4 and 5). The higher coefficient of variation values for the flooded area indicates that it is much more sensitive than the local water level. This result is important because in most of the applications, the hydrodynamic models are

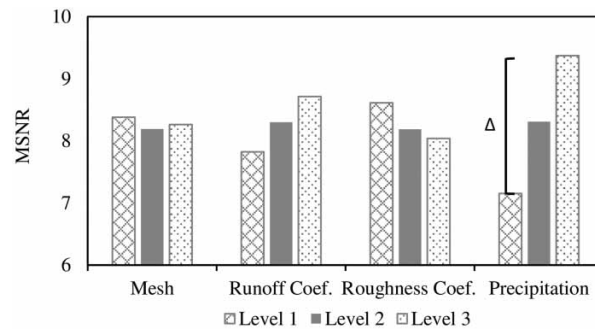


**Figure 7** | Calculated mean SNR for each parameter (considering the flooded area as a system response).

calibrated based on local variables (e.g., water level) with some known inputs (e.g., precipitation intensity) and some particular combinations of calibrated inputs (e.g., runoff coefficient, roughness coefficient, and mesh), which after all can correspond to a quite different flooded area if a different combination of calibrated inputs was used.

From Table 5, it can be seen that the highest SNR results from the combination 22 (1 3 1 3) for the water level and the flooded area, corresponding to the fine mesh size, highest runoff coefficient, smallest roughness coefficient, and highest precipitation intensity. This result is not surprising since the SNR is being computed with larger the better, i.e., the highest water level or the flood area will give the highest SNR.

In order to quantify the significance of each parameter, the mean of the SNR for each factor at the *i*th level was calculated using Equation (3) and is presented in Figures 6 and 7.

The results are compared and ranked based on  $\Delta$  parameter for the L9, the L27, and the full factorial design (L81) in Figure 8. Moreover, the *PC* of each factor obtained from ANOVA is presented for the mentioned designs in Figure 9 (further details of the Taguchi and ANOVA analyses results are presented in the Supplementary Material).

As it is shown in Figures 8 and 9, for both responses (water level (panel a) and flooded area (panel b)) in all types of the designs, the precipitation intensity is the most influencing parameter, followed by the runoff coefficient, the roughness coefficient, and lastly the mesh. The only exception can be seen for CS1 and CS9 in L9 design, in which the mesh size and the

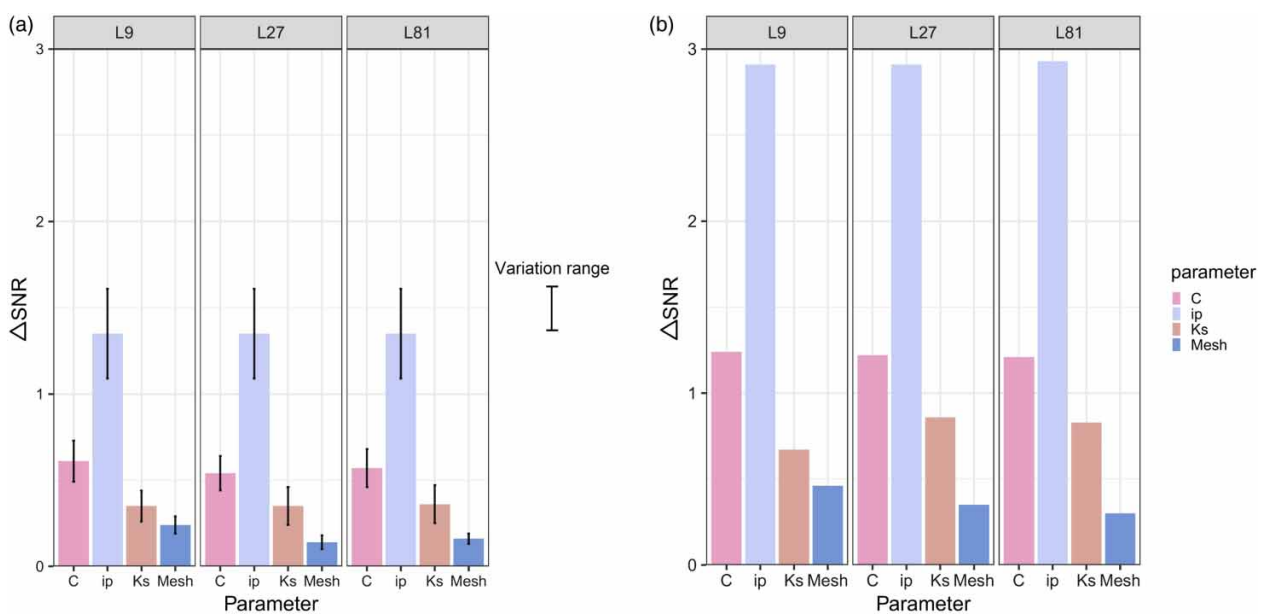


**Figure 8** | Overview of  $\Delta$ SNR variation for (a) local responses (the variation range shows the variation of  $\Delta$ SNR values at different CS) and (b) global response.

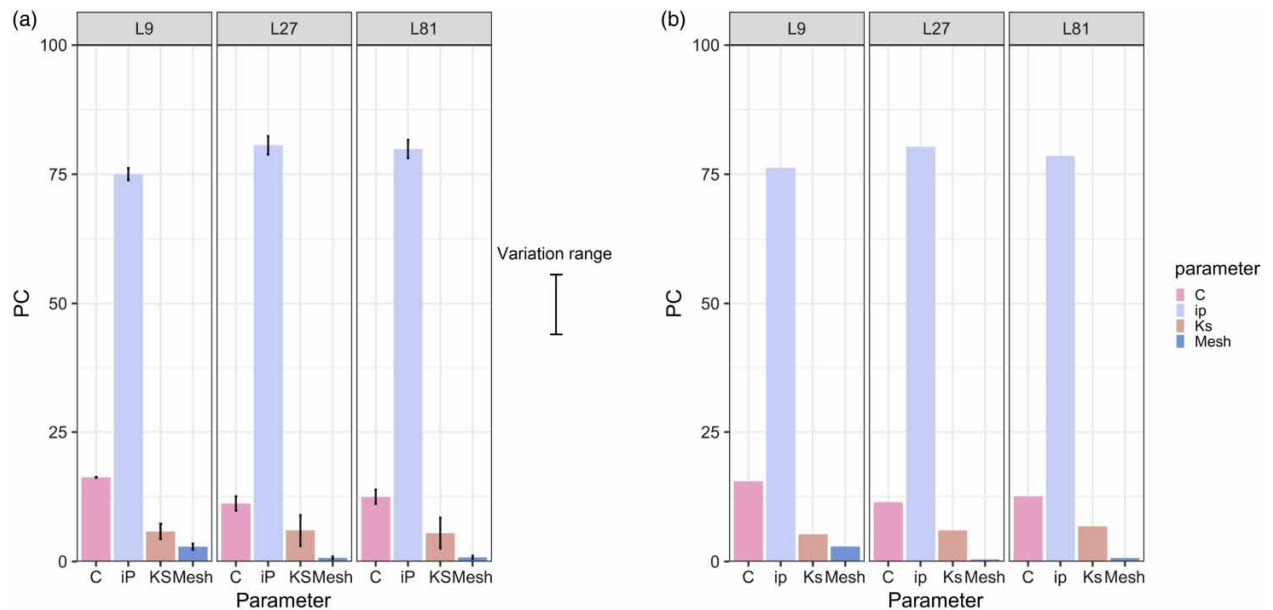


**Figure 9** | Overview of the ANOVA analysis results for (a) local responses (the variation range shows the variation of PC values at different CS) and (b) global response.

roughness effect have equal  $\Delta$ SNR values (0.12 and 0.3, respectively) and as a result are equally ranked as 3. However, comparing the L27 design results with the full factorial design (L81), it can be seen that there are no big differences between the results which means the results of the ANOVA and the Taguchi analyses using L27 combinations are consistent with those obtained from the full factorial design (L81). This finding confirms the effectiveness of the L27 design. Although the L9 design requires few numbers of experiments and provides results almost in accordance with full factorial design results, caution must be applied, as the findings in two of the CS (CS1 and CS9) showed that the mesh size effect has been overestimated by L9.

The results obtained from Figure 9 indicate that precipitation intensity is by far the most important factor, contributing about 80%, while the runoff coefficient and roughness coefficient contribute about 11 and 6%, respectively, and mesh accounts only for 1% contribution. This result highlights the huge importance of either estimating the precipitation intensity adequately with a given return period (which possibly has a big uncertainty due to climate change) for flood mapping or of predicting accurately the precipitation intensity (which has the uncertainty associated with the stochastic nature of weather) for flood forecasting systems. Also interesting is the fact that the runoff coefficient is slightly more relevant than the roughness coefficient. Usually, hydrology modelers attribute more relevance to the runoff coefficient, whereas hydraulic modelers focus on the importance of the roughness coefficient. From the joint hydrologic and hydraulic modeling, it seems that the runoff coefficient is quite relevant, which gives an indication to hydraulic modelers that the input discharge (usually coming from hydrological modeling, involving precipitation and runoff coefficient) influences their final results much more than the roughness coefficient.

The results in Figures 6 and 7 show that finer meshes (level 1) lead to slightly larger SNR values than coarser ones (levels 2 and 3). Nevertheless, the performance improvement with mesh refinement is not always true since the SNR value for the coarser mesh (level 3) is higher than the intermediate one (level 2). This puts in evidence that refining unstructured meshes with underlying complex topography can lead to no improvement. As stated before, for the runoff coefficient, roughness coefficient, and precipitation intensity, the performance results follow what is usually expected, i.e., the increase in runoff coefficient (levels 1–3) increases the SNR values, the increase in the Strickler coefficient (i.e., decrease in roughness, levels 1–3) reduces the SNR values and the increase in the precipitation intensity (levels 1–3) results in higher SNR values. This is confirmed by the maximum and minimum flooded areas, corresponding to combinations 22 and 15, respectively, that are presented in Figure 10.

In complex and nonlinear systems, the joint effects of input parameters can have a significant influence on the outputs. Thus, in order to have a complete SA, the interactions among parameters are analyzed using the ANOVA technique. In this regard,

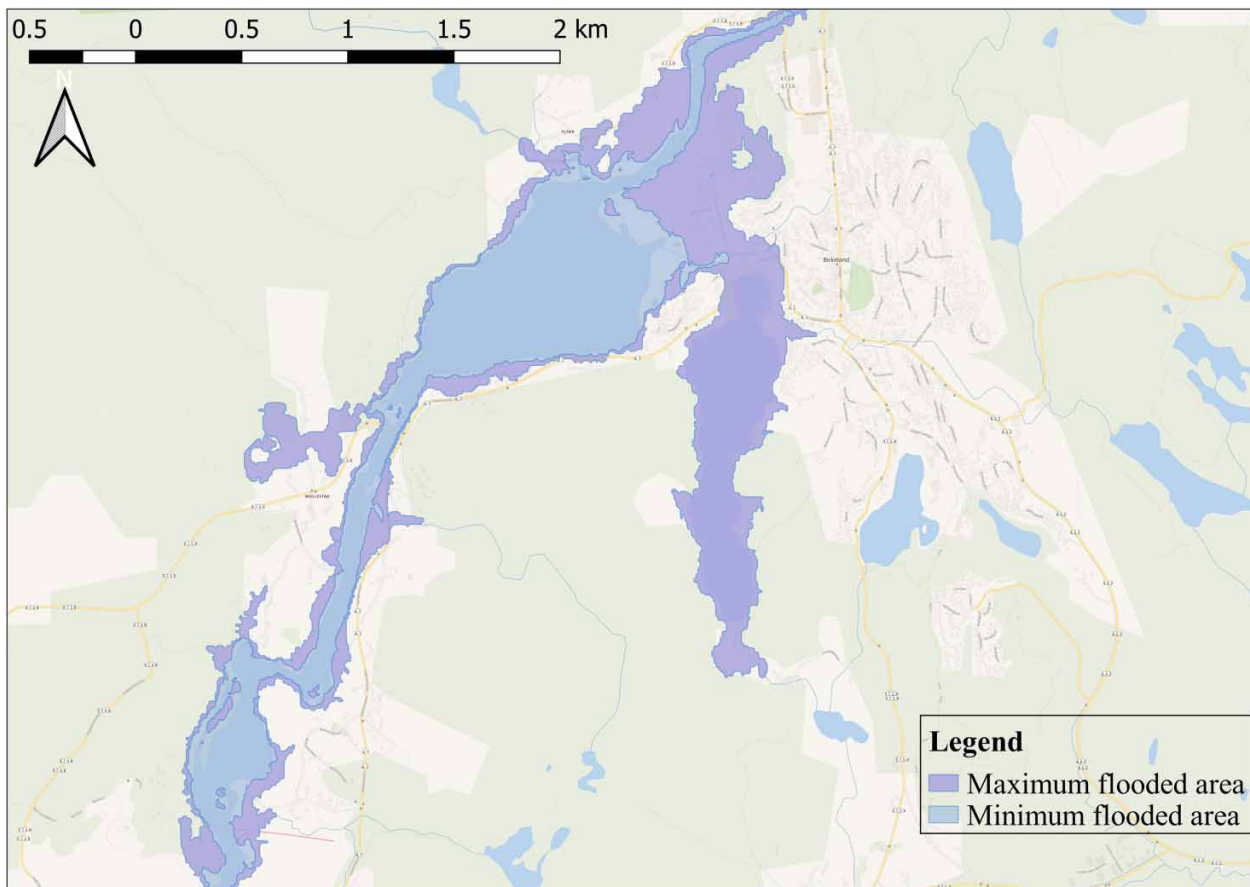


**Figure 10** | The variation in the calculated flooded area.

CS4, which is considered an important CS located in the Flaksvann lake where a hydrological station exists, was selected to explore the interaction between the parameters. The interactions are analyzed for both L27 and L81 at a specified CS. Since the results were similar, the interaction matrix of the parameters is only presented for the L27 design in [Figure 11](#). If the curves are parallel with each other, it means that there are no interaction effects of the two parameters ([Wang et al. 2017](#)).

The intersection lines in [Figure 11\(b\)](#) imply that the mesh size mostly interacts with the roughness coefficient, presenting similar performances for the rougher case (smaller Strickler coefficient, i.e., level 1), but a much more mixed behavior for less rough cases (levels 2 and 3). As can be seen in [Figure 11\(a\)–11\(c\)](#), and already mentioned, mesh refinement will not necessarily improve performance (i.e., the SNR). In [Figure 11\(b\)](#), the mesh refinement always improves the performance for the smoother case (roughness at level 3), but that is not true for the intermediate case (level 2), where a mesh refinement from level 3 to level 2 produces worse results. As stated before, this is related to the unstructured mesh generation, in particular, near the river main channel where the roughness coefficient varies. From those figures, it is seen that, in general, the intermediate mesh (level 2) presents lower performance, and the finer mesh (level 1) presents slightly better results than the coarser mesh (level 3). The latter becomes more evident for high-intensity precipitation (see level 3 in [Figure 11\(c\)](#)), which indicates that for simulating extreme flood events refining the mesh can originate a better performance.

The runoff coefficient slightly interacts with the precipitation intensity ([Figure 11\(e\)](#)). It is clear that runoff coefficients are more important for model performance as the intensity precipitation level is higher. This is logic since the runoff coefficient represents a precipitation percentage loss, which, for the same level (i.e., percentage) and higher intensity of precipitation, corresponds to a much higher amount of water flowing through the catchment (i.e., higher SNR). Nevertheless, this points out to the importance of a correct calibration of the runoff coefficient, especially for high-intensity precipitation events that originate floods.

Based on the mean response variation range (see blue dashed circles in [Figures 11\(e\)](#) and [11\(f\)](#)), it can be observed that the importance of the parameters changes depending on the precipitation intensity. At the lower intensity (level 1), the roughness

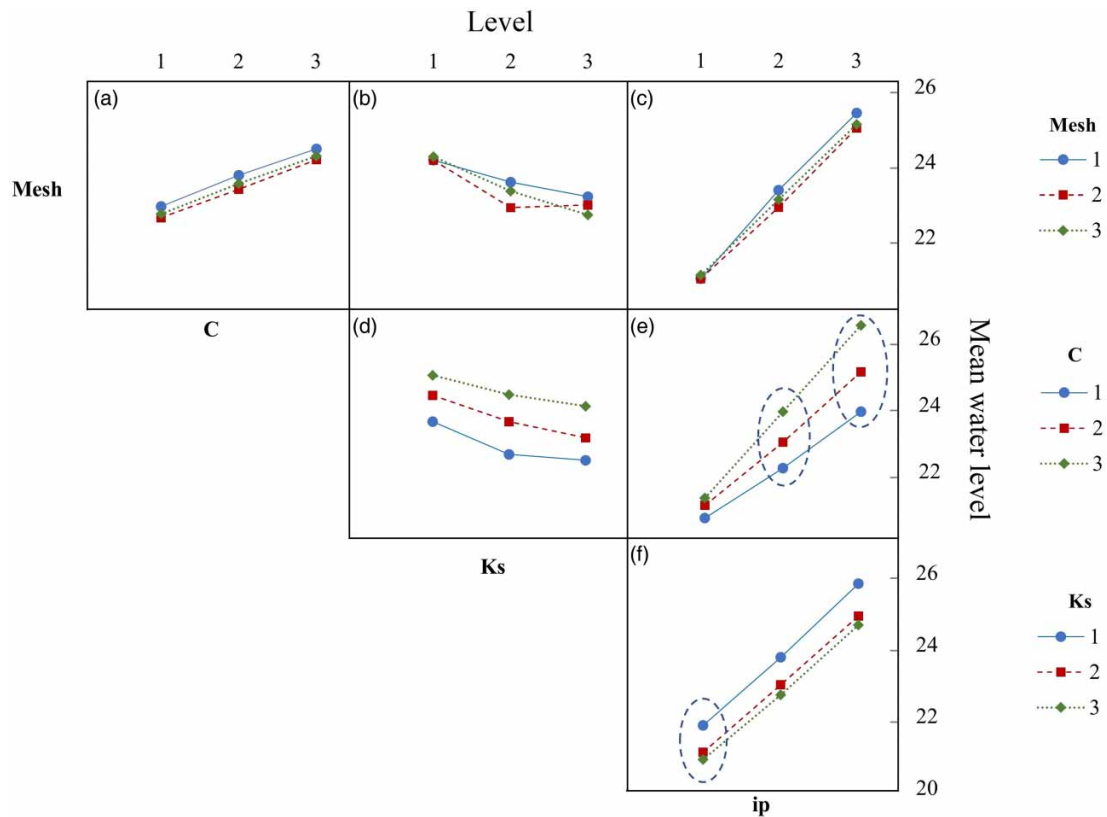


**Figure 11** | Interaction plots for the water level at CS4.  $C$  is the runoff coefficient,  $K_S$  is the roughness coefficient, and  $i_p$  is the precipitation intensity. Interactions between: (a) mesh and  $C$ , (b) mesh and  $K_S$ , (c) mesh and  $i_p$ , (d)  $C$  and  $K_S$ , (e)  $C$  and  $i_p$ , and (f)  $K_S$  and  $i_p$ .

parameter corresponds to higher variation comparing to the other parameters. Whereas, under moderate and high intensities (levels 2 and 3), the runoff coefficient is the most influencing parameter, which corresponds to the higher variation range in the mean water level.

## CONCLUSION

In this study, the application of the Taguchi technique and ANOVA was investigated to identify and rank the most influencing parameters in a 2D hydrodynamic flood simulation model. In general, this approach has several advantages: (i) it can effectively reduce the number of simulations needed for SA, (ii) it quantifies the contribution of each parameter and ranks them based on the associated variation in target outputs, and (iii) it explores the interaction between input parameters.

- The main conclusions of this study are: the implemented Taguchi–ANOVA approach can be used as an efficient SA method in 2D flood modeling to quantify and rank the affecting parameters. However, the results suggest that the minimum orthogonal array (L9) should be used cautiously and that an intermediate orthogonal array (L27) is preferred, if affordable.
- The considered global response (flooded area) is more sensitive to the input parameters variation comparing to the local response (cross-sectional water level). This shows the necessity of considering both local and global scale calibrations for flood simulation purposes.

The following secondary conclusions, which require further validation for a more complex hydrological approach, can be drawn from the results presented in this paper:

- The precipitation intensity is identified as the most significant parameter in flood modeling, accounting for about 80% contribution. Then follows runoff coefficients (11%), roughness coefficient (6%), and mesh size (1%). This highlights the great importance of accurate estimation of the precipitation intensity for flood modelers and decision makers. This can be a major challenge due to the uncertainties resulting from climate change and the stochastic nature of the weather.



- Generally, among the proposed mesh sizes, the finer mesh size (level 1) led to slightly better results compared with the other mesh sizes (levels 2 and 3). Especially, under high-intensity precipitation (level 3), the difference is clearer. However, the mesh refinement is not always a solution to improve the results due to the underlying complex gridded data, including topography, roughness, and runoff coefficient values. Moreover, the strong interaction between the roughness coefficient and the mesh size provides further support for the hypothesis that mesh refinement can, in some cases, negatively affect the results.
- The importance of the input parameters can change depending on the hydrological conditions. Under the low-intensity precipitation (level 1), the roughness parameter is affecting the results more than other parameters. Whereas, under moderate and high-intensity precipitations (levels 2 and 3), the runoff coefficient is the most influencing parameter, which corresponds to the higher variation in outputs.

## ACKNOWLEDGEMENTS

The work presented in this paper is funded by the University of Agder, Norway (project no. 63859). We would like to acknowledge the help of Daniel Conde and Rui Ferreira (IST, Portugal) on the HiSTAV model set-up.

## DATA REFERENCE

The data used in this work including precipitation data and measured discharge data are available at <http://www.senorge.no/>. The Digital Terrain Models and land cover maps are acquired from <https://hoydedata.no/LaserInnsyn/> and <https://land.copernicus.eu/pan-european/corine-land-cover>, respectively. The Taguchi and ANOVA analyses were implemented using the Minitab 19 software.

## DATA AVAILABILITY STATEMENT

All relevant data are included in the paper or its Supplementary Information.

## REFERENCES

- Abily, M., Delestre, O., Gourbesville, P., Bertrand, N., Duluc, C.-M. & Richet, Y. 2016 Global sensitivity analysis with 2D hydraulic codes: application on uncertainties related to high-resolution topographic data. *Advances in Hydroinformatics*. Springer, Berlin, pp. 301–315. [https://doi.org/10.1007/978-981-287-615-7\\_21](https://doi.org/10.1007/978-981-287-615-7_21).
- Ahmadisharaf, E., Kalyanapu, A. J. & Bates, P. D. 2018 A probabilistic framework for floodplain mapping using hydrological modeling and unsteady hydraulic modeling. *Hydrological Sciences Journal* **63** (12), 1759–1775. <https://doi.org/10.1080/02626667.2018.1525615>.
- Arcement, G. J. & Schneider, V. R. 1989 *Guide for selecting Manning's roughness coefficients for natural channels and flood plains*. US Government Printing Office Washington, DC. <https://doi.org/10.3133/wsp2339>.
- Bao, Z., Yang, F., Wu, Z., Nyamsi, S. N. & Zhang, Z. 2013 Optimal design of metal hydride reactors based on CFD-Taguchi combined method. *Energy Conversion and Management* **65**, 322–330. <https://doi.org/10.1016/j.enconman.2012.07.027>.
- Bellos, V., Papageorgaki, I., Kourtis, I., Vangelis, H., Kalogiros, I. & Tsakiris, G. 2020 Reconstruction of a flash flood event using a 2D hydrodynamic model under spatial and temporal variability of storm. *Natural Hazards* **101**, 711–726. <https://doi.org/10.1007/s11069-020-03891-3>.
- Bomers, A., Schielen, R. M. J. & Hulscher, S. J. 2019 The influence of grid shape and grid size on hydraulic river modelling performance. *Environmental Fluid Mechanics* **19** (5), 1273–1294.
- Campolongo, F., Saltelli, A. & Cariboni, J. 2011 From screening to quantitative sensitivity analysis. A unified approach. *Computer Physics Communications* **182** (4), 978–988. <https://doi.org/10.1016/j.cpc.2010.12.039>.
- Caviedes-Voullième, D., García-Navarro, P. & Murillo, J. 2012 Influence of mesh structure on 2D full shallow water equations and SCS Curve Number simulation of rainfall/runoff events. *Journal of Hydrology* **448**, 39–59.
- Chen, B., Krajewski, W. F., Helmers, M. J. & Zhang, Z. 2019 Spatial variability and temporal persistence of event runoff coefficients for cropland hillslopes. *Water Resources Research* **55** (2), 1583–1597.
- Chen, S., Garambois, P.-A., Finaud-Guyot, P., Dellinger, G., Mose, R., Terfous, A. & Ghenaim, A. 2018 Variance based sensitivity analysis of 1D and 2D hydraulic models: An experimental urban flood case. *Environmental Modelling & Software* **109**, 167–181. <https://doi.org/10.1016/j.envsoft.2018.08.008>.
- Conde, D. A., Canelas, R. B. & Ferreira, R. M. 2020 A unified object-oriented framework for CPU+ GPU explicit hyperbolic solvers. *Advances in Engineering Software* **148**, 102802. <https://doi.org/10.1016/j.advengsoft.2020.102802>.
- Conde, D. A., Telhado, M. J., Baptista, M. A. V. & Ferreira, R. M. 2015 Severity and exposure associated with tsunami actions in urban waterfronts: the case of Lisbon, Portugal. *Natural Hazards* **79** (3), 2125–2144. <https://doi.org/10.1007/s11069-015-1951-z>.

- Costabile, P. & Costanzo, C. 2021 A 2D-SWEs framework for efficient catchment-scale simulations: Hydrodynamic scaling properties of river networks and implications for non-uniform grids generation. *Journal of Hydrology* **599**, 126306.
- Dorn, H., Vetter, M. & Höfle, B. 2014 GIS-based roughness derivation for flood simulations: a comparison of orthophotos, LiDAR and crowdsourced geodata. *Remote Sensing* **6** (2), 1739–1759. <https://doi.org/10.3390/rs6021739>.
- Dottori, F., Di Baldassarre, G. & Todini, E. 2013 Detailed data is welcome, but with a pinch of salt: Accuracy, precision, and uncertainty in flood inundation modeling. *Water Resources Research* **49** (9), 6079–6085. <https://doi.org/10.1002/wrcr.20406>.
- Fanchi, J. R. 2005 *Principles of applied reservoir simulation*. Elsevier, Oxford. <https://doi.org/10.1016/C2017-0-00352-X>.
- Fernández-Pato, J., Caviedes-Voullième, D. & García-Navarro, P. 2016 Rainfall/runoff simulation with 2D full shallow water equations: Sensitivity analysis and calibration of infiltration parameters. *Journal of Hydrology* **536**, 496–513. <https://doi.org/10.1016/j.jhydrol.2016.03.021>.
- Ferraro, D., Costabile, P., Costanzo, C., Petaccia, G. & Macchione, F. 2020 A spectral analysis approach for the a priori generation of computational grids in the 2-D hydrodynamic-based runoff simulations at a basin scale. *Journal of Hydrology* **582**, 124508.
- Ferreira, R. M., Franca, M. J., Leal, J. G. & Cardoso, A. H. 2009 Mathematical modelling of shallow flows: Closure models drawn from grain-scale mechanics of sediment transport and flow hydrodynamics. *Canadian Journal of Civil Engineering* **36** (10), 1605–1621. <https://doi.org/10.1139/L09-033>.
- Geuzaine, C. & Remacle, J. F. 2009 Gmsh: A 3-D finite element mesh generator with built-in pre-and post-processing facilities. *International Journal for Numerical Methods in Engineering* **79** (11), 1309–1331. <https://doi.org/10.1002/nme.2579>.
- Ghasemzade, M., Baroni, G., Abbaspour, K. & Schirmer, M. 2017 Combined analysis of time-varying sensitivity and identifiability indices to diagnose the response of a complex environmental model. *Environmental Modelling & Software* **88**, 22–34. <https://doi.org/10.1016/j.envsoft.2016.10.011>.
- Gibson, M. J., Savic, D. A., Djordjevic, S., Chen, A.S., Fraser, S. & Watson, T. 2016 Accuracy and computational efficiency of 2D urban surface flood modelling based on cellular automata. *Procedia Engineering* **154**, 801–810.
- Hadi, M. N., Farhan, N. A. & Sheikh, M. N. 2017 Design of geopolymers concrete with GGBFS at ambient curing condition using Taguchi method. *Construction and Building Materials* **140**, 424–431. <https://doi.org/10.1016/j.conbuildmat.2017.02.131>.
- Hu, R., Fang, F., Salinas, P. & Pain, C. 2018 Unstructured mesh adaptivity for urban flooding modelling. *Journal of Hydrology* **560**, 354–363.
- Hu, R., Fang, F., Salinas, P., Pain, C., Domingo, N. S. & Mark, O. 2019 Numerical simulation of floods from multiple sources using an adaptive anisotropic unstructured mesh method. *Advances in Water Resources* **123**, 173–188. <https://doi.org/10.1016/j.advwatres.2018.11.011>.
- Kacker, R. N., Lagergren, E. S. & Filliben, J. J. 1991 Taguchi's orthogonal arrays are classical designs of experiments. *Journal of Research of the National Institute of Standards and Technology* **96** (5), 577. <https://dx.doi.org/10.6028/2Fjres.096.034>.
- Karmakar, B., Dhawane, S. H. & Halder, G. 2018 Optimization of biodiesel production from castor oil by Taguchi design. *Journal of Environmental Chemical Engineering* **6** (2), 2684–2695. <https://doi.org/10.1016/j.jece.2018.04.019>.
- Khang, D. S., Tan, R. R., Uy, O. M., Promentilla, M. A. B., Tuan, P. D., Abe, N. & Razon, L. F. 2017 Design of experiments for global sensitivity analysis in life cycle assessment: the case of biodiesel in Vietnam. *Resources, Conservation and Recycling* **119**, 12–23. <https://doi.org/10.1016/j.resconrec.2016.08.016>.
- Kim, B., Sanders, B. F., Schubert, J. E. & Famiglietti, J. S. 2014 Mesh type tradeoffs in 2D hydrodynamic modeling of flooding with a Godunov-based flow solver. *Advances in Water Resources* **68**, 42–61.
- LeVeque, R. J. 2002 Finite volume methods for hyperbolic problems, 31. Cambridge University Press, Cambridge. 10.1017/CBO9780511791253.
- Lim, N. J. & Brandt, S. A. 2019 Flood map boundary sensitivity due to combined effects of DEM resolution and roughness in relation to model performance. *Geomatics, Natural Hazards and Risk* **10** (1), 1613–1647. <https://doi.org/10.1080/19475705.2019.1604573>.
- Mejia, A. I. & Reed, S. 2011 Evaluating the effects of parameterized cross section shapes and simplified routing with a coupled distributed hydrologic and hydraulic model. *Journal of Hydrology* **409** (1-2), 512–524. <https://doi.org/10.1016/j.jhydrol.2011.08.050>.
- Merz, R. & Blöschl, G. 2009 A regional analysis of event runoff coefficients with respect to climate and catchment characteristics in Austria. *Water Resources Research* **45** (1), W01405. <https://doi.org/10.1029/2008WR007163>.
- Merz, R., Blöschl, G. & Parajka, J. 2006 Spatio-temporal variability of event runoff coefficients. *Journal of Hydrology* **331** (3-4), 591–604.
- Murray, P. M., Bellany, F., Benhamou, L., Bučar, D.-K., Tabor, A. B. & Sheppard, T. D. 2016 The application of design of experiments (DoE) reaction optimisation and solvent selection in the development of new synthetic chemistry. *Organic & Biomolecular Chemistry* **14** (8), 2373–2384. <https://doi.org/10.1039/C5OB01892G>.
- Neal, J. C., Odoni, N. A., Trigg, M. A., Freer, J. E., Garcia-Pintado, J., Mason, D. C., Wood, M. & Bates, P. D. 2015 Efficient incorporation of channel cross-section geometry uncertainty into regional and global scale flood inundation models. *Journal of Hydrology* **529**, 169–183. <https://doi.org/10.1016/j.jhydrol.2015.07.026>.
- Papaioannou, G., Vasiliades, L., Loukas, A. & Aronica, G. T. 2017 Probabilistic flood inundation mapping at ungauged streams due to roughness coefficient uncertainty in hydraulic modelling. *Advances in Geosciences* **44**, 23. <https://doi.org/10.5194/adgeo-44-23-2017>.
- Pappenberger, F., Beven, K., Horritt, M. & Blazkova, S. J. J. O. H. 2005 Uncertainty in the calibration of effective roughness parameters in HEC-RAS using inundation and downstream level observations. *Journal of Hydrology* **302** (1-4), 46–69. <https://doi.org/10.1016/j.jhydrol.2004.06.036>.
- Park, Y., Cho, K. H., Kang, J.-H., Lee, S. W. & Kim, J. H. 2014 Developing a flow control strategy to reduce nutrient load in a reclaimed multi-reservoir system using a 2D hydrodynamic and water quality model. *Science of The Total Environment* **466**, 871–880. <https://doi.org/10.1016/j.scitotenv.2013.07.041>.

- Pianosi, F., Beven, K., Freer, J., Hall, J. W., Rougier, J., Stephenson, D. B. & Wagener, T. 2016 Sensitivity analysis of environmental models: A systematic review with practical workflow. *Environmental Modelling & Software* **79**, 214–232. <https://doi.org/10.1016/j.envsoft.2016.02.008>.
- Plackett, R. L. & Burman, J. P. 1946 The design of optimum multifactorial experiments. *Biometrika* **33** (4), 305–325.
- Rao, C. R. 1947 Factorial experiments derivable from combinatorial arrangements of arrays. *Supplement to the Journal of the Royal Statistical Society* **9** (1), 128–139. <https://doi.org/10.2307/2983576>.
- Rao, R. S., Prakasham, R., Prasad, K. K., Rajesham, S., Sarma, P. & Rao, L. V. 2004 Xylitol production by *Candida* sp.: parameter optimization using Taguchi approach. *Process Biochemistry* **39** (8), 951–956. [https://doi.org/10.1016/S0032-9592\(03\)00207-3](https://doi.org/10.1016/S0032-9592(03)00207-3).
- Ross, P. J. & Ross, P. J. 1988 *Taguchi techniques for quality engineering: loss function, orthogonal experiments, parameter and tolerance design*. McGraw-Hill, New York.
- Sadeghi, S. H., Moosavi, V., Karami, A. & Behnia, N. 2012 Soil erosion assessment and prioritization of affecting factors at plot scale using the Taguchi method. *Journal of Hydrology* **448**, 174–180. <https://doi.org/10.1016/j.jhydrol.2012.04.038>.
- Sadrzadeh, M. & Mohammadi, T. 2008 Sea water desalination using electrodialysis. *Desalination* **221** (1-3), 440–447. <https://doi.org/10.1016/j.desal.2007.01.103>.
- Sauer, A. & Ortlepp, R. 2021 Parameter uncertainties in flood hazard analysis of heavy rain events. *ASCE-ASME Journal of Risk and Uncertainty in Engineering Systems, Part A: Civil Engineering* **7** (2), 04021016.
- Savage, J., Pianosi, F., Bates, P., Freer, J. & Wagener, T. 2016 Quantifying the importance of spatial resolution and other factors through global sensitivity analysis of a flood inundation model. *Water Resources Research* **52** (11), 9146–9163. <https://doi.org/10.1002/2015WR018198>.
- Schubert, J. E., Sanders, B. F., Smith, M. J. & Wright, N. G. 2008 Unstructured mesh generation and landcover-based resistance for hydrodynamic modeling of urban flooding. *Advances in Water Resources* **31** (12), 1603–1621. <https://doi.org/10.1016/j.advwatres.2008.07.012>.
- Schumann, G., Matgen, P., Hoffmann, L., Hostache, R., Pappenberger, F. & Pfister, L. 2007 Deriving distributed roughness values from satellite radar data for flood inundation modelling. *Journal of Hydrology* **344** (1-2), 96–111. <https://doi.org/10.1016/j.jhydrol.2007.06.024>.
- Song, X., Zhang, J., Zhan, C., Xuan, Y., Ye, M. & Xu, C. J. 2015 Global sensitivity analysis in hydrological modeling: Review of concepts, methods, theoretical framework, and applications. *Journal of Hydrology* **523**, 739–757. <https://doi.org/10.1016/j.jhydrol.2015.02.013>.
- Stahle, L. & Wold, S. 1989 Analysis of variance (ANOVA). *Chemometrics and Intelligent Laboratory Systems* **6** (4), 259–272. [https://doi.org/10.1016/0169-7439\(89\)80095-4](https://doi.org/10.1016/0169-7439(89)80095-4).
- Subramanya, K. 2013 *Engineering Hydrology*, 4e. Tata McGraw-Hill Education, New Delhi, India.
- Taguchi, G., Organization, A. P. & productivité, O. 1986 *Introduction to Quality Engineering: Designing Quality Into Products and Processes*. Asian Productivity Organization Tokyo.
- Teng, J., Jakeman, A. J., Vaze, J., Croke, B. F., Dutta, D. & Kim, S. J. E. M., Software, 2017. Flood inundation modelling: A review of methods, recent advances and uncertainty analysis. *Environmental Modelling & Software* **90**, 201–216. <https://doi.org/10.1016/j.envsoft.2017.01.006>.
- Tian, W. 2013 A review of sensitivity analysis methods in building energy analysis. *Renewable and Sustainable Energy Reviews* **20**, 411–419. <https://doi.org/10.1016/j.rser.2012.12.014>.
- van Griensven, A. v., Meixner, T., Grunwald, S., Bishop, T., Diluzio, M. & Srinivasan, R. 2006 A global sensitivity analysis tool for the parameters of multi-variable catchment models. *Journal of Hydrology* **324** (1-4), 10–23. <https://doi.org/10.1016/j.jhydrol.2005.09.008>.
- van Vuren, S., Paarlberg, A. & Havinga, H. 2015 The aftermath of ‘Room for the River’ and restoration works: Coping with excessive maintenance dredging. *Journal of Hydro-Environment Research* **9** (2), 172–186. <https://doi.org/10.1016/j.jher.2015.02.001>.
- Viglione, A., Merz, R. & Blöschl, G. 2009 On the role of the runoff coefficient in the mapping of rainfall to flood return periods. *Hydrology and Earth System Sciences* **13** (5), 577–593.
- Vojtek, M., Petroselli, A., Vojteková, J. & Asgharinia, S. 2019 Flood inundation mapping in small and ungauged basins: sensitivity analysis using the EBA4SUB and HEC-RAS modeling approach. *Hydrology Research* **50** (4), 1002–1019. <https://doi.org/10.2166/nh.2019.163>.
- Wang, C., Li, Y. & Huang, G. 2017 Taguchi-factorial type-2 fuzzy random optimization model for planning conjunctive water management with compound uncertainties. *Environmental Modelling & Software* **97**, 184–200. <https://doi.org/10.1016/j.envsoft.2017.08.007>.
- Werner, M., Hunter, N. & Bates, P. 2005 Identifiability of distributed floodplain roughness values in flood extent estimation. *Journal of Hydrology* **314** (1-4), 139–157. <https://doi.org/10.1016/j.jhydrol.2005.03.012>.
- Whitford, W. G., Lundgren, M. & Fairbank, A. 2018 *Cell Culture Media in Bioprocessing, Biopharmaceutical Processing*. Elsevier, Oxford, pp. 147–162. <https://doi.org/10.1016/B978-0-08-100623-8.00008-6>.
- Xing, Y., Shao, D., Ma, X., Zhang, S. & Jiang, G. 2021 Investigation of the importance of different factors of flood inundation modeling applied in urbanized area with variance-based global sensitivity analysis. *Science of The Total Environment* **772**, 145327.
- Yang, J. 2011 Convergence and uncertainty analyses in Monte-Carlo based sensitivity analysis. *Environmental Modelling & Software* **26** (4), 444–457. <https://doi.org/10.1016/j.envsoft.2010.10.007>.
- Yang, W. p. & Tarnq, Y. 1998 Design optimization of cutting parameters for turning operations based on the Taguchi method. *Journal of Materials Processing Technology* **84** (1-3), 122–129. [https://doi.org/10.1016/S0924-0136\(98\)00079-X](https://doi.org/10.1016/S0924-0136(98)00079-X).



- Yu, D. & Lane, S. N. 2006 Urban fluvial flood modelling using a two-dimensional diffusion-wave treatment, part 1: mesh resolution effects. *Hydrological Processes: An International Journal* **20** (7), 1541–1565. <https://doi.org/10.1002/hyp.5935>.
- Yuanyai, C. & Nembhard, H. B. 2015 Chapter 8 - Design of experiments: A key to innovation in nanotechnology. In: Ahmed, W., Jackson, M.J. (eds), *Emerging Nanotechnologies for Manufacturing (Second Edition)*. William Andrew Publishing, Boston, pp. 230–254. <https://doi.org/10.1016/B978-0-323-28990-0.00008-7>.
- Zadeh, F. K., Nossent, J., Sarrazin, F., Pianosi, F., van Griensven, A., Wagener, T. & Bauwens, W. 2017 Comparison of variance-based and moment-independent global sensitivity analysis approaches by application to the SWAT model. *Environmental Modelling & Software* **91**, 210–222. <https://doi.org/10.1016/j.envsoft.2017.02.001>.
- Zhang, T., Feng, P., Maksimović, Č. & Bates, P. D. 2016 Application of a three-dimensional unstructured-mesh finite-element flooding model and comparison with two-dimensional approaches. *Water Resources Management* **30** (2), 823–841. <https://doi.org/10.1007/s11269-015-1193-6>.
- Zischg, A. P., Felder, G., Weingartner, R., Quinn, N., Coxon, G., Neal, J., Freer, J. & Bates, P. 2018a Effects of variability in probable maximum precipitation patterns on flood losses. *Hydrology and Earth System Sciences* **22** (5), 2759–2773. <https://doi.org/10.5194/hess-22-2759-2018>.
- Zischg, A. P., Mosimann, M., Bernet, D. B. & Röthlisberger, V. 2018b Validation of 2D flood models with insurance claims. *Journal of Hydrology* **557**, 350–361. <https://doi.org/10.1016/j.jhydrol.2017.12.042>.

First received 23 April 2021; accepted in revised form 11 September 2021. Available online 30 September 2021



**Paper II:** Return levels uncertainty under effect of climate change

Alipour SM, Leal J., 2019. Return levels uncertainty under effect of climate change. Proceedings of the IAHR World Congress. ISSN: 2521-7119. s 256 - 264. DOI:[10.3850/38WC092019-1230](https://doi.org/10.3850/38WC092019-1230).



## **Return levels uncertainty under effect of climate change**

Saba Mirza Alipour<sup>(1)</sup>, Joao Leal<sup>(2)</sup>

<sup>(1,2)</sup> Department of Engineering Science

University of Agder, Faculty of Engineering and Science, Grimstad, Norway

Saba.m.alipour@uia.com ; joao.leal@uia.no

### **Abstract**

River flood return period estimation plays an important role in the engineering practices of water resources and flood management, but there are many parameters that accompany the calculation process. Typically, several return levels and return periods (e.g. 100, 200, etc.) are used to describe and quantify river flood discharge. Classical river flood modelling techniques assume a stationary climate. In the stationary case it is assumed that, there is a one-to-one relationship between the m-year return level and T-year return period which is defined implicitly as the reciprocal of the probability of an exceedance in any 1 year. However, in recent years, it has become increasingly evident that, magnitude and frequency of peak flow can no longer be assumed to be stationary due to the climate change effect. This paper aims to investigate the probabilistic behavior of the return period and reliability of 100-year return period peak flow under stationary and nonstationary conditions. For this purpose, we focused on stationary and non-stationary scenarios. Using existing annual maximum daily discharge data and annual maximum daily precipitation data various GEV models were developed and return levels under stationary and nonstationary scenarios were estimated. The results revealed the existence of a clear climate signal in flood water level and its return period. Also, the comparison of the results showed a significant difference between calculated return level in each scenario. As a result, return periods and return levels reliability should be assessed under climate change and the uncertainty associated with them should be quantified.

### **1 Introduction**

Recent reports from various locations around the world, exhibit changes in the frequency, severity and spatial pattern of climatic extremes. In particular, hydrological recorded data show nonstationary (as increasing or decreasing trends) and the possibility of severe flood events is increasing (Kiang et al., 2011; Machado et al 2015; Yan et al., 2017; Serago & Vogel, 2018). Therefore, the assumption of stationarity which has been made so far in assessment of climatic events is now being challenged. Accordingly, numerous studies with different approaches have been conducted to assess the effect of nonstationary in hydrologic extremes such as trend Analysis (e.g. Wi et al., 2016, Agilan & Umamahesh, 2017, Westra et al., 2013, Cheng et al., 2014), frequency analysis and concept of return level and return period where the parameters of a given distribution vary with time (e.g. Cooley, 2013, Obeysekera & Salas, 2016; Cheng et al., 2014).

Estimating flood frequency, quantifying the risk of flooding and presenting flood risk maps, directly depend on estimation of flood return-periods and return levels.

This paper first investigates the behavior of the GEV distribution to estimate the annual daily maximum precipitation and annual daily maximum discharge return level using MLE method, secondly, assessing their relative impacts on flood and the confidence interval widths.

### **2 Study area and data**

Bikeland, is a region in Aust Agder, Norway and is located beside Tovdal river. On 12 September 2017, this region experienced its worst flood for over 100 years. Two different data series were collected and the extreme value statistics for frequency analysis of extreme precipitation and extreme discharge were performed on them. The analyses were based on the data series of daily precipitation recorded at Senumstad, and daily river discharge recorded at Flaksvatn, Aust Agder, Norway. The data for the stations were obtained from the Norwegian Water

Resources and Energy Directorate website (NVE) and Norwegian Meteorological Institute. Table 1 summarizes data of the considered stations also annual maxima values for each station are plotted in the Figure 1.

**Table 1. Stations' Information**

Station	Location		Operation type	Dataset period	Data source
	x	y			
Flaksvatn	102562	6485578	Daily discharge (m <sup>3</sup> s <sup>-1</sup> )	1900-2018	www.nve.no
Senumstad	108446	6495230	Daily precipitation (mm)	1972-2018	www.eklima.met.no

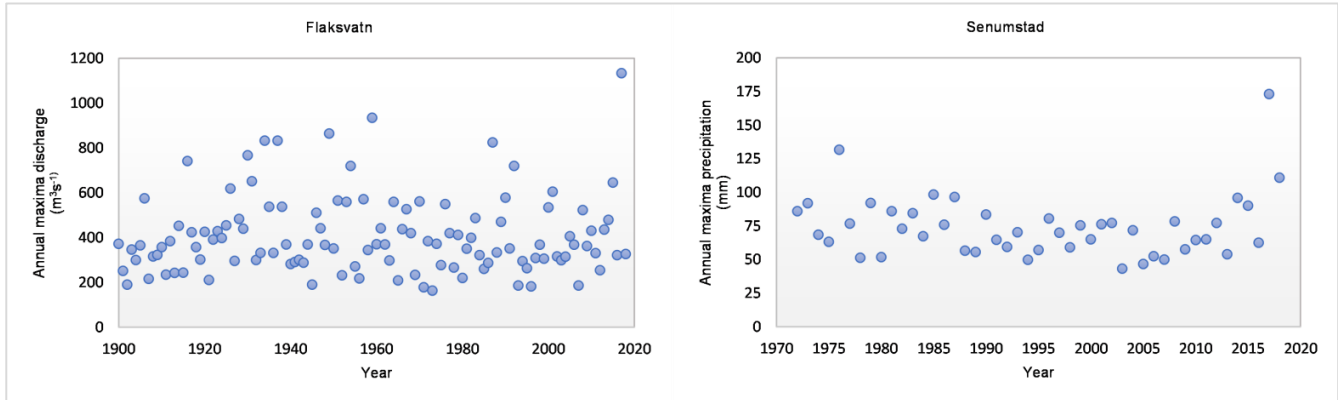


**Figure 1.** Annual maximum daily discharge and precipitation for Flaksvatn and Senumstad stations, respectively

### 3 Methods

#### 3.1 Extreme Value Theory

The Generalized Extreme Value (GEV) distribution was introduced into meteorology by Jenkinson (1955). The GEV approach is widely employed to model extremes in the environmental sciences specifically, hydrologic processes such as floods (Vogel et al., 2011, Durocher et al., 2018) and precipitation (Gellens, 2002, Vasiliades et al., 2015). The analysis of extremes in hydrometeorological data, such as the annual or monthly maxima in precipitation and discharge series, is fundamental for the design of engineering structures (Maidment, 1993).

The GEV distribution is a generalization of three extreme value distributions, including Fréchet, Weibull, and Gumbel and can be combined into a single distribution as Eq. [1]. The GEV distribution depends on three parameters: location ( $\mu$ ), scale ( $\sigma$ ), and shape ( $\xi$ ) and can be fitted to environmental time series of extreme values such as annual maxima.

$$F(x, \mu, \sigma, \xi) = \exp \left\{ - \left[ 1 + \xi \left( \frac{x - \mu}{\sigma} \right) \right]^{-1/\xi} \right\} \quad [1]$$

The location parameter specifies the center of the distribution, the scale parameter gives an indication of the size of deviations around the location, and the shape parameter governs the tail behavior of the GEV distribution.

The block maxima approach is predicated upon the Extremal Types Theorem. By supposing  $X_1, X_2, \dots, X_n$  as a sequence of independent random variables from a common distribution function  $F$ , the statistic order of interest is  $M_n = \max$ , namely, the maximal value of the independent identically distributed (i.i.d.) random variables. Here,  $X_i$  represents the daily discharge (m<sup>3</sup>s<sup>-1</sup>) and daily precipitation amount (mm) and  $n$  the number of observations during a specific time period, so that  $M_n$  is the annual maximum.

In a nonstationary GEV distribution, the GEV parameters can be expressed as various forms of time-dependent function. In this study, the location and scale parameters are expressed as a linear function of time ( $t$ ), as represented by Eq. [2] and [3], respectively. It can simply present the increasing or decreasing trend of the location and scale parameters interrelated with the mean and variance of the observed data.

$$\mu(t) = \beta_0 + \beta_1 t \quad [2]$$

$$\sigma(t) = \exp(\sigma_0 + \sigma_1 t) \quad [3]$$

The location parameter varies linearly with time, whereas the scale parameter varies exponentially with time since it is greater than zero (Coles, 2001). For the GEV model, it is difficult to estimate the shape parameter precisely (Coles, 2001). Therefore, this study assumes the shape parameter to be constant over time.

Table 2. Applied stationary and nonstationary GEV models.

Model	Name	Location parameter $\mu$	Scale parameter $\sigma$	Shape parameter
Stationary	GEV(0,0,0)	$\mu$	$\sigma$	$\xi$
Non-stationary	GEV(1,0,0)	$\mu_0 + \mu_1 t$	$\sigma$	$\xi$
Non-stationary	GEV(0,1,0)	$\mu$	$\exp(\sigma_0 + \sigma_1 t)$	$\xi$
Non-stationary	GEV(1,1,0)	$\mu_0 + \mu_1 t$	$\exp(\sigma_0 + \sigma_1 t)$	$\xi$

### 3.2 Return period

#### 3.2.1 Return Periods and Return Levels Under Stationarity

In many disciplines, return levels and return periods are used to describe and quantify risk Cooley, 2013. Classical methods assume a stationary climate to determine the return period and risk of extreme events. In other words, in this method the occurrences of extremes are independent, and the events arise from a stationary distribution. Nevertheless, recent studies have shown that climate change has accelerated over the past few decades and that climate will continue to change in the coming decades primarily due to anthropogenic modifications of the Earth's atmosphere Solomon, 2007. Consequently, to meet and satisfy safety requirements there is growing interest to consider and account for non-stationarity when assessing risk. the assumption of stationarity climate has pervaded concepts of return level and return period. Under stationary assumption, assume:  $\{X_t\}$  as a time series for a random future annual maximum extreme event,  $M_y$  as random variable representing the annual maximum for year  $y$ , which has a distribution function (F). Given a return period of interest  $T$ , we can solve the equation

$$F(r_t) = p(M_y < r_t) = 1 - \frac{1}{T} \quad [4]$$

In which,  $r_t$ , indicates the associated return level. Then using the notion of the return period as expected waiting time, an annual no exceedance probability, can be expressed as:  $F_X(x) = 1 - P(X > x)$ , and subsequently the design quantile for a return period  $T$  is readily determined by inverting  $F_X(X)$ , where  $P(X > x)$  is the exceedance probability. Under stationarity,  $P$  remains constant every year at a particular location, and the return period ( $T$ ) can be interpreted as the average recurrence interval between extreme events (Cooley, 2013), following a geometric distribution with probability mass function (pmf) given by Eq. [5]:

$$f(t) = P(T = t) = \left(1 - \frac{1}{T}\right)^{t-1} \frac{1}{T} \quad [5]$$

#### 3.2.2 Return Periods and Return Levels Under Non-stationarity

Olsen et al., 1998, interpreted return period as the expected waiting time until an exceedance occurs and computed an  $T$ -year return level for non-stationary time series and compare this to the  $1/T$  probability-of-exceedance level. Under non-stationary assumptions, this definition can be extended. Therefor for a known design flood event ( $x=0$ ),  $X$  is defined as the waiting time until the event reoccurs for the first time, the probability for  $X=x$  can be expressed as follows (Eq. [6]),

$$P(X = x) = P_x \prod_{i=1}^{x-1} (1 - P_i), x = 1, 2, \dots \quad [6]$$

Then, the expected return period  $T$  of the design event can be denoted as Eq. [7]:

$$T = E(X) = \sum_{x=i}^{\infty} x P_x \prod_{i=1}^{x-1} (1 - P_i) = 1 + \sum_{x=i}^{\infty} \prod_{i=1}^x (1 - P_i) \quad [7]$$

The other definition of return period is that the expected number of events in  $T$  years is one. For a period of  $T$  years,  $N$  is the number of the design events, the expected value of which is calculated by Eq. [8],

$$E(N) = \sum_{i=1}^T E(I(P_i)) = \sum_i^T P_i \quad [8]$$

Where "i" is an indicator variable. The expected number of events return period  $T$  is obtained by setting Eq. equal to 1, as follows (Eq. [9]),:

$$1 = \sum_i^T P_i \quad [9]$$

## 4 Results

### 4.1 Return level under stationary conditions

Understanding the behavior of the return level under stationary and non-stationary conditions is essential for hydrologic processes. In this section, we analyze the behavior of return level under stationary condition and its dependence on time ranges. Using equation [4] and different data sets, the return levels for different return points were calculated and results are displayed in Table 3 and Figure 2. We considered 7 time periods for Flaksvatn station and 3 time periods for Senumstad station to calculate maximum flow discharge and maximum precipitation. Results show that the maximum values for both stations were obtained for the recent 20 years and according to the Table 3 there is a considerable difference between maximum and minimum discharge and also precipitation values for each return level.

Table 3. Stationary return levels

Station	Data type	Time period	Duration (year)	50-year level	100-year level	200-year level	500-year level
Flaksvatn	Annual daily maximum discharge ( $m^3s^{-1}$ )	1900-2018	119	915.31	1056.44	1210.39	1435.97
		1919-2018	100	934.86	1074.04	1224.23	1441.59
		1939-2018	80	913.21	1056.13	1212.37	1441.91
		1949-2018	70	954.97	1107.75	1275.13	1521.68
		1969-2018	50	884.37	1020.89	1169.59	1387.14
		1989-2018	30	942.71	1097.75	1269.25	1524.69
		1999-2018	20	958.52	1119.01	1298.90	1571.01
Senumstad	Annual daily maximum precipitation (mm)	1972-2018	47	137.67	155.21	174.26	202.08
		1989-2018	30	136.67	157.24	180.56	216.38
		1999-2018	20	158.08	187.62	222.53	278.67

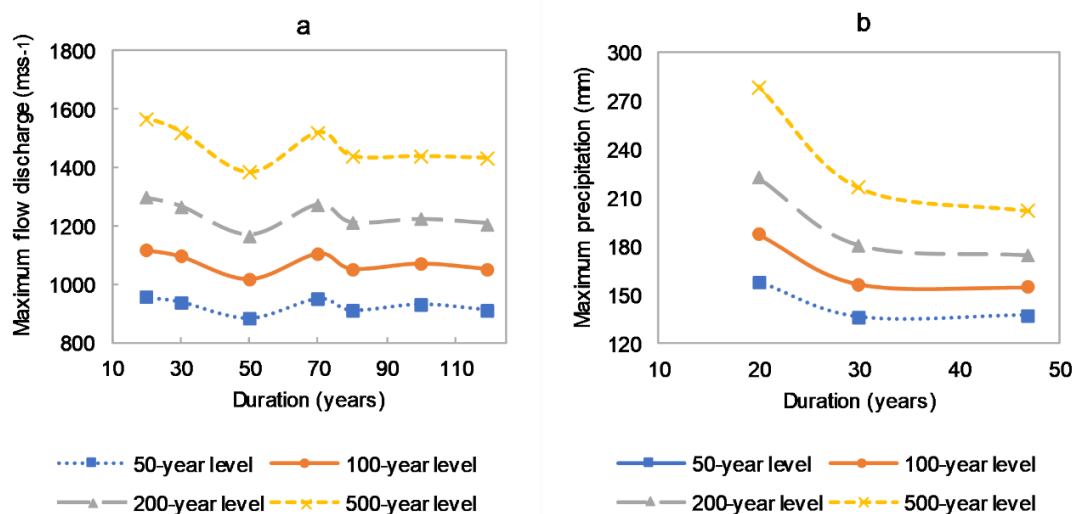


Figure 2. Stationary return levels: a) annual maximum daily discharge at Flaksvatn station; b) annual maximum daily precipitation at Senumstad station

Results from Figure 2 indicate that in both data sets, the return level is highly dependent on the time span. It can be seen that, for long data sets (more than 50 years) there is not a regular pattern and the values vary depending on the length of the data record (Figure 2a). For shorter and more recent data sets (less than 50 years, i.e. starting in the 70's last century) an increasing trend can be detected in both the discharge and precipitation, which may indicate the presence of climate change.

## 4.2 Return level under non-stationary conditions

### 4.2.1 Trend analysis

The widely used nonparametric test Mann–Kendall test is used in this study, to evaluate the presence of monotonic trends in the annual maximum series. The Mann–Kendall analysis was conducted using the R package “Kendall”



(McLeod, 2005). The results of the test with selected periods of annual maximum precipitation and annual maximum discharge series in Senumstad and Flaksvatn, respectively, are given in Table 4.

Table 4. Mann-Kendall test results

Data set	Tau	p-value
Flaksvatn 119	0.016	0.793
Flaksvatn 50	0.133	0.175
Flaksvatn 30	0.140	0.284
Flaksvatn 20	0.158	0.346
Senumstad 47	-0.074	0.460
Senumstad 30	0.200	0.124
Senumstad 20	0.337	0.040

In Table 4, the T value of the M-K test is similar to the correlation coefficient, and its value varies from -1 to 1 (i.e. positive values indicate increasing trend, and negative ones indicate decreasing trend (Agilan & Umamahesh, 2017). For Senumstad station, with 20-year period the two-sided p-value given in Table 4, confirms the presence of a trend at the 5 % significance level, but results did not show a trend for Flaksvatn station.

#### 4.2.2 Stationary and Nonstationary Model analyses

The purpose of a trend test is to determine whether the time series has a general increase or decrease. However, increasing or decreasing behavior of the series does not always indicate non-stationarity (Yilmaz et al., 2014). Moreover, the results of the M-K test (shown in the previous section) are contradictory to the increasing trend observed in the stationary analysis for shorter data sets (Figure 3). Therefore, in this section, this issue will be investigated in more detail by conducting nonstationary extreme value analyses. For this purpose four models were developed, namely: (1) stationary model with constant parameters GEV (0,0,0); (2) non-stationary model with time varying location parameter GEV (1,0,0); (3) non-stationary model with time varying scale parameter GEV (0,1,0), and (4) non-stationary model with time varying location and scale parameters GEV (1,1,0). These models were applied to the 7 data sets presented in Table 5. The estimated parameters and goodness-of-fit results are listed in Table 5. The R-package extRemes (Gilleland & Katz, 2016) was used to fit the nonstationary GEV model and the resulting parameters.

The models with minimum AIC values were selected (model rank equal to 1) as best-fitted models. Many studies recommend the Akaike's information criterion (AIC), corrected Akaike's information criterion (AICc), and Bayesian information criterion (BIC) for the selection of probability distribution models (Cannon & geosciences, 2011; Sugahara et al., 2009; Villarini et al., 2009). Kim et al., 2017, performed Monte Carlo simulations to compare the performances of these three tests, with regard to nonstationary as well as stationary GEV distributions. They concluded that for relatively small sample sizes, in case of stationarity, the BIC performance is better and in case of nonstationary, the AIC proved to be better than the other two methods. In this study AIC and BIC tests are used to evaluate the goodness of fit.

Table 5. Estimated parameters and goodness-of-fit results

ID	Models	location	scale	shape	AIC	BIC	Model Rank
1	Flaksvatn119						
	GEV(0,0,0)	324.186	116.335	0.130	1531.457	1531.457	1
	GEV(1,0,0)	324.0439-0.007t	116.064	0.131	1533.454	1544.571	3
	GEV(0,1,0)	323.6	exp(4.684+0.001t)	0.132	1533.153	1544.269	2
2	Flaksvatn50						
	GEV(0,0,0)	310.133	113.492	0.128	644.233	652.970	2
	GEV(1,0,0)	270.467+1.5877t	109.469	0.144	643.712	651.360	1
	GEV(0,1,0)	311.488	exp(4.809-0.003t)	0.146	646.047	653.695	4
3	Flaksvatn30						
	GEV(0,0,0)	320.565	117.313	0.149	391.4995	395.7031	1
	GEV(1,0,0)	280.927+2.757t	113.703	0.170	392.129	397.734	2
	GEV(0,1,0)	323.882	exp(4.872 -0.007t)	0.171	393.317	398.922	3
4	Flaksvatn20						
	GEV(1,1,0)	280.330+2.681t	exp(4.736-0.001t)	0.173	394.123	401.129	4
	GEV(0,0,0)	339.774	111.995	0.168	261.822	264.809	1

	GEV(1,0,0)	321.977+1.946t	112.219	0.164	263.636	267.619	3
	GEV(0,1,0)	337.106	exp(4.313+0.039t)	0.103	263.0251	267.008	2
	GEV(1,1,0)	321.113+2.122t	exp(0.038+0.038t)	0.099	264.842	269.820	4
5	Senumstad47						
	GEV(0,0,0)	63.622	14.715	0.125	413.682	419.233	1
	GEV(1,0,0)	68.333-0.198t	14.370	0.141	414.348	421.748	2
	GEV(0,1,0)	63.994	exp(2.518+0.006t)	0.122	415.037	422.437	3
	GEV(1,1,0)	67.817-0.172t	exp(2.555+0.004t)	0.125	416.050	425.300	4
6	Senumstad30						
	GEV(0,0,0)	60.485	13.251	0.187	262.0367	266.2403	3
	GEV(1,0,0)	58.33+0.154t	13.341	0.170	263.845	269.450	4
	GEV(0,1,0)	60.154	exp(1.866+0.046t)	-0.002	258.827	264.431	1
	GEV(1,1,0)	58.545+0.179t	exp(1.874+0.046t)	-0.005	260.478	267.484	2
7	Senumstad20						
	GEV(0,0,0)	60.510	14.940	0.245	182.870	185.858	3
	GEV(1,0,0)	48.840+1.1286t	13.0474	0.356	181.746	185.729	2
	GEV(0,1,0)	60.707	exp(1.8305+0.10358t)	-0.279	181.102	185.085	1
	GEV(1,1,0)	61.527-0.125t	exp(1.798+0.108t)	-0.301	183.094	188.073	4

The small differences in ACI values for all the models within each data set (Table 5) unable any definitive conclusion about which model is better and if there is a clear signal of nonstationary. Nevertheless, it can be seen that even if trend analyses did not show any significant trend in Flaksvatn and Senumstad data sets, the results displayed in Table 5, indicate that in some cases nonstationary models adjust slightly better than the stationary model.

#### **Uncertainty in the return levels**

Since the comparison between stationary and nonstationary models does not allow to reach definitive conclusions, it is important to access the impact of adopting each of those models in the return levels. This will allow an estimation of the uncertainty arising from possible effects of climate change.

Using Eqs. [1], [4] and [9], the return levels for 100 year flood were calculated for stationary and all nonstationary models. The results are presented in Figure 3, where the stationary model results are shown along with the best model (according to the AIC values in Table 5) marked with a \*, and with envelop curves of the maximum and minimum values of all models' results.

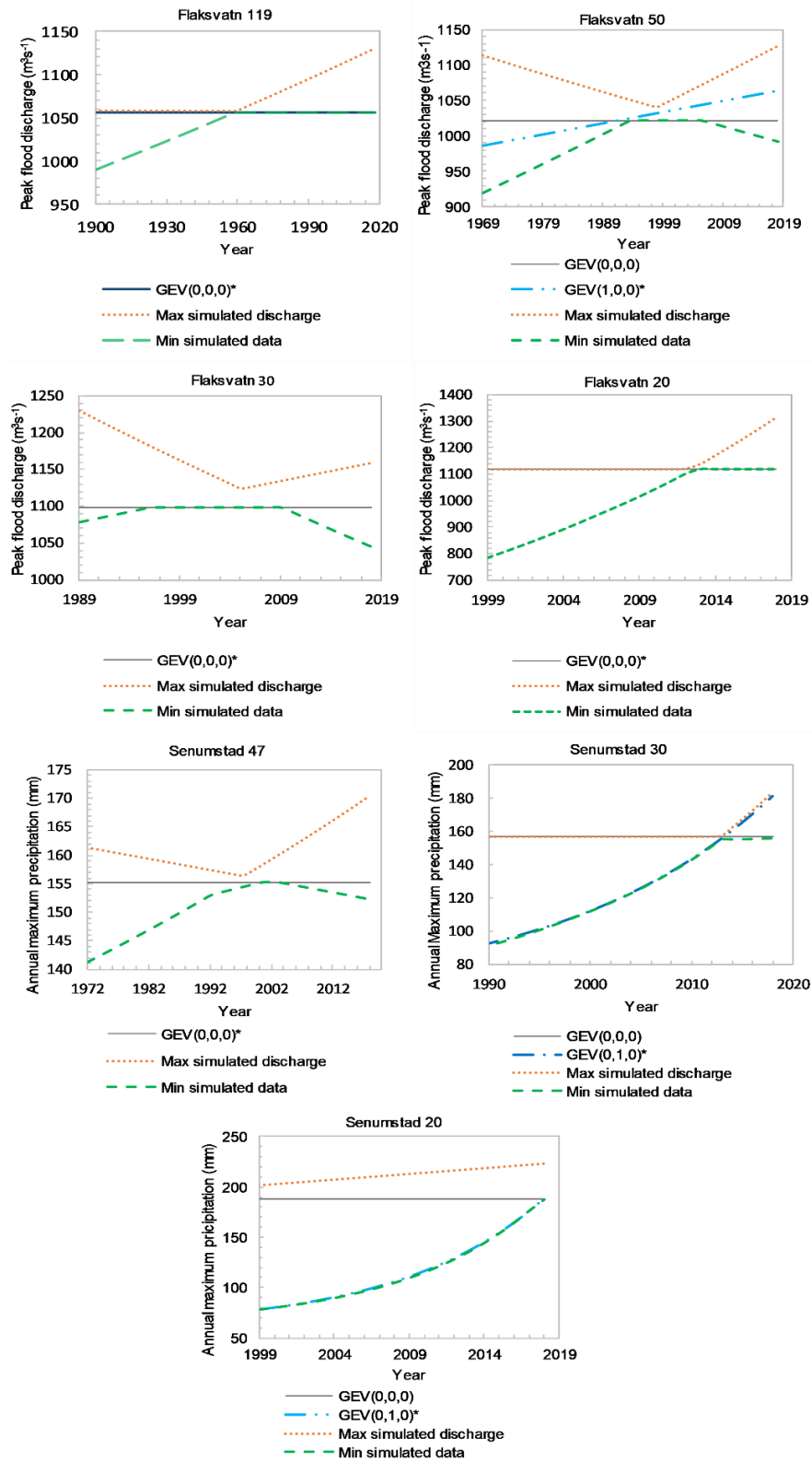


Figure 3. 100 year return level along all data sets. Stationary model, best fitted model (marked with \*) and maximum and minimum envelop curves for all models results

The results show significant differences on the maximum and minimum return levels given by the different models. Those differences are also dependent on the year where the 100 year flood is being computed, which is a consequence of using a simple linear function of time for GEV distribution parameters (see Eqs. [2] and [3]). Here we will focus on the results obtained for the most recent year (2018).

The results illustrate that the maximum difference between stationary model and nonstationary models in 2018, varies between [1056.44, 1129.67] for Flaksvatn 119, [991.16, 1127.31] for Flaksvatn 50, [1045.85, 1158.11] for Flaksvatn 30 and [1119.01, 1315.88] for Flaksvatn 20. The largest difference between the maximum and minimum discharge relates to Flaksvatn 20 and the smallest is computed for Flaksvatn 119. The same analyses were performed for Senumstad station rendering: Senumstad 47: [152.25, 170.96], Senumstad 30: [156.26, 183.60], Senumstad 20: [187.62, 223.27]. According to the reported values, the largest and the smallest band width resulted from Senumstad 20 and Senumstad 47, respectively. It can be concluded that non-stationary models can result in return values larger or smaller values than stationary models. Therefore, it is safer to use stationary and nonstationary models, selecting the maximum return value of all models.

## 5 Conclusion and discussion

Present study, used 119 years annual daily maximum discharge data and 47 years annual daily maximum precipitation to analyze the effect of climate change on flood return level. The analyses were based on the application of two complementary statistical methods: (1) The Mann-Kendall trend test to detect possible trends (2) A non-stationary GEV model with time varying location and scale parameters. Four GEV models were developed and their performance were compared. Main results of this paper are as follows:

- The estimated stationary return levels for the time period between 1970-2018 is larger than those return levels that are corresponding to the time period before 1970. (1900-1970).
- Despite the results of trend analyses that did not show any trend, there was evidence of nonstationary in some data sets according to statistical values.
- There is a considerable difference between nonstationary and stationary return levels, and it would be more safe to use different models before selecting a return level for design processes.

This research used only two stations, further analyses should be performed using more stations. Also the nonstationary effect is complicated and many other influencing parameters (such as: temperature, emission scenarios,...) should be considered for developing covariates.

## REFERENCES

- Agilan, V., & Umamahesh, N. J. I. J. o. C. (2017). Modelling nonlinear trend for developing non-stationary rainfall intensity–duration–frequency curve. 37(3), 1265-1281.
- Cannon, A. J. J. C., & geosciences. (2011). GEVcdn: an R package for nonstationary extreme value analysis by generalized extreme value conditional density estimation network. 37(9), 1532-1533.
- Cheng, L., AghaKouchak, A., Gilleland, E., & Katz, R. W. J. C. c. (2014). Non-stationary extreme value analysis in a changing climate. 127(2), 353-369.
- Cooley, D. (2013). Return periods and return levels under climate change. In *Extremes in a changing climate* (pp. 97-114): Springer.
- Durocher, M., Burn, D., Mostofi Zadeh, S., & Ashkar, F. (2018). *Nonstationary index-flood models for threshold-Based methods: from threshold modeling to nonstationary return period*. Paper presented at the AGU Fall Meeting Abstracts.
- Gellens, D. J. J. o. H. (2002). Combining regional approach and data extension procedure for assessing GEV distribution of extreme precipitation in Belgium. 268(1-4), 113-126.
- Gilleland, E., & Katz, R. W. J. J. o. S. S. (2016). extRemes 2.0: An extreme value analysis package in R. 72(8), 1-39.
- Kiang, J. E., Olsen, J. R., & Waskom, R. M. J. J. o. t. A. W. R. A. (2011). Introduction to the Featured Collection on “Nonstationarity, Hydrologic Frequency Analysis, and Water Management” 1. 47(3), 433-435.

- Kim, H., Kim, S., Shin, H., & Heo, J.-H. J. J. o. h. (2017). Appropriate model selection methods for nonstationary generalized extreme value models. *547*, 557-574.
- Maidment, D. R. (1993). *Handbook of hydrology* (Vol. 9780070): McGraw-Hill New York.
- McLeod, A. I. J. R. P. K. (2005). Kendall rank correlation and Mann-Kendall trend test.
- Obeysekera, J., & Salas, J. D. J. J. o. H. E. (2016). Frequency of recurrent extremes under nonstationarity. *21*(5), 04016005.
- Olsen, J. R., Lambert, J. H., & Haines, Y. Y. J. R. A. (1998). Risk of extreme events under nonstationary conditions. *18*(4), 497-510.
- Serago, J. M., & Vogel, R. M. J. A. i. w. r. (2018). Parsimonious nonstationary flood frequency analysis. *112*, 1-16.
- Solomon, S. (2007). *IPCC (2007): climate change the physical science basis*. Paper presented at the AGU Fall Meeting Abstracts.
- Sugahara, S., Da Rocha, R. P., & Silveira, R. J. I. J. o. C. A. J. o. t. R. M. S. (2009). Non-stationary frequency analysis of extreme daily rainfall in Sao Paulo, Brazil. *29*(9), 1339-1349.
- Vasiliades, L., Galiatsatou, P., & Loukas, A. J. W. R. M. (2015). Nonstationary frequency analysis of annual maximum rainfall using climate covariates. *29*(2), 339-358.
- Villarini, G., Serinaldi, F., Smith, J. A., & Krajewski, W. F. J. W. R. R. (2009). On the stationarity of annual flood peaks in the continental United States during the 20th century. *45*(8).
- Vogel, R. M., Yaindl, C., & Walter, M. J. J. o. t. A. W. R. A. (2011). Nonstationarity: Flood Magnification and Recurrence Reduction Factors in the United States 1. *47*(3), 464-474.
- Westra, S., Alexander, L. V., & Zwiers, F. W. J. J. o. C. (2013). Global increasing trends in annual maximum daily precipitation. *26*(11), 3904-3918.
- Wi, S., Valdés, J. B., Steinschneider, S., Kim, T.-W. J. S. e. r., & assessment, r. (2016). Non-stationary frequency analysis of extreme precipitation in South Korea using peaks-over-threshold and annual maxima. *30*(2), 583-606.
- Yan, L., Xiong, L., Guo, S., Xu, C.-Y., Xia, J., & Du, T. J. J. o. H. (2017). Comparison of four nonstationary hydrologic design methods for changing environment. *551*, 132-150.
- Yilmaz, A., Hossain, I., Perera, B. J. H., & Sciences, E. S. (2014). Effect of climate change and variability on extreme rainfall intensity–frequency–duration relationships: a case study of Melbourne. *18*(10), 4065-4076.



**Paper III:** Representation of 100-year design rainfall uncertainty in catchment-scale flood modeling: A MCMC Bayesian approach

Alipour, S.M., Engeland, K., Leal, J., 2021b. Representation of 100-year design rainfall uncertainty in catchment-scale flood modeling: A MCMC bayesian approach. [VANN](#), 04.





# Representation of 100-year design rainfall uncertainty in catchment-scale flood modeling: A MCMC bayesian approach

By Saba Mirza Alipour, Kolbjørn Engeland and Joao Leal

Saba Mirza Alipour is a Ph.D research fellow at Department of Engineering and Science, University of Agder.

Kolbjørn Engeland is a researcher at Norwegian Water Resources and Energy Directorate (NVE).

Joao Leal is a professor at Department of Engineering and Science, University of Agder.

## Sammendrag

*Representasjon av usikkerhet i 100-års nedbøren for flommodellering på nedbørfelt-skala: En MCMC tilnærming.* Usikkerheter knyttet til estimering av nedbørmengder er en av de viktigste kildene til usikkerhet i flommodellering. Representasjon av disse usikkerhetene kan være utfordrende på grunn av ufullstendige historiske data, klimaendringer og værets stokastiske natur. I denne studien ble det brukt en Bayesiansk tilnærming med forkunnskaper om formparameteren for å tilpasse den generelle ekstremverdi (GEV) -fordelingen til årlige maksimalverdier for døgnnedbør. Metoden ble brukt for forskjellige datasett (stasjonsbaserte data, feltbaserte data og griddede data). Til slutt ble det valgt et konfidensintervall for 100-års nedbøren for hele nedbørfeltet. Resultatene illustrerer en betydelig forskjell i de beregnede konfidensintervallene avhengig av om man gjør en lokal analyse med stasjonsbaserte data, eller en analyse på nedbørfelt-skala med feltbaserte data eller griddede data. Funnene viser også at konfidensintervallene kan endres betydelig avhengig av den valgte perioden for analysene. Ingen signifikante trender i ekstremnedbør ble identifisert.

## Summary

Uncertainties associated with the estimation of design rainfall is one of the major sources of uncertainty in flood modelling. Representation of these uncertainties can be challenging due to the incomplete historical data, climate change effect and the stochastic nature of the weather. In this study, a Bayesian inference with prior knowledge about the shape parameter was applied to fit the Generalised Extreme Value (GEV) distribution for annual maximum rainfall data. The method was used for different data sets (station-based data, catchment-based data, and gridded data) and finally, a range was selected as a 100-year design rainfall as the catchment precipitation. The results illustrate a considerable difference in the calculated ranges resulting from local scale analyses (station-based data) and catchment scale analysis (catchment-based and gridded data). The findings also show that the confidence intervals of the quantiles can considerably change depending on the selected period for the analyses. No significant trends in extreme precipitation were found.

## Introduction

Estimation of design rainfall over a catchment area is an important task in engineering practice related to water resources and flood management. However, due to the complex and chaotic nature of weather and precipitation generating processes, there is a considerable degree of uncertainty in the design rainfall estimates. This uncertainty will, in subsequent steps, contribute to uncertainty in design flood estimates, flood zone mapping and flood risk assessments. Assessing uncertainty in design rainfall estimates is therefore an important task. Uncertainty sources for design rainfall estimates are the limited sample size, the aggregation of design rainfall from point measurements to the catchment scale, and climate variability and trends. The sample uncertainty is explained by the limited sample size, i.e., we need to estimate a design rainfall of 200 years return period based on much less than 200 years of data. The estimated design precipitation will therefore, in many cases, be higher than any observed precipitation. The actual areal precipitation is unknown since the precipitation is measured in gauges. The uncertainty in estimated areal rainfall depends on the spatial variability of the precipitation events that generate the extreme events. Convective precipitation with a high spatial variability dominates in small catchments whereas stratiform precipitation dominates in larger catchments. Relatively small catchments far away from precipitation gauges have therefore the largest uncertainty in design rainfall estimates. The design rainfall for a catchment area will be smaller than the design rainfall for a point. Therefore, in engineering, area reduction factors (ARFs) are used to adjust design values from point measurements to the catchment area. Climate trends and changes introduce an additional challenge since the basic assumption of stationarity is no longer fulfilled resulting in a design rainfall that is time dependent.

A large and growing body of literature has investigated different approaches and methods to estimate design rainfall. The most widely used methods is based on fitting a probability distri-

bution to annual maxima data. Extreme Value theory shows that the Generalized Extreme Value (GEV) distribution is the asymptotic distribution for maxima extracted from sufficient large blocks of data (Fisher and Tippett, 1928, Coles, 2001). The GEV distribution is therefore a good approximation for the maxima of long, but finite, sequences of random variables, such as annual rainfall maxima (Pelosi et al., 2020). In addition to the basic form of GEV distribution, the GEV model is applied in other forms such as mixed GEV distribution to account for different flood generating processes (e.g., Kedem et al., 1990, Yoon et al., 2013) and nonstationary GEV distribution (e.g., Cunderlik and Burn, 2003, Leclerc and Ouarda, 2007, Agilan and Uma-mahesh, 2017). As mentioned before, the nonstationary GEV models are applied to non-stationary time series (i.e., series with statistical properties varying in time due to changes in the dynamic system) to reflect the effect of long-term climate change on a phenomenon. In the nonstationary case, the parameters of the model are expressed as a function of time  $t$  and possibly other covariates as well (Coles, 2001). Different examples of nonstationary GEV models can be found in the works conducted by Khaliq et al. (2006), Cannon (2010), Um et al. (2017) and Ouarda and Charron (2019). One important and influencing part in GEV modeling process is the length of time series. Ideally the longer time series are selected to fit the GEV distribution and for the shorter records ISO standard ISO 19901-1 recommends to not use return periods more than a factor of four beyond the length of the data set (e.g., for the data covering a period of 30 years, the longest return periods that should be investigated is 120 years) (Vanem, 2015). However, DeGaetano and Castellano (2018) showed that the use of long, nonstationary precipitation records has the potential to yield precipitation-frequency estimates that are not representative of the current (or future) extreme rainfall climatology.

When estimating design rainfall, we need to estimate the parameters of the GEV distribution

so that it gives the best possible fit to the observed data. Typical estimators are ordinary moments (OM), L-moments (LM), Maximum likelihood (ML), generalized maximum likelihood (GML) and Bayesian approaches. A comparative study of performance of different estimators can be found in the works presented by Martins and Stedinger (2000) and Kobierska et al. (2018). In most applications the l-moments, GML or Bayesian approaches are recommended since they are robust with respect to outliers and either explicitly or implicitly apply constraints on the shape parameter. Bayesian approach is now widely used for inference (e.g., Yan and Moradkhani, 2016, Lima et al., 2018, Lutz et al., 2020). Some important advantages of the Bayesian methods are (i) the possibility to set prior information (i.e., on the shape parameter) (ii) the uncertainty in design flood estimates can easily be extracted and (iii) it is easy to introduce and make inference for non-stationary models. Many studies have proposed the Bayesian framework as a satisfactory method to estimate confidence intervals for flood quantiles (e.g., Martins and Stedinger, 2000, Renard et al., 2006, Lima et al., 2016, Lima et al., 2018). The Bayesian approach is also recommended by the Norwegian meteorological institute (Lutz et al., 2020).

Estimation of design rainfall over an area/catchment, is one of the subjects that has received considerable attention in recent years. This issue is particularly important for rainfall-runoff modeling of extreme hydrometeorological events. There is a large volume of published studies describing methods to transfer local/station measurements to larger scales such as catchment scale. Among the proposed methods, Area Reduction Factors (ARFs), are widely used to convert estimates of extreme point rainfall to estimates of extreme area-averaged rainfall (Wright et al., 2014). The design precipitation for a catchment area will decrease with increasing catchment area due to the spatial averaging of precipitation and the transition from convective to stratiform precipitation as the most relevant extreme precipitation generating process. The target duration of extreme precipitation will

also depend on catchment size. In Svensson and Jones (2010), different methods for estimating the ARF were critically reviewed. They reported that there is no obvious preferred method for estimating extreme areal precipitation.. Dyrddal (2012) provided a summary of existing methodology applied by the Norwegian Meteorological Institute (MET Norway) for estimating extreme precipitation in station sites and catchments in Norway. She found that existing methods are laborious and outdated, and proposed a grid-based methodology as an alternative to using ARFs. An example of grid based methodology where the annual maximum area rainfall is extracted from gridded precipitation data is applied in Dyrddal et al. (2016). They conclude that using a grid-based approach is efficient, and more objective than station-based methods combined with ARFs. However, the grid-based estimates are generally lower than the station-based estimates that use ARFs.

In this study we want to demonstrate how the choice of approach affects the design precipitation estimates for one catchment in southern Norway. The main goal of this study is to estimate 100-year rainfall for a catchment with several precipitation stations inside or in the proximity (described in next section) with the associated uncertainty using both stations based and grid-based approaches. We compared estimates using three different approaches i) use annual maxima for each station (experiment 1), ii) the estimates from the previous step are combined to establish a mixture distribution (experiment 2) and iii) use annual maxima from catchment average precipitation extracted from gridded precipitation data (experiment 3). In (i) and (ii) ARF were used to get the catchment design rainfall. For all approaches, a Bayesian methodology was used to estimate the design rainfall and the associated uncertainty.

In addition to the proposed procedure, this paper aims to highlight the importance of time series length by comparing the estimated design rainfalls for different periods in the same station.

## Study area

The study catchment is upstream the gauging station Flaksvatn in Tovdalselva river, located in Agder province (Norway) (Fig. 1). The catchment area is 1867 km<sup>2</sup>. The mean annual precipitation in the catchment is approximately 1260 mm, with most of the rainfall occurring between October and March (about 60%) (Data collected from <http://nevina.nve.no/>). On 02.10.2017, an extreme flood event occurred in the downstream parts of the river and inundated Birkeland city that is located beside this river. This event was the highest ever recorded flood in this river. The information of this event,

measured at Flaksvatn station and Senumstad station (Fig. 1), is presented in Table 1.

## Data

Annual maximum daily rainfall data recorded from 6 stations operated by the Norwegian meteorological institute were collected from SeKlima.met.no. Information about the stations is listed in Table 2 and their locations on the map are displayed in Fig. 2. Two stations, namely Herefoss and Rislå have been relocated (about 500 m and 700 m respectively) and are now operating as Herefoss and Senumstad stations. (The Meteorological institute has established

Table 1. Summary of the recorded data of the flood event in the study area. Discharge and precipitation data belong to Flaksvatn and Senumstad stations, respectively. The max discharge 30.09 and 01.10 were observed at 23:00, whereas the 02.10, the discharge culminated at 09:00

Date	Rainfall (mm)	Max Water level (m)	Max Discharge (m <sup>3</sup> .s <sup>-1</sup> )
30.09.2017	45.1	21.40	501.3
01.10.2017	173.1	24.57	1062
02.10.2017	63.6	25.56	1195

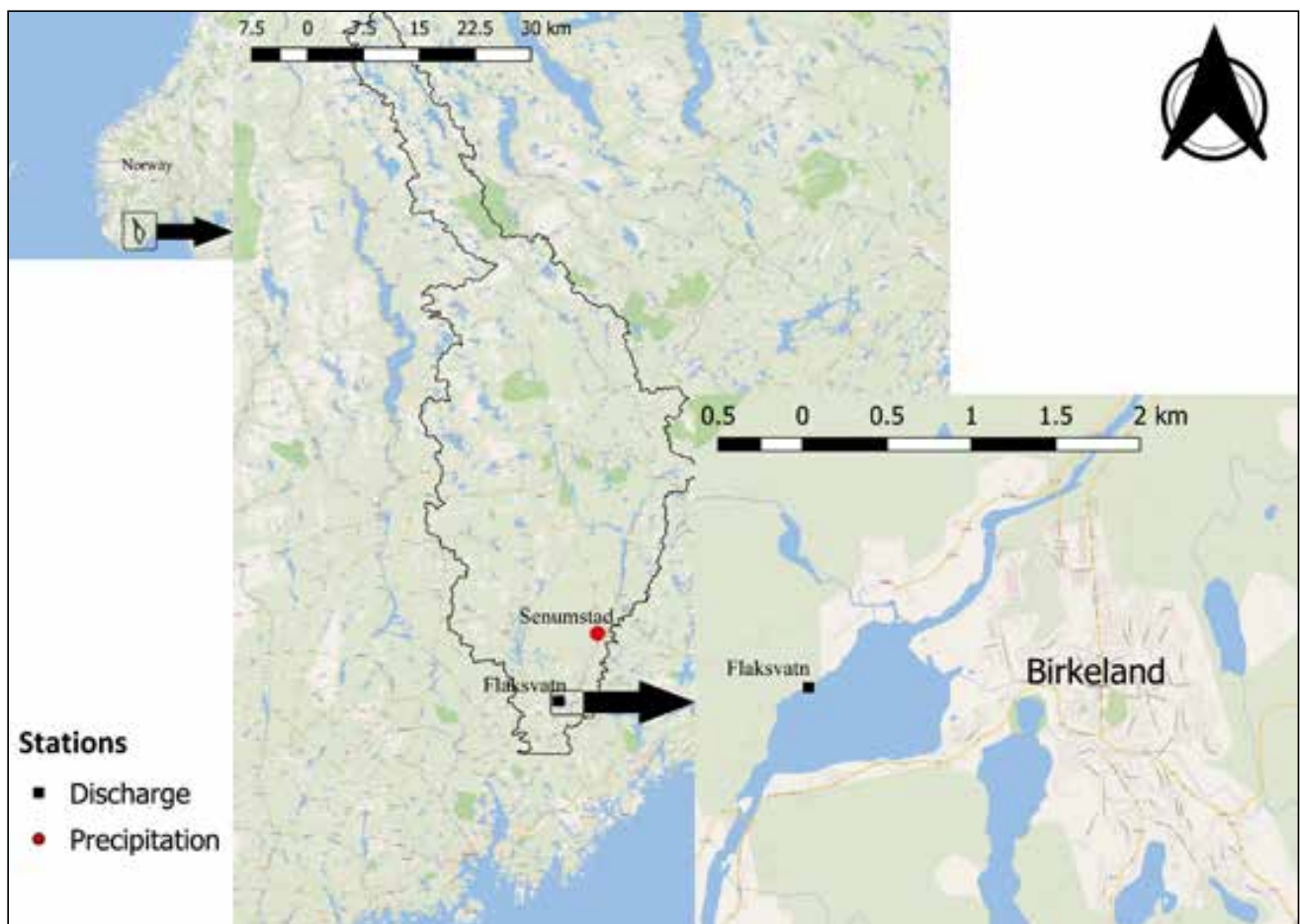


Figure 1. Tovdal river catchment and the study area



Table 2. Operation periods and length of the recorded timeseries for the stations of the catchment

Station	Operation period	Time series length (years)
Dovland	From Sep 1958	54
Herefoss	From Jul 1895	123
Kjevik	From Jun 1939	75
Mykland	From Jul 1895	126
Senumstad-Rislå	From Sep 1958	54
Tovdal	From Jul 1895	95

homogenized time series that merge the observations from before and after the relocation). Among the stations presented in Table 2, Mykland station was removed from the study because of missing data in the daily rainfall records.

In Norway, estimates of daily precipitation on a 1x1 km grid, presented by MET Norway, can be found in [www.seNorge.no](http://www.seNorge.no). The gridded data are based on interpolation of observations at approximately 400 precipitation stations (Dyrredal et al., 2016). We used the gridded data to extract daily precipitation averaged for the

catchment upstream the streamflow station at Flaksvatn (Fig. 1). Subsequently the annual maximum rainfall data for the years from 1961 to 2019 were extracted.

### Methods

In this study, we used the annual maximum precipitation data and therefore assumed that the data follows the generalized extreme value (GEV) distribution (Jenkinson, 1955):

$$F(x|\mu, \sigma, \xi) = \exp \left\{ - \left[ 1 + \xi \left( \frac{x - \mu}{\sigma} \right) \right]^{-1/\xi} \right\} \quad \text{Eq. 1}$$

where  $x$  is annual maximum rainfall,  $\mu$  is the location parameter,  $\sigma$  is the scale parameter and  $\xi$  is the shape parameter.

The challenge of statistical inference is to estimate the parameter vector  $\theta = [\mu, \sigma, \xi]$  so that the GEV distribution has the best fit to the data  $x$ . In this study we used Bayesian inference.

Bayesian inference is based on the Bayes' theorem (Bayes, 1763) and states that the posterior probability  $P(\theta|x)$  of the parameters  $\theta$  given the data depends on the likelihood of the parameters given data  $L(\theta|x)$  and the prior knowledge of the parameters  $P(\theta)$ :

$$\frac{L(\theta|x)P(\theta)}{P(x)} \quad \text{Eq. 2}$$

the likelihood function is specified as the product of the probability density function (pdf) of the GEV distribution evaluated at all observations.  $P(x)$  is or marginal probability of  $x$  and acts as a normalizing constant. Since  $P(x)$  is a constant, Eq. 2 can be written as:

$$P(\theta|x) \propto L(x|\theta)P(\theta) \quad \text{Eq. 3}$$



Figure 2. The locations of stations

Table 3. The prediction intervals (5% and 95% CI) for 100-year flood quantiles.

ID	100-year design rainfall (mm/day)			ARF effect (*0.88) Climate factor (*1.2) Time resolution (*1.13) (mm/day) (ARF is not used for Experiment 3)		
	ML	0.05	0.95	ML	0.05	0.95
<b>Experiment 1</b>						
Dovland	120	102	162	144	122	194
Herefoss	120	109	141	143	130	168
Kjevik	114	99	145	136	118	174
Senumstad	147	128	198	175	152	236
Tovdal	124	108	154	148	129	184
<b>Experiment 2</b>						
Catchment	123	116	136	147	138	162
<b>Experiment 3</b>						
Grid data	104	92	134	141	125	182

In this study we selected the prior distribution for the GEV parameters, based on the recommendations in Martins and Stedinger, 2000 and Lutz et al., 2020. Accordingly, we used uninformative prior distributions for location ( $\mu$ ) and scale ( $\sigma$ ) and beta distribution for shape parameter ( $\xi \sim B(p=6, q=9)$ ) which is defined on the interval  $[-0.5, 0.5]$ .

We used a Markov Chain Monte Carlo (MCMC) algorithm to estimate the posterior probability distribution of the parameter set  $\theta$ . We used the algorithm implemented in the R-package nsRFA (Viglione et al., 2020), where a Metropolis Hastings algorithm is implemented, and carried out 50,000 iterations to obtain a sample of the posterior distribution of the GEV parameters  $\theta$ . This posterior sample of GEV parameters was subsequently used by the GEV distribution to provide a predictive distribution of the design rainfall (i.e., in our case the 100-year rainfall where the cumulative GEV distribution equals 0.99) in the form of a sample. From this sample the 90% prediction interval for the design rainfall was calculated.

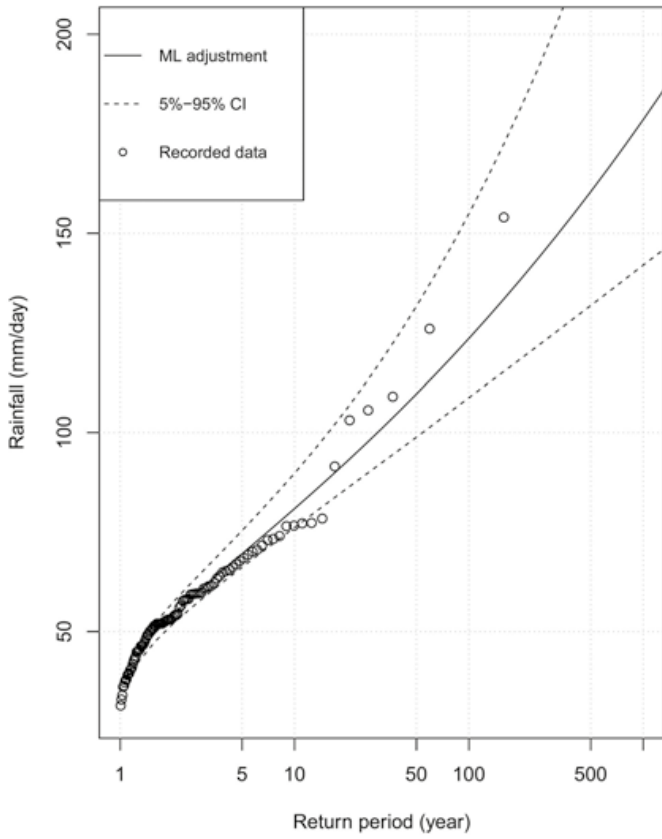
To transfer the climate change effects and possible future changes, the design rainfall values are multiplied by climate factors. The climate factors are calculated based on return period, rainfall duration, geographical location, reference period, scenario period and climate

models (global/regional) (Hanssen-Bauer et al., 2009). In this study the defined rainfall interval is multiplied by a climate factor equal to 1.2. The factor is selected based on the values reported by Hanssen-Bauer et al. (2009), for the case study region (Agder) under high emissions scenario (RCP8.5) (Table 3). In order to achieve design values that represent 24 hour duration and not a calendar day, we multiplied all estimates by 1.13 as recommended by the Norwegian meteorological institute (<https://klimaservicesenter.no/kss/vrdata/ivf-veiledning>). Further, we needed to convert point (station) rainfall estimates to catchment-averaged estimates for experiment 1 and 2 where station data were used. We used area reduction factor recommended by the Norwegian meteorological institute (<https://klimaservicesenter.no/kss/laermer/kraftig-nedbor>). For daily precipitation in a catchment of 1867 km<sup>2</sup>, the ARF value is 0.88.

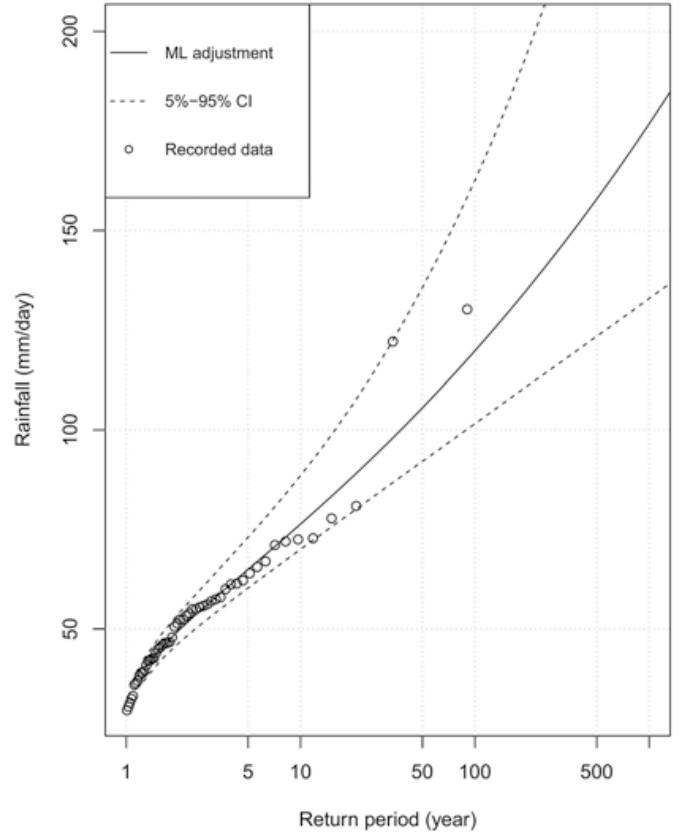
## Results and discussion

Following the approaches described in the previous section, the design rainfall ranges (or prediction intervals) were estimated using Bayesian MCMC and results are presented in Table 3 and Figs. 3 and 4, displays the 100-year design rainfall value with the associated prediction intervals for each experiment.

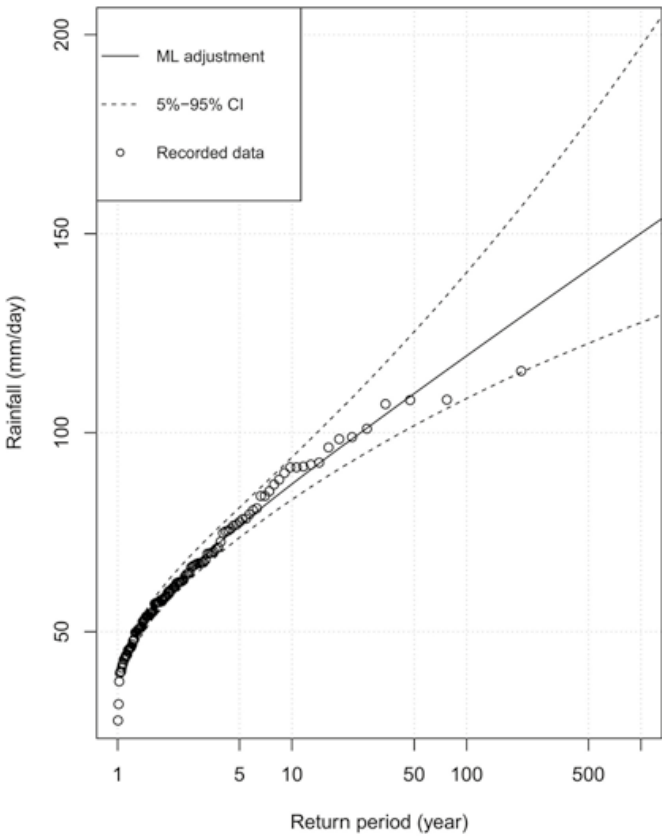
Tovdal



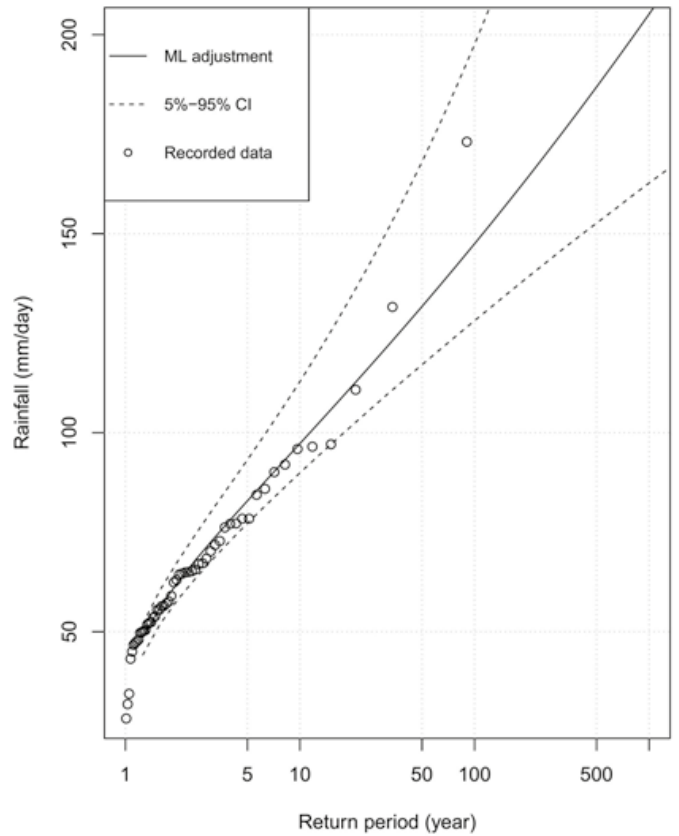
Dovland



Herefoss



Senumstad



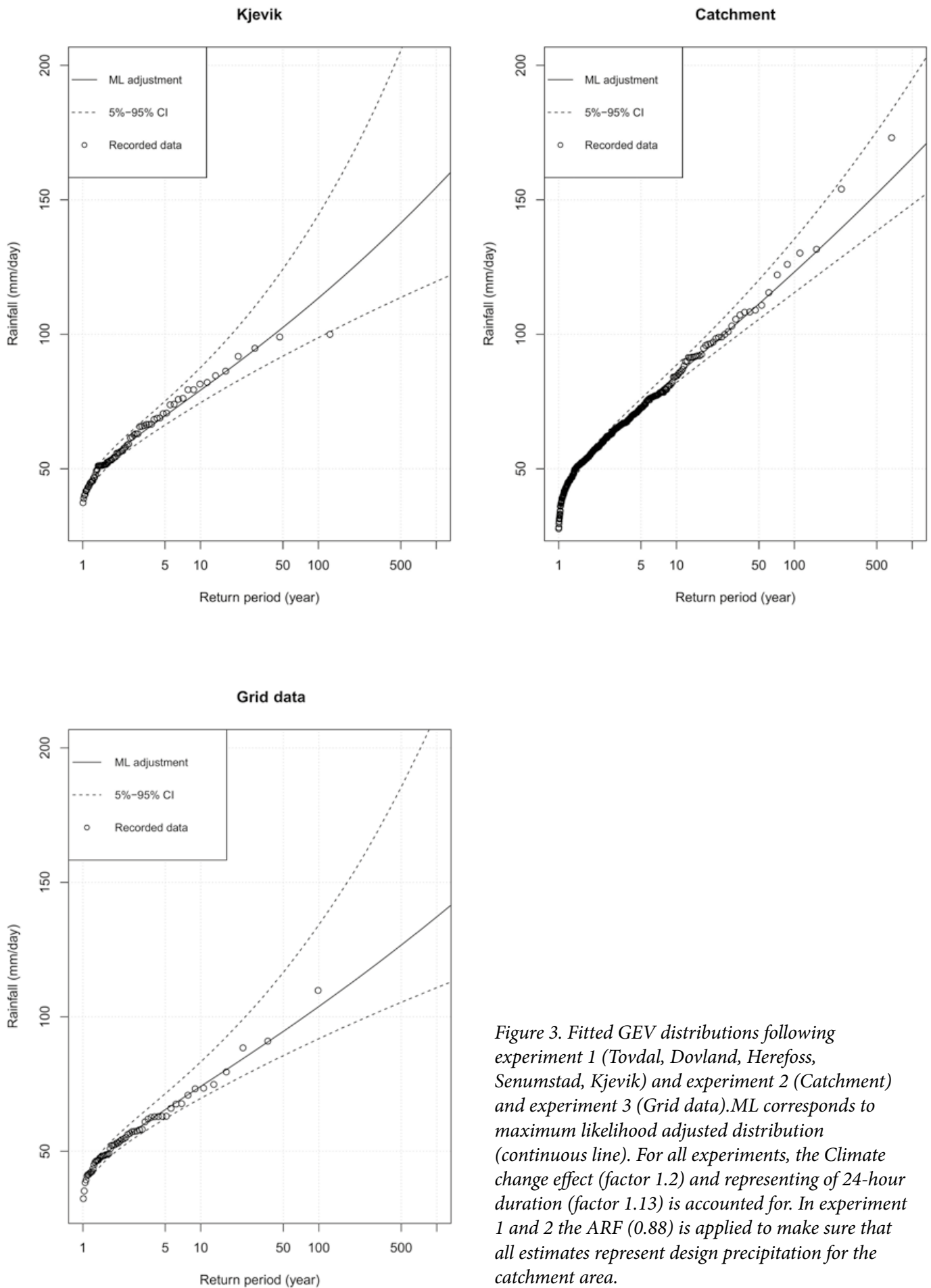


Figure 3. Fitted GEV distributions following experiment 1 (Tovdal, Dovland, Herefoss, Senumstad, Kjevik) and experiment 2 (Catchment) and experiment 3 (Grid data). ML corresponds to maximum likelihood adjusted distribution (continuous line). For all experiments, the Climate change effect (factor 1.2) and representing of 24-hour duration (factor 1.13) is accounted for. In experiment 1 and 2 the ARF (0.88) is applied to make sure that all estimates represent design precipitation for the catchment area.



For experiment 1, we see from Table 3 and Fig. 4 that the highest design rainfall value (ML) and its confidence intervals is estimated for Senumstad station, and the lowest values are obtained for Kjevnik (lowest ML and 5% CI) and Herefoss (lowest 95% CI). From the table it can be seen that the data from the stations Tovdal, Kjevnik and Dovland results in rather similar ranges.

Comparing the ranges obtained from experiment 1 and 2, it can be seen that the second experiment (catchment) leads to more narrow prediction intervals whereas the ML estimate is practically similar to the estimated design precipitation at the Tovdal station and slightly smaller than the average of the design rainfall estimated at each station.

Using the gridded data in experiment 3 (Grid data) results in slightly smaller ML estimates than the values obtained from experiment 1 and 2. The only exception can be seen for Senumstad station, which is considerably higher than the Grid-based ML value, and Kjevnik which corresponds to smaller ML value. Likewise, the 5% CI value for the grid-based estimate is lower than the other stations except for Dovland and

Kjevnik, whereas the 95% CI value is below the values obtained from Dovland, Senumstad and Tovdal.

The results from experiment 1 shows that using data from only one precipitation station when estimating a design rainfall for a large catchment might be challenging since the selected station might not be representative for the whole catchment. In this study, Senumstad provides the highest estimates (147 mm) whereas Kjevnik provides the lowest estimate (114 mm). Using several precipitation stations inside and close to the catchment, allows us to provide more robust estimates.

The estimates from Herefoss, Dovland, Kjevnik, Tovdal and SeNorge are not significantly different, and the estimates are practically similar. This shows that for this particular catchment, the gridded data are useful for estimating design rainfall, and we avoid the use of ARFs and the need to select one particular precipitation station. Since we in this study do not want to under-estimate the uncertainty, we selected to use the estimates from Dovland station. However, we recognize, that in areas with a larger spatial variability in precipitation, the use of one single station would be even more challenging.

One important issue that should be considered in time series analyses, is the selection of the length of the time series. To investigate the effect of time series period on the estimated design rainfall, various time spans that consist of the most recent 30, 40, 50, 60, 70,80, 90 and 100 years of data were used to estimate the 100-year design rainfall and the results are displayed in Fig. 5 for each of the stations. According to the results, the changes in the modified ML estimates are not significantly different (Fig. 5 (a)). Unlike the ML line, the variation in upper bound (0.95 CI) is considerable when moving from shorter to longer periods. A decreasing trend can be observed in 0.95 CI values by increasing the data length. However, there are exceptions such as in Kjevnik (70 years), Tovdal (90 years) and Senumstad (50 years). The variation of 0.95 CI line can to a large degree be

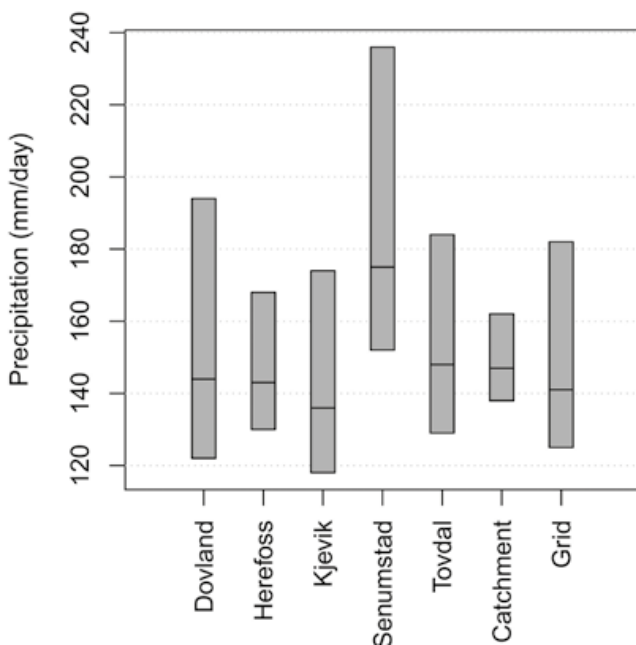


Figure 4. Comparing the estimated 100-year design rainfall values resulted from experiment 1 (Dovland, Herefoss, Kjevnik, Senumstad and Tovdal), experiment 2 (Catchment), and experiment 3 with grid data.

attributed to the uncertainty in the estimated shape parameter which depends on the length of data.

According to Fig. 5, using the longer time spans narrows down the estimated interval or in other words results in smaller uncertainties. This is a direct effect of the increasing sample size that decreases the sample uncertainty. In extreme value analysis, there is a strong tradition for using the maximum possible amount of data when estimating design values to reduce estimation uncertainties. However, in the presence of changes in the climate, using long time series might result in biased estimates. Detecting trends in extremes is challenging since strong variability from year-to-year masks possible trends. To investigate the presence of trends in location and scale parameters, the nonstationary GEV models were developed and tested for each of the stations (location and scale parameters as time varying parameters) and no significant trends were found, neither in the location nor the scale parameters. A stationary model was therefore used for this catchment.

## Conclusions

In this study, a Bayesian inference is used along with prior knowledge about the shape parameter to fit the Generalised Extreme Value (GEV) distribution for annual maximum rainfall data. The method was used for three experiments. Firstly, the method was applied for each station. Secondly, the estimated posteriors of the stations were merged into one sample and the design rainfall range was identified. Thirdly, the catchment average precipitation from SeNorge was used in the estimations. The results of the experiments were compared with each other. Furthermore, the effect of selecting different periods to estimate the quantiles intervals were assessed. The main results of this paper are as follows:

- Using precipitation data from only one station to estimate design rainfall might result in biased estimates. Hence, it is better to use several stations within or close to the target catchment.
- Using one sample involving all the posteriors (experiment 2, catchment-based scenario)

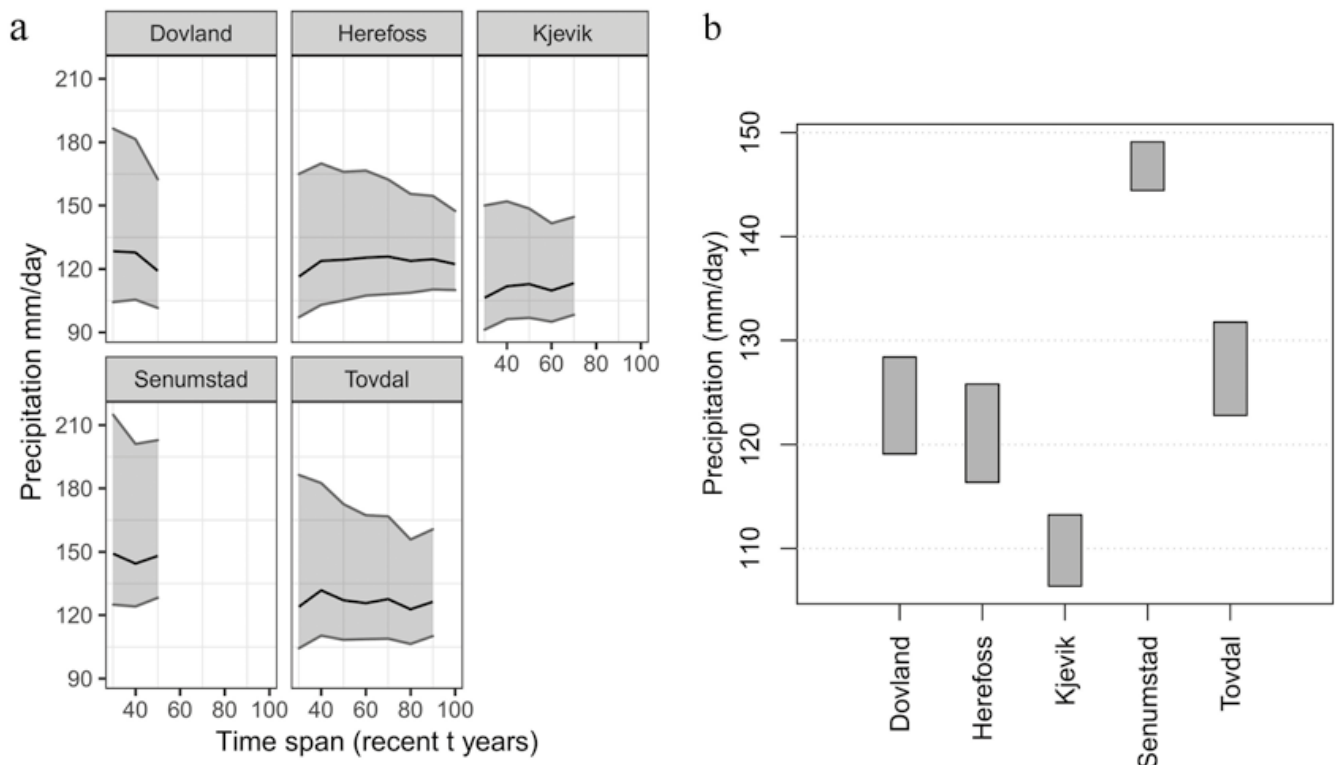


Figure 5. a. The effect of time series length on the estimated 100-year design rainfall (the middle black line presents the ML values, and the upper and lower lines display the 95% and 5% CI). b. the variation ranges for ML values displayed in panel a.

may narrow down the estimated design rainfall interval but it may result into small predictive uncertainty and therefore fail to cover possible extreme events.

- Using gridded precipitation data gave similar results to using station-based data combined with area reduction factor.
- The length of the time series and the number of years that are representing the extremes is a trade-off between having sufficient data to reduce sampling uncertainty and avoiding possible non-stationarities in the extremes. For this study, the stationarity assumption was fulfilled.

The estimated 100-year precipitation based on the data from Dovland was selected to be used to represent the uncertainty in design precipitation and will be used for further analysis of flood zones. We believe that the prediction range is in particular useful for risk-assessments and could also be used to provide safety factor that reflects the knowledge (and uncertainty) in our estimates and are therefore more tailored to each application.

## References

Agilan, V., Umamahesh, N., 2017. What are the best covariates for developing non-stationary rainfall intensity-duration-frequency relationship? *Advances in Water Resources*, 101: 11-22.

Bayes, T., 1763. LII. An essay towards solving a problem in the doctrine of chances. By the late Rev. Mr. Bayes, FRS communicated by Mr. Price, in a letter to John Canton, AMFR S. *Philosophical transactions of the Royal Society of London*(53): 370-418.

Cannon, A.J., 2010. A flexible nonlinear modelling framework for nonstationary generalized extreme value analysis in hydroclimatology. *Hydrological Processes: An International Journal*, 24(6): 673-685.

Coles, S., 2001. *Extremes of non-stationary sequences, An introduction to statistical modeling of extreme values*. Springer, pp. 105-123.

Cunderlik, J.M., Burn, D.H., 2003. Non-stationary pooled flood frequency analysis. *Journal of Hydrology*, 276(1-4): 210-223.

DeGaetano, A.T., Castellano, C., 2018. Selecting time series length to moderate the impact of nonstationarity in extreme rainfall analyses. *Journal of Applied Meteorology and Climatology*, 57(10): 2285-2296.

Dyrddal, A.V., 2012. Estimation of extreme precipitation in Norway and a summary of the state-of-the-art. *Meteorologisk institutt. met. no rapport*, 8: 19.

Dyrddal, A.V., Skaugen, T., Stordal, F., Førland, E.J., 2016. Estimating extreme areal precipitation in Norway from a gridded dataset. *Hydrological Sciences Journal*, 61(3): 483-494.

Fisher, R.A., Tippett, L.H.C., 1928. Limiting forms of the frequency distribution of the largest or smallest member of a sample, *Mathematical proceedings of the Cambridge philosophical society*. Cambridge University Press, pp. 180-190.

Hanssen-Bauer, I., Drange, H., Førland, E., Roald, L., Børsheim, K., Hisdal, H., Lawrence, D., Nesje, A., Sandven, S., Sorteberg, A., 2009. *Climate in Norway 2100. Background information to NOU Climate adaptation (In Norwegian: Klima i Norge 2100. Bakgrunnsmateriale til NOU Klimatilpassing)*, Oslo: Norsk klimasenter.

Jenkinson, A.F., 1955. The frequency distribution of the annual maximum (or minimum) values of meteorological elements. *Quarterly Journal of the Royal Meteorological Society*, 81(348): 158-171.

Kedem, B., Chiu, L.S., Karni, Z., 1990. An analysis of the threshold method for measuring area-average rainfall. *Journal of Applied Meteorology and Climatology*, 29(1): 3-20.

Khaliq, M.N., Ouarda, T.B., Ondo, J.-C., Gachon, P., Bobée, B., 2006. Frequency analysis of a sequence of dependent and/or non-stationary hydro-meteorological observations: A review. *Journal of hydrology*, 329(3-4): 534-552.

Kobierska, F., Engeland, K., Thorarinsdottir, T., 2018. Evaluation of design flood estimates—a case study for Norway. *Hydrology Research*, 49(2): 450-465.

Leclerc, M., Ouarda, T.B., 2007. Non-stationary regional flood frequency analysis at ungauged sites. *Journal of hydrology*, 343(3-4): 254-265.

Lima, C.H., Kwon, H.-H., Kim, Y.-T., 2018. A local-regional scaling-invariant Bayesian GEV model for estimating rainfall IDF curves in a future climate. *Journal of Hydrology*, 566: 73-88.

Lima, C.H., Lall, U., Troy, T., Devineni, N., 2016. A hierarchical Bayesian GEV model for improving local and regional flood quantile estimates. *Journal of Hydrology*, 541: 816-823.

- Lutz, J., Grinde, L., Dyrddal, A.V., 2020. Estimating Rainfall Design Values for the City of Oslo, Norway—Comparison of Methods and Quantification of Uncertainty. *Water*, 12(6): 1735. DOI: <https://doi.org/10.3390/w12061735>
- Martins, E.S., Stedinger, J.R., 2000. Generalized maximum-likelihood generalized extreme-value quantile estimators for hydrologic data. *Water Resources Research*, 36(3): 737-744.
- Ouarda, T.B., Charron, C., 2019. Changes in the distribution of hydro-climatic extremes in a non-stationary framework. *Scientific reports*, 9(1): 1-8.
- Pelosi, A., Furcolo, P., Rossi, F., Villani, P., 2020. The characterization of extraordinary extreme events (EEEs) for the assessment of design rainfall depths with high return periods. *Hydrological Processes*, 34(11): 2543-2559.
- Renard, B., Lang, M., Bois, P., 2006. Statistical analysis of extreme events in a non-stationary context via a Bayesian framework: case study with peak-over-threshold data. *Stochastic environmental research and risk assessment*, 21(2): 97-112.
- Svensson, C., Jones, D.A., 2010. Review of methods for deriving areal reduction factors. *Journal of Flood Risk Management*, 3(3): 232-245.
- Um, M.-J., Kim, Y., Markus, M., Wuebbles, D.J., 2017. Modeling nonstationary extreme value distributions with nonlinear functions: an application using multiple precipitation projections for US cities. *Journal of Hydrology*, 552: 396-406.
- Vanem, E., 2015. Uncertainties in extreme value modeling of wave data in a climate change perspective. *Journal of Ocean Engineering and Marine Energy*, 1(4): 339-359.
- Viglione, A., Hosking, J.R., Laio, F., Miller, A., Gaume, E., Payrastre, O., Salinas, J.L., N'guyen, C.C., Halbert, K., Viglione, M.A., 2020. Package 'nsRFA'. Non-supervised Regional Frequency Analysis. CRAN Repository, Version 0.7-15.
- Wright, D.B., Smith, J.A., Baeck, M.L., 2014. Critical examination of area reduction factors. *Journal of Hydrologic Engineering*, 19(4): 769-776.
- Yan, H., Moradkhani, H., 2016. Toward more robust extreme flood prediction by Bayesian hierarchical and multimodeling. *Natural Hazards*, 81(1): 203-225.
- Yoon, P., Kim, T.-W., Yoo, C., 2013. Rainfall frequency analysis using a mixed GEV distribution: a case study for annual maximum rainfalls in South Korea. *Stochastic Environmental Research and Risk Assessment*, 27(5): 1143-1153.



**Paper IV:** Emulation of 2D Hydrodynamic Flood Simulations at Catchment Scale  
Using ANN and SVR

Alipour, S.M., Leal, J., 2021. Emulation of 2D Hydrodynamic Flood Simulations at Catchment Scale Using ANN and SVR. *Water*, 13(20): 2858.  
[DOI:10.3390/w13202858](https://doi.org/10.3390/w13202858)



## Article

# Emulation of 2D Hydrodynamic Flood Simulations at Catchment Scale Using ANN and SVR

Saba Mirza Alipour \*  and Joao Leal 

Department of Engineering and Science, University of Agder, Jon Lilletuns vei 9, 4879 Grimstad, Norway; Joao.leal@uia.no

\* Correspondence: Saba.m.Alipour@uia.no; Tel.: +47-9251-4142

**Abstract:** Two-dimensional (2D) hydrodynamic models are one of the most widely used tools for flood modeling practices and risk estimation. The 2D models provide accurate results; however, they are computationally costly and therefore unsuitable for many real time applications and uncertainty analysis that requires a large number of model realizations. Therefore, the present study aims to (i) develop emulators based on SVR and ANN as an alternative for predicting the 100-year flood water level, (ii) improve the performance of the emulators through dimensionality reduction techniques, and (iii) assess the required training sample size to develop an accurate emulator. Our results indicate that SVR based emulator is a fast and reliable alternative that can predict the water level accurately. Moreover, the performance of the models can improve by identifying the most influencing input variables and eliminating redundant inputs from the training process. The findings in this study suggest that the training data size equal to 70% (or more) of data results in reliable and accurate predictions.

**Keywords:** emulators; artificial neural network; support vector regression; training set size; error structure



**Citation:** Mirza Alipour, S.; Leal, J. Emulation of 2D Hydrodynamic Flood Simulations at Catchment Scale Using ANN and SVR. *Water* **2021**, *13*, 2858. <https://doi.org/10.3390/w13202858>

Academic Editor: Chris Bradley

Received: 10 August 2021

Accepted: 10 October 2021

Published: 13 October 2021

**Publisher's Note:** MDPI stays neutral with regard to jurisdictional claims in published maps and institutional affiliations.



**Copyright:** © 2021 by the authors. Licensee MDPI, Basel, Switzerland. This article is an open access article distributed under the terms and conditions of the Creative Commons Attribution (CC BY) license (<https://creativecommons.org/licenses/by/4.0/>).

## 1. Introduction

Floods are one of the most frequent and costly natural disasters that happen throughout the world and are likely to increase in number and severity as a result of climate change [1,2]. As a result, flood related topics including flood modeling, risk analysis, flood management, etc., have always been the subject of research from the past to the present. There are a variety of tools and approaches for flood modeling purposes, such as empirical methods (e.g., measurements, surveys, remote sensing, and statistical models) and hydrodynamic models (1D, 2D, and 3D models) [3].

Two-dimensional (2D) models, as a class of hydrodynamic models, are one of the popular tools that are based on the numerical solution of the 2D Shallow Water Equations (SWE) and use different types of input parameters with complex domain spaces (e.g., hydrological data, floodplain and channel geometry, initial and boundary conditions, roughness) and provide outputs such as flow velocity, water level, and inundation extent. Two-dimensional hydrodynamic models provide accurate results. However, they are usually computationally intensive and require long run time. Therefore, these tools might not be a proper choice (i) when a large number of model realizations is needed (such as required in uncertainty analysis with GLUE, Monte Carlo, or Bayesian approaches, or in optimization studies), or (ii) for applications that require rapid model response [4] (e.g., rapid flood risk analysis or real time flood modeling). There are alternative solutions to overcome these constraints, such as simplification of the model (e.g., [5,6]) or using data-driven surrogate models or emulators.

In literature, emulators, metamodels, response surface modeling, and surrogate modeling are often considered as interchangeable concepts and generally are referred to as



metamodels [7]. The principal idea of these models is to find relationships between the system state variables (input and output) without explicit knowledge of the physical behavior of the system [8]. In recent years, the application of emulators in hydraulic/hydrological modeling practices has received considerable attention and a variety of methods have been developed and used as emulators such as: polynomial regression [9,10], radial basis functions [11], kriging methods [12], and smoothing splines [13]. A comprehensive review of different emulation methods can be found in [7], in which different approaches for optimization purposes were critically reviewed. Amongst the proposed methods for development of the surrogates or emulators, artificial intelligent (AI) techniques are popular methods that have been widely applied in flood related studies. Ghalkhani et al. [14] applied Artificial Neural Network (ANN) and Adaptive Neuro-Fuzzy Inference System (ANFIS) to develop a surrogate model to emulate HEC-RAS model outputs for flood routing in rivers. Chu et al. [4] developed an ANN-based emulation modelling framework to simulate flood inundation based on information obtained from a 2D hydrodynamic model. Xie et al. [15] applied ANN-based hybrid modeling approach to improve the model performance in data-sparse regions by training an emulator using data-rich regions.

In addition to ANN, successful application of other AI techniques has also been reported in literature. The authors of [16] compared ANN and Support Vector Regression (SVR) performance for approximating the Soil and Water Assessment Tool (SWAT) model in two watersheds and reported the better performance of SVR model. Xu et al. [17] implemented SVR to investigate the effect of model structural error on calibration and prediction of real-world groundwater flows. Numerous types of emulators have been developed for different classes of 2D models such as: HecRAS2D, TELEMAC2D, TUFLOW, and MIKE FLOOD (e.g., [4,9,18,19]). According to the literature, most of the 2D models simulate flood flow for a given discharge or inflow hydrograph and accordingly the simulation scale is constrained to a limited river reach. For these 2D models, the emulators are trained based on inputs such as discharge, roughness values along river, topographic features of river channel and floodplain, and the outputs such as flood discharge or volume and flood level. Only a small number of 2D models use direct rainfall at catchment scale (global scale) to model flood, thus, the application of emulators for hydrology-hydraulic coupled models is rare. A few studies have used emulators for catchment scale flood modeling such as Bass and Bedient [20] that used a supervised machine learning approach based on coupled hydrodynamic and hydrologic modeling results to provide rapid, probabilistic estimates of joint flooding from Tropical Cyclones at the catchment scale.

Catchment or so-called global scale flood modeling is particularly important in catchments with complex topography and rivers with multiple tributaries originating from different parts of the catchment where the land cover and topography features effect can play important roles. Thus, their effect should be considered in the emulation process. In recent years, due to the advances in computational power and accessibility of graphics processing units (GPU), flood simulation at global scale has become feasible but is still time consuming. Therefore, it is important to develop accurate emulators and to do it in an efficient way.

Typically, the performance and accuracy of the trained emulators are assessed through aggregated error metrics such as root mean squared error (*RMSE*) and correlation coefficient (*R*). Al Kajbaf and Bensi [21] showed that aggregated error metrics give incomplete measures of the performance, and the accuracy of the models must be assessed beyond these metrics.

Thus, this study aims to: (i) develop an emulator by using ANN and SVR, considering inputs such as rainfall intensity, land features and outputs simulated by a coupled hydrology-hydraulic 2D model, (ii) simplify the models' structures and improve the performance of the emulators by applying correlation tests and ANOVA analyses, (iii) investigate the predictive error structure of the emulators and select the most accurate emulator, and (iv) assess the required training sample size to develop an accurate emulator.



## 2. Materials and Methods

### 2.1. Case Study

Birkeland, located in Agder province (Norway), was selected as the case study, as floods have become a major concern there in recent years. Birkeland is located beside a river named Tovdal, where the river debouches into a small natural lake called Flakksvann (Figure 1). The length of the main river is approximately 130 km, and the catchment has an area of about 1767 km<sup>2</sup> dominated by forests (about 74%). The elevation ranges from 10.00 to 872.34 m.a.s.l., and the average slope of the catchment along the river is about 0.65%. The mean annual precipitation is approximately 1261 mm, with most of the rainfall occurring between October and March (about 60%). On 2 October 2017, an extreme flood event occurred in the downstream parts of the river and inundated Birkeland. This event was the highest ever recorded flooding of this river. The recorded data of the event can be found in the study by [22].

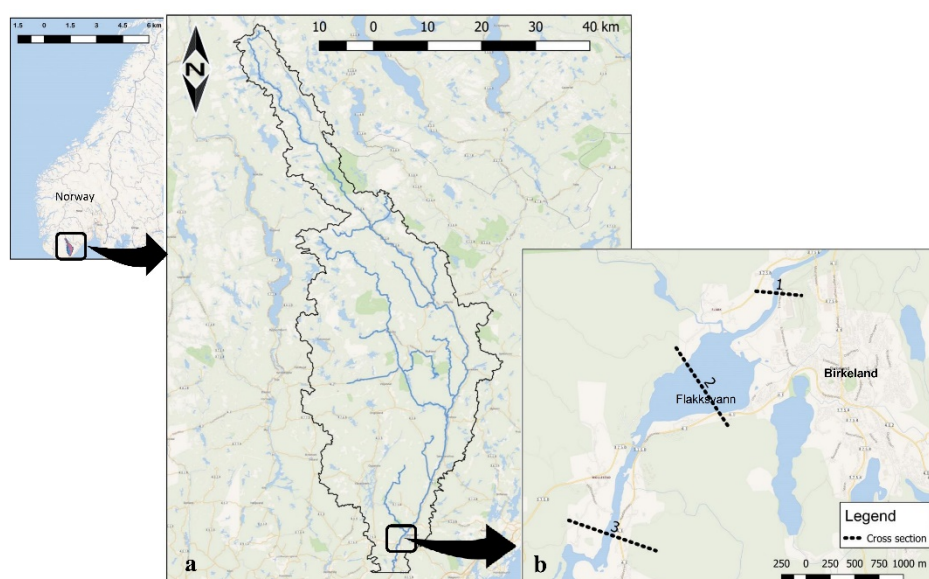


**Figure 1.** (a) Map of Tovdal river's catchment area. (b) The case study area with specified cross sections.

### 2.2. Hydrodynamic Simulations and Input Ranges

In the current study, a GPU based 2DH (two dimensional horizontal) hydrodynamic model named HiSTAV was used to simulate floods. The model was originally proposed by in [23] and optimized in [24]. The core of the model is a hyperbolic system of partial differential equations expressing mass and momentum conservation principles for shallow-water flows. The equations are solved using a finite volume scheme, which is applied on a spatial discretization using unstructured meshes. The initial conditions for the equations are zero water depth and zero discharge everywhere (dry surface conditions). Water enters the domain only through rainfall; hence there are no inlet boundaries. The only open boundary is at the outlet (downstream), where free outflow is assumed. For detailed information about HiSTAV and the model structure we refer the readers to the study presented by [23].

The model employs adaptable triangular meshes over the study domain to discretize the catchment and terrain parameters (i.e., elevation, bathymetry, land use, etc.). The computational domain for the simulations is the part of the catchment upstream of the small lake named Flakksvann, just beside Birkeland (Figure 1a). In order to avoid outlet boundary interference, the domain was extended 11 km further to the downstream of the lake. In this study, by employing Godunov's finite-volume approach ([25]) a total of 401,769 mixed mesh of triangular cells are constructed in three sizes over the computational domain (Figure 1a) by Gmsh ([26]), which is a free finite element grid generator with a

build-in CAD engine and post-processor. The small cells or so-called finer resolutions are assigned to the cells where the flow gradients are expected to be large, such as the river channel; medium sized cells, or average resolution over the flood plain; and coarser resolution over other parts of the catchment, where flow gradients are expected to be mild.

Prior to undertaking the simulations, warm-up simulations were performed until reaching the normal water level in the river network. A 9-day precipitation with an intensity of 2 mm/h was found to be long enough to fill the river basin and the lakes with the steady flow. Using the filled catchment (in water courses parts) as the base time step, the model was calibrated and validated using the recorded data of the 2017 flood event (including water level, discharge, hydrograph at Flakksvann cross section, and flood maps). Further details of the calibration process are presented in [22].

Once the calibration and validation were done, reasonable ranges were established for the inputs, taking into consideration the calibrated values and based on the land type, vegetation, and average antecedent soil moisture. In the present study, each simulation started from the warm-up simulation results and ran for a computational time of 34 h. The calibration simulation's result in terms of flow depth is displayed in Figure 2.

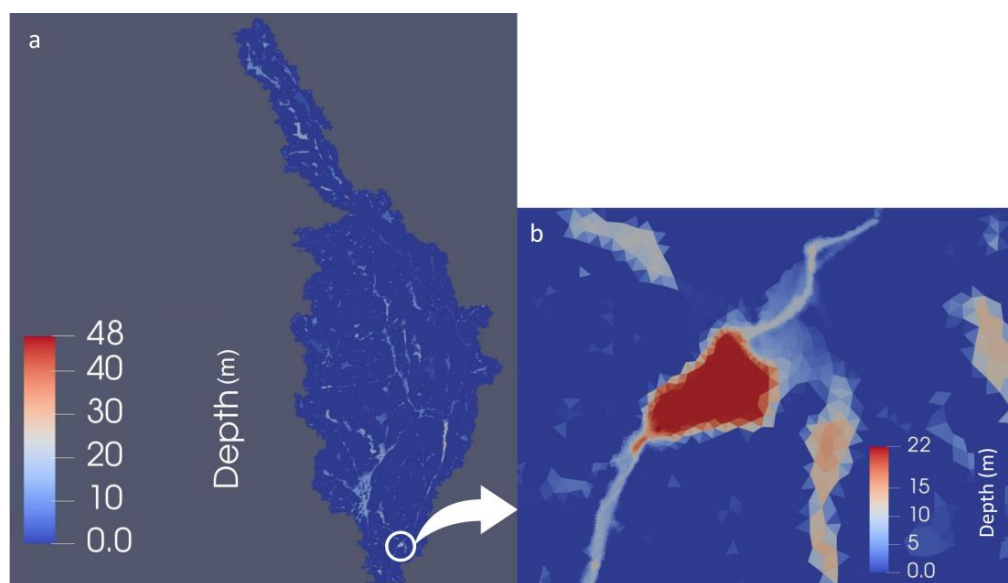


**Figure 2.** Water depth ranges in the calibrated model: (a) computational domain, (b) case study region.

HiSTAV requires different data sets as input to simulate the flow, namely: the topobathymetric dataset, Strickler roughness coefficient values, runoff coefficient values (in form of raster files), and precipitation intensity.

A  $10 \times 10 \text{ m}^2$  Digital Terrain Model (DTM) including the river bathymetry information is used to represent topographic features and derive hydrologic characteristics (i.e., slope, flow direction, flow accumulation, stream network, computational cascade for flow routing, etc.).

Hydraulic roughness is inserted in the model in the form of a grid structure raster file ( $100 \times 100 \text{ m}^2$  resolution), in which each cell represents Strickler roughness values. The spatial distribution of roughness values is determined based on  $100 \times 100 \text{ m}^2$  land cover maps (obtained from <https://land.copernicus.eu/>—“Corine Land Cover (CLC) 2018, Version 20” (accessed on 10 April 2021)). Subsequently, using typical Strickler roughness coefficient tables, the roughness values were assigned for each cell [27,28].

The runoff coefficient  $C$  is a dimensionless factor that is used by HiSTAV to convert the rainfall amounts to runoff (i.e., effective precipitation  $h_p = C \cdot i_p$ , being  $i_p$  the precipitation intensity). Similar to the hydraulic roughness values, the runoff coefficient is used in the form of raster data and represents the integrated effect of catchment losses (like infiltration

and surface retention). Therefore, the coefficient depends on different parameters such as land cover and use, slope, soil moisture, and rainfall intensity [29].

In this study, a combination of two different approaches to calculate the runoff coefficient was used. First, by using land cover maps and recommended values of runoff coefficients for different types of areas [30], a range was determined for each cell. Second, since the HiSTAV model assumes a uniform spatial distribution of precipitation as input, the runoff coefficient was used as an artifact to introduce spatial variability of the precipitation. For this purpose, daily precipitation data were obtained from 37 stations (Figure 3) for one of the recorded extreme floods (flood of 2 October 2017). The rainfall observations at the stations were interpolated to delineate the spatial distribution of precipitation using the inverse distance weighting interpolation method (IDW), which gave similar precipitation patterns like the ones presented by the Norwegian Meteorological Institute (<http://www.senorge.no/> (accessed on 20 March 2021)). Thereafter, precipitation zones were delineated as in Figure 3. The combination of the two described approaches was used to calculate the final runoff coefficient in each cell,  $C_t$ , as follows:

$$C_t = C \times \left( \frac{i_{P_{cell}}}{i_{P_{max}}} \right) \quad (1)$$

where  $i_{P_{max}}$  is the maximum amount of precipitation intensity among the recorded values,  $i_{P_{cell}}$  is the recorded precipitation intensity in each cell, and  $C$  is the runoff coefficient.

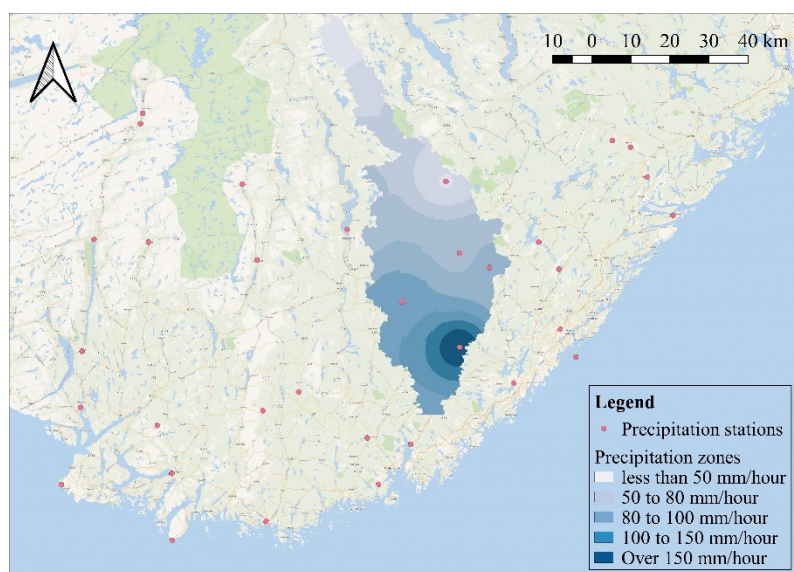


**Figure 3.** Spatial distribution of the precipitation stations and the interpolated precipitation over the catchment.

The input parameters, namely hydraulic roughness parameter ( $K_S$ ), runoff coefficient ( $C$ ), and precipitation intensity ( $i_p$ ), were selected as the uncertain input variables that HiSTAV uses to simulate the flow. The hydraulic roughness and runoff coefficient parameter spaces are constructed for each of them based on a range that reflects the possible variation range.

The choice of ranges was based on the land type, vegetation, and average antecedent soil moisture.

Estimation of precipitation intensity is a crucial step in rainfall-runoff modelling practices, but it is incorporated with uncertainty due to the limited historical data, climate variability/change, and the complex and chaotic nature of climate. In this study, we used a Bayesian MCMC approach to define a range for precipitation intensity. For this purpose, annual maximum precipitation data were collected from different stations in the catchment and the generalized extreme value distribution (GEV) was fitted to each data series using a Bayesian MCMC approach. This approach uses a Markov chain Monte

Carlo (MCMC) algorithm to estimate the GEV distribution for each data set. We used the algorithm implemented in the R-package nsRFA [31], where a Metropolis Hastings algorithm is implemented, and carried out 50,000 iterations to fit the GEV distribution.

In this study we aimed to emulate the 100-year return period flood water level. Therefore, using the fitted GEV distribution for the 100-year return period, the design rainfall and the corresponding 5% and 95% confidence intervals are selected as the precipitation range for each station. The estimated ranges for different stations were compared and finally a sufficiently wide range was selected as the catchment precipitation range. In order to consider future climate change effects, the defined precipitation interval was multiplied by a climate factor equal to 1.2. The factor was selected based on the values reported by Hanssen-Bauer et al. [32] for the case study region (Agder) under high emissions scenario (RCP8.5). For details of the Bayesian MCMC method, we refer the reader to the studies by Reis Jr and Stedinger [33], Gaume et al. [34], and Lutz et al. [35].

Table 1 presents the considered input variables with their descriptions and specified ranges used in this study. Runoff coefficient values and Strickler roughness values were assigned to each cell based on the land type.

**Table 1.** Selected input descriptions and assigned ranges.

Parameters		Acronym	Range	
Precipitation intensity (mm/h)		$i_p$	5–8.1	
Strickler roughness ( $m^{1/3}/s$ )	Urban lands	$K_s\_U$	40–70	
	Forests (broad-leaved, coniferous)	$K_s\_F$	15–40	
	Moors and heathland	$K_s\_Mo$	18–30	
	Arable lands	$K_s\_A$	18–37	
	Agriculture and vegetated areas	$K_s\_Ag$	18–37	
	River and water courses	$K_s\_R$	20–50	
	Mineral sites	$K_s\_Mi$	30–60	
	Runoff coefficient (%)	Urban lands	$C\_U$	80–90
		Forests (broad-leaved, coniferous)	$C\_F$	50–70
Moors and heathland		$C\_Mo$	60–80	
Arable lands		$C\_A$	40–60	
Agriculture and vegetated areas		$C\_Ag$	40–60	
Mineral sites		$C\_Mi$	70–90	

In total, there were 14 potential input variables (seven different  $K_s$  values assigned for each land type, six types of runoff coefficient values assigned for each land type, and precipitation intensity) used to simulate the flow. The values for each of the inputs were randomly sampled assuming uniform probability distribution within the specified range (Table 1). Uniform distribution was selected ensuring equal probability for each value and avoiding any prior assumptions about the parameter distribution. The reasoning behind the use of a uniform distribution for roughness and runoff coefficients was that there was insufficient information to assume that any value in the range was more likely than any other value [36]. As displayed in Table 1, the selected range for precipitation was wide compared to the other ranges. Thus, the precipitation intensity probability distribution was divided into three equal uniformly distributed intervals with equal probabilities (1/3) and the values were sampled from these intervals. The choice of the uniform distribution for precipitation intensity was made to ensure that all possible precipitation intensities from low to extreme rainfalls were presented for training the emulator.

A total of 1100 input data sets were randomly generated, and simulations were performed using HiSTAV. Because it is crucial to predict associated extreme rainfall events (i.e., real time flood prediction purposes as in early warning systems), in addition to the 1100 samples, another 100 samples that resulted in extreme events (higher  $C$  and  $i_p$  values and lower  $K_s$  values in river section) were simulated and were added to the total data set.



In this study we intended to emulate the numerical flood inundation modeling. Therefore, water level was considered as the output of interest in the simulations and the values were observed in three cross sections (CS), specified along the study area (Figure 1b).

### 2.3. Emulation Methods

#### 2.3.1. Support Vector Regression (SVR)

Support Vector Regression (SVR) is a supervised learning algorithm that estimates the connection between the input and output of a system from the existing samples [37]. This method attempts to identify correlations by transferring data to a higher dimension according to Equation (2) and solving the equation with the help of structural risk minimization based on Equation (3) [38]. If the relationship between the dependent and predictor variables is captured correctly, it can be used to predict the system outputs from the inputs [39].

$$f(x) = \omega\varphi(x) + b \quad (2)$$

$$\text{Minimize : } \left[ \frac{1}{2} \|\omega\|^2 + C \sum \xi_i + \xi_i^* \right] \quad \text{Subject to : } \begin{cases} y_i - (\omega\varphi(x_i) + b_i) \leq \varepsilon + \xi_i \\ (\omega\varphi(x_i) + b_i) - y_i \leq \varepsilon + \xi_i^* \\ \xi_i, \xi_i^* \geq 0 \end{cases} \quad (3)$$

Given a training data set  $(x_i, y_i), i = 1, 2, 3, \dots, n$   $x_i \in R^n, y_i \in R^n, x_i$  is the input vector,  $y_i$  shows the corresponding output, and  $i$  denotes the  $i$ th training sample. The variable  $\omega \in R^n$  denotes the weight factor,  $b \in R$  indicates the deviation and is constant,  $n$  is the size of data, and  $f(x)$  is the estimated target that is applied to calculate the output based on the actual input data, which has tolerance error and negligible complexity (Agustina et al., 2018). The expression  $\varphi(x_i)$  is a nonlinear transfer function that maps input data to the higher dimensional feature space;  $\xi_i$  and  $\xi_i^*$  are slack variables that specify the upper and the lower training errors subject to an error tolerance  $\varepsilon$ , and  $C$  is a positive constant that determines the degree of penalized loss when a training error occurs. Using the Lagrange relations, the nonlinear regression function will be as follows:

$$f(x) = \sum_{i=1}^n (a_i - a_i^*) k(x, x_i) + b \quad (4)$$

where,  $a_i, a_i^*$  are Lagrange coefficients and  $k(x, x_i) = \langle \varphi(x), \varphi(x_i) \rangle$  is called the kernel function [38]. There are different kernel functions such as: polynomial, Gaussian radial basis, exponential radial basis, and wavelet kernel. To have an accurate model, the models' parameters including  $C, \varepsilon$ , and the parameters of the kernel function should be determined appropriately. As a result, in the current study a grid search algorithm combined with the cross-validation method was used to optimize (tune) the different hyperparameters and models' architecture.

#### 2.3.2. Artificial Neural Networks (ANN)

Artificial neural networks (ANN) are nonlinear, multi-dimensional interpolating functions capable of capturing complex nonlinear relationships in the underlying data that can be missed by conventional regression methods. The topology structure of ANN is displayed in Figure 4. The network displayed in Figure 4 consists of a number of interconnected nodes (called neurons) arranged into three layers: input layer (receives input), hidden layer (represents the relationship between the input layer and the output layer), and output layer (releases the output). The implementation of the ANN model is based on three phases: a training phase to determine the model parameters from a set of training data, a validation phase to estimate the generalization ability of the model, and a test phase to calculate the output using the optimized model [40].

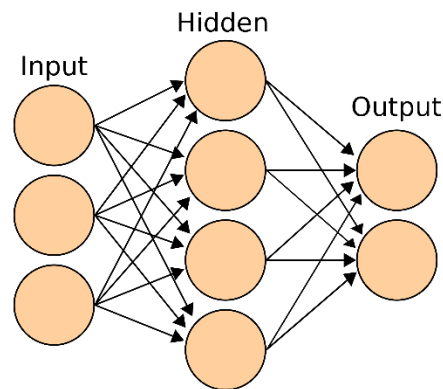


Figure 4. ANN topology.

### 2.3.3. Performance Criteria

The performance of the proposed emulators is assessed by computing several metrics: root mean square error (*RMSE*), mean relative absolute error (*MRAE*), and coefficient of determination ( $R^2$ ). In addition to these metrics, maximum absolute error (*MaxAE*) is also selected to assess the performance of the emulator in prediction of individual extreme values (Equations (5)–(9)). The *RMSE*, *MRAE*, and *MaxAE* metrics have ideal values equal to zero, and the ideal value for  $R^2$  is one.

$$Error = y_i - \hat{y}_i \quad (5)$$

$$RMSE = \sqrt{\frac{1}{n} \sum_{i=1}^n (y_i - \hat{y}_i)^2} \quad (6)$$

$$MRAE = \frac{1}{n} \sum_{i=1}^n \frac{|y_i - \hat{y}_i|}{\hat{y}_i} \quad (7)$$

$$R^2 = 1 - \frac{\sum_{i=1}^n (y_i - \hat{y}_i)^2}{\sum_{i=1}^n (y_i - \bar{y})^2} \quad (8)$$

$$MaxAE = Max|y_i - \hat{y}_i| \quad (9)$$

where  $n$  represents the number of observations,  $y_i$ ,  $\bar{y}$  and  $\hat{y}_i$  are observed, mean of observed, and predicted values, respectively.

### 2.4. Development of the Emulator

As was noted previously, 2D hydrodynamic models are usually computationally intensive and require long run time. In the current catchment considering the resolution of DTM and the number of mesh elements, each simulation takes about 1.5 h using  $8 \times$  NVIDIA Tesla P100 (16GB) GPU (Model:  $2 \times$  Intel(R) Xeon(R) CPU E5-2698 v4 @ 2.20GHz). Therefore, the main objective of this study is to produce an emulator to predict water level as close as possible to the 2D model outputs. In this section, we develop an emulator focusing on two questions: (i) how to increase the accuracy of the emulator and (ii) how much training data are required for developing an accurate emulator. We follow three steps: (1) develop the initial emulator using all the inputs, (2) improve the accuracy of the emulator by reducing the dimensionality, and (3) address the minimum data set size required for training an accurate emulator. A general overview of the workflow in this study is presented in Figure 5.

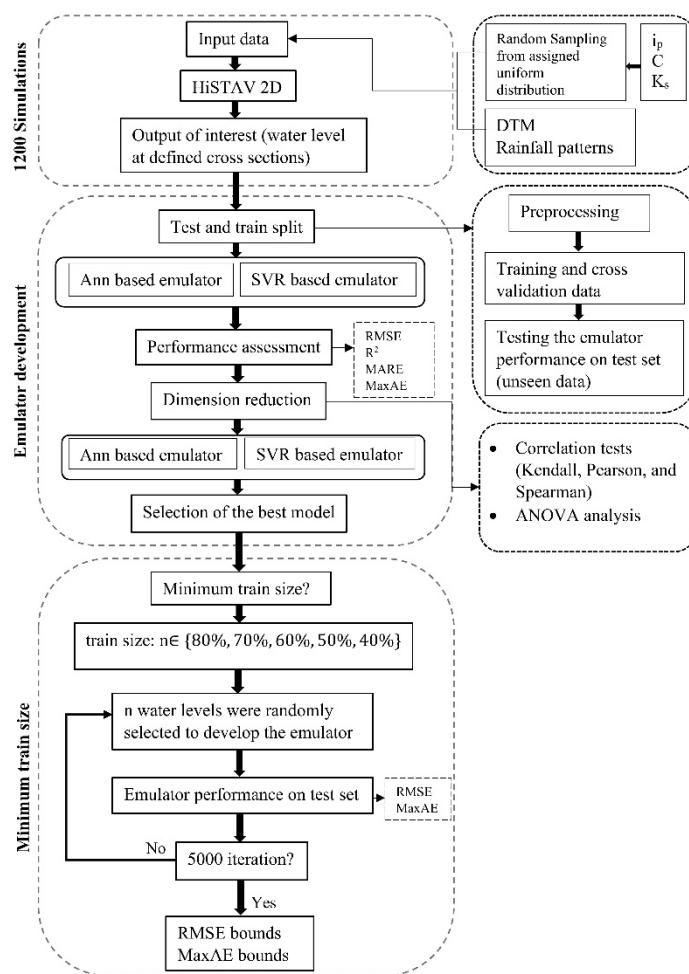


Figure 5. General overview of the methods.

To develop the emulator, the data set is split into test and training sets. Eighty percent of the data are randomly selected as the training set and 20% as the test set for model validation. Two emulators were developed, one using SVR and another using ANN.

To configure the artificial neural networks, a trial-and-error procedure was used to identify the number of hidden layers and nodes and fix the final architecture of the neural network model. Several different model structures were tested using 1 to 4 hidden layers and 4 to 30 hidden nodes, and the number of epochs was set as four epochs of 1000 iterations each. Finally, a model with two hidden layers with 10 and 12 hidden neurons in each was selected as the optimal structure. To determine the optimal structure for SVR a grid search algorithm was used, combined with the cross-validation method to optimize (tune) the different hyperparameters and models' architecture, and a model with parameters  $C = 10$ ,  $\gamma = 0.1$ ,  $\epsilon = 0.01$  and Radial basis function (RBF) kernel was selected as the optimal model.

The performance and accuracy of data driven approaches highly depend on the input selection and their functional relationship with outputs. Identifying suitable input variables reduces the model complexity and prevents redundant information being added into the model (i.e., input dependence), which avoids the negative impact of these inputs on model performance [41]. There are several approaches for dimensionality reduction purposes such as screening methods, correlation-based methods, variance-based techniques, principal component analysis, etc.

In this study three correlation tests—Pearson, Kendall, and Spearman—were used to identify the most correlated inputs and reduce the dimensionality. Pearson's correlation test is the most widely used correlation statistic to measure the degree of linear association

between two variables, whereas Kendall's and Spearman's correlation coefficients are based on ranks and measure the ranked order correlation. Further details of different correlation tests can be found in the study conducted by [42].

In addition to the correlation tests, analysis of variance (ANOVA) was performed to identify the most significant factors. This method focuses on the analysis of the variance explained by each input and is accomplished by estimating the Fischer's test value ( $F$ -value). The impact of any factor is explained by its  $F$ -value and the corresponding sum of squares that represent variance. A higher  $F$ -value and sum of squares of any factor indicates its relative importance in the process of the response [43]. To represent the impacts of each individual parameter, the percentage contribution ( $PC$ ) of each input is calculated using the following equation [44,45]:

$$PC = \frac{SS_j}{SS_T} \times 100 \quad (10)$$

where  $SS_T$  is the total sum of squares, and  $SS_j$  is the sum of squared deviations for each parameter  $j$ . Both can be calculated using Equations (11) and (12), respectively:

$$SS_T = \sum_{i=1}^n (Y_i - \bar{Y})^2 \quad (11)$$

$$SS_j = n_{jl} \sum_{i=1}^l (\bar{Y}_{ji} - \bar{Y})^2 \quad (12)$$

where  $n$  is the number of observations,  $Y_i$  represents the  $i$ th observed result in the result set,  $\bar{Y}$  is the average of the results,  $\bar{Y}_{ji}$  is the mean of results for the factor  $j$  at level  $i$ , and  $n_{jl}$  is the number of experiments that have factor  $j$  at level  $l$  [46].

To successfully train an emulator, the dataset on which the emulator is trained needs to be sufficiently large (i.e., consist of a sufficient number of observations) [47]. This can be challenging when the generation or collection of training data is subject to certain limitations. A number of studies have highlighted the importance of sampling and the effect of sample size on the accuracy of the models.

Hjort and Marmion [48] investigated the sample size effect on the accuracy of a geomorphological model using an ANN approach. Heckmann et al. [49] analyzed the sample size effects on logistic regression (LR) model accuracy for predicting debris flow spatial distribution and showed the negative effect of both inadequate sample size and too large sample size on results. Kalantar et al. [50] investigated the effect of different training samples on parameter estimation in SVR, LR, and ANN models and reported that the ANN model was performing better in terms of sensitivity to training samples. In this study training datasets with different sizes were created using random sampling. The procedure was repeated for +5000 times for each size and the variability in performance of the trained emulator was assessed through its predictive ability on the test set (unseen data).

### 3. Results and Discussion

Following the 1200 simulations obtained from random input data sets, two emulators were developed using ANN and SVR to predict water level at three different cross sections. The required time to predict 1200 water levels using ANN and SVR was about 1 min, which is 100,000 times faster compared to the simulation time using HiSTAV.

Figure 6 displays the water level predicted by ANN and SVR against the corresponding results of the 2D simulator. Moreover, to evaluate the performance of the initial emulators using a full set of inputs (14 input parameters), four statistical metrics,  $RMSE$ ,  $R^2$ ,  $MRAE$ , and  $MaxAE$  (Equations (6)–(9)) were calculated at each of three cross sections and the results are presented in Table 2.



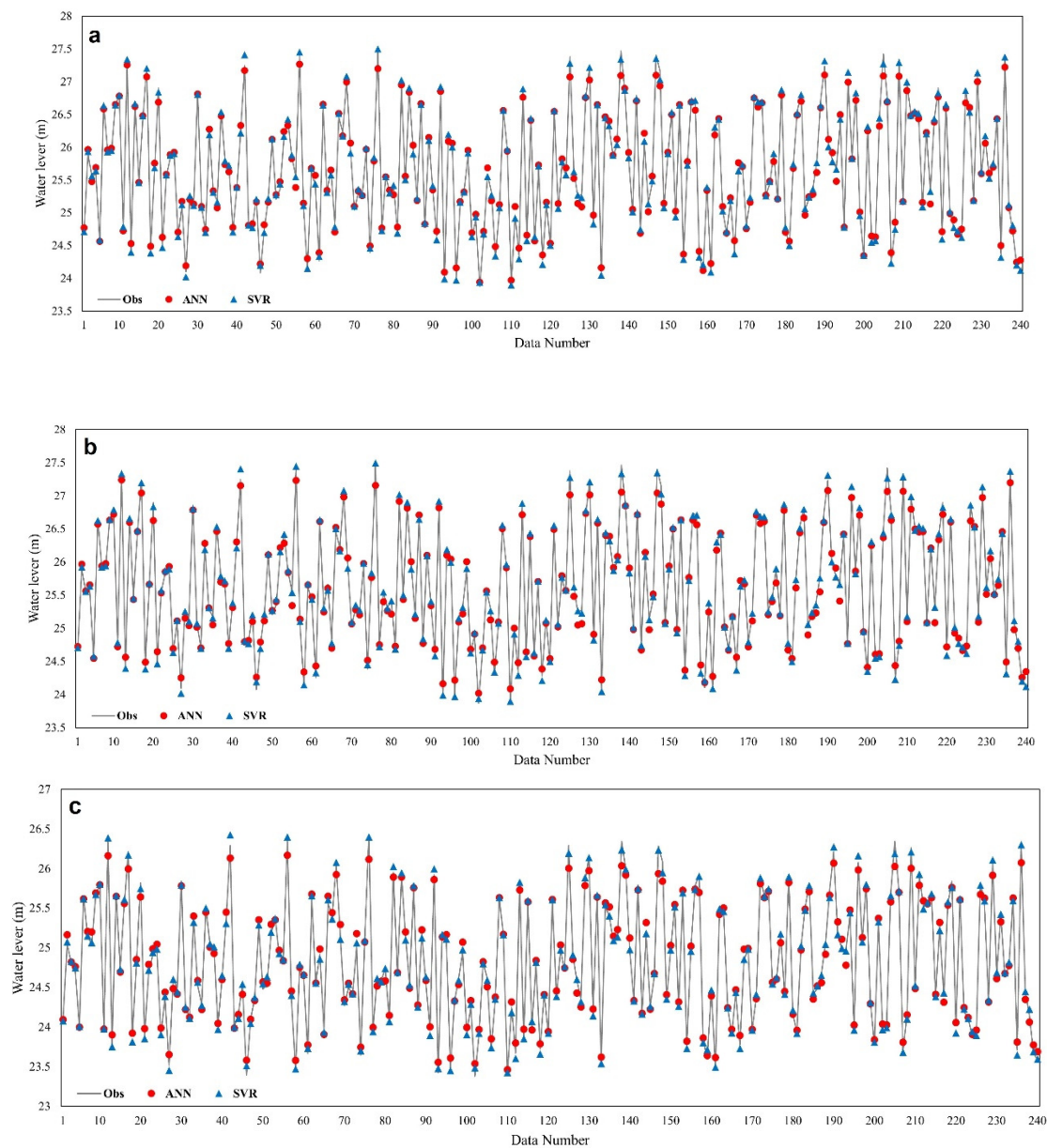


**Figure 6.** Comparison of observed and predicted water level for test set by ANN and SVR at cross section 1 (a), cross section 2 (b), and cross section 3 (c).

**Table 2.** Initial emulator performance (developed using 14 inputs) on test set.

Location	SVR				ANN			
	RMSE	R <sup>2</sup>	MRAE	MaxAE	RMSE	R <sup>2</sup>	MRAE	MaxAE
CS1	0.043	0.998	0.001	0.163	0.093	0.989	0.003	0.381
CS2	0.043	0.999	0.001	0.163	0.106	0.985	0.003	0.493
CS3	0.042	0.997	0.001	0.153	0.094	0.986	0.003	0.299

According to the performance statistics presented in Table 2 and the plots displayed in Figure 6, it can be seen that the SVR with optimized model parameters  $C = 10$ ,  $\gamma = 0.1$ ,  $\epsilon = 0.01$ , and Radial basis function (RBF) kernel, outperformed the ANN emulator and led to more accurate results. Looking at the *MaxAE* values in Table 2 and also the peak and minimum points in Figure 6, it can be observed that the performance of the emulators was

not accurate enough and, in some cases, they made errors as large as 16 cm (by SVR) and 50 cm (by ANN). Therefore, in next section we try to enhance the accuracy of the models.

### 3.1. Dimensionality Reduction

In this section three correlation tests—namely Kendall, Pearson, and Spearman—and ANOVA were used to identify the most important inputs and reduce the dimensionality. Using 1200 simulations obtained with 14 parameters with different spaces as inputs, the correlation tests and ANOVA analysis were applied in the specified cross sections, and the results are displayed in Figure 7.

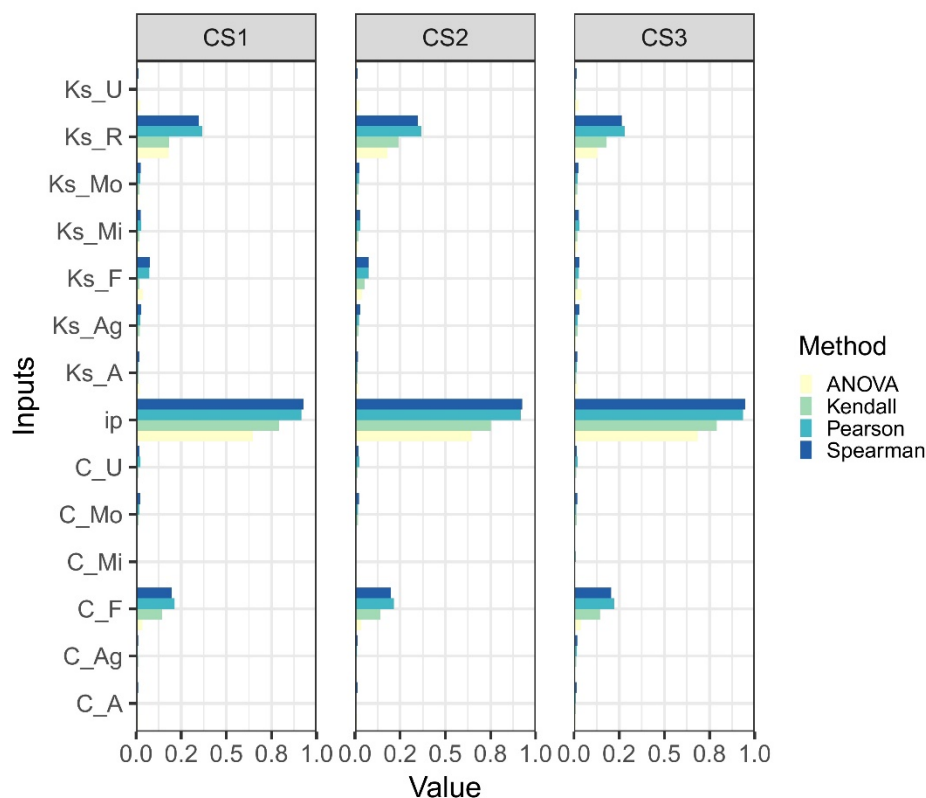


**Figure 7.** Absolute correlation values resulting from Kendall, Pearson, and Spearman tests and percentage of contribution (PC) values resulting from ANOVA test (Equation (10)).

The results of the different implemented techniques presented in Figure 7 indicate a significant correlation between rainfall ( $i_p$ ) and water level followed by river friction ( $K_s_R$ ) and forest runoff coefficient ( $C_F$ ). The findings of the correlation tests and ANOVA test are consistent; however, the ANOVA results are more stable at different locations compared to the correlation tests. According to the correlation values displayed in Figure 7, forest friction ( $K_s_F$ ) shows a weak correlation with water level at cross sections CS1 and CS2 and a negligible correlation at cross section CS3. Unlike correlation values, the calculated contribution value resulted from the ANOVA test shows an almost constant contribution of forest friction ( $K_s_F$  with about 4%) at different cross sections. Accordingly, two alternative approaches were adopted to train the emulators: first, the four highest correlated parameters (rainfall ( $i_p$ ), forest runoff coefficient ( $C_F$ ), river friction ( $K_s_R$ ), and forest friction ( $K_s_F$ )) were used to develop the emulators. In the second approach forest friction ( $K_s_F$ ) was removed from the input set and emulators were trained using only three inputs. The results of the first approach (four inputs) are presented in Table 3. Comparing Tables 2 and 3 (i.e., fourteen inputs and four inputs, respectively), shows that the performance of both emulators considerably improves (about 50% reduction in error values) when the number of the inputs decreases to four inputs. The results of the second

approach (three inputs) showed that the predictive ability of the models considerably deteriorates when the number of inputs is decreased to three parameters. Therefore, the results are only presented for the emulators with four inputs (Table 3).

**Table 3.** Emulator (with four inputs) performance on test set.

Location	SVR				ANN			
	RMSE	$R^2$	MRAE	MaxAE	RMSE	$R^2$	MRAE	MaxAE
CS1	0.024	0.999	0.001	0.084	0.099	0.987	0.003	0.291
CS2	0.024	0.999	0.001	0.084	0.121	0.983	0.004	0.426
CS3	0.022	0.999	0.001	0.078	0.085	0.988	0.003	0.363

The results presented in Table 3 indicate the efficiency of the methods used for detecting the main influencing parameters. However, caution must be taken in selection of inputs. As an example, the correlation tests detected the forest friction as a weakly correlated parameter, but the performance of the models improved considerably when this parameter was added into input set.

### 3.2. Error Structure Analysis

In order to gain insight into the predictive ability of the selected emulators (ANN and SVR with four inputs), the error values (Equation (5)) were plotted versus observed water level for the test set in the specified locations (CS1 to CS3). Moreover, to assess the error trend and change point, linear regression and polynomial regression were used. The slope of the linear regression line indicates if there is a trend in the plotted error values. Positive values of the slope show increasing error trends, whereas negative values indicate decreasing trends. A polynomial (quadratic) line that deviates strongly from the linear regression line provides further insights regarding how “severe” the potential over- or under-prediction may be for large target response values [21]. As it is displayed in Figure 8, the linear and polynomial regression lines for SVR model are close to each other and are approximately horizontal in all three cross sections. This result indicates that the performance of the SVR model for different magnitudes of floods were similar and relatively constant. In contrast, the ANN model showed an increasing trend of error. The error values were negative for the smaller water levels and positive for the higher water levels. This result indicates that the ANN model tends to overpredict the smaller floods and underpredict the extreme floods. The steep slope of the polynomial regression line for ANN indicates that the potential of underprediction of extreme events is even higher than overprediction of small floods by ANN. As can be seen in the plots, the best performance of ANN was achieved for the medium size floods. Moreover, from the plots it is apparent that the error ranges for SVR were much smaller than those for ANN.

In flood modeling/prediction processes the normality assumption for error values is quite common, whereas potentially error values can follow any distribution. Therefore, in this section the distribution of error is investigated using the histograms displayed in Figure 9. The histograms show that the ANN error distributions were non-symmetric and were skewed to the left (positively skewed). This result indicates that ANN generally overpredicts the water level. Unlike the ANN, the SVR error distributions were approximately symmetric, and the error ranges were much smaller compared to the ANN ones. The fitted SVR distributions in CS2 and CS3 were close to normal distribution. However, in CS1, the distribution was more peaked than the normal distribution. Thus, blindly assuming normality for errors, whereas data come from non-normal data (which is even more common), can eventuate to critical statistical inference problems.

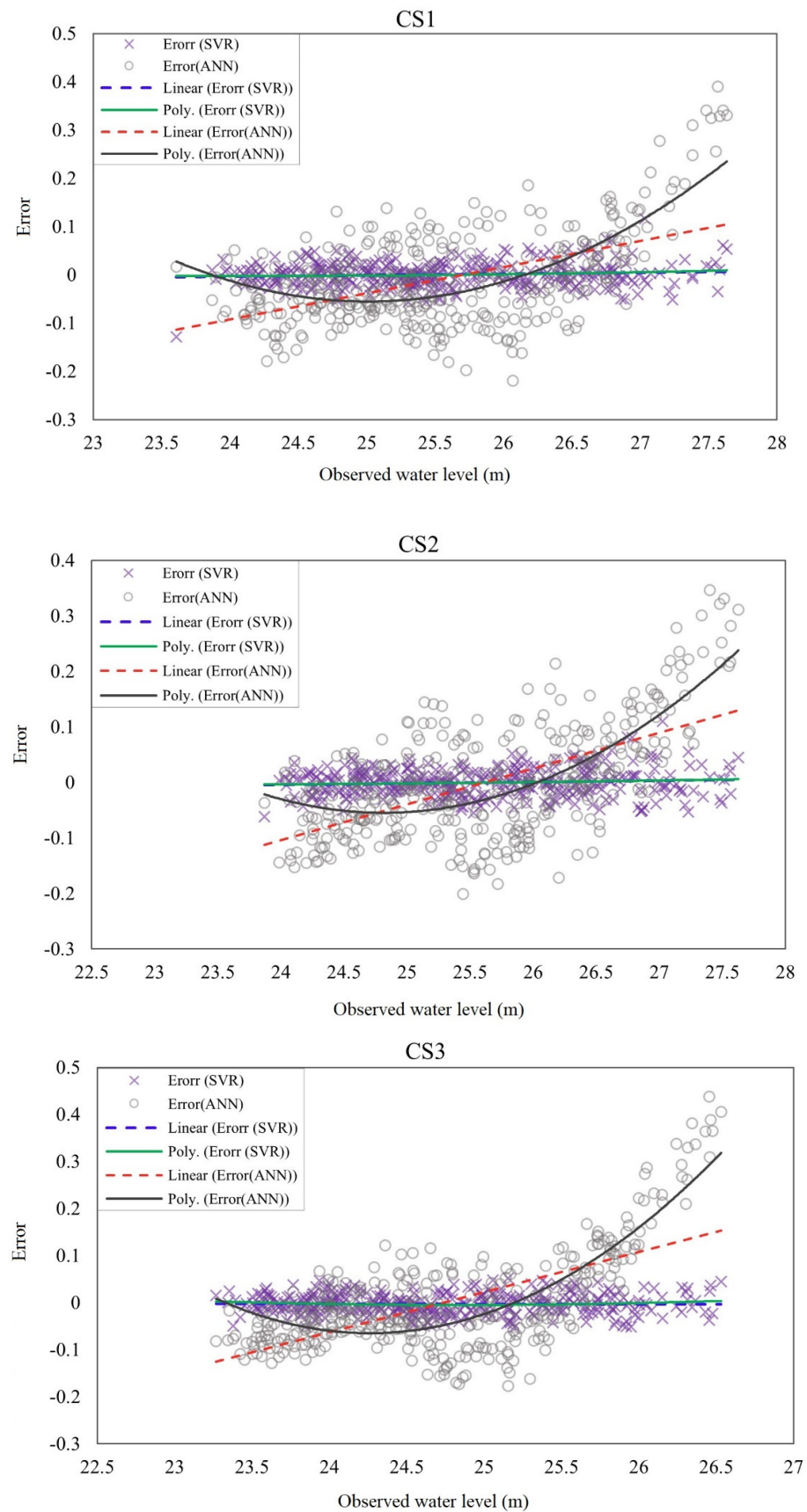


**Figure 8.** Error trend and linear and polynomial regression of error values resulted from SVR and ANN predicted water level at the specified cross sections (CS1 to CS3).

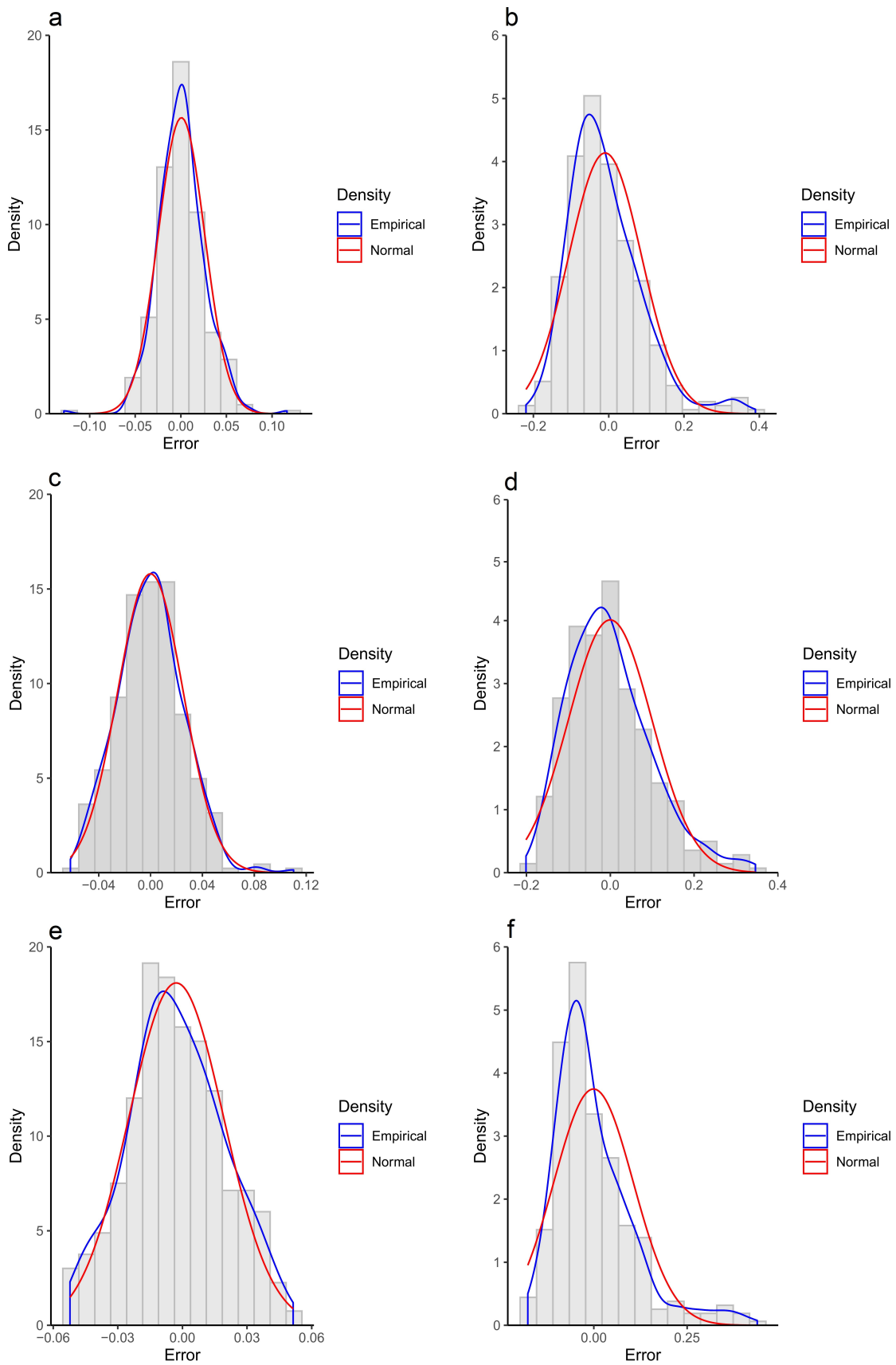


**Figure 9.** Empirical distribution of error values versus the normal distribution for the SVR and ANN based emulators. (a) SVR error distribution-CS1, (b) ANN error distribution-CS1, (c) SVR error distribution-CS2, (d) ANN error distribution-CS2, (e) SVR error distribution-CS3, (f) ANN error distribution-CS3.

### 3.3. Sample Size

In the previous section the SVR emulator with four inputs was selected as a reliable emulator. Therefore, in this section, we aim to extend our analysis by addressing the effect of sample size on the model accuracy. For this purpose, different training sample sizes equal to 80%, 70%, 60%, 50%, and 40% of the entire data set (1200 simulations) were generated by randomly selecting the required number of observations, and the performance of the emulator is assessed through *RMSE* and *MaxAE*. As an example, the training sample size equal to 70% was obtained with 840 observations randomly selected as the training set and the remaining (30%) used as the test set. The process was repeated for +5000 times for each training sample size to ensure that different possible events were sampled for training the emulator. The effect of selecting different training samples is displayed in Figure 10.

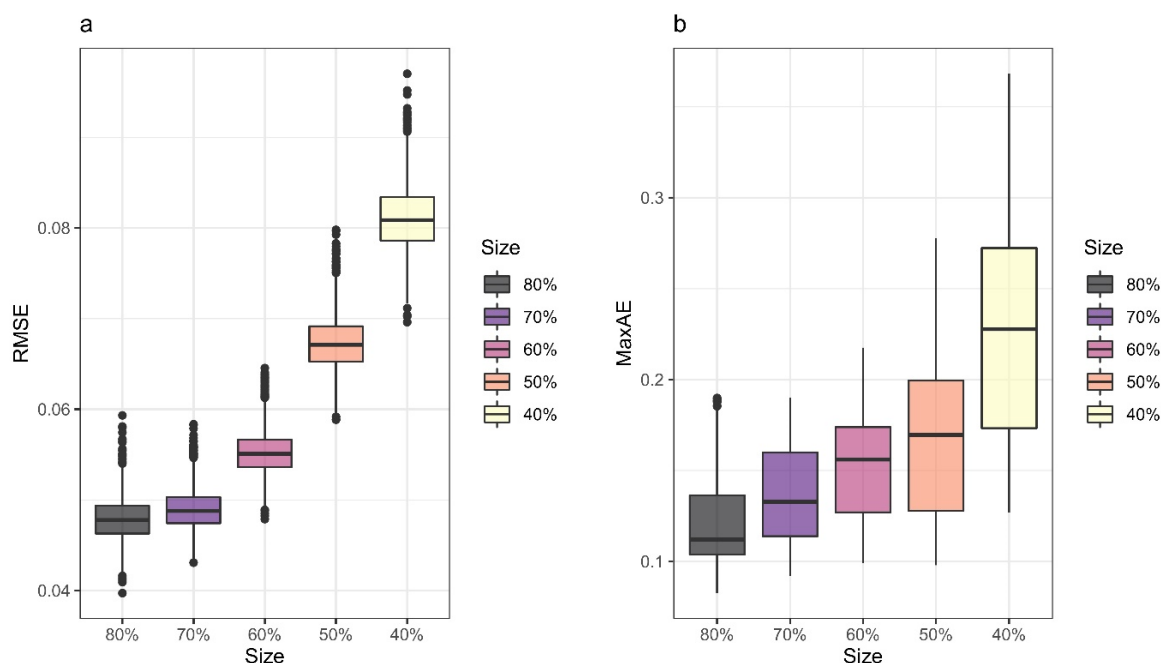


**Figure 10.** The calculated (a) *RMSE* and (b) *MaxAE* box plots for test sets resulting from the models trained by different sample sizes for 5000 times.

According to the *RMSE* values variation (Figure 10a), the larger training sets (80% and 70%) resulted in the smaller error values. Assuming 7 cm as an acceptable performance threshold, Figure 10a indicates that the *RMSE* values less than 7 cm can be achieved for training sizes equal to 60% or more. As shown in Figure 10a, decreasing the training size to 50%, led to a sudden increase in *RMSE* values (ranges between 6 cm to 8 cm). The box plot for the 50% size shows that 75% of the provided *RMSE* values were less than 7 cm. This result indicates that it is possible to train an acceptable emulator using 50% of data, but this requires a proper selection of the data.

Since extreme values are the major area of interest in flood studies and play an important role in defining confidence intervals or creating flood probability distributions, maximum absolute error (*MaxAE*) was also considered as a performance evaluation criterion in this section. Figure 10b displays the maximum error variation for each size resulting from 5000 iterations for each sample. Based on the Figure 10b, as it was expected the larger training sets (70% and 80%) were performing well. Looking at the median line for 80% and 70% sizes in the plots, it can be seen that the maximum difference between the observed and predicted water level mostly (75% of the time) varied between 8 cm to 13 cm. Although the size of 70% may produce error values as big as 16 cm to 19 cm (the *MaxAE* values above third quartile) (Figure 10b), it should be noted that the probability of getting such values is low, and in 75% of the time the *MaxAE* values never exceed 16 cm.



As much as the training size decreased, the *MaxAE* range increased. For training size equal to 60%, a comparison between the *RMSE* values (Figure 10a) and *MaxAE* values (Figure 10b), indicated that the overall performance of the emulator was acceptable (small *RMSE* values), but according to the *MaxAE* values, it may be prone to low probable values such as extremes floods. Furthermore, assuming 15 cm as the error threshold for *MaxAE*, it can be seen that about 50% of the *MaxAE* values (for training sample size of 60%) were above this limit. Accordingly, it was not reliable to train an emulator with less than 50% of the data (corresponding to 600 simulations), because the errors were typically beyond the acceptable limit. As it is displayed for the size equal to 40%, there is a big difference between the minimum and maximum calculated *MaxAE* values (about 25 cm), which means there is a large uncertainty associated with predicted extreme water levels that can bias the performance of the emulator.

#### 4. Conclusions

In the present study, two emulators were developed to predict cross sectional water level based on information obtained from coupled hydrology-hydraulic 2D simulations at the catchment scale. The following conclusions can be drawn from the present study:

- The statistical metrics for the developed emulators confirm the applicability of surrogates for predicting the cross-sectional water level. However, evaluating the results from different aspects (performance metrics, error trends, ranges, and distributions) showed that SVR has a better performance compared to ANN.
- Inclusion of too many variables as inputs can deteriorate the performance of the emulators; thus, simplification of the model structure through dimension reduction techniques can be used to obtain the most accurate model. The implemented correlation tests and ANOVA used in this study provided consistent results and showed that they can be a good choice to reduce the dimension of input data, improving the accuracy of the models.
- The error trend and regression plots for the SVR model and ANN model indicate that the performance of the SVR model for different magnitudes of floods are similar and relatively constant, whereas the ANN model tends to overpredict the smaller floods and underpredict the extreme floods. The best and worst performance of the ANN-based emulator is achieved for the medium size and extreme floods, respectively. Therefore, the application of the ANN model may not be safe for prediction of extreme flood events.
- The normality assumption for errors, which is typically undertaken in hazard assessment and decision making, is not always true and can eventuate to incorrect statistical inferences.
- The findings in this study suggest that the training data set size equal to 70% (or more) of data results in reliable and accurate predictions. The results also showed that it is not reliable to train an emulator with less than 50% of the data (corresponding to 600 simulations).

The use of data-driven models to emulate 2D hydrodynamic simulations at the catchment scale is feasible and will help to overcome the unaffordable computational resources of physical-based models. Finally, it is important to bear in mind the limitations of the current study. First, the time-consuming simulations prevented us from adopting a more complex approach such as synthetic hyetographs, which would increase the number of inputs and consequently would increase the total number of simulations. Therefore, we have used a time invariant precipitation intensity in this study. Second, the study is limited to 100-year design rainfall range; for the values outside of this range, the training process should be updated. Finally, this study has only focused on the water level as the output of interest. Further analyses should be done to develop an emulator to predict other important outputs such as the velocity. Nevertheless, the noted limitations do not invalidate the main conclusions presented above.

**Author Contributions:** Conceptualization, S.M.A. and J.L.; methodology, S.M.A.; software, S.M.A.; validation, J.L.; formal analysis, S.M.A.; investigation, J.L.; data curation, S.M.A.; writing—original draft preparation, S.M.A.; writing—review and editing, J.L.; visualization, S.M.A.; supervision, J.L. All authors have read and agreed to the published version of the manuscript.

**Funding:** The work presented in this paper is funded by the University of Agder, Norway (project number: 63859).

**Institutional Review Board Statement:** Not applicable.

**Informed Consent Statement:** Not applicable.

**Data Availability Statement:** The data used in this work including precipitation data and measured flow data are available at <http://www.senorge.no/> (accessed on 20 March 2021). The land cover maps are acquired from <https://land.copernicus.eu/pan-european/corine-land-cover> (accessed on 10 April 2021).

**Acknowledgments:** We would like to acknowledge the help of Ghali Yakoub in the Python coding of ANN and SVR algorithms.

**Conflicts of Interest:** The authors declare no conflict of interest.

## References

1. Panagoulia, D.; Dimou, G. Sensitivity of flood events to global climate change. *J. Hydrol.* **1997**, *191*, 208–222. [[CrossRef](#)]
2. Panagoulia, D. From low-flows to floods under global warming. In *EGU General Assembly 2009*; EGU General Assembly Conference Abstracts: Vienna, Austria, 2009; p. 4511.
3. Teng, J.; Jakeman, A.J.; Vaze, J.; Croke, B.F.; Dutta, D.; Kim, S.J.E.M. Software Flood inundation modelling: A review of methods, recent advances and uncertainty analysis. *Environ. Model. Softw.* **2017**, *90*, 201–216. [[CrossRef](#)]
4. Chu, H.; Wu, W.; Wang, Q.; Nathan, R.; Wei, J. An ANN-based emulation modelling framework for flood inundation modelling: Application, challenges and future directions. *Environ. Model. Softw.* **2020**, *124*, 104587. [[CrossRef](#)]
5. Jamieson, R.S.; Lhomme, J.; Wright, G.; Gouldby, B. A highly efficient 2D flood model with sub-element topography. *Proc. Inst. Civ. Eng. Water Manag.* **2012**, *165*, 581–595. [[CrossRef](#)]
6. Davidsen, S.; Löwe, R.; Thryssøe, C.; Arnbjerg-Nielsen, K. Simplification of one-dimensional hydraulic networks by automated processes evaluated on 1D/2D deterministic flood models. *J. Hydroinform.* **2017**, *19*, 686–700. [[CrossRef](#)]
7. Razavi, S.; Tolson, B.A.; Burn, D.H. Numerical assessment of metamodelling strategies in computationally intensive optimization. *Environ. Model. Softw.* **2012**, *34*, 67–86. [[CrossRef](#)]
8. Solomatine, D.P.; Ostfeld, A. Data-driven modelling: Some past experiences and new approaches. *J. Hydroinform.* **2008**, *10*, 3–22. [[CrossRef](#)]
9. Yu, J.; Qin, X.; Larsen, O. Uncertainty analysis of flood inundation modelling using GLUE with surrogate models in stochastic sampling. *Hydrol. Process.* **2015**, *29*, 1267–1279. [[CrossRef](#)]
10. Castro-Gama, M.E.; Popescu, I.; Li, S.; Mynett, A.; van Dam, A. Flood inference simulation using surrogate modelling for the Yellow River multiple reservoir system. *Environ. Model. Softw.* **2014**, *55*, 250–265. [[CrossRef](#)]
11. Luo, J.; Lu, W. Comparison of surrogate models with different methods in groundwater remediation process. *J. Earth Syst. Sci.* **2014**, *123*, 1579–1589. [[CrossRef](#)]
12. Bacchi, V.; Hamdi, Y.; Foch, M.; Pheulpin, L. Development of a new approach for the assessment of Flood Hazard through a kriging surrogate: Application to the bi-dimensional model of the Loire River. In *Advances in Extreme Value Analysis and Application to Natural Hazards, EVAN; CHATOU*: Paris, France, 2019.
13. Villa-Vialaneix, N.; Follador, M.; Ratto, M.; Leip, A. A comparison of eight metamodelling techniques for the simulation of N<sub>2</sub>O fluxes and N leaching from corn crops. *Environ. Model. Softw.* **2012**, *34*, 51–66. [[CrossRef](#)]
14. Ghalkhani, H.; Golian, S.; Saghafian, B.; Farokhnia, A.; Shamseldin, A. Application of surrogate artificial intelligent models for real-time flood routing. *Water Environ. J.* **2013**, *27*, 535–548. [[CrossRef](#)]
15. Xie, S.; Wu, W.; Mooser, S.; Wang, Q.; Nathan, R.; Huang, Y. Artificial neural network based hybrid modeling approach for flood inundation modeling. *J. Hydrol.* **2021**, *592*, 125605. [[CrossRef](#)]
16. Zhang, X.; Srinivasan, R.; Van Liew, M. Approximating SWAT model using artificial neural network and support vector machine 1. *JAWRA J. Am. Water Resour. Assoc.* **2009**, *45*, 460–474. [[CrossRef](#)]
17. Xu, T.; Valocchi, A.J.; Ye, M.; Liang, F. Quantifying model structural error: Efficient Bayesian calibration of a regional groundwater flow model using surrogates and a data-driven error model. *Water Resour. Res.* **2017**, *53*, 4084–4105. [[CrossRef](#)]
18. Liu, Y.; Pender, G. A flood inundation modelling using v-support vector machine regression model. *Eng. Appl. Artif. Intell.* **2015**, *46*, 223–231. [[CrossRef](#)]
19. Bermúdez, M.; Ntegeka, V.; Wolfs, V.; Willems, P. Development and comparison of two fast surrogate models for urban pluvial flood simulations. *Water Resour. Manag.* **2018**, *32*, 2801–2815. [[CrossRef](#)]
20. Bass, B.; Bedient, P. Surrogate modeling of joint flood risk across coastal watersheds. *J. Hydrol.* **2018**, *558*, 159–173. [[CrossRef](#)]



21. Al Kajbaf, A.; Bensi, M. Application of surrogate models in estimation of storm surge: A comparative assessment. *Appl. Soft Comput.* **2020**, *91*, 106184. [CrossRef]
22. Alipour, S.M.; Engeland, K.; Leal, J. A practical methodology to perform global sensitivity analysis for 2D hydrodynamic computationally intensive simulations. *Hydrol. Res.* **2021**, in press. [CrossRef]
23. Ferreira, R.M.; Franca, M.J.; Leal, J.G.; Cardoso, A.H. Mathematical modelling of shallow flows: Closure models drawn from grain-scale mechanics of sediment transport and flow hydrodynamics. *Can. J. Civ. Eng.* **2009**, *36*, 1605–1621. [CrossRef]
24. Conde, D.A.; Canelas, R.B.; Ferreira, R.M. A unified object-oriented framework for CPU+ GPU explicit hyperbolic solvers. *Adv. Eng. Softw.* **2020**, *148*, 102802. [CrossRef]
25. LeVeque, R.J. *Finite Volume METHODS for Hyperbolic Problems*; Cambridge University Press: Cambridge, UK, 2002; Volume 31. [CrossRef]
26. Geuzaine, C.; Remacle, J.F. Gmsh: A 3-D finite element mesh generator with built-in pre-and post-processing facilities. *Int. J. Numer. Methods Eng.* **2009**, *79*, 1309–1331. [CrossRef]
27. Arcement, G.J.; Schneider, V.R. *Guide for Selecting Manning's Roughness Coefficients for Natural Channels and Flood Plains*; US Government Printing Office: Washington, DC, USA, 1989.
28. Dorn, H.; Vetter, M.; Höfle, B. GIS-based roughness derivation for flood simulations: A comparison of orthophotos, LiDAR and crowdsourced geodata. *Remote Sens.* **2014**, *6*, 1739–1759. [CrossRef]
29. Goel, M.K. *Runoff Coefficient*, in *Encyclopedia of Snow, Ice and Glaciers*; Singh, V.P., Singh, P., Haritashya, U.K., Eds.; Springer: Dordrecht, The Netherlands, 2011; pp. 952–953. [CrossRef]
30. Subramanya, K. *Engineering Hydrology*, 4th ed.; Tata McGraw-Hill Education: New Delhi, India, 2013.
31. Viglione, A.; Hosking, J.R.; Laio, F.; Miller, A.; Gaume, E.; Payrastre, O.; Salinas, J.L.; N'guyen, C.C.; Halbert, K.; Viglione, M.A. *Package 'nsRFA'*. Non-supervised Regional Frequency Analysis. CRAN Repository, 2020. Version 0.7-15. Available online: <http://cran.r-project.org/web/packages/nsRFA/> (accessed on 20 March 2021).
32. Hanssen-Bauer, I.; Drange, H.; Førland, E.; Roald, L.; Børsheim, K.; Hisdal, H.; Lawrence, D.; Nesje, A.; Sandven, S.; Sorteberg, A. Climate in Norway 2100. In *Background Information to NOU Climate Adaptation (In Norwegian: Klima i Norge 2100. Bakgrunnsmateriale til NOU Klimatilpassing)*; Norsk Klimasenter: Oslo, Norway, 2009.
33. Reis, D.S., Jr.; Stedinger, J.R. Bayesian MCMC flood frequency analysis with historical information. *J. Hydrol.* **2005**, *313*, 97–116. [CrossRef]
34. Gaume, E.; Gaál, L.; Viglione, A.; Szolgay, J.; Kohnová, S.; Blöschl, G. Bayesian MCMC approach to regional flood frequency analyses involving extraordinary flood events at ungauged sites. *J. Hydrol.* **2010**, *394*, 101–117. [CrossRef]
35. Lutz, J.; Grinde, L.; Dyrddal, A.V. Estimating Rainfall Design Values for the City of Oslo, Norway—Comparison of Methods and Quantification of Uncertainty. *Water* **2020**, *12*, 1735. [CrossRef]
36. Dalbey, K.; Patra, A.; Pitman, E.; Bursik, M.; Sheridan, M. Input uncertainty propagation methods and hazard mapping of geophysical mass flows. *J. Geophys. Res. Solid Earth* **2008**, *113*, B05203. [CrossRef]
37. Vapnik, V. *The Nature of Statistical Learning Theory*; Springer Science & Business Media: Berlin/Heidelberg, Germany, 2013.
38. Dodangeh, E.; Panahi, M.; Rezaie, F.; Lee, S.; Bui, D.T.; Lee, C.-W.; Pradhan, B. Novel hybrid intelligence models for flood-susceptibility prediction: Meta optimization of the GMDH and SVR models with the genetic algorithm and harmony search. *J. Hydrol.* **2020**, *590*, 125423. [CrossRef]
39. Smola, A.J.; Schölkopf, B. A tutorial on support vector regression. *Stat. Comput.* **2004**, *14*, 199–222. [CrossRef]
40. Shu, C.; Burn, D.H. Artificial neural network ensembles and their application in pooled flood frequency analysis. *Water Resour. Res.* **2004**, *40*, W09301. [CrossRef]
41. Fernando, T.; Maier, H.; Dandy, G. Selection of input variables for data driven models: An average shifted histogram partial mutual information estimator approach. *J. Hydrol.* **2009**, *367*, 165–176. [CrossRef]
42. Lee Rodgers, J.; Nicewander, W.A. Thirteen ways to look at the correlation coefficient. *Am. Stat.* **1988**, *42*, 59–66. [CrossRef]
43. Karmakar, B.; Dhawane, S.H.; Halder, G. Optimization of biodiesel production from castor oil by Taguchi design. *J. Environ. Chem. Eng.* **2018**, *6*, 2684–2695. [CrossRef]
44. Yang, W.p.; Tarng, Y. Design optimization of cutting parameters for turning operations based on the Taguchi method. *J. Mater. Process. Technol.* **1998**, *84*, 122–129. [CrossRef]
45. Sadrzadeh, M.; Mohammadi, T. Sea water desalination using electro dialysis. *Desalination* **2008**, *221*, 440–447. [CrossRef]
46. Stahle, L.; Wold, S. Analysis of variance (ANOVA). *Chemom. Intell. Lab. Syst.* **1989**, *6*, 259–272. [CrossRef]
47. Alwosheel, A.; van Cranenburgh, S.; Chorus, C.G. Is your dataset big enough? Sample size requirements when using artificial neural networks for discrete choice analysis. *J. Choice Model.* **2018**, *28*, 167–182. [CrossRef]
48. Hjort, J.; Marmion, M. Effects of sample size on the accuracy of geomorphological models. *Geomorphology* **2008**, *102*, 341–350. [CrossRef]
49. Heckmann, T.; Gegg, K.; Gegg, A.; Becht, M. Sample size matters: Investigating the effect of sample size on a logistic regression susceptibility model for debris flows. *Nat. Hazards Earth Syst. Sci.* **2014**, *14*, 259–278. [CrossRef]
50. Kalantar, B.; Pradhan, B.; Naghibi, S.A.; Motevalli, A.; Mansor, S. Assessment of the effects of training data selection on the landslide susceptibility mapping: A comparison between support vector machine (SVM), logistic regression (LR) and artificial neural networks (ANN). *Geomat. Nat. Hazards Risk* **2018**, *9*, 49–69. [CrossRef]



**Paper IV:** Uncertainty Assessment of Flood Maps: A Comparison of Bootstrap and Monte Carlo Methods

Alipour, S.M., Leal, J., Engeland, K., 2022. Uncertainty Assessment of Flood Maps: A Comparison of Bootstrap and Monte Carlo Methods. Proceedings of the 39th IAHR World Congress(19–24 June 2022, Granada, Spain): 6422-6430.  
DOI:[doi://10.3850/IAHR-39WC2521716X2022651](https://doi.org/10.3850/IAHR-39WC2521716X2022651)



## Uncertainty Assessment of Flood Maps: A Comparison of Bootstrap and Monte Carlo Methods

Saba Mirza Alipour<sup>(1)</sup>, Kolbjørn Engeland<sup>(2)</sup>, Joao Leal<sup>(3)</sup>

<sup>(1)</sup> Department of Engineering and Science, University of Agder, Jon Lilletuns vei 9, 4879 Grimstad, Norway,  
Email: Saba.m.alipour@uia.no

<sup>(2)</sup> Norwegian Water Resources and Energy Directorate (NVE), PO Box 5091 Maj., 0301 Oslo, Norway,  
Email: koe@nve.no

<sup>(3)</sup> Department of Engineering and Science, University of Agder, Jon Lilletuns vei 9, 4879 Grimstad, Norway,  
Email: joao.leal@uia.no

### Abstract

Uncertainty is unavoidable in flood modeling practices and should be properly communicated. There are a variety of methods and techniques for uncertainty analysis, but normally they require a large number of hydrological/hydrodynamic model realizations. Among several uncertainty analysis methods, bootstrap is a popular technique which is carried out to make statistical inferences by using limited (or small) number of realizations without imposing much structural assumptions. This study has critically assessed the applicability of bootstrap method for assessing the uncertainty in flood mapping and compared the results with those that are obtained from Monte Carlo method. The results challenge the applicability of bootstrap method as an alternative to the more computationally intensive methods such as Monte Carlo. Furthermore, the results suggest that the mean parameter's variation, which is typically undertaken as a convergence criterion in uncertainty analysis, can lead to early stopping of the process and consequently wrong statistical inferences.

**Keywords:** Bootstrap; Monte Carlo; Uncertainty analysis; Flood modeling

### 1. INTRODUCTION

Floods are one of the main natural hazards affecting millions of human lives and cause large economic losses. The increasing number of severe flood events in recent years has motivated the development of safe and reliable flood maps. However, due to the complex nature of floods and the uncertain nature of parameters affecting flood generation process, there is a considerable degree of uncertainty in flood estimates, flood zone mapping and flood risk assessments. In addition to the uncertain nature of flood events, the uncertainty is introduced into the flood modeling process by different sources of uncertainty. These sources such as input parameters, model structure, simplifications and assumptions that are made throughout the modeling process, or analysis can play important role and significantly influence the final outputs.

In the past decades, despite the great improvement in flood inundation modelling tools and approaches, accurate flood modeling and methods to deal with the associated uncertainty are still the subject of ongoing research. Teng et al. (2017), has provided a comprehensive review of different flood modeling methods and uncertainty analyses in this field. Among various types of the flood modeling approaches, 2D hydrodynamic models are one of the popular tools which represent floodplain flow as a two-dimensional field with the assumption that the third dimension (corresponding to the depth) is shallow in comparison to the other two dimensions (Teng et al., 2017). 2D hydrodynamic models are based on the numerical solution of the 2D Shallow Water Equations (SWE), use different types of input parameters with complex domain spaces (e.g., hydrological data, floodplain and channel geometry, initial and boundary conditions, roughness, etc.) and provide outputs such as flow velocity, water level, discharge, and inundation extent. However, uncertainty is an inevitable part of the simulated outputs and uncertainty analyses have therefore become an essential part of flood modelling practices.

A large and growing body of literature has investigated the uncertainty associated with input parameters such as hydraulic roughness coefficient in the river channel and flood plains, precipitation, discharge and design hydrograph (e.g., Sampson et al., 2014, Das and Umamahesh, 2018, Vojtek et al., 2019, Chen et al., 2018, Ahmadisharaf et al., 2018), topography/bathymetry and digital terrain models (DTM) (e.g., Savage et al. (2016), Abily et al., 2016, Lim and Brandt, 2019, Neal et al., 2015, van Vuren et al., 2015, Mejia and Reed, 2011). A considerable amount of literature has explored the propagated uncertainty in the model's outputs such as flood

inundation map (e.g., Merwade et al., 2008, Jung and Merwade, 2012, Liu and Merwade, 2018), flood volume and discharge (Dung et al., 2015, Lumbroso and Gaume, 2012), and flood risk analyses (e.g., Apel et al., 2004, Apel et al., 2009, Vousdoukas et al., 2018).

A majority of these studies attempt to represent the uncertainty using either frequentist methods (e.g. Gallagher and Doherty, 2007, Montanari and Grossi, 2008, Bomers et al., 2019) or Bayesian methods (e.g., Bates et al., 2004, Reis Jr and Stedinger, 2005, Hall et al., 2011, Parkes and Demeritt, 2016). Bayesian approach requires a parametric model defined by the likelihood. In contrast to Bayesian methods, nonparametric bootstrap represents a frequentist approach that doesn't require any parametric distributions, and therefore involves fewer assumptions (Selle and Hannah, 2010). The bootstrap method, initially introduced by Efron (1979) is a class of nonparametric resampling methods which relies on drawing random samples with replacement from the available dataset and thereby allow to carry out statistical inference on a wide range of estimators like the mean value without imposing much structural assumptions on the underlying data-generating random process (Kreiss and Lahiri, 2012). The essential idea of the nonparametric bootstrap approach is that the data provide the best estimate of the distribution from which the data were drawn (Tibshirani and Efron, 1993).

Several studies thus far have implemented bootstrap technique in hydrology and environmental modeling practices for a variety of purposes including frequency analysis (e.g., Cunderlik and Burn, 2003, 2003, Engeland et al., 2004, Overeem et al., 2008, Bomers et al., 2019), model and parameter uncertainty analyses (e.g., Selle and Hannah, 2010, Li et al., 2010, Zhang et al., 2018, Gopalan et al., 2019), uncertainty assessment of water quality trends (e.g., Srinivas and Srinivasan, 2005, Hirsch et al., 2015., Uddameri et al., 2018) and uncertainty analyses in flood forecasting models in combination with artificial neural networks (ANN) (e.g., Han et al., 2007, Tiwari and Chatterjee, 2010).

There are different approaches for application of the bootstrap technique, namely residual bootstrap, Markovian bootstrap, the prominent block bootstrap and frequency domain resampling procedures (Kreiss and Lahiri, 2012). In fact the original bootstrap idea of Efron (1979) fails to provide satisfactory answers to general statistical inference problems for dependent data such as time series data, since the assumption of independently and identically distributed (i.i.d.) data is violated (Beyaztas et al., 2018). In order to overcome this problem, the bootstrap method can be extended either as a block bootstrap (Davison and Hinkley, 1997, Kunsch, 1989;), which divides the time series into different blocks and draws samples from these blocks (Lahiri, 2003, Selle and Hannah, 2010), or as a residual based bootstrap (or model based bootstrap) (Freedman, 1981, Efron and Tibshirani, 1986) in which the residuals obtained from the original dataset by fitting some general models, such as linear regression, autoregression, or nonparametric regression models, are resampled to obtain the bootstrap sample of the data (Beyaztas et al., 2018, Gopalan et al., 2019).

In this study we aim to implement the bootstrap method to assess the uncertainty associated with 100-year flood water level and maps and we attempt to answer the following questions:

- What is the smallest sample size that can accurately represent the original sample and its uncertainty?
- Can bootstrap method capture the incorporated uncertainty as well as the Monte Carlo method does?
- Does increasing the number of bootstrap replications, compensate the smallness of sample size?

## 2. METHODS

### 2.1. Hydrodynamic Simulations (Emulator) and Input Data

In the current study, a GPU based 2DH (two dimensional horizontal) hydrodynamic model named HiSTAV (developed by Conde et al., 2020) has been used to simulate flow using different input sets. The 2D model provide accurate results but it is computationally intensive. Therefore, these types of tools might not be a proper choice when a large number of model realizations is needed (such as required in uncertainty analysis). To overcome this constrain we simulated 1,300 different flood events and used these simulations to develop an emulator to replace the original hydrodynamic model. The details of the process are presented in the study by Alipour and Leal (2021). The developed emulator gives as output the water level and requires the following input parameters: hydraulic roughness parameter ( $K_S$ ), runoff coefficient ( $C$ ) and precipitation intensity ( $i_P$ ).

To generate the input set, hydraulic roughness ( $K_S$ ) and runoff coefficient ( $C$ ) parameters are randomly sampled assuming a uniform probability distribution within a specified range which was established based on tabled values and engineering expertise, reflecting the possible variation range for each parameter. The uniform distribution is selected since it makes no assumptions about prior parameter distribution other than specifying a



feasible range and scale (Freer et al., 1996). Table 1 presents the considered uncertain input parameters with their descriptions and specified ranges used in this study.

**Table 1.** Selected input descriptions and assigned ranges

Parameters		Acronym	Range
Strickler roughness ( $m^{1/3}/s$ )	Forests (broad-leaved, coniferous)	$Ks\_F$	15-40
	River and water courses	$Ks\_R$	20-50
Runoff coefficient (%)	Forests (broad-leaved, coniferous)	$C\_F$	50-70

To generate the precipitation sample, we have used daily precipitation data acquired from bias-adjusted climate projections for Norway. The data are presented as  $1 \times 1$  km grid data and are made available by Norwegian Centre for Climate Services (NCCS) (<https://klimaservicesenter.no/>). Further details about the data and bias correction procedure can be found in the study by Wong et al. (2016).

It should be noted that the model uses a spatially varying precipitation over the catchment (Fig. 1) and Birkeland region at the down part of catchment receives the highest amount of precipitation (100%) (Fig. 1). Thus, we have selected the cells covering Birkeland region and extracted the time series for this region to develop area averaged annual maximum precipitation (AMP) series.

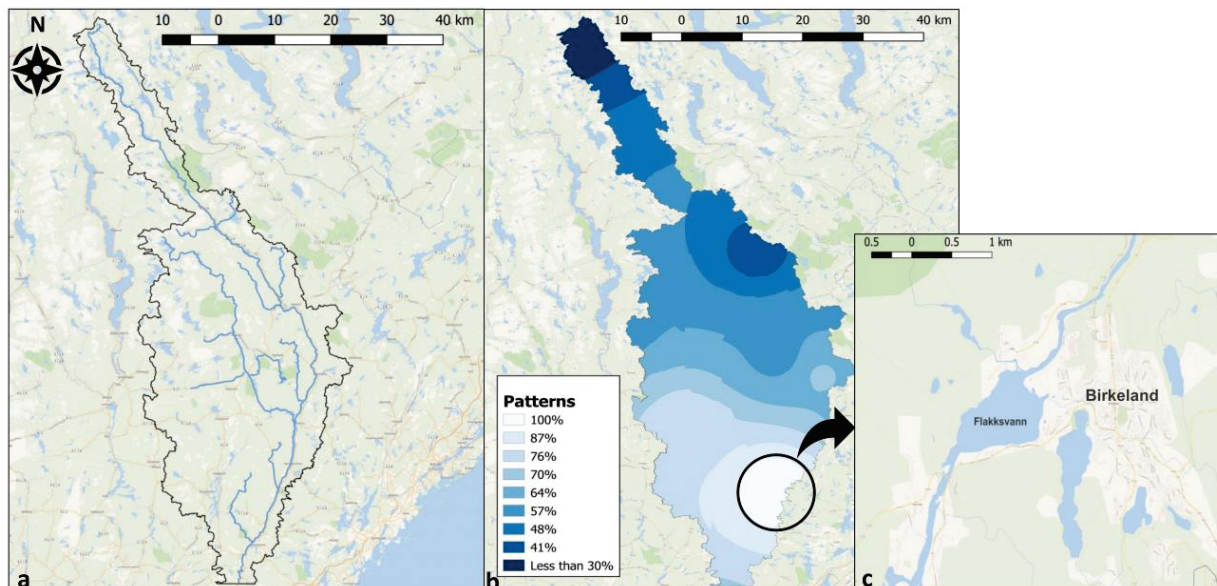


**Figure 1.** a) The study area and, b) precipitation patterns adopted by the model over the catchment. The Birkeland region (panel c) receives 100% of the precipitation. The patterns are generated using the interpolation of measured rainfall values in different stations and resembles the 2017 precipitation pattern which is used as the reference event for uncertainty analysis (details in Alipour et al., 2021).

10 AMP series are developed using 10 EURO-CORDEX RCMs (Regional Climate Models) for a future period (2071–2100) under a representative concentration pathway (RCP), namely RCP4.5. The information of the models is displayed in Table 2.

**Table 2.** The climate models information

Institute	Global Climate Model (GCM)	Regional Climate Model (RCM)
CLM-Community	CNRM-CER-FACS-CM5	CCLM4-8-17
SMHI	CNRM-CER-FACS-CM5	RCA4
CLM-Community	ICHEC-EC-EARTH	CCLM4-8-17
DMI	ICHEC-EC-EARTH	HIRHAM5
KNMI	ICHEC-EC-EARTH	RACMO22E
SMHI	ICHEC-EC-EARTH	RCA4
SMHI	IPSL-CM5A-MR	RCA4
SMHI	MOHC-HADGEM2-ES	RCA4
CLM-Community	MPI-ESM-LR	CCLM4-8-17
SMHI	MPI-ESM-LR	RCA4

Once the AMP series are obtained, the Gumbel distribution was fitted to them, using Bayesian Markov Chain Monte Carlo (MCMC) method. For the Bayesian inference, we created Markov Chain Monte Carlo chains (number of chains = 3) of length 50,000 and estimated the posterior probability of the 100-year precipitation values for each AMP. In other words, 3 (number of chains)×50,000 (length of each chain)×10 (AMP series) values of 100-year precipitation are ensembled and the values within the 90% CI are used as the precipitation sample. The Bayesian MCMC process was applied in nsRFA package (Viglione et al., 2020).

Using a Monte Carlo process, the inputs are randomly sampled to simulate the water level in Flaksvan lake using the emulator. In this study, we carried out 100,000 Monte Carlo simulations and obtained an extensive sample of water levels in Flaksvan lake. We selected the extensive number of 100,000, insuring a stable and converged sample to be used as the original sample whose statistical characteristics are considered as certain.

## 2.2. Application of Bootstrap Approach

In this study a bootstrap method based on sampling with replacement is used to represent the uncertainty in flood inundation mapping. Assume that the data consists of a random sample  $T_n = \{(x_1, y_1), (x_2, y_2), \dots, (x_n, y_n)\}$  of size  $n$  sampled from an unknown probability distribution  $F$ , where  $t_i = (x_i, y_i)$  is a realization sampled independently and identically distributed (i.i.d.) from  $F$  and consists of a predictor vector  $x_i$ , and the corresponding output variable  $y_i$ . The samples have the same number of elements that the original set has and since the samples are made with replacement, they can contain some elements several times and might not contain some of the original elements at all (for details please see, Schnaidt and Heinson, 2015). The set of  $B$  bootstrap samples can be represented as  $T_1, T_2, \dots, T_b, \dots, T_B$ , in which  $B$  is the total number of bootstrap samples and ranges usually from 50 to 200 (Efron and Tibshirani, 1993). The process repeated many times, provides a large sample of bootstrap estimates from which standard errors or confidence intervals for the original corresponding parameter estimates may be calculated.

## 3. RESULTS AND DISCUSSION

As mentioned before, this study seeks to (i) determine the adequate original sample size for representing the associated uncertainty of the statistical parameters of the original sample (i.e., Mean, 0.025 quantile, 0.975 quantile), (ii) identify the size of bootstrap samples (i.e., the required replication), and (iii) represent the uncertainty associated with the probabilistic 100-year return period flood maps.

To determine the adequate sample size that represents the original sample distribution, the following procedure was used: i) sample of sizes 100, 200, 500, 1000, 2000, 5000, 10000 20000 and 100000 were extracted from the original MC sample, one sample for each sample size. (ii) For each sample from (i), we created 10 000 bootstrap samples. (iii) For each bootstrap sample we estimated the mean, the 0.025 quantile (q1) and the 0.975 quantile (q2) resulting in 10 000 estimates of each statistical parameters. (iv) We calculated the 95% CI for each statistical parameter. Fig. 2, displays the constructed CI for each of the statistical parameters and bootstrap sample size. The dashed red line shows the statistical parameters calculated for the original sample (100,000 water level simulations, resulted from random sampling from inputs (Monte Carlo process)). As displayed in the figure, the constructed bounds for the mean and q2, cover the true mean and true q2 values



(displayed with red dashed line) for all the sample sizes. However, the estimated bounds for the q1, do not cover the true value in sizes equal to 1,000 and 500. According to the figure, the CI gets narrower by increasing sample size, providing smaller uncertainty. The results from Fig. 2 suggest that the size equal to 2,000 (or more) provides 100% coverage of true statistical parameters. The uncertainty converges for sizes bigger than 5,000, and as it was expected the mean parameter converges faster than the tail quantiles. Therefore, the mean parameter's variation, which is typically undertaken as a convergence criterion in uncertainty analysis, can lead to early stopping of the process and consequently wrong statistical inferences. The estimated CI, for 0.975 percentile converges slower than the other parameters and has the highest uncertainty. The size of 10,000 can be selected as the converged and stabilized CI, which corresponds to 7 cm uncertainty in q1 and q2, and 3 cm uncertainty in the mean value.

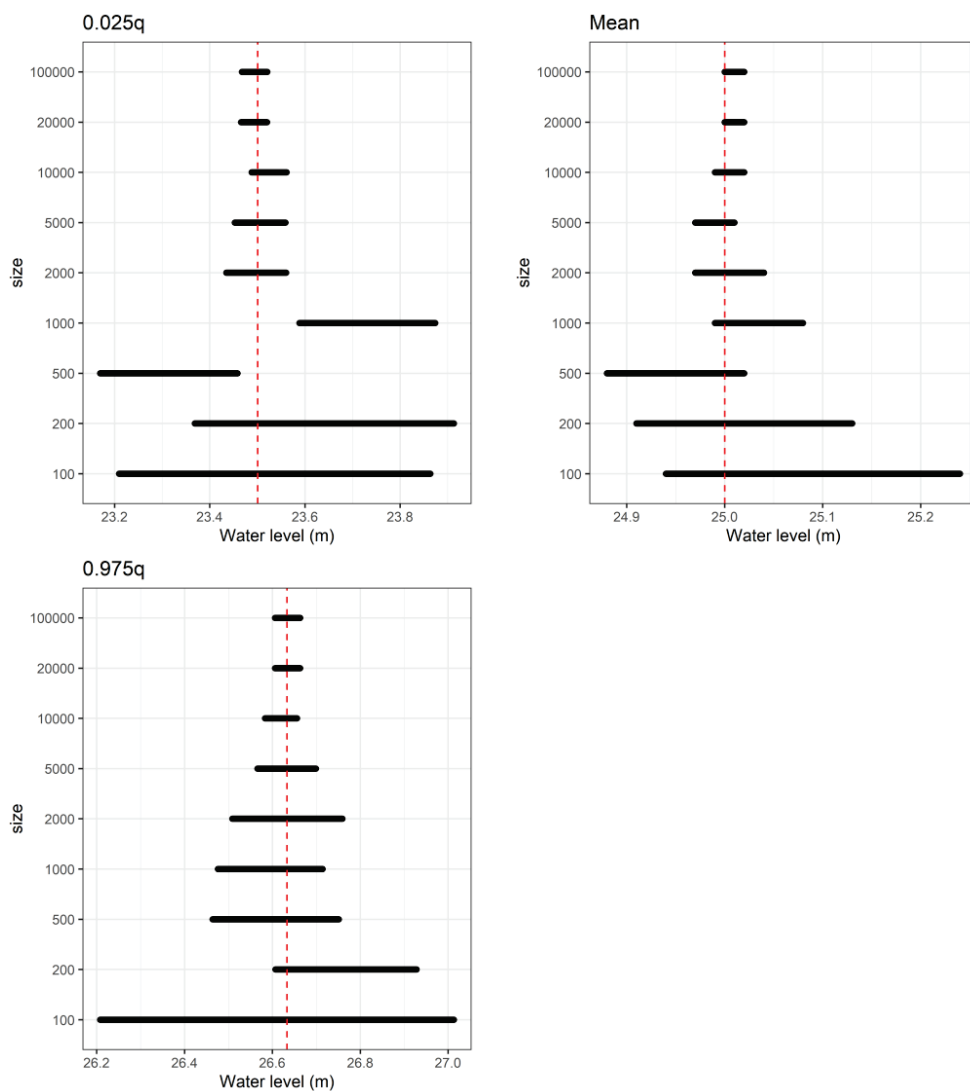


**Figure 2.** The uncertainty associated with 0.025q, Mean and 0.975q parameters, represented by bootstrap method. The red dashed line represents the estimated statistics for the sample size of 100,000 (assumed as the true values).

As stated earlier, the bootstrap assumes the observations in the original sample are the only ones that can ever be observed. Therefore, as it can be seen in the Fig. 2, the bootstrap does not work well with small sample sizes which are not adequately representative and provides inaccurate CIs. According to the importance of the sample size, a question arises: when the sample is not large enough, are we able to reduce the uncertainty by increasing the number of replications of bootstrapping (even more than 10,000)? To answer this question, we have performed bootstrapping on a sample size equal to 5,000 for different number of replications (i.e., bootstrap

samples). Here we presented the results only for  $q_2$  in Fig. 3. We start with replication equal to 1,000 and increased it to 100,000 and obtained almost same CI's. Therefore, increasing the number of replications, doesn't avoid the shortcomings of having small sample size.

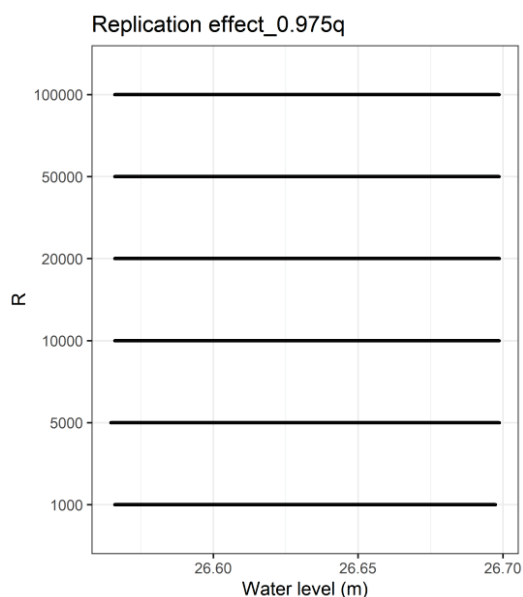


**Figure 3.** The influence of replication (number of bootstrap samples) in bootstrap method with a sample size of 5,000

In the present study, the uncertainty of the 100-year flood map, is defined as the difference between  $q_1$  and  $q_2$ . By selecting the lower bound of estimated CI for  $q_1$  (23.47 m), and the upper bound for  $q_2$  (26.66 m) in the converged samples (those that have size larger than 5,000), the uncertainty of water level is calculated as 3.19 m. The estimated uncertainty in terms of flood map is presented in the Fig. 4.

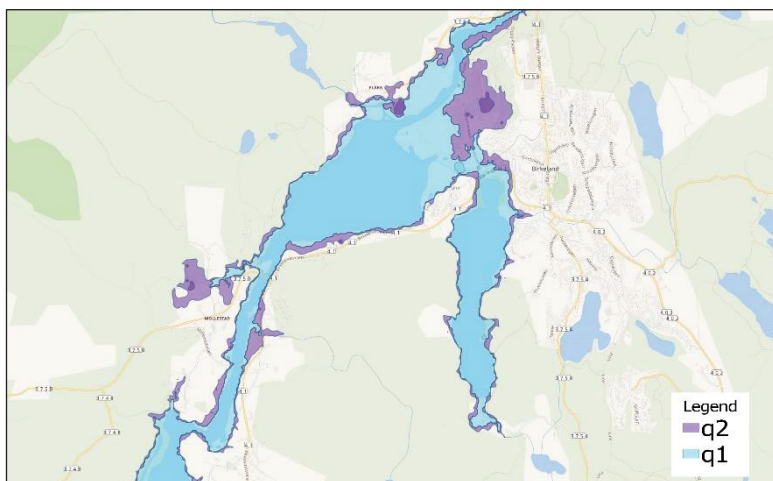


**Figure 4.** The flooded area uncertainty estimated by the water levels resulted from the lower bound ( $q_1$ ) and upper bound value ( $q_2$ ) of water level probability distribution.

According to the results, the bootstrap technique can give a rough estimate of the uncertainty of parameters such as the mean. Nevertheless, the uncertainty of parameters such as  $q_1$  and  $q_2$  that converge slowly, needs to be captured using large samples. The bootstrap method usually is used when limited number of data are available, however, as it has been discussed bootstrap technique performs poorly for relatively small samples,

requiring large samples that cannot be avoided by increasing the number of bootstrap samples (repetitions). In comparison to the Monte Carlo method, bootstrap provides same uncertainty bounds only for large samples, therefore this result challenges the applicability of this less computationally intense as an alternative to the more computationally intensive uncertainty analysis methods such as Monte Carlo.

#### 4. CONCLUSION

The bootstrap method is usually introduced as robust and powerful technique for uncertainty analysis in limited and small samples where the large number of realizations are not feasible. This study set out to determine the applicability of bootstrap method in uncertainty analysis and tries to demonstrate its limitations and reliability. The following conclusions can be drawn from the present study:

- The bootstrap technique is dependent on the original sample and the degree of representativeness of the original sample significantly influences the bootstrap results. Therefore, in small samples, bootstrap method performs poorly and provides unrealistic statistical inferences.
- Bootstrap technique performs well in large samples, and to achieve reliable inferences, it requires samples sizes as large as the Monte Carlo method does.
- Increasing the number of replications, doesn't avoid the shortcomings of having small sample size.
- A comparison between three statistics namely means, 0.025 and 0.975 quantiles, in both Monte Carlo analysis and bootstrap analysis, showed that the mean parameter converges faster than the other parameters. Therefore, the mean parameter's variation, which is typically undertaken as a convergence criterion in uncertainty analysis, can lead to early stopping of the process and consequently wrong statistical inferences.

#### 5. REFERENCES

- Abily, M., Delestre, O., Gourbesville, P., Bertrand, N., Duluc, C.-M., Richet, Y., 2016. Global sensitivity analysis with 2D hydraulic codes: application on uncertainties related to high-resolution topographic data, *Advances in Hydroinformatics*. Springer, pp. 301-315. DOI:[https://doi.org/10.1007/978-981-287-615-7\\_21](https://doi.org/10.1007/978-981-287-615-7_21)
- Ahmadisharaf, E., Kalyanapu, A.J., Bates, P.D., 2018. A probabilistic framework for floodplain mapping using hydrological modeling and unsteady hydraulic modeling. *Hydrological Sciences Journal*, 63(12): 1759-1775. DOI:<https://doi.org/10.1080/02626667.2018.1525615>
- Alipour, S.M., Engeland, K., Leal, J., 2021. A practical methodology to perform global sensitivity analysis for 2D hydrodynamic computationally intensive simulations. *Hydrology Research*. DOI:<https://doi.org/10.2166/nh.2021.243>
- Alipour, S.M., Leal, J., 2021. Emulation of 2D Hydrodynamic Flood Simulations at Catchment Scale Using ANN and SVR. *Water*, 13(20): 2858.
- Apel, H., Aronica, G., Kreibich, H., Thielen, A., 2009. Flood risk analyses—how detailed do we need to be? *Natural hazards*, 49(1): 79-98.
- Apel, H., Thielen, A.H., Merz, B., Blöschl, G., 2004. Flood risk assessment and associated uncertainty. *Natural Hazards and Earth System Sciences*, 4(2): 295-308.
- Bates, P.D., Horritt, M.S., Aronica, G., Beven, K., 2004. Bayesian updating of flood inundation likelihoods conditioned on flood extent data. *Hydrological processes*, 18(17): 3347-3370.
- Beyaztas, U., Arikan, B.B., Beyaztas, B.H., Kahya, E., 2018. Construction of prediction intervals for Palmer Drought Severity Index using bootstrap. *Journal of Hydrology*, 559: 461-470.
- Bomers, A., Schielen, R.M., Hulscher, S.J., 2019. Decreasing uncertainty in flood frequency analyses by including historic flood events in an efficient bootstrap approach. *Natural hazards and earth system sciences*, 19(8): 1895-1908.
- Chen, S., Garambois, P.-A., Finaud-Guyot, P., Dellinger, G., Mose, R., Terfous, A., Ghennaim, A., 2018. Variance based sensitivity analysis of 1D and 2D hydraulic models: An experimental urban flood case. *Environmental Modelling & Software*, 109: 167-181. DOI:<https://doi.org/10.1016/j.envsoft.2018.08.008>
- Conde, D.A., Canelas, R.B., Ferreira, R.M., 2020. A unified object-oriented framework for CPU+ GPU explicit hyperbolic solvers. *Advances in Engineering Software*, 148: 102802. DOI:<https://doi.org/10.1016/j.advengsoft.2020.102802>
- Cunderlik, J.M., Burn, D.H., 2003. Non-stationary pooled flood frequency analysis. *Journal of Hydrology*, 276(1-4): 210-223.

- Das, J., Umamahesh, N., 2018. Assessment of uncertainty in estimating future flood return levels under climate change. *Natural Hazards*, 93(1): 109-124.
- Davison, A.C., Hinkley, D.V., 1997. *Bootstrap methods and their application*. Cambridge university press.
- Dung, N.V., Merz, B., Bárdossy, A., Apel, H., 2015. Handling uncertainty in bivariate quantile estimation—An application to flood hazard analysis in the Mekong Delta. *Journal of Hydrology*, 527: 704-717.
- Efron, B., 1979. Bootstrap methods: another look at the jackknife, *Breakthroughs in statistics*. Springer, pp. 569-593.
- Efron, B., Tibshirani, R., 1986. Bootstrap methods for standard errors, confidence intervals, and other measures of statistical accuracy. *Statistical science*: 54-75.
- Engeland, K., Hisdal, H., Frigessi, A., 2004. Practical extreme value modelling of hydrological floods and droughts: a case study. *Extremes*, 7(1): 5-30.
- Freedman, D.A., 1981. Bootstrapping regression models. *The Annals of Statistics*, 9(6): 1218-1228.
- Gopalan, S.P., Kawamura, A., Amaguchi, H., Takasaki, T., Azhikodan, G., 2019. A bootstrap approach for the parameter uncertainty of an urban-specific rainfall-runoff model. *Journal of Hydrology*, 579: 124-195.
- Hall, J.W., Manning, L.J., Hankin, R.K., 2011. Bayesian calibration of a flood inundation model using spatial data. *Water Resources Research*, 47(5).
- Han, D., Kwong, T., Li, S., 2007. Uncertainties in real-time flood forecasting with neural networks. *Hydrological Processes: An International Journal*, 21(2): 223-228.
- Hirsch, R.M., Archfield, S.A., De Cicco, L.A., 2015. A bootstrap method for estimating uncertainty of water quality trends. *Environmental Modelling & Software*, 73: 148-166.
- Jung, Y., Merwade, V., 2012. Uncertainty quantification in flood inundation mapping using generalized likelihood uncertainty estimate and sensitivity analysis. *Journal of Hydrologic Engineering*, 17(4): 507-520.
- Kreiss, J.-P., Lahiri, S.N., 2012. Bootstrap methods for time series, *Handbook of statistics*. Elsevier, pp. 3-26.
- Kunsch, H.R., 1989. The jackknife and the bootstrap for general stationary observations. *The annals of Statistics*: 1217-1241.
- Lahiri, P., 2003. On the impact of bootstrap in survey sampling and small-area estimation. *Statistical Science*, 18(2): 199-210.
- Li, Z., Shao, Q., Xu, Z., Cai, X., 2010. Analysis of parameter uncertainty in semi-distributed hydrological models using bootstrap method: A case study of SWAT model applied to Yingluoxia watershed in northwest China. *Journal of Hydrology*, 385(1-4): 76-83.
- Lim, N.J., Brandt, S.A., 2019. Flood map boundary sensitivity due to combined effects of DEM resolution and roughness in relation to model performance. *Geomatics, Natural Hazards and Risk*, 10(1): 1613-1647. DOI:<https://doi.org/10.1080/19475705.2019.1604573>
- Liu, Z., Merwade, V., 2018. Accounting for model structure, parameter and input forcing uncertainty in flood inundation modeling using Bayesian model averaging. *Journal of hydrology*, 565: 138-149.
- Lumbroso, D., Gaume, E., 2012. Reducing the uncertainty in indirect estimates of extreme flash flood discharges. *Journal of hydrology*, 414: 16-30.
- Mejia, A.I., Reed, S., 2011. Evaluating the effects of parameterized cross section shapes and simplified routing with a coupled distributed hydrologic and hydraulic model. *Journal of Hydrology*, 409(1-2): 512-524. DOI:<https://doi.org/10.1016/j.jhydrol.2011.08.050>
- Merwade, V., Olivera, F., Arabi, M., Edleman, S., 2008. Uncertainty in flood inundation mapping: current issues and future directions. *Journal of Hydrologic Engineering*, 13(7): 608-620.
- Montanari, A., Grossi, G., 2008. Estimating the uncertainty of hydrological forecasts: A statistical approach. *Water Resources Research*, 44(12).
- Neal, J.C., Odoni, N.A., Trigg, M.A., Freer, J.E., Garcia-Pintado, J., Mason, D.C., Wood, M., Bates, P.D., 2015. Efficient incorporation of channel cross-section geometry uncertainty into regional and global scale flood inundation models. *Journal of Hydrology*, 529: 169-183. DOI:<https://doi.org/10.1016/j.jhydrol.2015.07.026>
- Overeem, A., Buishand, A., Holleman, I., 2008. Rainfall depth-duration-frequency curves and their uncertainties. *Journal of Hydrology*, 348(1-2): 124-134.
- Parkes, B., Demeritt, D., 2016. Defining the hundred year flood: A Bayesian approach for using historic data to reduce uncertainty in flood frequency estimates. *Journal of Hydrology*, 540: 1189-1208.
- Reis Jr, D.S., Stedinger, J.R., 2005. Bayesian MCMC flood frequency analysis with historical information. *Journal of hydrology*, 313(1-2): 97-116. DOI:<https://doi.org/10.1016/j.jhydrol.2005.02.028>
- Sampson, C.C., Fewtrell, T.J., O'Loughlin, F., Pappenberger, F., Bates, P.B., Freer, J.E., Cloke, H.L., 2014. The impact of uncertain precipitation data on insurance loss estimates using a flood catastrophe model. *Hydrology and Earth System Sciences*, 18(6): 2305-2324.

- Savage, J., Pianosi, F., Bates, P., Freer, J., Wagener, T., 2016. Quantifying the importance of spatial resolution and other factors through global sensitivity analysis of a flood inundation model. *Water Resources Research*, 52(11): 9146-9163. DOI:<https://doi.org/10.1002/2015WR018198>
- Schnaidt, S., Heinson, G., 2015. Bootstrap resampling as a tool for uncertainty analysis in 2-D magnetotelluric inversion modelling. *Geophysical Journal International*, 203(1): 92-106.
- Selle, B., Hannah, M., 2010. A bootstrap approach to assess parameter uncertainty in simple catchment models. *Environmental Modelling & Software*, 25(8): 919-926.
- Srinivas, V., Srinivasan, K., 2005. Matched block bootstrap for resampling multiseason hydrologic time series. *Hydrological Processes: An International Journal*, 19(18): 3659-3682.
- Teng, J., Jakeman, A.J., Vaze, J., Croke, B.F., Dutta, D., Kim, S.J.E.M., 2017. Flood inundation modelling: A review of methods, recent advances and uncertainty analysis. 90: 201-216. DOI:<https://doi.org/10.1016/j.envsoft.2017.01.006>
- Tibshirani, R.J., Efron, B., 1993. An introduction to the bootstrap. *Monographs on statistics and applied probability*, 57: 1-436.
- Tiwari, M.K., Chatterjee, C., 2010. Development of an accurate and reliable hourly flood forecasting model using wavelet-bootstrap-ANN (WBANN) hybrid approach. *Journal of Hydrology*, 394(3-4): 458-470.
- Uddameri, V., Singaraju, S., Hernandez, E.A., 2018. Detecting seasonal and cyclical trends in agricultural runoff water quality—hypothesis tests and block bootstrap power analysis. *Environmental monitoring and assessment*, 190(3): 157.
- van Vuren, S., Paarlberg, A., Havinga, H., 2015. The aftermath of “Room for the River” and restoration works: Coping with excessive maintenance dredging. *Journal of hydro-environment research*, 9(2): 172-186. DOI:<https://doi.org/10.1016/j.jher.2015.02.001>
- Viglione, A., Hosking, J.R., Laio, F., Miller, A., Gaume, E., Payrastre, O., Salinas, J.L., N'guyen, C.C., Halbert, K., Viglione, M.A., 2020. Package ‘nsRFA’. Non-supervised Regional Frequency Analysis. CRAN Repository, Version 0.7-15.
- Vojtek, M., Petroselli, A., Vojteková, J., Asgharina, S., 2019. Flood inundation mapping in small and ungauged basins: sensitivity analysis using the EBA4SUB and HEC-RAS modeling approach. *Hydrology Research*, 50(4): 1002-1019. DOI:<https://doi.org/10.2166/nh.2019.163>
- Vousdoukas, M.I., Bouziotas, D., Giardino, A., Bouwer, L.M., Mentaschi, L., Voukouvalas, E., Feyen, L., 2018. Understanding epistemic uncertainty in large-scale coastal flood risk assessment for present and future climates. *Natural Hazards and Earth System Sciences*, 18(8): 2127-2142.
- Wong, W.K., Haddeland, I., Lawrence, D., Beldring, S., 2016. Gridded 1 x 1 km climate and hydrological projections for Norway.
- Zhang, A., Shi, H., Li, T., Fu, X., 2018. Analysis of the influence of rainfall spatial uncertainty on hydrological simulations using the bootstrap method. *Atmosphere*, 9(2): 71.



**Paper VI:** Uncertainty analysis of 100-year flood maps under climate change scenarios

Alipour, S.M., Leal, J., Engeland, K., 2022. Uncertainty analysis of 100-year flood maps under climate change scenarios. (Submitted to the Journal of Hydrology, Manuscript Number: HYDROL47552)





## **Uncertainty analysis of 100-year flood maps under climate change scenarios**

Saba Mirza Alipour<sup>a</sup>, Kolbjørn Engeland<sup>b</sup>, Joao Leal<sup>a</sup>

<sup>a</sup> Department of Engineering and Science, University of Agder, Jon Lilletuns vei 9, 4879, Grimstad, Norway

<sup>b</sup> Norwegian Water Resources and Energy Directorate (NVE), PO Box 5091 Maj., 0301 Oslo, Norway

### **Abstract**

In this study, the uncertainty of 100-year flood maps under 3 scenarios (present and future RCP4.5 and RCP8.5) is assessed through intensive Monte Carlo simulations. The uncertainty introduced by model input data namely, roughness coefficient, runoff coefficient and precipitation intensity (which incorporates three different sources of uncertainty (RCP scenario, climate model, and probability distribution function), propagated through a surrogate hydrodynamic/hydrologic model developed based on a physical 2D model. The results obtained from this study challenge the use of deterministic flood maps and climate factors and suggests using probabilistic approaches for developing safe and reliable flood maps. Furthermore, they show that the main source of uncertainty comes from the precipitation, namely the selected probability distribution compared to the selected RCP and climate model.

**Keywords:** deterministic approach, probabilistic approach, 100-year flood maps, uncertainty, climate change

### **Introduction**

Flood inundation maps are useful tools to delineate inundated regions. Generally, those maps are developed using deterministic modeling techniques to represent inundated zones in terms of floodplain boundaries as a single line. However, due to the complex and chaotic nature of flooding and considerable degree of uncertainty which stem from different sources, the flood maps should not be defined as a single deterministic border. Evidence for this can be found looking at flood insurance claims of recent flood events, where a remarkable number of claims have occurred out of the identified hazard zones (Brody et al., 2013). This confirms the inefficiency of deterministic maps to present a safe realization of flood extends. In recent years,

according to the increase in frequency and severity of floods and their disastrous influence on society, the need for developing accurate flood maps has been increased. In the past decades, despite the great improvement in flood inundation modelling tools and approaches, accurate flood modeling and methods to deal with the incorporated uncertainty are still the subject of ongoing research. Teng et al. (2017) provided a comprehensive review of different flood modeling methods and uncertainty analyses techniques implemented to quantify the associated uncertainty. Among various types of the flood modeling approaches, 2D hydrodynamic models are one of the popular tools which represent floodplain flow as a two-dimensional field with the assumption that the third dimension (water depth) is shallow in comparison to the other two dimensions (Teng et al., 2017). 2D hydrodynamic models are based on the numerical solution of the 2D Shallow Water Equations (SWE), use different types of input parameters with complex domain spaces (e.g., hydrological data, floodplain and channel geometry, initial and boundary conditions, roughness, etc.) and provide outputs such as flow velocity, water level, discharge, and inundation extent. However, uncertainty is an unavoidable part of the simulated outputs and uncertainty analyses therefore become an essential part of flood modelling practices. A considerable amount of literature has been published on investigating the uncertainty associated with the flood modeling outputs such as flood inundation map (e.g., Merwade et al., 2008, Jung and Merwade, 2012, Liu and Merwade, 2018), flood volume and discharge (Dung et al., 2015, Leandro et al., 2019) and flood risk analyses (e.g., Apel et al., 2004, Apel et al., 2009, Vousdoukas et al., 2018).

According to the literature, the key sources of uncertainty in flood modeling are (1) input parameters such as hydraulic roughness coefficient in the river channel and flood plains, precipitation, discharge and design hydrograph (e.g., Sampson et al., 2014, Das and Umamahesh, 2018, Vojtek et al., 2019, Chen et al., 2018, Ahmadisharaf et al., 2018, Lawrence, 2020), topography/bathymetry and digital terrain models (DTM) (e.g., Savage et al. (2016), Abily et al., 2016, Lim and Brandt, 2019, Neal et al., 2015, Van Vuren et al., 2015, Mejia and Reed, 2011), (2) model parameters and structures (e.g., boundary conditions Pappenberger et al., 2006b, mesh generation Kim et al., 2014, modeling assumptions and simplifications Wagenaar et al., 2016) and (3) validation data (Stephens et al., 2012, Thielen et al., 2015).

There are several frameworks and approaches that have been proposed in literature to address uncertainty issues systematically (e.g., Pappenberger et al., 2006a, Beven et al., 2011, Beven et al., 2015, Teng et al., 2017, Ahmadisharaf et al., 2018). One of the widely used approaches for uncertainty analyses purposes, is the probabilistic approach in which the uncertainty is described by means of probability distributions. Input parameters are treated as random variables with known probability distributions, and the result is a probability distribution of an output parameter (Komatina and Branisavljevic, 2005). In the present study we follow three main steps that are identified by Beven et al. (2015) to address the uncertainty associated with 100-year flood inundation map: firstly, the sources of uncertainty are to be identified; secondly, uncertainty from different sources need to be quantified (or at least ranked qualitatively) and then prioritized; and lastly, uncertainty should be properly communicated (Beven et al., 2015, Dottori et al., 2013).

The existing uncertainty in the input parameters can arise from different sources, such as inconsistent or unavailable data, measurement errors, sampling errors and selection of a probability distribution function (PDF). Determining the input uncertainty is one of the major tasks in flood uncertainty analyses since many parameters are not directly measurable, it is generally not possible to collect a large, random sample of parameter values and test various PDFs for their ability to describe uncertainty in the parameters (Haan et al., 1998). Among various uncertain input parameters required for flood simulation, estimation of precipitation is a significant challenge due to several reasons such as complex and chaotic nature of weather, unavailable or incomplete records and the estimation methods. This is even more challenging and entails considerable uncertainty under future climate conditions due to simulation assumptions, uncertainty of climate models, climate change effect, downscaling errors and bias adjustment methods.

Generally, the uncertainty associated with inputs is defined through assigning particular PDFs to the inputs. However, as it is mentioned earlier it is often difficult to identify the correct and representative PDF for the inputs and several studies have shown the importance of this issue (e.g., Haan et al., 1998, Merz and Thielen, 2009, Winter et al., 2018, Annis et al., 2020, Moccia et al., 2021).

Choosing PDFs for inputs requires a reasonable description of that particular input and arbitrary selection of PDFs can eventuate to unreliable results. According to the literature review, the commonly used distributions for roughness parameter are uniform distribution (e.g., Pappenberger et al., 2005, Warmink et al., 2013, Annis et al., 2020), Lognormal (mainly used for channel roughness) (e.g., Hall et al., 2005, Papaioannou et al., 2017) and Beta distribution (Hall et al., 2005). The PDFs that are widely used to estimate design extreme precipitation are Gumbel and generalized extreme value (GEV) (Papalexiou and Koutsoyiannis, 2013, Kobierska et al., 2013).

Once the uncertainty sources are identified, the key preliminary step is the selection of the methods to represent the propagated uncertainty. One of the popular and widely used methods for uncertainty analysis is Monte Carlo (MC) method (e.g., Loveridge and Rahman, 2014, Vousdoukas et al., 2018). Nevertheless, this method requires a large number of realizations (often more than 1,000), and this constrain limits the application of the MC method in the flood models with a long execution time such as in catchment scale modeling.

To date, numerous studies have attempted to analyze and represent the propagated uncertainty in flood maps through different methods. Most of these studies have been performed in small or limited areas such as river reaches. Few studies in the literature have investigated the associated uncertainty of flood maps in catchment scale while considering both hydrological and hydraulic properties of the catchment. Furthermore, usually due to the computational constrains intensive number of MC simulations ( $>10,000$ ) has not been performed. Therefore, in this study we aim to i) explore the effect of assigning different PDFs for inputs on the output and its uncertainty, ii) estimate the future 100-year flood magnitude, iii) represent the 100-year flood map uncertainty in different scenarios including present, and future through intensive number (100,000) of MC simulations, iv) delineate the differences between deterministic and probabilistic maps and vi) decompose the uncertainty into its sources.

## **Method**

Surrogate hydrodynamic model

In the current study, a surrogate model (called emulator here after) which was developed to mimic a physical 2D model has been used to simulate floods. The physical model named HiSTAV, is a GPU based 2DH (two dimensional horizontal) hydrodynamic model, originally proposed by Ferreira et al. (2009) and optimized by Conde et al. (2020). The core of the model is a hyperbolic system of partial differential equations expressing mass and momentum conservation principles for shallow-water flows. The equations are solved using a finite volume scheme, which is applied on a spatial discretization using unstructured meshes. The model requires different data sets such as topo-bathymetric dataset, Strickler roughness coefficient values, runoff coefficient values (in form of raster files) and precipitation intensity as input to simulate the flow. The case of this study is Birkeland town area, located in Agder province (Norway). In recent years floods have become a major concern there. Birkeland is located beside a river named Tovdal, where the river debouches into a small natural lake called Flakksvann (Fig. 1). The length of the main river is approximately 130 km, and the catchment has an area of about 1767 km<sup>2</sup> dominated by forests (about 74%). The elevation ranges from 10.00 to 872.34 m.a.s.l., and the average slope of the catchment along the river is about 0.65%. The mean annual precipitation is approximately 1261 mm, with most of the rainfall occurring between October and March (about 60%).

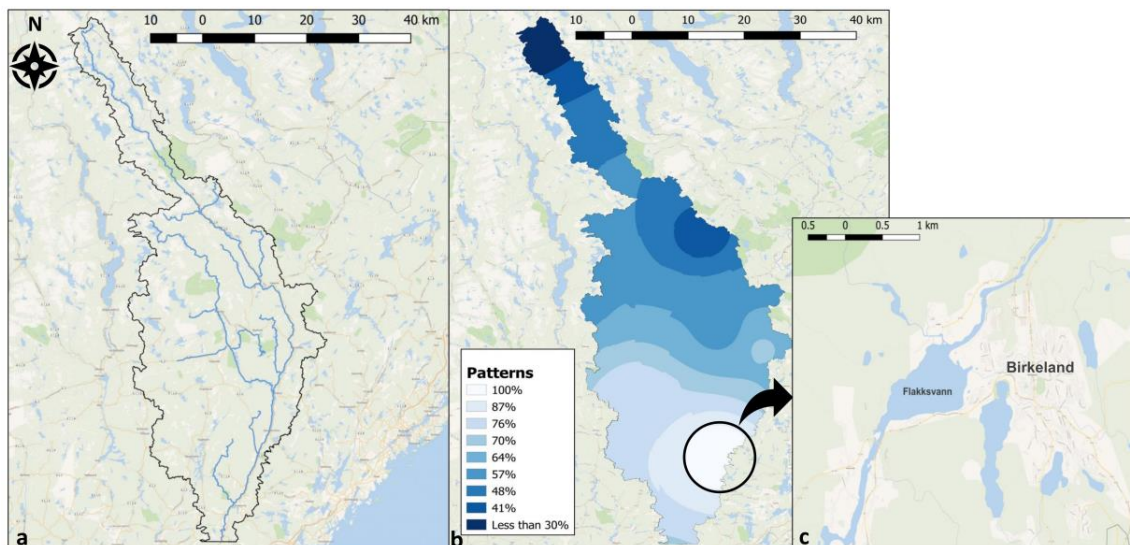


Figure 1. a. Catchment of Tovdal river, b. the spatially varying precipitation over the catchment adopted by model to apply precipitation over the catchment, c. zoom of Flakksvann lake near Birkeland town.

The simulation time for the considered computational domain (composed of 401,769 mixed mesh elements) is about 12 GPU hours. As a result, this long run time inhibits the application of HiSTAV for uncertainty analysis in which a large number of realizations is required. To overcome this limitation, we developed an emulator based on 1,200 different simulations performed with the physical 2D model. The details of the model and the process of the emulation can be found in Alipour and Leal (2021). In summary, by sampling the input parameters spaces namely precipitation intensity, roughness, and runoff coefficient values for each land type in the catchment, 1,200 simulations were performed. These simulations were then used to develop two emulators using Artificial Neural Network (ANN) and Support Vector Regression (SVR) to predict cross sectional water level. The developed emulators were optimized in a subsequent step by dimension reduction techniques and removing the less correlated inputs. Finally, the SVR based emulator which uses as input set the precipitation ( $i_p$ ), the forest runoff coefficient ( $C_F$ ), the river friction ( $K_s_R$ ) and the forest friction ( $K_s_F$ ), was selected as the best model that mimics the physical 2D model. The trained emulator (at Flakksvann lake cross section) was updated later with more simulations, covering wider ranges of the precipitation, to be used in this study. The use of this surrogate 2D hydrodynamic model (with an accuracy of  $R^2 = 0.999$ ) allows us to overcome the unaffordable computational resources of running the physical-based model. Fig. 2, displays the performance of the surrogate model against the physical 2D hydrodynamic model.

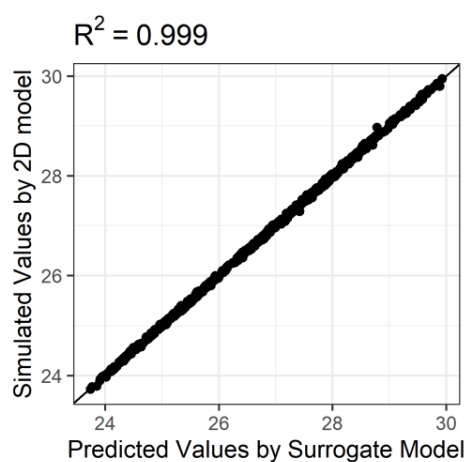


Figure 2. Performance of the developed surrogate model

### Probabilistic approach (Monte Carlo simulations)

As stated earlier there are several frameworks to capture and communicate the uncertainty, and one is probabilistic framework. In a broader sense, this approach involves, (i) investigating different, plausible scenarios such as parameter variation and future conditions, (ii) identifying statistical distributions for uncertain inputs and parameters, (iii) simultaneously sampling each distribution as input, (iv) executing the model for each of the sampled input series and finally (vi) constructing the probability distribution of the output of interest. This procedure, which is called Monte Carlo simulation (MC), is continued until reaching an adequate number of realizations or in other words until reaching convergence. In the current study, the use of the emulator enables us to perform thousands of simulations for uncertainty analysis without having the computational time constrains. The inputs precipitation ( $i_p$ ), forest runoff coefficient ( $C_F$ ), river friction ( $K_s_R$ ) and forest friction ( $K_s_F$ ) used by the emulator, are considered as uncertain parameters. The hydraulic roughness and runoff coefficient parameter spaces are constructed reflecting a wide variation range withing reasonable engineering practice. The choice of ranges was made based on the land type, vegetation, and average antecedent soil moisture and are presented in Table 1.

Table 1. Selected input descriptions and assigned ranges

Parameters		Acronym	Range
Strickler roughness ( $m^{1/3}/s$ )	Forests (broad-leaved, coniferous)	$K_s_F$	15-40
	River and water courses	$K_s_R$	20-50
Runoff coefficient (%)	Forests (broad-leaved, coniferous)	$C_F$	50-70

Estimation of precipitation intensity is a crucial step in rainfall-runoff modelling practices which is incorporated with uncertainty due to the limited historical data, climate variability/change and complex and chaotic nature of climate. In this study we have used three climate scenarios, namely, present scenario and two future scenarios (i.e., two representative concentration pathways RCPs 4.5 and 8.5), to obtain the 100-year precipitation range.

The present scenario involves the probabilistic calculation of the 100-year precipitation based on the recorded data in a station named Dovland. This station is selected based on several reasons such as, it has a sufficient length of data (54 years daily records), is located at the center of the catchment and is close to the study area. Furthermore based on the comparison performed in the study by Alipour et al. (2021b), this station is selected as the station which gives a better estimate of the catchment's 100-year precipitation.

To estimate future 100-year precipitation under two future scenarios, we have used downscaled bias-adjusted daily precipitation data at a  $1 \times 1 \text{ km}^2$  resolution provided by Norwegian Centre for Climate Services (NCCS) (<https://klimaservicesenter.no/>) (further details on data and bias correction procedure can be found in Wong et al. (2016)). These data were acquired from 10 EURO-CORDEX regional climate models (CM) simulations for a future period (2071–2100) under two representative concentration pathways RCP4.5 and RCP8.5. The information of the models is displayed in Table 2.

Table 2. The climate models information

Institute	Global Climate Model	Regional Climate Model (CM)
CLM-Community	CNRM-CER-FACS-CM5	CCLM4-8-17
SMHI	CNRM-CER-FACS-CM5	RCA4
CLM-Community	ICHEC-EC-EARTH	CCLM4-8-17
DMI	ICHEC-EC-EARTH	HIRHAM5
KNMI	ICHEC-EC-EARTH	RACMO22E
SMHI	ICHEC-EC-EARTH	RCA4
SMHI	IPSL-CM5A-MR	RCA4
SMHI	MOHC-HADGEM2-ES	RCA4
CLM-Community	MPI-ESM-LR	CCLM4-8-17
SMHI	MPI-ESM-LR	RCA4

The 2D model used in this study, adopts a spatially varying precipitation over the catchment (Fig. 1.b) and Birkeland region receives the highest amount of precipitation (100%) (Fig. 1.c) (further details of the model and the precipitation patterns can be found in Alipour et al. (2021a)). Accordingly, we have selected the grids (as mentioned earlier the precipitation data are in form of grid data) covering Birkeland



region and extracted the time series for this region to develop area averaged annual maximum precipitation (AMP) series.

Overall, 20 AMP series for a future period (2071–2100) are obtained using 10 EURO-CORDEX regional climate models for RCP4.5 and RCP8.5.

To calculate the 100-year precipitation using the AMP series (from the three scenarios), we need to choose a flood frequency analysis method. However, there is no general rule to choose a probability distribution function (PDF) for precipitation series and typically distributions such GEV, Gumbel, GP, etc., are used to describe extreme events. Therefore, in this study we explore the effect of assigning different distributions for precipitation and accordingly compare the simulated 100-year flood magnitude. For this purpose, six different distributions namely: 1) Gumbel, 2) GEV, (3) GEV with prior on shape (GEV\_WPS hereafter), (4) Log-normal (LN), (5) Generalize Logistic (GenLog) and (6) Pearson type III (P3) were selected for fitting to the AMP series. The prior distribution for the GEV parameters, are assigned based on the recommendations in Martins and Stedinger (2000) and Lutz et al. (2020). Accordingly, we used uninformative prior distributions for location ( $\mu$ ) and scale ( $\sigma$ ) and beta distribution for shape parameter ( $\xi \sim B(p=6, q=9)$ ) which is defined on the interval  $[-0.5, 0.5]$ . The explanation of the adopted distributions including equations for the quantile functions and the probability density functions (PDFs) can be found in Kobierska et al. (2018).

There are several methods for fitting theoretical distributions to data series (for example, ordinary moments (OM), L-moments (LM), Maximum likelihood (ML), generalized maximum likelihood (GML), and Bayesian approaches). A comparative study of performance of different estimators can be found in the works by Martins and Stedinger (2000) and Kobierska et al. (2018). In most applications, the L-moments, GML or Bayesian approaches are recommended since they are robust with respect to outliers and either explicitly or implicitly apply constraints on the shape parameter. In the current study we used Bayesian approach due to the following reasons: (i) allows to set prior information (i.e., on the shape parameter) (ii) the uncertainty in design flood estimates can easily be extracted (iii) it is easy to introduce and make inference for non-stationary models (iv) and it is recommended by several studies and also by Norwegian meteorological institute (Lutz et al., 2020, Martins and Stedinger, 2000, Renard et al., 2006, Lima et al., 2016, Lima et al., 2018). Further details of

determining a range for 100-year design rainfall using MCMC Bayesian method can be found in Alipour et al. (2021b).

In summary, we applied the Bayesian approach using the algorithm implemented in the R-package nsRFA (Viglione et al., 2020) and created three Markov Chain Monte Carlo (MCMC) chains of length 50,000 and estimated the posterior probability distributions for each data series (10 AMP series under RCP 4.5, 10 AMP series under RCP 8.5 and 1 AMP series under present scenario). These posterior samples were subsequently used to provide posterior samples of 100-year precipitation (a series of the quantiles that corresponds to 100-year return period in each chain) from which the 90% credibility intervals were calculated. Subsequently, the 100-year precipitation estimates of each scenario are ensembled and the results are shown in Fig. 3.

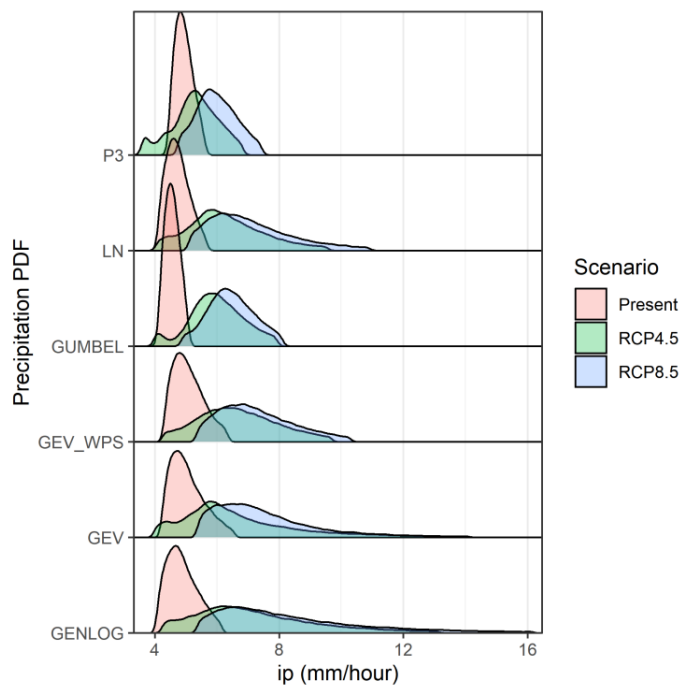


Figure 3. The 100-year precipitation probability distributions under three scenarios. The two future scenarios are ensembles of the 100-year precipitation derived from 10 CM.

These distributions represent the uncertainty of 100-year precipitation and will be used as the precipitation parameter spaces along with the other input spaces (Table 1) for MC simulations.

### **Deterministic approach**

In contrast to the probabilistic approach, deterministic approach assumes known values for input data and provides fixed outputs. These methods are subjected to considerable criticism since they inevitably mask out a wide range of probable outputs. In this study, to explore the difference between the probabilistic and deterministic modeling, we present the flood maps based on both approaches. The deterministic approach explained in this section is the typical approach which is widely used for case studies in Norway.

To obtain the deterministic water level, the 100-year precipitation value is estimated by fitting the GEV distribution to the AMP series observed in Dovland station, identifying the quantile which corresponds to the probability of 0.99 of not being exceeded (0.99 quantile). We only have considered the GEV distribution, since it is the distribution which is widely used to estimate extreme events such as 100-year precipitation. Similar to the probabilistic approach, we used Bayesian MCMC method to fit the distribution to the data series, however instead of a range of values, the value with the highest probability (maximum likelihood) is selected as the deterministic 100-year precipitation (i.e., the peak point of the GEV distribution in Fig. 3).

To transfer the climate change effects and possible future changes, the estimated rainfall value is multiplied by climate factor. Climate factors are calculated based on return period, rainfall duration, geographical location, reference period, scenario period and climate models (global/regional) (Hanssen-Bauer et al., 2009). In this study, the estimated rainfall value is multiplied by a climate factor equal to 1.2. The factor is selected based on the values reported by Hanssen-Bauer et al. (2009), for the case study region (Agder) under high emissions scenario (RCP8.5) (Table 3). We used RCP 8.5, regarding the current national guidance for adaptation related to climate change in Norway which recommends that estimates for the likely effects of climate change are based on concentration pathways representing a high level of emissions (Miljøverndepartement, 2012). The future deterministic 100-year precipitation is calculated as 144 mm/day (6 mm/hour). The details of the applied methodology can be found in Alipour et al. (2021b). To simulate flood water level based on the deterministic precipitation, the other inputs namely, roughness and runoff coefficient values, were determined based on the median values of the specified ranges of the parameters presented in Table 1.

### **Uncertainty and sensitivity analysis**

Uncertainty analysis represent the uncertainty as an ensemble or range of probable model outputs. These outputs are result of uncertain or imprecisely known inputs which are sampled from different input values using a Monte Carlo based sampling methods. However, different uncertainty sources have different contributions to the total uncertainty. Performing sensitivity analysis allows us to assess how the uncertainty in the output of a model can be apportioned to different sources of uncertainty in the model input (Saltelli et al., 2004) and accordingly, pay more attention to the parameters with larger effect on the output.

Sensitivity analysis methods can be broadly classified into local and global methods (for further details see Saltelli et al. (2004), and Pianosi et al. (2016)). In this study first, we used analysis of variance (ANOVA) as a global sensitivity analysis method to identify the most significant factors. Subsequently, ANOVA method is used to decompose the output uncertainty into the uncertainty of each individual input parameters.

ANOVA method focuses on the analysis of the variance explained by each factor and is accomplished by estimating the Fischer's test value ( $F$ -value). The impact of any factor is explained by its  $F$ -value and the corresponding sum of squares that represent variance. Higher  $F$ -value and sum of squares of any factor indicates its relative importance in the process of the response (Karmakar et al., 2018). Moreover, to explore the impacts of individual factors, the percentage contribution ( $PC$ ) of each factor is calculated using the following equation (Yang and Tarn, 1998, Sadrzadeh and Mohammadi, 2008):

$$PC = \frac{SS_j}{SS_T} \times 100 \quad \text{Eq. 4}$$

where  $SS_T$  is the total sum of squares, and  $SS_j$  is the sum of squared deviations for each factor  $j$ . Both can be calculated using Eqs. 5 and 6, respectively:

$$SS_T = \sum_{i=1}^n (Y_i - \bar{Y})^2 \quad \text{Eq. 5}$$

$$SS_j = \sum_{i=1}^l n_{jl} (\bar{Y}_{jl} - \bar{Y})^2 \quad \text{Eq. 6}$$

where  $n$  is the number of experiments/simulations,  $Y_i$  represents the measured results in the  $i$ th experiment/simulation,  $\bar{Y}$  is the average of results,  $\bar{Y}_{jl}$  is the mean of results

for the factor  $j$  at level  $i$ ,  $n_{jl}$  is the number of simulations that have factor  $j$  at level  $l$  (Stahle and Wold, 1989).

## Results

As an initial step in the uncertainty analysis framework, a sensitivity analysis was performed using ANOVA, to assess the influence of input parameters and quantify the relative contribution of each parameter to the variability of the output. The sensitivity analysis was performed on all the water level ensembles resulted from different scenarios. The results are presented in Table 3 displaying the average contribution of the inputs. As shown in the table, water levels are significantly influenced by precipitation by a contribution of 85% and accordingly the uncertainty of this parameter can be the main source of uncertainty of the output (water level).

Table 3. Input parameters contributions through ANOVA analysis

Source	SS	Contribution	F-Value	P-Value
K <sub>S</sub> _R	0.17	7.2%	2530.75	0.00
K <sub>S</sub> _F	0.08	3.2%	552.43	0.00
C_F	0.10	4.1%	2063.39	0.00
i <sub>p</sub>	2.02	85.4%	123918.25	0.00

In order to explore the future floods magnitude and present the incorporated uncertainty, the input parameters including 12 precipitation ensembles were sampled to generate 100,000 MC simulations and consequently to construct a probability distribution for the water level under two RCPs. We have used an extensive number of 100,000 simulations to ensure a sufficiently large, stabilized ensemble of probable 100-year flood events.

The probable future 100-year flood levels following three scenarios are displayed in Fig. 4. According to this figure, the 100-year flood is likely to become more severe in future specially under RCP 8.5. The results demonstrate a large variability in water level distributions.

In the present scenario, different precipitation PDFs lead to approximately similar water level estimates, however under future scenarios these estimates are considerably different.

To illustrate these differences and to explore the probable changes in flood magnitudes, basic descriptive parameters of the distributions namely, mean, median, minimum, maximum, standard deviation, skewness, kurtosis, 0.05 and 0.95 quantiles

were adopted (see Table A.1 in appendix). Furthermore, the inter-quantile range (called uncertainty index (UI) hereafter) which is defined as the difference between 0.05 and 0.95 quantiles, is also calculated as a parameter that reflects the uncertainty in each distribution.

A comparison between different quantiles (e.g., q1, median, mean, and q2) indicates that under both future scenarios, GenLog and GEV (with and without prior) distributions tend to give larger estimates. The lowest water level values belong to those simulations whose precipitation is estimated using Gumbel and P3 distributions. A quantile-by-quantile comparison between the present scenario and the future scenarios indicates that, the changes are not homogeneous between different quantiles and become more pronounced in higher quantiles. For example, comparing the means shows that under RCP 8.5, the values have an increment between 5% to 12% and under RCP 4.5, the changes are between 3% to 8%, depending on the precipitation PDFs. The increase in q2 values is between 8% to 22% for RCP 8.5 and between 5% to 17% under RCP 4.5. The largest differences under different scenarios, were obtained from the water level ensembles whose precipitation was derived from GenLog distribution. While Gumbel distribution provides the lowest amount of change in different quantiles.

The non-homogeneous changes in different quantiles, challenges the application of climate factors for projecting the future changes. In fact, in probabilistic approaches with a range of values, the application of these factors is questionable since they cannot be multiplied as a constant to whole range.

The calculated UI values can vary between 2 m to 5.83 m under future scenarios. The most uncertain estimates were obtained from GenLog derived water level (5.83 m under RCP 8.5 and 5.24 m under RCP 4.5). The P3 based simulations provide the smallest uncertainty (about 2.20 m in both RCPs). Comparing the GEV distributions with and without a prior for shape parameter, indicates that, assuming a prior for shape parameter eventuates to smaller estimates for q2 value (about 4%) and as a result decreases the uncertainty. The estimated uncertainty is remarkably larger for the GEV (three parameter EVD) compared to the Gumbel (two parameter EVD) which are from the same family named EVD. This means that shape parameter estimation can introduce a large uncertainty into the results. However, despite the larger uncertainty, GEV provides remarkably larger estimates compared to the Gumbel. This suggest that

the use of two parameter EVD (Gumbel) may be unsafe. The ranking order based on the estimated water level quantile values sorted from the largest to smallest are as follow: 1. GenLog, 2. GEV, 3. GEV\_WSP, 4. LN, 5. Gumbel and 6. P3.

The deterministic future water level which is estimated based on deterministic 100-year precipitation multiplied by a climate factor, has been estimated equal to 24.34 m (see dashed line in Fig. 4). As displayed in the Fig. 4, this estimate is located at the lower quantiles of the future estimates. The only exception is for P3 estimate under RCP 4.5 in which deterministic approach is close to the maximum likelihood value. This means the deterministic approach along with climate factors which is typically undertaken in hydrology and flood modeling practices, largely underestimates the flood magnitude.

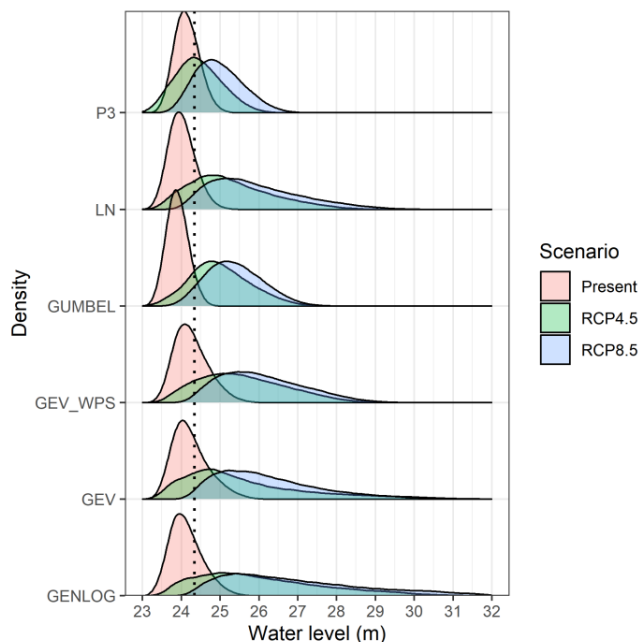


Figure 4. The water level distribution resulted from different input sets (uniformly distributed  $K_s$  and  $C$  values, and 100-year precipitation distributions resulted from different precipitation PDFs shown in the y axis). The dotted black line represents the future deterministic water level.

Having discussed the uncertainty of flood estimates, in this section we aim to develop a probabilistic flood map. The selection of the best distribution for flood frequency analyses has been the subject of ongoing research in recent years. A study by Kobierska et al. (2018) on 526 number of catchments in Norway, indicates that the 3-

parameter GEV (with assuming a prior for shape parameter) gives good fit and reliable estimates for 30 year data records. Therefore, in this study we focus on the estimates resulted from GEV-WPS (RCP 8.5) distribution for precipitation and uniform distributions for roughness and runoff coefficients, as the probabilistic future 100-year flood. The RCP 8.5 is selected here since it is recommended by the current national guidance for adaptation related to climate change in Norway (Miljøverndepartement, 2012).

These estimates in terms of flood map are presented in Fig. 5. As it is displayed in the figure, many critical regions are not considered in deterministic flood map. These regions include industrial regions which in case of flood, in addition to financial losses to these properties, chemical contamination of this river as a salmon fish habitat can happen.

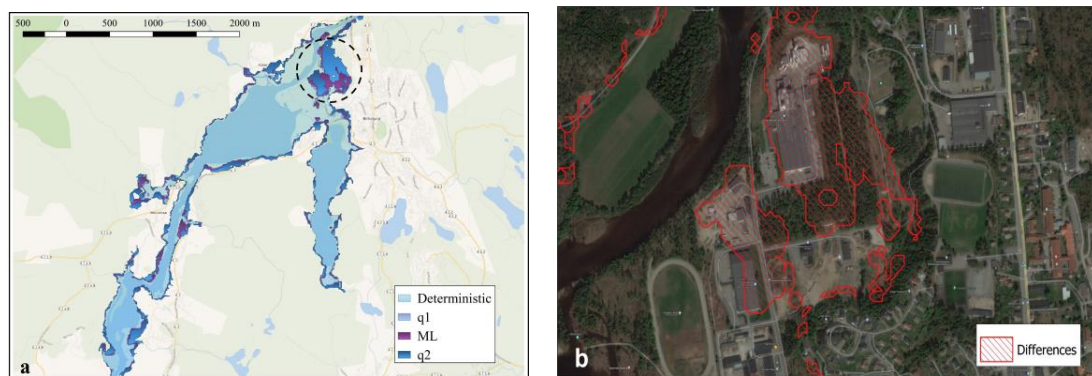


Figure 5.a. The flood map modified based on the deterministic water level value versus different quantiles of the water level PDF resulted from future (RCP 8.5) scenario whose inputs as: 100-year precipitation derived from GEV\_WPS under RCP 8.5, roughness and runoff values as the values reported in Table 1. b. The area identified by dashed circle in panel “a” is the industry park and is represented in detail as panel “b”. The hashed red area displays the difference between the flooded area calculated based on q2 and ML.

### **How many simulations are needed?**

In the current study, using the emulator enabled us to perform 100,000 simulations. However, performing a large number of realizations is not feasible in case of using a physical model. As a result, in this section we aim to identify the required number of simulations to reliably terminate the Monte Carlo process. We have assessed the



convergence of the MC simulations through, different parameters. In this study, the convergence criteria is defined as the fluctuation in mean, standard deviation (SD), 0.05 and 0.95 quantiles, and coefficient of variation (CV) (Ballio and Guadagnini, 2004, Ehlers et al., 2019). Additionally, Root Mean Square Error (RMSE) values which is the standard deviation of the residuals were also calculated to measure the difference between the water level distributions with different sizes (100, 200, ..., 20,000) and the reference distribution consist of 100,000 water levels. The results are displayed in Fig. 6 for the Mean, SD, q2 and RMSE (for future scenario RCP 8.5). The detailed results are presented in Table A.2 of the appendix.

Depending on the precipitation PDF, convergence is achieved in different number of realizations. As an example, Gumbel converges faster than more uncertain distributions such as GENLOG. According to the results the mean parameter and SD converge after about 1,000 realizations (assuming fluctuation < 5 cm as converged), whereas the higher quantiles converge later. As an example, q2 values converge after about 3,000 realizations. The RMSE value converges after all of the parameters at about 4,000 realizations. If we assume more restrict fluctuation threshold (e.g., fluctuation  $\leq 2$  cm), the required number of simulations will increase to much higher numbers (more than 10,000).

The mean parameter's variation, which is typically adopted as a convergence criterion in uncertainty analysis, can lead to early stopping of the process and consequently wrong statistical inferences. Consequently, we suggest assessing the convergence in higher quantiles in addition to the other parameters. Specially in uncertainty analysis, risk assessment or any other practices that higher quantiles are subject of the analysis.

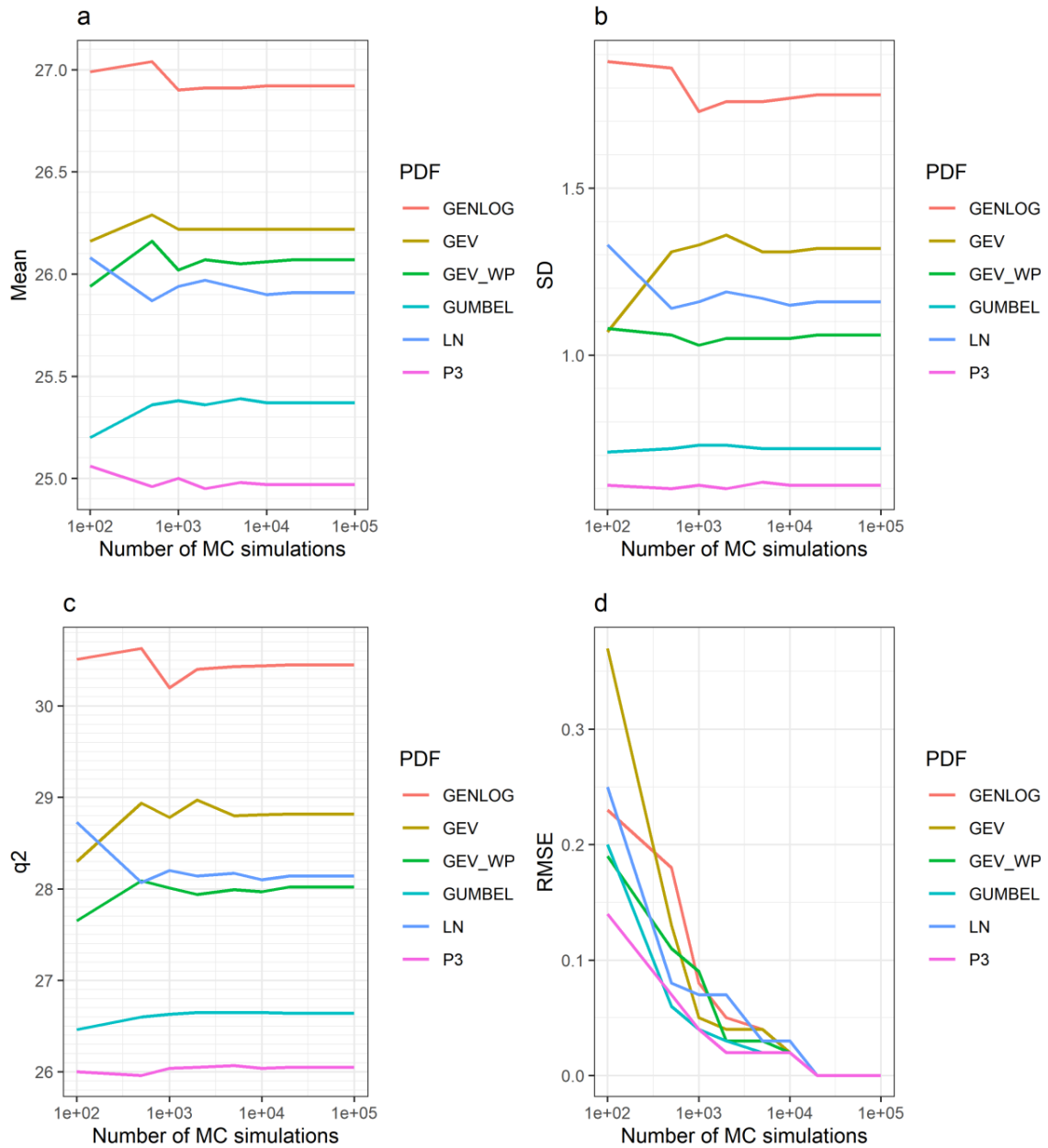


Figure 6. Convergence in the MC simulations. Variation of different parameters with the number of simulations: a. Mean, b. standard deviation, c.  $q_2$ , and d. RMSE.

### Uncertainty decomposition

According to the sensitivity analysis results, precipitation is ranked as the most significant parameter. As a result, the uncertainty of water level is mainly influenced by the uncertainty of this parameter. In this section we decomposed the uncertainty of precipitation into the following components, Climate models, RCP and PDFs and identified their relative contribution to overall uncertainty through ANOVA analysis.

To explore the associated uncertainty in 100-year precipitation, the UI values were calculated for 100-year precipitation estimates obtained from fitting different PDFs into the data simulated by different climate models. The calculated UI values are displayed in Fig. 7.

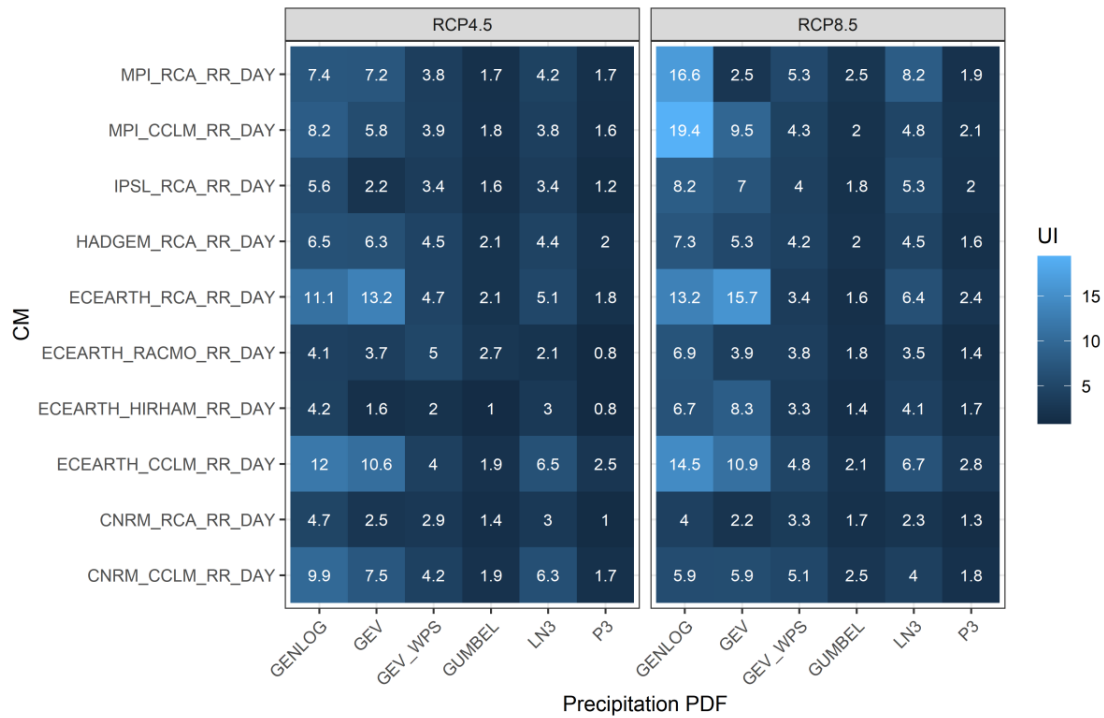


Figure 7. The estimated uncertainty index value calculated for the 100-year precipitation derived from different PDFs.

The ANOVA analysis identified the contribution of uncertainty of each individual parameter as the values displayed in Table 4.

Table 4. Relative contribution of the uncertainty sources into the total uncertainty of precipitation

Source	Seq SS	Contribution	F-Value	P-Value
PDF	1.341	73%	93.15	0.000
CM	0.361	20%	11.12	0.000
RCP	0.125	7%	11.85	0.001

According to the results, the precipitation PDF has the highest contribution to the total uncertainty (about 73%). Climate models contribute about 20% and are ranked as second contributor and RCP has the lowest contribution (about 7%). This result

highlights the huge importance of selecting a proper distribution for flood frequency analysis. In contrast to PDF, selection of the future scenario is the least important parameter for uncertainty estimation. A comparison between the climate models showed that on average, the highest and the lowest uncertainty values are obtained from “ECEARTH\_RCA\_RR\_DAY” and “CNRM\_RCA\_RR\_DAY” climate models, respectively.

Furthermore, the influence of the climate models, PDFs and RCPs on different quantiles of the 100-year precipitation distributions (Fig. 3) (such as q1, mean, median, maximum likelihood value and q2) were also assessed through ANOVA and the results are displayed in Fig. 8.

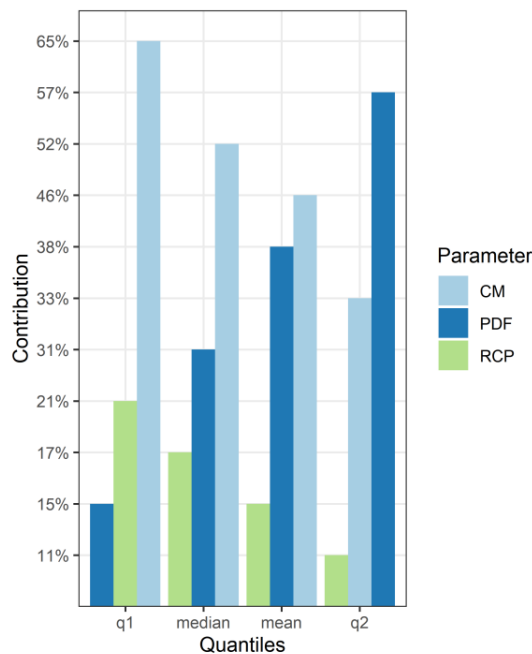


Figure 8. The influence of the parameters, climate models, precipitation PDFs and RCP on different quantiles.

The results show that the lower quantiles (such as q1 and median) are mostly influenced by climate models and as we move to the higher quantiles the PDF effect becomes more important. Both CM and RCP decrease their contribution for overall uncertainty as we move from lower to higher quantiles, while the opposite is observed for the PDF. This finding suggests that the PDFs highly influence the higher quantiles such as the values that are in the tail of the distribution and the upper bound of the uncertainty (q2). In other words, in deterministic approaches or in the flood modeling practices, where typically the maximum likelihood value is used as the

design rainfall value without taking the uncertainty into account, the climate models are the most influencing parameters. The PDF plays a key role when the higher quantiles are of major interest such as in uncertainty studies and risk analysis.

### **Conclusion**

This study (i) has presented 100-year flood maps under 3 scenarios (present, RCP 4.5 and RCP 8.5) through probabilistic and deterministic approaches, (ii) subsequently, the uncertainty of 100-year flood maps, due to alternative input assumptions, were explored through intensive Monte Carlo simulations (100,000 simulations) and finally (iii) the uncertainty is decomposed into the uncertainty of individual sources. The following conclusions can be drawn from the present study.

- Despite the wide ranges for the inputs roughness and runoff coefficients, precipitation uncertainty, which incorporates three different sources of uncertainty (RCP, PDF, CM), is the main source of uncertainty in flood simulations.
- A quantile-by-quantile comparison between the water level distributions resulted from different scenarios, indicates that, the changes are not homogeneous between different quantiles and become more pronounced in higher quantiles. This result challenges the application of climate factors for projecting the future changes.
- The flood maps based on the deterministic approach even with the inclusion of a climate factor, considerably underestimate the future flood's magnitude.
- To avoid early stopping of the MC process, we suggest assessing the convergence in higher quantiles or through the aggregated metrics such as RMSE which contains all the quantiles and displays a general picture of convergence.
- Decomposing the uncertainty of precipitation into different sources illustrated that, selection of the precipitation PDF is the main source of uncertainty, while selection of the future RCP scenario (which is the subject of debate in climate change mitigation and adaptation guidelines) is the least important parameter for uncertainty estimation.
- ANOVA analysis showed that, the lower quantiles (such as q1 and median) are mostly influenced by climate models and as we move to the higher quantiles the PDFs influence becomes larger. As a result, we suggest in studies where

highly likely situations or the most likely situation is the focus (for example, design based on the maximum likelihood value), the attention should be paid to the selection of climate models. Conversely, if the focus is on highly unlikely extreme events, such as in risk analysis, the PDF selection for precipitation should be considered as the major uncertainty source that can considerably change the results.

Finally, according to the results presented in this study, we highly recommend taking the uncertainty into the account in flood studies. To overcome the computational constrains, which is the main obstacle in probabilistic approaches, surrogate models can be a efficient alternative. In fact, using the surrogate model enabled us to perform this study with intensive number of MC simulations (a total of 1,800,000 simulations were performed in this study). Therefore, we suggest flood modelers to use surrogate models as a complementary tool to consider the uncertainty and make more safe decisions.

### **Acknowledgements**

The work presented in this paper is funded by the University of Agder, Norway (project no. 63859).

### References

- Abily, M., Delestre, O., Gourbesville, P., Bertrand, N., Duluc, C.-M., Richet, Y., 2016. Global sensitivity analysis with 2D hydraulic codes: application on uncertainties related to high-resolution topographic data, *Advances in Hydroinformatics*. Springer, pp. 301-315. DOI:[https://doi.org/10.1007/978-981-287-615-7\\_21](https://doi.org/10.1007/978-981-287-615-7_21)
- Ahmadisharaf, E., Kalyanapu, A.J., Bates, P.D., 2018. A probabilistic framework for floodplain mapping using hydrological modeling and unsteady hydraulic modeling. *Hydrological Sciences Journal*, 63(12): 1759-1775.
- Alipour, S.M., Engeland, K., Leal, J., 2021a. A practical methodology to perform global sensitivity analysis for 2D hydrodynamic computationally intensive simulations. *Hydrology Research*. DOI:<https://doi.org/10.2166/nh.2021.243>

- Alipour, S.M., Engeland, K., Leal, J., 2021b. Representation of 100-year design rainfall uncertainty in catchment-scale flood modeling: A MCMC bayesian approach. Norsk Vannforening, 04.
- Alipour, S.M., Leal, J., 2021. Emulation of 2D Hydrodynamic Flood Simulations at Catchment Scale Using ANN and SVR. *Water*, 13(20): 2858.
- Annis, A., Nardi, F., Volpi, E., Fiori, A., 2020. Quantifying the relative impact of hydrological and hydraulic modelling parameterizations on uncertainty of inundation maps. *Hydrological Sciences Journal*, 65(4): 507-523.
- Apel, H., Aronica, G., Kreibich, H., Thielen, A., 2009. Flood risk analyses—how detailed do we need to be? *Natural hazards*, 49(1): 79-98.
- Apel, H., Thielen, A.H., Merz, B., Blöschl, G., 2004. Flood risk assessment and associated uncertainty. *Natural Hazards and Earth System Sciences*, 4(2): 295-308.
- Ballio, F., Guadagnini, A., 2004. Convergence assessment of numerical Monte Carlo simulations in groundwater hydrology. *Water resources research*, 40(4).
- Beven, K., Lamb, R., Leedal, D., Hunter, N., 2015. Communicating uncertainty in flood inundation mapping: a case study. *International Journal of River Basin Management*, 13(3): 285-295.
- Beven, K., Leedal, D., McCarthy, S., Lamb, R., Hunter, N., Keef, C., Bates, P., Neal, J., Wicks, J., 2011. Framework for assessing uncertainty in fluvial flood risk mapping. FRMRC Research Rep. SWP1, 7.
- Brody, S.D., Blessing, R., Sebastian, A., Bedient, P., 2013. Delineating the reality of flood risk and loss in Southeast Texas. *Natural Hazards Review*, 14(2): 89-97.
- Chen, S., Garambois, P.-A., Finaud-Guyot, P., Dellinger, G., Mose, R., Terfous, A., Ghenaim, A., 2018. Variance based sensitivity analysis of 1D and 2D hydraulic models: An experimental urban flood case. *Environmental Modelling & Software*, 109: 167-181.  
DOI:<https://doi.org/10.1016/j.envsoft.2018.08.008>
- Conde, D.A., Canelas, R.B., Ferreira, R.M., 2020. A unified object-oriented framework for CPU+ GPU explicit hyperbolic solvers. *Advances in*

Engineering Software, 148: 102802.

DOI:<https://doi.org/10.1016/j.advengsoft.2020.102802>

Das, J., Umamahesh, N., 2018. Assessment of uncertainty in estimating future flood return levels under climate change. *Natural Hazards*, 93(1): 109-124.

Dottori, F., Di Baldassarre, G., Todini, E., 2013. Detailed data is welcome, but with a pinch of salt: Accuracy, precision, and uncertainty in flood inundation modeling. *Water Resources Research*, 49(9): 6079-6085.

DOI:<https://doi.org/10.1002/wrcr.20406>

Dung, N.V., Merz, B., Bárdossy, A., Apel, H., 2015. Handling uncertainty in bivariate quantile estimation—An application to flood hazard analysis in the Mekong Delta. *Journal of Hydrology*, 527: 704-717.

Ehlers, L.B., Sonnenborg, T.O., Refsgaard, J.C., 2019. Observational and predictive uncertainties for multiple variables in a spatially distributed hydrological model. *Hydrological Processes*, 33(5): 833-848.

Ferreira, R.M., Franca, M.J., Leal, J.G., Cardoso, A.H., 2009. Mathematical modelling of shallow flows: Closure models drawn from grain-scale mechanics of sediment transport and flow hydrodynamics. *Canadian journal of civil engineering*, 36(10): 1605-1621. DOI:<https://doi.org/10.1139/L09-033>

Haan, C.T., Storm, D.E., Al-Issa, T., Prabhu, S., Sabbagh, G.J., Edwards, D.R., 1998. Effect of parameter distributions on uncertainty analysis of hydrologic models. *Transactions of the ASAE*, 41(1): 65.

Hall, J., Tarantola, S., Bates, P., Horritt, M., 2005. Distributed sensitivity analysis of flood inundation model calibration. *Journal of Hydraulic Engineering*, 131(2): 117-126.

Hanssen-Bauer, I., Drange, H., Førland, E., Roald, L., Børsheim, K., Hisdal, H., Lawrence, D., Nesje, A., Sandven, S., Sorteberg, A., 2009. Climate in Norway 2100. Background information to NOU Climate adaptation (In Norwegian: Klima i Norge 2100. Bakgrunnsmateriale til NOU Klimatilpassing), Oslo: Norsk klimasenter.



- Jung, Y., Merwade, V., 2012. Uncertainty quantification in flood inundation mapping using generalized likelihood uncertainty estimate and sensitivity analysis. *Journal of Hydrologic Engineering*, 17(4): 507-520.
- Karmakar, B., Dhawane, S.H., Halder, G., 2018. Optimization of biodiesel production from castor oil by Taguchi design. *Journal of Environmental Chemical Engineering*, 6(2): 2684-2695.  
DOI:<https://doi.org/10.1016/j.jece.2018.04.019>
- Kim, B., Sanders, B.F., Schubert, J.E., Famiglietti, J.S., 2014. Mesh type tradeoffs in 2D hydrodynamic modeling of flooding with a Godunov-based flow solver. *Advances in Water Resources*, 68: 42-61.
- Kobierska, F., Engeland, K., Thorarinsdottir, T., 2018. Evaluation of design flood estimates—a case study for Norway. *Hydrology Research*, 49(2): 450-465.
- Kobierska, F., Jonas, T., Zappa, M., Bavay, M., Magnusson, J., Bernasconi, S.M.J.A.i.W.R., 2013. Future runoff from a partly glacierized watershed in Central Switzerland: A two-model approach. 55: 204-214.
- Komatina, D., Branisavljevic, N., 2005. Uncertainty analysis as a complement to flood risk assessment. Faculty of Civil Engineering University of Belgrade: Beograd, Serbia.
- Lawrence, D., 2020. Uncertainty introduced by flood frequency analysis in projections for changes in flood magnitudes under a future climate in Norway. *Journal of Hydrology: Regional Studies*, 28: 100675.
- Leandro, J., Gander, A., Beg, M., Bholá, P., Konnerth, I., Willems, W., Carvalho, R., Disse, M., 2019. Forecasting upper and lower uncertainty bands of river flood discharges with high predictive skill. *Journal of Hydrology*, 576: 749-763.
- Lim, N.J., Brandt, S.A., 2019. Flood map boundary sensitivity due to combined effects of DEM resolution and roughness in relation to model performance. *Geomatics, Natural Hazards and Risk*, 10(1): 1613-1647.  
DOI:<https://doi.org/10.1080/19475705.2019.1604573>

- Lima, C.H., Kwon, H.-H., Kim, Y.-T., 2018. A local-regional scaling-invariant Bayesian GEV model for estimating rainfall IDF curves in a future climate. *Journal of Hydrology*, 566: 73-88.
- Lima, C.H., Lall, U., Troy, T., Devineni, N., 2016. A hierarchical Bayesian GEV model for improving local and regional flood quantile estimates. *Journal of Hydrology*, 541: 816-823.
- Liu, Z., Merwade, V., 2018. Accounting for model structure, parameter and input forcing uncertainty in flood inundation modeling using Bayesian model averaging. *Journal of hydrology*, 565: 138-149.
- Loveridge, M., Rahman, A., 2014. Quantifying uncertainty in rainfall–runoff models due to design losses using Monte Carlo simulation: a case study in New South Wales, Australia. *Stochastic environmental research and risk assessment*, 28(8): 2149-2159.
- Lutz, J., Grinde, L., Dyrddal, A.V., 2020. Estimating Rainfall Design Values for the City of Oslo, Norway—Comparison of Methods and Quantification of Uncertainty. *Water*, 12(6): 1735. DOI:<https://doi.org/10.3390/w12061735>
- Martins, E.S., Stedinger, J.R., 2000. Generalized maximum-likelihood generalized extreme-value quantile estimators for hydrologic data. *Water Resources Research*, 36(3): 737-744.
- Mejia, A.I., Reed, S., 2011. Evaluating the effects of parameterized cross section shapes and simplified routing with a coupled distributed hydrologic and hydraulic model. *Journal of Hydrology*, 409(1-2): 512-524.  
DOI:<https://doi.org/10.1016/j.jhydrol.2011.08.050>
- Merwade, V., Olivera, F., Arabi, M., Edleman, S., 2008. Uncertainty in flood inundation mapping: current issues and future directions. *Journal of Hydrologic Engineering*, 13(7): 608-620.
- Merz, B., Thielen, A.H., 2009. Flood risk curves and uncertainty bounds. *Natural hazards*, 51(3): 437-458.
- Miljøverndepartement, 2012. Klimatilpasning i Norge (Climate change adaptation in Norway) Meld. St. nr. 33 (2012–2013). .

- Moccia, B., Mineo, C., Ridolfi, E., Russo, F., Napolitano, F., 2021. Probability distributions of daily rainfall extremes in Lazio and Sicily, Italy, and design rainfall inferences. *Journal of Hydrology: Regional Studies*, 33: 100771.
- Neal, J.C., Odoni, N.A., Trigg, M.A., Freer, J.E., Garcia-Pintado, J., Mason, D.C., Wood, M., Bates, P.D., 2015. Efficient incorporation of channel cross-section geometry uncertainty into regional and global scale flood inundation models. *Journal of Hydrology*, 529: 169-183.  
DOI:<https://doi.org/10.1016/j.jhydrol.2015.07.026>
- Papaioannou, G., Vasiliades, L., Loukas, A., Aronica, G.T., 2017. Probabilistic flood inundation mapping at ungauged streams due to roughness coefficient uncertainty in hydraulic modelling. *Advances in Geosciences*, 44: 23.  
DOI:<https://doi.org/10.5194/adgeo-44-23-2017>.
- Papalexiou, S.M., Koutsoyiannis, D., 2013. Battle of extreme value distributions: A global survey on extreme daily rainfall. *Water Resources Research*, 49(1): 187-201.
- Pappenberger, F., Beven, K., Horritt, M., Blazkova, S.J.J.o.H., 2005. Uncertainty in the calibration of effective roughness parameters in HEC-RAS using inundation and downstream level observations. 302(1-4): 46-69.  
DOI:<https://doi.org/10.1016/j.jhydrol.2004.06.036>
- Pappenberger, F., Harvey, H., Beven, K., Hall, J., Meadowcroft, I., 2006a. Decision tree for choosing an uncertainty analysis methodology: a wiki experiment <http://www.floodrisknet.org.uk/methods> <http://www.floodrisk.net>. *Hydrological processes*, 20(17): 3793-3798.
- Pappenberger, F., Matgen, P., Beven, K.J., Henry, J.-B., Pfister, L., 2006b. Influence of uncertain boundary conditions and model structure on flood inundation predictions. *Advances in water resources*, 29(10): 1430-1449.
- Pianosi, F., Beven, K., Freer, J., Hall, J.W., Rougier, J., Stephenson, D.B., Wagener, T., 2016. Sensitivity analysis of environmental models: A systematic review with practical workflow. *Environmental Modelling & Software*, 79: 214-232.  
DOI:<https://doi.org/10.1016/j.envsoft.2016.02.008>

- Renard, B., Lang, M., Bois, P., 2006. Statistical analysis of extreme events in a non-stationary context via a Bayesian framework: case study with peak-over-threshold data. *Stochastic environmental research and risk assessment*, 21(2): 97-112.
- Sadrzadeh, M., Mohammadi, T., 2008. Sea water desalination using electro dialysis. *Desalination*, 221(1-3): 440-447.  
DOI:<https://doi.org/10.1016/j.desal.2007.01.103>
- Saltelli, A., Tarantola, S., Campolongo, F., Ratto, M., 2004. *Sensitivity analysis in practice: a guide to assessing scientific models*, 1. Wiley Online Library.
- Sampson, C.C., Fewtrell, T.J., O'Loughlin, F., Pappenberger, F., Bates, P.B., Freer, J.E., Cloke, H.L., 2014. The impact of uncertain precipitation data on insurance loss estimates using a flood catastrophe model. *Hydrology and Earth System Sciences*, 18(6): 2305-2324.
- Savage, J., Pianosi, F., Bates, P., Freer, J., Wagener, T., 2016. Quantifying the importance of spatial resolution and other factors through global sensitivity analysis of a flood inundation model. *Water Resources Research*, 52(11): 9146-9163. DOI:<https://doi.org/10.1002/2015WR018198>
- Stahle, L., Wold, S., 1989. Analysis of variance (ANOVA). *Chemometrics and intelligent laboratory systems*, 6(4): 259-272.  
DOI:[https://doi.org/10.1016/0169-7439\(89\)80095-4](https://doi.org/10.1016/0169-7439(89)80095-4)
- Stephens, E.M., Bates, P., Freer, J., Mason, D., 2012. The impact of uncertainty in satellite data on the assessment of flood inundation models. *Journal of Hydrology*, 414: 162-173.
- Teng, J., Jakeman, A.J., Vaze, J., Croke, B.F., Dutta, D., Kim, S.J.E.M., 2017. *Software*, 2017. Flood inundation modelling: A review of methods, recent advances and uncertainty analysis. 90: 201-216.  
DOI:<https://doi.org/10.1016/j.envsoft.2017.01.006>
- Thieken, A.H., Apel, H., Merz, B., 2015. Assessing the probability of large-scale flood loss events: a case study for the river Rhine, Germany. *Journal of Flood Risk Management*, 8(3): 247-262.

- Van Vuren, S., Paarlberg, A., Havinga, H., 2015. The aftermath of “Room for the River” and restoration works: Coping with excessive maintenance dredging. *Journal of hydro-environment research*, 9(2): 172-186.  
DOI:<https://doi.org/10.1016/j.jher.2015.02.001>
- Viglione, A., Hosking, J.R., Laio, F., Miller, A., Gaume, E., Payrastre, O., Salinas, J.L., N'guyen, C.C., Halbert, K., Viglione, M.A., 2020. Package ‘nsRFA’. Non-supervised Regional Frequency Analysis. CRAN Repository, Version 0.7-15.
- Vojtek, M., Petroselli, A., Vojteková, J., Asgharina, S., 2019. Flood inundation mapping in small and ungauged basins: sensitivity analysis using the EBA4SUB and HEC-RAS modeling approach. *Hydrology Research*, 50(4): 1002-1019. DOI:<https://doi.org/10.2166/nh.2019.163>
- Vousdoukas, M.I., Bouziotas, D., Giardino, A., Bouwer, L.M., Mentaschi, L., Voukouvalas, E., Feyen, L., 2018. Understanding epistemic uncertainty in large-scale coastal flood risk assessment for present and future climates. *Natural Hazards and Earth System Sciences*, 18(8): 2127-2142.
- Wagenaar, D., De Bruijn, K., Bouwer, L., Moel, H.d., 2016. Uncertainty in flood damage estimates and its potential effect on investment decisions. *Natural Hazards and Earth System Sciences*, 16(1): 1-14.
- Warmink, J.J., Straatsma, M., Huthoff, F., 2013. The effect of hydraulic roughness on design water levels in river models. *Comprehensive Flood Risk Management*; Klijn, Schweckendiek, Eds.; Taylor & Francis: Abingdon, UK.
- Winter, B., Schneeberger, K., Huttenlau, M., Stötter, J., 2018. Sources of uncertainty in a probabilistic flood risk model. *Natural hazards*, 91(2): 431-446.
- Wong, W.K., Haddeland, I., Lawrence, D., Beldring, S., 2016. Gridded 1 x 1 km climate and hydrological projections for Norway.
- Yang, W.p., Tarng, Y., 1998. Design optimization of cutting parameters for turning operations based on the Taguchi method. *Journal of materials processing technology*, 84(1-3): 122-129. DOI:[https://doi.org/10.1016/S0924-0136\(98\)00079-X](https://doi.org/10.1016/S0924-0136(98)00079-X)

## APPENDIX

Table A.1. Different quantile values of water level distributions displayed in Fig.4.

Scenari	PDF	min	max	med	mean	SD	skew	kurtosis	q1	q2	ML	UI
o												
RCP 8.5												
	GenLog	23.81	32.39	26.55	26.93	1.79	0.73	2.77	24.64	30.47	25.46	5.83
	GEV_W	23.83	29.87	25.94	26.07	1.06	0.50	2.67	24.57	28.01	25.48	3.44
PS												
	GEV	23.83	31.51	25.97	26.22	1.31	0.86	3.37	24.54	28.81	25.25	4.27
	Gumbel	23.49	27.97	25.32	25.37	0.71	0.31	2.71	24.28	26.63	25.17	2.35
	LN	23.68	30.28	25.70	25.91	1.16	0.70	2.98	24.37	28.14	25.18	3.78
	P3	23.44	27.23	24.92	24.98	0.61	0.39	2.78	24.06	26.07	24.76	2.01
RCP 4.5												
	GenLog	23.18	31.78	25.76	26.06	1.60	0.71	2.93	23.93	29.17	25.08	5.24
	GEV_W	23.17	29.28	25.47	25.58	1.10	0.41	2.57	23.96	27.56	25.11	3.60
PS												
	GEV	23.06	32.29	25.22	25.65	1.62	1.15	3.98	23.75	29.07	24.74	5.32
	Gumbel	23.05	27.83	24.95	25.01	0.76	0.34	2.82	23.83	26.38	24.78	2.54
	LN	23.10	29.27	25.11	25.27	1.05	0.62	2.96	23.80	27.26	24.78	3.46
	P3	22.91	26.64	24.41	24.45	0.60	0.28	2.76	23.52	25.49	24.32	1.97
Present												
	GenLog	23.11	25.92	24.07	24.13	0.42	0.59	3.21	23.52	24.91	23.92	1.39
	GEV_W	23.21	26.13	24.21	24.26	0.44	0.60	3.18	23.64	25.08	24.09	1.44
PS												
	GEV	23.16	26.30	24.17	24.24	0.47	0.75	3.43	23.60	25.14	24.03	1.54
	Gumbel	23.12	24.96	23.89	23.90	0.27	0.22	2.85	23.47	24.37	23.88	0.90
	LN	23.10	25.44	23.99	24.02	0.34	0.42	3.10	23.51	24.62	23.95	1.11
	P3	23.03	24.88	23.78	23.79	0.27	0.23	2.92	23.37	24.25	23.76	0.88

Table A.2. Different water level distribution quantiles values base on the number of MC simulations

Scenario	PDF	min	max	med	mean	sd	CV	skew	kurtosis	q1	q2	RMSE	MC size
RCP 4.5	GENLOG	23.43	29.82	25.62	25.86	1.46	6%	0.67	2.78	23.85	28.51	0.31	100
RCP 4.5	GENLOG	23.36	30.89	25.75	25.97	1.59	6%	0.67	2.91	23.86	29.05	0.12	500
RCP 4.5	GENLOG	23.4	31.42	25.7	26	1.59	6%	0.85	3.35	23.94	29.25	0.08	1,000

RCP 4.5	GENLOG	23.2	31.49	25.7	26.04	1.6	6%	0.73	2.94	23.92	29.14	0.05	2,000
RCP 4.5	GENLOG	23.34	31.44	25.78	26.07	1.61	6%	0.72	2.94	23.96	29.22	0.06	5,000
RCP 4.5	GENLOG	23.25	31.48	25.75	26.06	1.62	6%	0.71	2.89	23.94	29.22	0.05	10,000
RCP 4.5	GENLOG	23.22	31.69	25.75	26.03	1.59	6%	0.73	2.98	23.93	29.14	0	20,000
RCP 4.5	GENLOG	23.22	31.69	25.75	26.03	1.59	6%	0.73	2.98	23.93	29.14	0	100,000
RCP 4.5	GEV	23.3	31.37	25.11	25.56	1.54	6%	1.08	4.18	23.63	28.6	0.26	100
RCP 4.5	GEV	23.28	31.71	25.33	25.75	1.66	6%	1.1	3.79	23.78	29.2	0.11	500
RCP 4.5	GEV	23.24	31.56	25.18	25.6	1.57	6%	1.13	3.91	23.75	28.92	0.1	1,000
RCP 4.5	GEV	23.19	31.44	25.22	25.67	1.63	6%	1.17	4.02	23.78	29.12	0.07	2,000
RCP 4.5	GEV	23.1	32.28	25.19	25.64	1.62	6%	1.15	3.97	23.75	29.07	0.03	5,000
RCP 4.5	GEV	23.1	31.84	25.22	25.65	1.61	6%	1.12	3.87	23.75	29.06	0.03	10,000
RCP 4.5	GEV	23.09	32.04	25.22	25.66	1.62	6%	1.14	3.92	23.75	29.08	0	20,000
RCP 4.5	GEV	23.09	32.04	25.22	25.66	1.62	6%	1.14	3.92	23.75	29.08	0	100,000
RCP 4.5	GEV_WPS	23.59	28.49	25.46	25.45	1.16	5%	0.31	2.45	23.69	27.35	0.18	100
RCP 4.5	GEV_WPS	23.41	28.85	25.36	25.54	1.07	4%	0.42	2.65	23.93	27.52	0.08	500
RCP 4.5	GEV_WPS	23.31	28.59	25.5	25.6	1.08	4%	0.35	2.44	24.01	27.5	0.08	1,000
RCP 4.5	GEV_WPS	23.4	28.9	25.51	25.6	1.09	4%	0.4	2.54	23.99	27.62	0.06	2,000
RCP 4.5	GEV_WPS	23.27	29.3	25.44	25.56	1.1	4%	0.43	2.62	23.95	27.54	0.02	5,000
RCP 4.5	GEV_WPS	23.19	29.26	25.45	25.57	1.09	4%	0.39	2.57	23.95	27.54	0.01	10,000
RCP 4.5	GEV_WPS	23.17	29.27	25.46	25.57	1.1	4%	0.4	2.54	23.96	27.54	0	20,000
RCP 4.5	GEV_WPS	23.17	29.27	25.46	25.57	1.1	4%	0.4	2.54	23.96	27.54	0	100,000
RCP 4.5	GUMBEL	23.35	27.18	25.01	25.05	0.77	3%	0.28	3.16	23.85	26.5	0.1	100
RCP 4.5	GUMBEL	23.21	27.37	24.99	25.04	0.78	3%	0.3	2.87	23.78	26.34	0.05	500
RCP 4.5	GUMBEL	23.19	27.67	25	25.03	0.79	3%	0.31	2.67	23.78	26.49	0.04	1,000
RCP 4.5	GUMBEL	23.37	27.57	24.97	25.04	0.77	3%	0.35	2.83	23.86	26.34	0.04	2,000
RCP 4.5	GUMBEL	23.04	27.81	24.95	25.02	0.78	3%	0.34	2.83	23.81	26.41	0.02	5,000
RCP 4.5	GUMBEL	23.11	27.65	24.95	25.02	0.76	3%	0.32	2.78	23.85	26.37	0.01	10,000
RCP 4.5	GUMBEL	23.16	27.69	24.95	25.01	0.77	3%	0.32	2.75	23.82	26.37	0	20,000
RCP 4.5	GUMBEL	23.16	27.69	24.95	25.01	0.77	3%	0.32	2.75	23.82	26.37	0	100,000
RCP 4.5	LN	23.38	28.41	25.15	25.34	1.09	4%	0.69	3.09	23.97	27.28	0.12	100
RCP 4.5	LN	23.26	29.09	25.09	25.28	1.07	4%	0.65	2.91	23.86	27.42	0.06	500
RCP 4.5	LN	23.14	28.63	25.07	25.22	1.02	4%	0.71	3.21	23.79	27.16	0.07	1,000
RCP 4.5	LN	23.13	28.91	25.08	25.21	1.03	4%	0.62	3.05	23.74	27.17	0.06	2,000
RCP 4.5	LN	23.2	28.96	25.07	25.24	1.03	4%	0.65	3.02	23.8	27.22	0.04	5,000
RCP 4.5	LN	23.09	28.99	25.07	25.24	1.03	4%	0.68	3.09	23.8	27.23	0.03	10,000
RCP 4.5	LN	23.11	29.04	25.1	25.26	1.05	4%	0.63	2.97	23.8	27.25	0	20,000

RCP 4.5	LN	23.11	29.04	25.1	25.26	1.05	4%	0.63	2.97	23.8	27.25	0	100,000
RCP 4.5	P3	23.18	26.47	24.35	24.39	0.65	3%	0.34	2.99	23.41	25.39	0.09	100
RCP 4.5	P3	23.06	26.26	24.42	24.44	0.63	3%	0.22	2.68	23.45	25.53	0.05	500
RCP 4.5	P3	22.95	26.56	24.41	24.44	0.59	2%	0.26	2.7	23.53	25.42	0.03	1,000
RCP 4.5	P3	22.99	26.27	24.43	24.46	0.61	2%	0.3	2.68	23.52	25.55	0.03	2,000
RCP 4.5	P3	22.96	26.42	24.42	24.46	0.6	2%	0.29	2.73	23.55	25.52	0.02	5,000
RCP 4.5	P3	22.96	26.66	24.42	24.45	0.6	2%	0.28	2.71	23.52	25.51	0.01	10,000
RCP 4.5	P3	22.92	26.54	24.41	24.45	0.6	2%	0.29	2.75	23.52	25.51	0	20,000
RCP 4.5	P3	22.92	26.54	24.41	24.45	0.6	2%	0.29	2.75	23.52	25.51	0	100,000
RCP 8.5	GENLOG	24.47	31.67	26.38	26.99	1.88	7%	0.86	2.82	24.74	30.51	0.23	100
RCP 8.5	GENLOG	24.1	31.68	26.58	27.04	1.86	7%	0.64	2.45	24.69	30.63	0.18	500
RCP 8.5	GENLOG	24.1	32.11	26.56	26.9	1.73	6%	0.7	2.78	24.64	30.2	0.08	1,000
RCP 8.5	GENLOG	24.01	32.24	26.55	26.91	1.76	7%	0.77	2.96	24.67	30.4	0.05	2,000
RCP 8.5	GENLOG	23.98	32.19	26.54	26.91	1.76	7%	0.71	2.73	24.65	30.43	0.04	5,000
RCP 8.5	GENLOG	23.9	32.29	26.55	26.92	1.77	7%	0.74	2.83	24.66	30.44	0.02	10,000
RCP 8.5	GENLOG	23.88	32.34	26.54	26.92	1.78	7%	0.75	2.83	24.66	30.45	0	20,000
RCP 8.5	GENLOG	23.88	32.34	26.54	26.92	1.78	7%	0.75	2.83	24.66	30.45	0	100,000
RCP 8.5	GEV	24.48	29.68	26.16	26.16	1.07	4%	0.8	3.46	24.82	28.3	0.37	100
RCP 8.5	GEV	24.15	30.57	26.04	26.29	1.31	5%	0.78	3.14	24.56	28.94	0.13	500
RCP 8.5	GEV	24.08	31.2	25.98	26.22	1.33	5%	0.84	3.3	24.53	28.78	0.05	1,000
RCP 8.5	GEV	23.86	31.55	25.95	26.22	1.36	5%	0.91	3.52	24.51	28.97	0.04	2,000
RCP 8.5	GEV	23.97	31.24	25.99	26.22	1.31	5%	0.84	3.37	24.55	28.8	0.04	5,000
RCP 8.5	GEV	23.89	31.53	25.98	26.22	1.31	5%	0.85	3.33	24.54	28.81	0.02	10,000
RCP 8.5	GEV	23.86	31.43	25.97	26.22	1.32	5%	0.87	3.4	24.53	28.82	0	20,000
RCP 8.5	GEV	23.86	31.43	25.97	26.22	1.32	5%	0.87	3.4	24.53	28.82	0	100,000
RCP 8.5	GEV_WPS	24.14	29.73	25.81	25.94	1.08	4%	0.78	3.92	24.52	27.65	0.19	100
RCP 8.5	GEV_WPS	24.12	29.27	26.1	26.16	1.06	4%	0.39	2.67	24.56	28.09	0.11	500
RCP 8.5	GEV_WPS	24.01	29.2	25.88	26.02	1.03	4%	0.57	2.86	24.57	28.01	0.09	1,000
RCP 8.5	GEV_WPS	23.97	29.46	25.96	26.07	1.05	4%	0.46	2.65	24.59	27.94	0.03	2,000
RCP 8.5	GEV_WPS	23.95	29.62	25.9	26.05	1.05	4%	0.5	2.63	24.57	27.99	0.03	5,000
RCP 8.5	GEV_WPS	23.87	29.51	25.93	26.06	1.05	4%	0.47	2.64	24.57	27.97	0.02	10,000
RCP 8.5	GEV_WPS	23.88	29.58	25.93	26.07	1.06	4%	0.5	2.64	24.57	28.02	0	20,000
RCP 8.5	GEV_WPS	23.88	29.58	25.93	26.07	1.06	4%	0.5	2.64	24.57	28.02	0	100,000
RCP 8.5	GUMBEL	23.76	27.01	25.14	25.2	0.71	3%	0.34	2.91	24.05	26.46	0.2	100
RCP 8.5	GUMBEL	23.78	27.58	25.35	25.36	0.72	3%	0.16	2.78	24.17	26.6	0.06	500
RCP 8.5	GUMBEL	23.58	27.57	25.33	25.38	0.73	3%	0.24	2.54	24.25	26.63	0.04	1,000



RCP 8.5	GUMBEL	23.74	27.81	25.31	25.36	0.73	3%	0.34	2.78	24.25	26.65	0.03	2,000
RCP 8.5	GUMBEL	23.57	27.85	25.35	25.39	0.72	3%	0.28	2.71	24.27	26.65	0.02	5,000
RCP 8.5	GUMBEL	23.57	27.77	25.31	25.37	0.72	3%	0.33	2.71	24.27	26.65	0.02	10,000
RCP 8.5	GUMBEL	23.56	27.85	25.32	25.37	0.72	3%	0.3	2.67	24.27	26.64	0	20,000
RCP 8.5	GUMBEL	23.56	27.85	25.32	25.37	0.72	3%	0.3	2.67	24.27	26.64	0	100,000
RCP 8.5	LN	24.26	29.57	25.83	26.08	1.33	5%	0.76	2.72	24.48	28.73	0.25	100
RCP 8.5	LN	23.88	29.61	25.74	25.87	1.14	4%	0.61	2.83	24.29	28.07	0.08	500
RCP 8.5	LN	23.67	29.62	25.71	25.94	1.16	4%	0.71	2.87	24.43	28.2	0.07	1,000
RCP 8.5	LN	23.79	30.14	25.76	25.97	1.19	5%	0.65	2.84	24.36	28.14	0.07	2,000
RCP 8.5	LN	23.73	29.88	25.74	25.93	1.17	5%	0.67	2.89	24.36	28.17	0.03	5,000
RCP 8.5	LN	23.75	30.19	25.69	25.9	1.15	4%	0.69	2.93	24.37	28.1	0.03	10,000
RCP 8.5	LN	23.68	30.02	25.71	25.91	1.16	4%	0.7	2.97	24.37	28.14	0	20,000
RCP 8.5	LN	23.68	30.02	25.71	25.91	1.16	4%	0.7	2.97	24.37	28.14	0	100,000
RCP 8.5	P3	23.82	26.56	25.07	25.06	0.61	2%	0.07	2.54	24.08	26	0.14	100
RCP 8.5	P3	23.67	26.78	24.96	24.96	0.6	2%	0.28	2.74	24	25.96	0.07	500
RCP 8.5	P3	23.6	27.2	24.96	25	0.61	2%	0.3	2.7	24.06	26.04	0.04	1,000
RCP 8.5	P3	23.5	27.2	24.89	24.95	0.6	2%	0.45	2.9	24.08	26.05	0.02	2,000
RCP 8.5	P3	23.54	27.2	24.93	24.98	0.62	2%	0.38	2.78	24.06	26.07	0.02	5,000
RCP 8.5	P3	23.43	27.13	24.91	24.97	0.61	2%	0.38	2.77	24.06	26.04	0.02	10,000
RCP 8.5	P3	23.45	27.28	24.92	24.97	0.61	2%	0.39	2.79	24.05	26.05	0	20,000
RCP 8.5	P3	23.45	27.28	24.92	24.97	0.61	2%	0.39	2.79	24.05	26.05	0	100,000